

Revision of the Late Triassic metoposaurid “*Metoposaurus*” *bakeri* (Amphibia: Temnospondyli) from Texas, USA and a phylogenetic analysis of the Metoposauridae

[Research article](#)

[Evolutionary Studies](#)

[Paleontology](#)

[Taxonomy](#)

[Zoology](#)

Bryan M. Gee^{1,2}, Aaron M. Kufner³

October 12, 2022

Author and article information

Abstract

Metoposaurids are a clade of large-bodied temnospondyls commonly found in non-marine Late Triassic deposits across northern Pangea. Three taxa are known from North America: *Anaschisma browni*, *Apachesaurus gregorii*, and “*Metoposaurus*” *bakeri*. While the osteology of most metoposaurids has been recently revised, that of a few taxa, including “*Metoposaurus*” *bakeri* remains poorly characterized. This taxon was formally described in 1931 as “*Buettneria bakeri*,” and its taxonomy has remained in flux ever since then. “*Metoposaurus*” *bakeri* is the earliest appearing metoposaurid in North America (Carnian of Texas), and *Metoposaurus* has frequently been utilized as an index taxon of the Otischalkian estimated holochron (‘land vertebrate faunachron’) and for biostratigraphic correlations with other geographic regions. The taxonomy of this species is therefore relevant for both taxonomic experts and biostratigraphers. Here we redescribe all material from the type locality of “*M.*” *bakeri*, the Elkins Place bone bed, and perform a phylogenetic analysis using a revised matrix assembled from several previous studies. Anatomical comparisons and phylogenetic analyses do not support placement in either *Metoposaurus*, a taxon otherwise only found in Europe, or *Anaschisma*, the only other large-bodied taxon from North America. Therefore, we erect a new genus, *Buettnererpeton* gen. nov., to accommodate this species. *Metoposaurus* is consequently absent from North America, and this genus cannot be used in global biostratigraphy. Phylogenetic analyses provide evidence that the phylogeny of the Metoposauridae remains extremely labile, with drastic differences in topological resolution and structure being linked to just a handful of characters and scores. Metoposaurids’ morphological conservatism and the increased recognition of intraspecific variation thus continue to be major confounds to elucidating the evolutionary history of this clade.

Cite this as

Main article text

Introduction

Metoposaurids are a clade of large-bodied temnospondyls that are common constituents of non-marine Late Triassic deposits in North America, western and central Europe, northern Africa, Madagascar, and India ([Colbert & Imbrie, 1956](#); [Hunt, 1993](#); [Sulej, 2002](#)). Within North America, metoposaurids are found across the continental United States but are best represented from the Carnian- and Norian-aged formations of the southwestern United States ([Long & Murry, 1995](#)). Over a dozen taxa have been named from North America, but only three are presently valid: *Anaschisma browni* [Branson, 1905](#), *Apachesaurus gregorii* [Hunt, 1993](#), and “*Metoposaurus*” *bakeri* [Case, 1931](#). “*Metoposaurus*” *bakeri* was described from the Late Triassic Dockum Group exposures in Scurry County, TX by [Case \(1931\)](#) as the third species of “*Buettneria*” [Case, 1922](#) (= *Anaschisma* [Branson, 1905](#); [Gee, Parker & Marsh, 2019](#)) on the basis of three medium-sized skulls ([Fig. 1](#)). The osteology of “*M.*” *bakeri* was subsequently expanded through substantial amounts of new material from the type locality, the Elkins Place bone bed ([Case, 1932](#); alternatively termed the ‘Elkins bone bed’). [Baird & Olsen \(1983\)](#) later reported the presence of “*M.*” *bakeri* from the Wolfville Formation of Nova Scotia based on the natural mold of a small, complete skull; this is the only published occurrence of “*M.*” *bakeri* outside of central Texas. Additional indeterminate metoposaurid material is also known from Nova Scotia ([Sues & Olsen, 2015](#)). [Houle & Mueller \(2004\)](#), [Martz \(2008\)](#), and [Mueller et al. \(2016\)](#) reported substantially larger specimens from the Boren Quarry in Garza County, TX ([Fig. 1](#)); two of these are conference abstracts, and the third is a publicly available, unpublished doctoral dissertation.

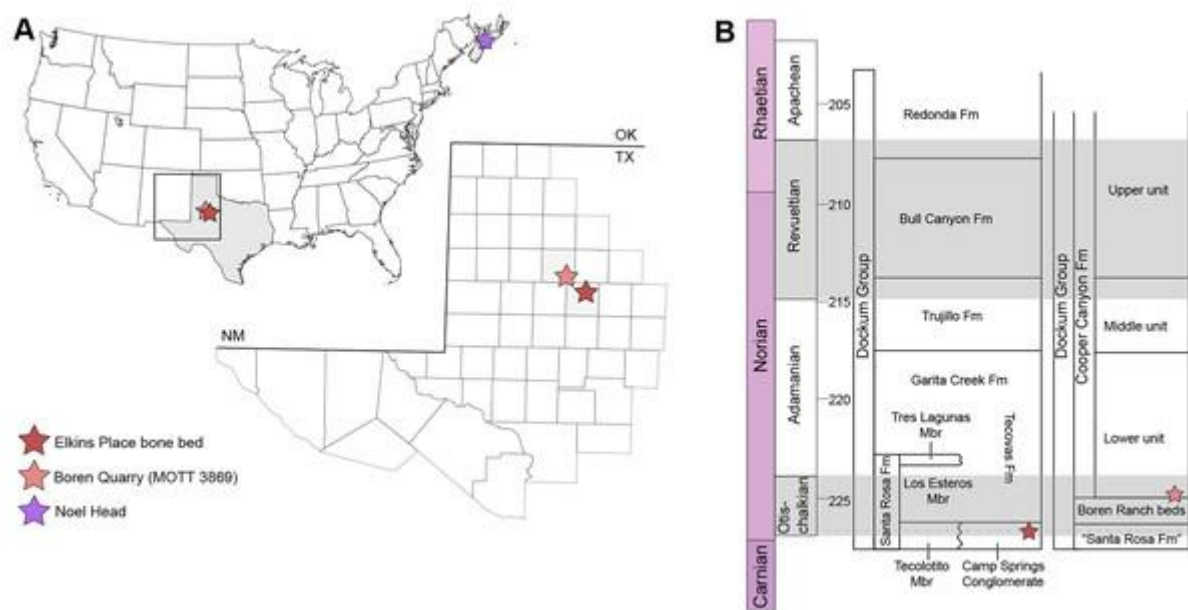


Figure 1: Map showing geographic and stratigraphic distribution of known occurrences of *Buettnererpeton bakeri*.

(A) Map of the lower 48 states (U.S.A.) and the province of Nova Scotia (Canada) showing the three published localities from which *B. bakeri* is known; inset represents close-up view of northwestern Texas showing localities on a county grid; (B) stratigraphic columns showing the approximate position of the two Texas localities. The two columns are based on local stratigraphy in the Dockum Group exposures of New Mexico and the Texas panhandle (on left) and the Dockum Group exposures in Garza County in west Texas (on right); note that the position of the Elkins Place bone bed within the Camp Springs Conglomerate is not well-constrained. Figure adapted from [Martz & Parker \(2017\):fig. 14](#).

[Download full-size image](#)

DOI: [10.7717/peerj.14065/fig-1](https://doi.org/10.7717/peerj.14065/fig-1)

Reexamination of historic metoposaurid specimens by numerous workers in the 21st century has produced a marked improvement in our understanding of the Metoposauridae, one of the last-surviving and most morphologically conserved temnospondyl clades. Within North America, the osteology and taxonomy of both *Anaschisma browni* ([Lucas et al., 2016](#); [Gee, Parker & Marsh, 2019](#); [Kufner & Gee, 2021](#)) and *Apachesaurus gregorii* ([Spielmann & Lucas, 2012](#); [Gee & Parker, 2018](#); [Rinehart & Lucas, 2018](#)) have been updated in recent years. A complementary suite of work on non-North American metoposaurids includes: (1) revision of the first described metoposaurid, *Metoposaurus diagnosticus* ([von Meyer, 1842](#)) [Lydekker, 1890](#) ([Sulej, 2002](#)); (2) description of a new taxon from Poland, *Metoposaurus krasiejowensis* [Sulej, 2002](#) ([Milner & Schoch, 2004](#); [Sulej, 2007](#)); (3) description of a new taxon from Portugal, *Metoposaurus algarvensis* [Brusatte et al., 2015](#); (4) revision of the Indian taxon, “*Koskinonodon*” *maleriensis*, also variably placed in different genera but most recently renamed as *Panthesaurus malerensis* [Chakravorti & Sengupta, 2018](#); (5) reevaluation of the Malagasy taxon “*Metoposaurus hoffmani*” [Dutuit, 1978](#) ([Fortuny et al., 2019](#)); and (6) revision of the poorly known Moroccan taxon “*Metoposaurus*” *azerouali* [Dutuit, 1976](#), long considered to be a *nomen dubium* but recently renamed as *Arganasaurus azerouali* [Buffa, Jalil & Steyer, 2019](#). As a

result, nearly all the presently recognized metoposaurid taxa have been recently revised through detailed study that facilitates thorough examination of their comparative morphology and phylogenetic relationships.

The three taxa that have not been recently re-studied beyond systematic reviews ([Colbert & Imbrie, 1956](#); [Hunt, 1993](#); [Schoch & Milner, 2000](#)) are *Arganasaurus lyazidi* ([Dutuit, 1976](#)) [Hunt, 1993](#) and *Dutuitosaurus ouazzoui* ([Dutuit, 1976](#)) [Hunt, 1993](#) from Morocco and “*Metoposaurus*” *bakeri*. *Arganasaurus lyazidi* and *D. ouazzoui* were detailed in [Dutuit’s \(1976\)](#) monographic work, and their taxonomic validity and status are considered stable. These taxa have also been reexamined first-hand by other workers as part of other studies (e.g., [Khaldoune et al., 2016](#); [Chakravorti & Sengupta, 2018](#); [Buffa, Jalil & Steyer, 2019](#)) such that explicit comparisons of anatomy and phylogenetic scorings are available. By comparison, [Case’s \(1931, 1932\)](#) descriptions and photographs of “*M.*” *bakeri* from the Dockum Group of Texas are detailed but also more dated and are understandably limited in relevant comparative information. Over the subsequent 90 years, substantial amounts of new metoposaurid material have been recovered that have greatly altered the framework of metoposaurid paleobiology and phylogenetics.

The taxonomy of “*Metoposaurus*” *bakeri* has shifted considerably since Case named the species ([Fig. 2](#)). “*Buettneria*” was synonymized with *Eupelor* [Cope, 1868](#) by [Colbert & Imbrie \(1956\)](#) and then with *Metoposaurus* [Lydekker, 1890](#) by [Roychowdhury \(1965\)](#); restored to *Buettneria* by [Hunt \(1993\)](#); replaced by *Koskinonodon* [Branson & Mehl, 1929](#) by [Mueller \(2007\)](#) due to nomenclatural preoccupation of *Buettneria*; and most recently synonymized with *Anaschisma* [Branson, 1905](#) by [Gee, Parker & Marsh \(2019\)](#).

“*Metoposaurus*” *bakeri* was synonymized with “*Buettneria perfecta*” (= *An. browni*) under “*Eupelor fraasi jonesi*” [Case, 1920](#) by [Colbert & Imbrie \(1956\)](#), who separated the North American taxa into subspecies delineated by geographic occurrence, largely along present-day state boundaries; “*E. f. jonesi*” was restricted to the Dockum Group. The species-level synonymy of these two taxa was maintained by [Roychowdhury \(1965\)](#), who placed all metoposaurids within *Metoposaurus* while preserving Colbert & Imbrie’s framework of subspecies. [Hunt’s \(1993\)](#) review of the Metoposauridae abandoned subspecies and removed “*M.*” *bakeri* to *Metoposaurus*, which only included “*M.*” *bakeri* and the European *M. diagnosticus* based on the shared exclusion of the lacrimal from the orbit. [Sulej \(2002\)](#) returned “*M.*” *bakeri* to “*Buettneria*” after identifying a lacrimal entering the orbit in *M. diagnosticus* but maintained “*B. bakeri*” as distinct from “*Buettneria perfecta*.” As this contact was subsequently found in two other European species, *M. krasiejowensis* and *M. algarvensis*, a lacrimal-orbit contact is considered diagnostic of *Metoposaurus sensu* [Brusatte et al. \(2015\)](#). This taxonomy has been adopted by practically every worker (but see [Lucas, Spielmann & Hunt, 2007](#)), and this feature is shared with *Anaschisma* (“*Buettneria*”), which would exclude “*M.*” *bakeri* from both genera based on their present diagnoses.

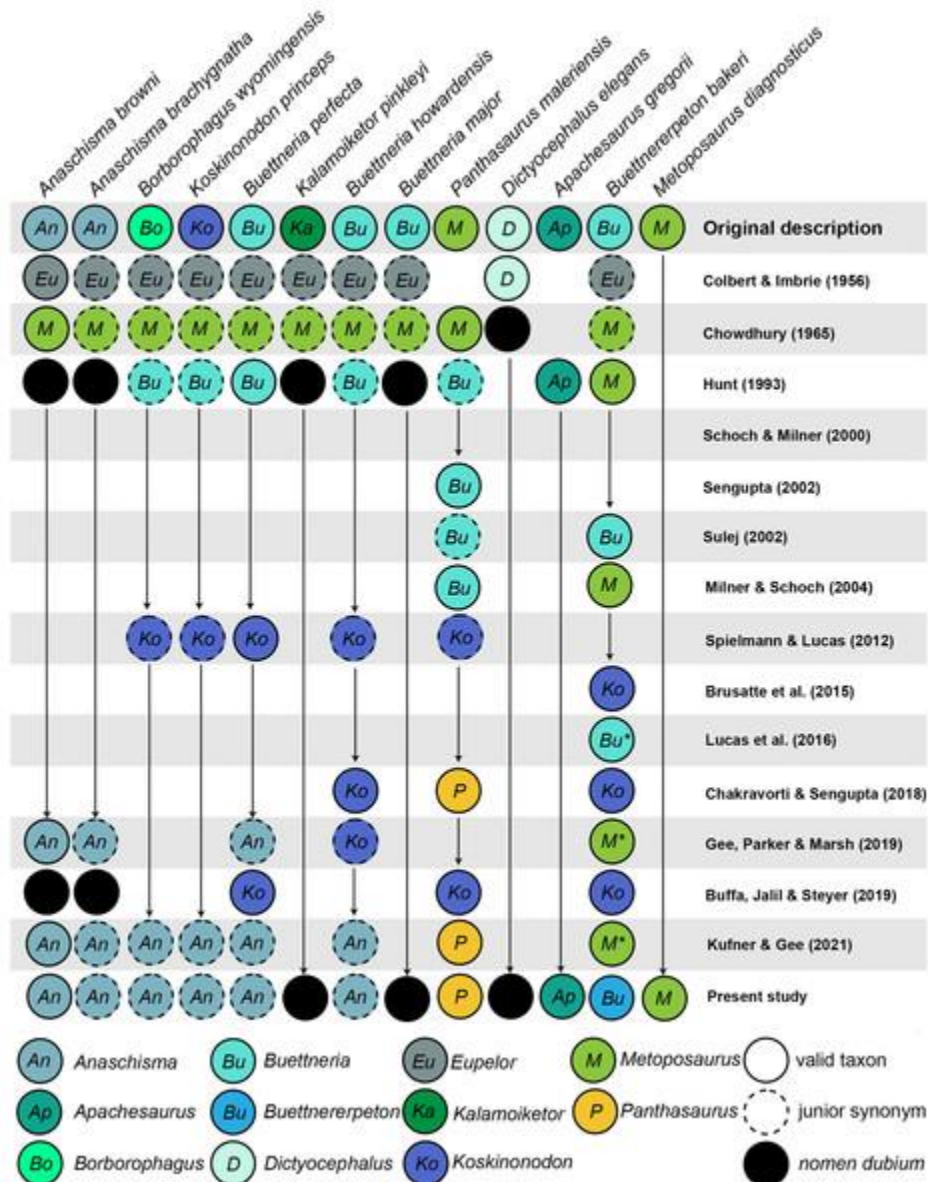


Figure 2: Comparison of genus-level placement of *Buettnererpeton bakeri* relative to other metoposaurids over time, with an emphasis on North American taxa.

Studies are ordered chronologically from top to bottom and are not an exhaustive list. Note that highly fragmentary taxa (*Eupelor durus*, *Metoposaurus fraasi*, *Metoposaurus jonesi*) are excluded due to space constraints. *Metoposaurus diagnosticus* is included as an ‘outgroup,’ and *Panthasaurus maleriensis* is included because it has sometimes been synonymized with *Anaschisma browni*. Arrows represent implicit or explicit continuity of genus-level placements. Asterisks indicate that the placement was marked as questionable by those authors based on the use of quotation marks.

[Download full-size image](#)

DOI: [10.7717/peerj.14065/fig-2](https://doi.org/10.7717/peerj.14065/fig-2)

As a result of the constant flux of metoposaurid anatomy and systematics, “*Metoposaurus*” *bakeri* has been referred to in nearly every possible taxonomic combination in the past two decades alone (Fig. 2), such as *Metoposaurus bakeri* (e.g., [Hunt, 1993](#); [Long & Murry, 1995](#); [Sengupta, 2002](#); [Witzmann & Gassner, 2008](#); [Parker & Martz, 2010](#); [McHugh, 2012](#); [Spielmann & Lucas,](#)

2012; [Sues & Olsen, 2015](#); [Lucas, 2021](#)), “*Metoposaurus*” *bakeri* (e.g., [Gee & Parker, 2018](#)), *Buettneria bakeri* (e.g., [Sulej, 2002](#)), “*Buettneria*” *bakeri* (e.g., [Lucas et al., 2016](#)), or *Koskinonodon bakeri* (e.g., [Brusatte et al., 2015](#); [Chakravorti & Sengupta, 2018](#); [Buffa, Jalil & Steyer, 2019](#); [Fortuny et al., 2019](#)). Phylogenetic inference has not resolved this matter, as three independent, computationally-derived analyses ([Chakravorti & Sengupta, 2018](#); [Buffa, Jalil & Steyer, 2019](#); [Gee, Parker & Marsh, 2019](#)) have recovered drastically different degrees of resolution and topology ([Fig. 3](#)).

“*Metoposaurus*” *bakeri* is also of interest beyond the confines of metoposaurid taxonomy because it was long considered to be an index taxon for the Otischalkian LVF (land vertebrate faunachron) and to be useful for correlation with European *Metoposaurus*-bearing deposits (e.g., [Lucas & Hunt, 1993](#); [Lucas, 1998, 2021](#)). However, the shifting taxonomy of both this taxon and of *Metoposaurus* has led to the abandonment of its usage in this biostratigraphic context by virtually all workers other than Lucas (e.g., [Langer, 2005](#); [Kammerer, Nesbitt & Shubin, 2011](#); [Martz & Parker, 2017](#)). This study thus has two objectives: (1) to provide a detailed, updated osteology of Case’s original material for use in comparative anatomical descriptions and phylogenetic analyses; and (2) to resolve the taxonomic status of this species, thereby clarifying its informativeness for biostratigraphy or lack thereof.

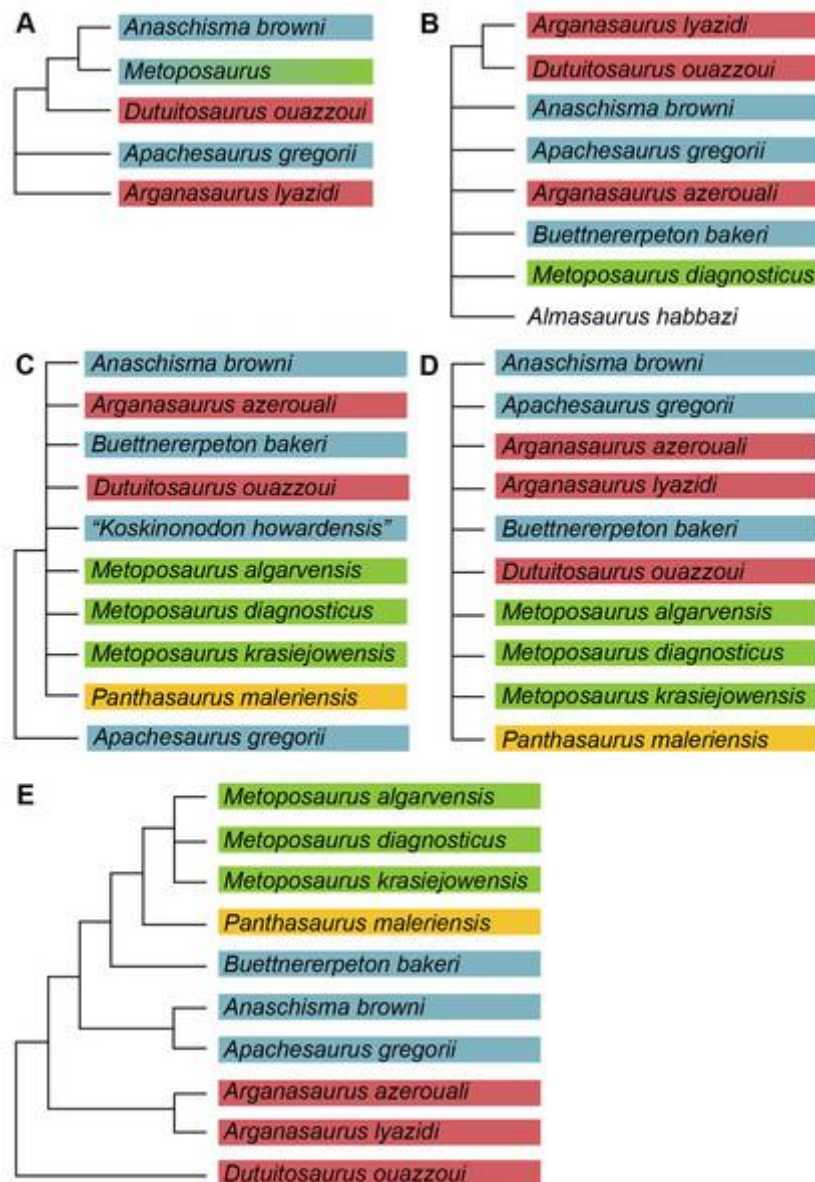


Figure 3: Comparison of previous phylogenetic hypotheses of the Metoposauridae.

(A) Non-computer-assisted topology of [Hunt \(1993\)](#); (B) pruned clade from the computer-assisted analysis of [McHugh \(2012\)](#); (C) topology from the computer-assisted analysis of [Chakravorti & Sengupta \(2018\)](#); (D) topology from the computer-assisted analysis of [Gee, Parker & Marsh \(2019\)](#); (E) topology from the computer-assisted analysis of [Buffa, Jalil & Steyer \(2019\)](#). Colors represent geographic regions. Names are updated to those employed in the current framework.

[Download full-size image](#)

DOI: [10.7717/peerj.14065/fig-3](https://doi.org/10.7717/peerj.14065/fig-3)

Materials and Methods

Examined specimens

A full list of the specimens of this taxon that we personally examined at the University of Michigan Museum of Paleontology (UMMP) is included in [Table 1](#).

Other referred specimens from the type locality that we did not personally examine include MCZ 1054, a complete skull that was exchanged as part of a loan (originally UMMP 13821 per [Case, 1932](#)) and MCZ 1056, a hemimandible (formerly UMMP 13946) that is listed as also having been exchanged on a collections card at the UMMP but not by Case. MCZ 1054 was most recently figured (photographs) by [Schoch & Milner \(2000\)](#):pl. 8A-B).

Table 1:

Complete listing of specimens of *Buettnererpeton bakeri* repositied at the University of Michigan Museum of Paleontology (UMMP) that were examined as part of this study.

UMMP number	ID	UMMP number	ID
12945	13 intercentra	13800	R tabular and postparietal
12946	R femur	13801	2 R postparietals
12947	L femur	13802	2 L prefrontals
12969	4 exoccipitals	13803	L and R maxillae
12970	L hemimandible	13804	L quadratojugal
13027	Interclavicle	13805	R prefrontal
13028	L clavicle	13806	2 R quadratojugals
13029	Interclavicle	13807	R postorbital
13055	Cranium (holotype)	13808	L postfrontal
13771	R pterygoid	13809	3 L nasals
13772	L humerus	13810	R quadrate
13773	1 R radius and 2 R femora	13811	1 R and 3 L nasals
13774	1 L and 2 R tibiae	13812	3 R parietals
13775	L humerus	13813	2 L parietals
13776	6 ribs	13814	3 R frontals
13777	R and L partial stapes	13815	2 L frontals
13778	Rib	13816	3 L squamosals
13779	2 partial R chevrons	13817	2 R squamosals
13780	Partial R and L caudal neural arches	13818	3 R quadratojugals
13781	L and R fibulae	13819	4 R and 3 L exoccipitals
13782	R ulna	13820	Cranium and R hemimandible

UMMP number	ID	UMMP number	ID
13783	Rib	13822	Partial cranium
13784	4 metapodials	13823	Cranium
13785	2 phalanges	13824	L clavicle
13786	L scapula	13825	L clavicle
13787	L epipterygoid	13826	R parietal
13788	11 ribs	13827	R surangular
13789	4 L and 2 R ilia	13828	L surangular
13792	Atlas	13829	R squamosal
13793	4 supratemporals	13830	L squamosal
13794	R pterygoid	13896	L clavicle
13795	R pterygoid	13897	L clavicle
13796	R pterygoid	13898	R clavicle
13797	Postparietals	13899	L clavicle
13798	2 L tabulars	13900	R clavicle
13799	L postparietal and L tabular	13901	R clavicle
13902	R clavicle	13949	L hemimandible
13903	R clavicle	13956	Cranium
13904	R clavicle	13966	R postfrontal
13905	Interclavicle	13967	L postparietal and tabular
13906	Interclavicle	13968	L squamosal
13907	Interclavicle	13969	2 L quadratojugals
13908	Interclavicle	13970	R postfrontal and postorbital
13910	Interclavicle	13975	L hemimandible
13911	Interclavicle	14098	Partial skull; R pterygoid, exoccipital, and quadratojugal
13912	Interclavicle	14099	R pterygoid, R exoccipital, R squamosal, and R cleithrum
13913	Interclavicle	14154	Cranium
13914	Interclavicle	14205	Neural arch

UMMP number	ID	UMMP number	ID
13915	Interclavicle	14262	Unidentified fragment
13944	R hemimandible	118526	5 intercentra
13945	L hemimandible	118527	6 intercentra
13947	L hemimandible	118525	17 intercentra
13948	R hemimandible		

DOI: [10.7717/peerj.14065/table-1](https://doi.org/10.7717/peerj.14065/table-1)

A few specimens have been reported from other localities that we did not examine ([Fig. 1](#)). YPM VPPU 021742 is a natural mold of a small specimen from Nova Scotia, the only species-level record of a metoposaurid from Canada and of the taxon outside of Texas ([Gregory, 1980](#); [Baird & Olsen, 1983](#); [Hopson, 1984](#); [Baird, 1986](#)). Figures of the specimen, especially a recent photograph by [Sues & Olsen \(2015\)](#) that is reproduced here alongside an interpretive drawing ([Fig. 4](#)), confirm the historic referral based on a lacrimal excluded from the orbit. It is not described in detail due to both lack of personal observation and the nature of the specimen (two-dimensional mold), but it is further contextualized with other material of this taxon in the discussion. [Martz \(2008\)](#) reported two specimens (TTU P-11046, TTU P-10530) from the Boren Quarry (MOTT VPL 3869), Garza Co., TX in his doctoral dissertation. These specimens were first noted in a conference abstract by [Houle & Mueller \(2004\)](#), who suggested that it might be a new subspecies of “*Buettneria bakeri*.” This is the same locality and material referenced in a later conference abstract ([Mueller et al., 2016](#)). We agree with the referral of these specimens to “*Metoposaurus*” *bakeri* based on Martz’s figures, although these specimens have yet to be published.

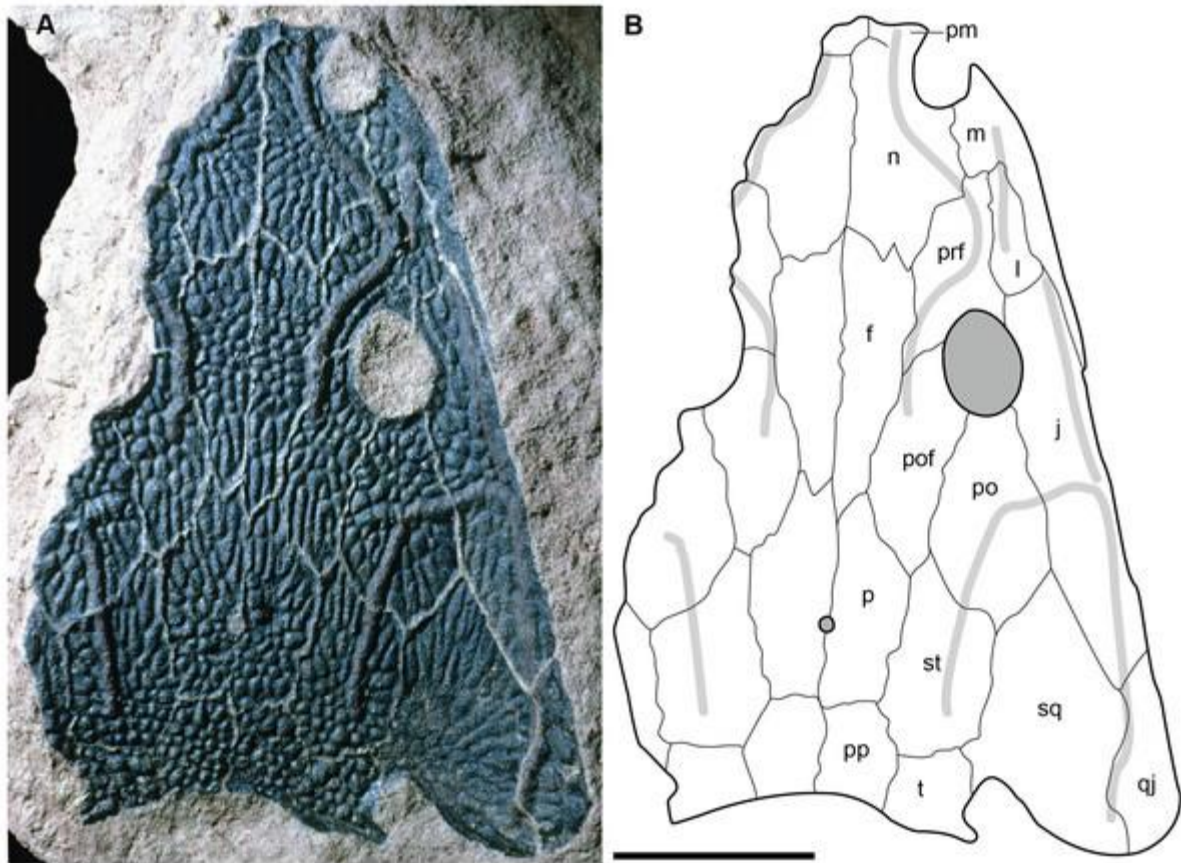


Figure 4: Referred specimen of *Buettnererpeton bakeri* from the Wolfville Formation of Nova Scotia, YPM VPPU 021742.

(A) Photograph (image credit: Hans-Dieter Sues); (B) interpretive line drawing. Note that the specimen is a natural mold and is therefore a mirrored impression of the dorsal surface of the skull. Abbreviations: f, frontal; j, jugal; l, lacrimal; m, maxilla; n, nasal; p, parietal; pm, premaxilla; po, postorbital; pof, postfrontal; pp, postparietal; prf, prefrontal; qj, quadratojugal; sq, squamosal; st, supratemporal; t, tabular. Scale bar equal to 5 cm.

[Download full-size image](#)

DOI: [10.7717/peerj.14065/fig-4](https://doi.org/10.7717/peerj.14065/fig-4)

Lastly, [Chakravorti & Sengupta \(2018\)](#) listed a never-before-reported specimen of this taxon in the Natural History Museum London (AB8948), but it was not described and was figured at an insufficient size to assess its anatomy. S.

Chakravorti graciously sent BMG a higher-resolution photograph, which permitted us to identify it as a cast of a published skull of a small-bodied specimen (TMM 31099-12B) from Quarry 2 near Otis Chalk, Howard County, TX ([Sawin, 1945](#)).

Our association was made on the basis of the cast's relatively small size and a distinctive pattern of fractures on the dorsal surface. TMM 31099-12B was listed by Sawin as a specimen of "*Buettneria bakeri?*," which likely accounts for the identification of the cast, but Sawin did not provide any figures or details other than to say that it was comparable to "*B. bakeri*" in form and size. TMM 31099-12B was then mentioned as a "juvenile metoposaur" by [Davidow-Henry \(1987\)](#) and was most recently figured by [Hunt \(1993\)](#) as a referred specimen of "*Buettneria perfecta*" (= *Anaschisma browni*). Although Hunt's figure is also too small to allow us to assess the anatomy, we consider Hunt's taxonomic referral, based on his

personal examination and its recency, to be the most reliable interpretation here, and AB8948 is not regarded as a specimen of “*Metoposaurus*” *bakeri*. This clarification underscores the need to exercise caution with identifications listed on collections cards and labels, especially for taxa with frequent shifts in taxonomy such as metoposaurids.

Locality & horizon

All material re-described here, which represents the only detailed published occurrence of the taxon in Texas, comes from the Elkins Place bonebed in Scurry County Texas (Fig. 1). Per [Long & Murry \(1995:14\)](#), the site was discovered by A.N. Huddleston on the P.L. Fuller Ranch approximately 37 km north of the town of Snyder in Scurry County (23 miles per [Case, 1932](#)). This locality has typically been situated within the Camp Springs Conglomerate at the base of the Dockum Group just above the TR-3 unconformity. There has been great historical debate over the rank of this unit (e.g., [Lehman, 1994](#)); it has been variably termed the Camp Springs Member (e.g., [Lucas & Anderson, 1993, 1994](#); [Ray et al., 2016](#); [Datta, Kumar & Ray, 2019](#)), the Camp Springs Formation (e.g., [Stocker, 2012](#); [Heckert et al., 2013](#); [Sues, Fitch & Whatley, 2020](#)), the Camp Springs Conglomerate (e.g., [Martz et al., 2012](#); [Martz & Parker, 2017](#)), and the pre-Tecovas Horizon (in part; e.g., [Long & Murry, 1995](#)). We refer to it as the Camp Springs Conglomerate here. This unit, regardless of its geologic rank, is less controversially accepted to be equivalent to the lowest portion (Tecolotito Member) of the Santa Rosa Formation elsewhere in Texas (e.g., [Martz & Parker, 2017](#)).

The lithology of the site has been described in detail by [Case \(1932\)](#) and is only briefly repeated here. All bones occurred in the lowest part of a half-meter thick coarse gray sandstone with no clear association beyond one jaw with a skull. Examples of the matrix can be seen in the palate of several of the complete skulls or within the braincase in partial specimens. Some elements were clustered, such as a number of skulls, but no association of cranial and postcranial elements was reported. The only remains of other taxa from the locality are fragmentary and isolated material (e.g., phytosaur teeth, coprolites) from a higher stratigraphic horizon in a clay conglomerate that is of a poorer quality of preservation. The monotaxicity of the metoposaurid-bearing horizon is therefore more similar to Lamy, NM (*Anaschisma browni*) and the type locality of *Dutuitosaurus ouazzoui* in Morocco ([Dutuit, 1976](#); [Lucas et al., 2010](#)) than to the mixed-taxa assemblages at Krasiejów and Rotten Hill ([Sulej, 2007](#); [Lucas et al., 2016](#)). The general state of disarticulation mirrors that observed for most other metoposaurid accumulations (e.g., [Sulej, 2007](#); [Lucas et al., 2010, 2016](#)). [Lehman & Chatterjee \(2005\)](#) interpreted the deposit as the infilling of an abandoned stream channel that probably held ephemeral bodies of water. Similar concentrations of small-bodied metoposaurids in abandoned channel fills also occur in the Chinle Formation of Arizona ([Loughney, Fastovsky & Parker, 2011](#)).

Photography

Specimens were photographed at the University of Michigan, Museum of Paleontology in Ann Arbor, Michigan, U.S.A. using a Nikon D3500 DSLR camera with an 18–55 mm and a 70–100 mm lens. All specimens were photographed in standard anatomical profiles, but some specimens, especially the large pectoral elements, are embedded in plaster from at least one side (usually the unornamented surfaces) and could not be photographed in certain profiles. Other specimens were originally stabilized using Japanese rice paper and are uninformative on one side. Figures were prepared using Adobe Photoshop and Illustrator.

Phylogenetic analysis

Our character matrix was derived from previous matrices ([Buffa, Jalil & Steyer, 2019](#); [Chakravorti & Sengupta, 2018](#); [Gee, Parker & Marsh, 2019](#)). We began with the matrix of [Buffa, Jalil & Steyer \(2019\)](#) because this matrix utilizes traditional discrete characters (rather than [Chakravorti & Sengupta \(2018\)](#), many of which are discrete binning of continuous data) and because this matrix produced good resolution in the original study compared to that of [Gee, Parker & Marsh \(2019\)](#), which also used discrete characters. Since one of us (BMG) authored the latter matrix, this provided a good opportunity to compare character sampling and scoring approaches to work towards an improved phylogenetic consensus for the clade. We then added additional characters utilized by one of the other two studies and removed several that were primarily used to differentiate the specific outgroups utilized by Buffa, Jalil & Steyer relative to metoposaurids. This produced a total of 139 characters; the character list of this study is listed in [Appendix 1](#), and the associated NEXUS file is appended as [Appendix 2](#). The matrix was compiled using Mesquite version 3.6 (build 197) ([Maddison & Maddison, 2018](#)).

For outgroups, we sampled the stereospondylomorph *Sclerocephalus haeuseri* [Goldfuß, 1847](#) (the operational outgroup), the Middle Triassic metoposauroid *Callistomordax kugleri* [Schoch, 2008](#) (the only unequivocal non-metoposaurid metoposauroid), the Early Triassic trematosauroid *Lyrocephaliscus euri* ([Wiman, 1914](#)) [Kuhn, 1961](#); the Middle Triassic trematosauroid *Trematolestes hagdorni* [Schoch, 2006](#); the Early Triassic lydekkerinid *Lydekkerina huxleyi* ([Lydekker, 1889](#)) [Broom, 1915](#); the late Permian rhinesuchid *Rhineceps nyasaensis* ([Haughton, 1927](#)) [Watson, 1962](#) (from the original sampling of Buffa, Jalil & Steyer); two brachyopoids, the late Permian or Early Triassic *Bothriceps australis* [Huxley, 1859](#), and the Late Triassic *Compsocerops cosgriffi* [Sengupta, 1995](#); and four capitosaurids, the Late Triassic *Cyclotosaurus intermedius* [Sulej & Majer, 2005](#), the Middle Triassic *Eocyclotosaurus appetolatus* [Rinehart, Lucas & Schoch, 2015](#), the Middle Triassic *Quasicyclotosaurus campi* [Schoch, 2000](#), and the Middle Triassic *Mastodonsaurus giganteus* [Jaeger, 1828](#).

We also retained the Late Triassic *Almasaurus habbazi* [Dutuit, 1976](#), from the analysis of [Buffa, Jalil & Steyer, 2019](#), but it should be noted that the position of this small-bodied taxon is strongly influenced by the interpretation and inclusion of two other small-bodied Late Triassic taxa: *Rileymillerus cosgriffi* [Bolt & Chatterjee, 2000](#), and *Chinlestegophis jenkinsi* [Pardo, Small & Huttenlocker, 2017](#).

These three taxa are contemporaneous with metoposaurids, and *A. habbazi* and *R. cosgriffi* were sometimes thought to be closely related to each other and to metoposaurids (e.g., [Schoch, 2008](#); [McHugh, 2012](#), but see original interpretations by [Bolt & Chatterjee, 2000](#)) but have been more recently recovered as being closely related to brachyopoids ([Pardo, Small & Huttenlocker, 2017](#)). [Gee, Makovicky & Sidor \(2022\)](#), an expansion of Pardo, Small & Huttenlocker, with the addition of *A. habbazi* (among other small-bodied stereospondyls), recovered *A. habbazi* as a trematosaur but *R. cosgriffi* and *C. jenkinsi* as the sister taxa of brachyopoids. The latter two were also sampled here.

We manually rescored all previously utilized characters based on a combination of personal observation (of North American metoposaurids) and the literature ([Table 2](#)). Characters were ordered when it could be reasonably inferred that character transformations occurred along a morphocline; an example is the progression of the lacrimal from being excluded from the orbit (16-0) to narrowly contacting the orbit (16-1) to broadly contacting the orbit (16-2). We elected to order such characters because leaving all multistate characters unordered is not a neutral stance like equal weighting. Instead, doing so presents an alternative hypothesis for the evolution of these characters in which transformations between all states are equally likely (e.g., [Slowinski, 1993](#); [Wiens, 2001](#)). Previous studies have demonstrated that ordering these types of characters improves both resolution and accuracy (e.g., [Fröbisch & Schoch, 2009](#); [Grand et al., 2013](#); [Rineau et al., 2015](#); [Rineau, Zaragüeta i Bagils & Laurin, 2018](#)). Characters were left equally weighted.

Table 2:

Literature sources used for phylogenetic scoring of matrices.

Taxon	References
<i>Almasaurus habbazi</i>	Dutuit (1976)
<i>Anaschisma browni</i>	Lucas et al. (2016) , Gee, Parker & Marsh (2019) , Kufner & Gee (2021)
<i>Apachesaurus gregorii</i>	Hunt (1993) , Spielmann & Lucas (2012)
<i>Arganasaurus lyazidi</i>	Dutuit (1976) , Hunt (1993)
<i>Bothriceps australis</i>	Warren, Rozefelds & Bull (2011)
<i>Buettnererpeton bakeri</i>	Case (1931, 1932) ; this study
<i>Callistomordax kugleri</i>	Schoch (2008)
<i>Chinlestegophis jenkinsi</i>	Pardo, Small & Huttenlocker (2017)
<i>Compsocerops cosgriffi</i>	Sengupta (1995)
<i>Cyclotosaurus intermedius</i>	Sulej & Majer (2005)
<i>Dutuitosaurus ouazzoui</i>	Dutuit (1976)
<i>Eryops megacephalus</i>	Sawin (1941) , Moulton (1974) , Pawley & Warren (2006)

Taxon	References
<i>Eocyclotosaurus appetolatus</i>	Rinehart, Lucas & Schoch (2015) , Rinehart & Lucas (2016)
<i>Lydekkerina huxleyi</i>	Pawley & Warren (2005) , Hewison (2007, 2008) , Jeannot, Damiani & Rubidge (2006)
<i>Lyrocephaliscus euri</i>	Säve-Söderbergh (1936) , Mazin & Janvier (1983)
<i>Mastodonsaurus giganteus</i>	Schoch (1999)
<i>Metoposaurus algarvensis</i>	Brusatte et al. (2015)
<i>Metoposaurus diagnosticus</i>	Fraas (1889) , Sulej (2002)
<i>Metoposaurus krasiejowensis</i>	Sulej (2002, 2007)
<i>Quasicyclotosaurus campi</i>	Schoch (2000)
<i>Rhineceps nyasaensis</i>	Watson (1962)
<i>Rileymillerus cosgriffi</i>	Bolt & Chatterjee (2000)
<i>Sclerocephalus haeuseri</i>	Schoch & Witzmann (2009)
<i>Trematolestes hagdorni</i>	Schoch (2006)
<i>Trimerorhachis insignis</i>	Pawley (2007) , Milner & Schoch (2013)

DOI: [10.7717/peerj.14065/table-2](https://doi.org/10.7717/peerj.14065/table-2)

Note:

Taxa are listed in alphabetical order.

Parsimony analysis was performed in PAUP* 4.0a169 for MacIntosh ([Swofford, 2002](#)) using a heuristic search with 10,000 random addition sequence replicates, holding 10 trees per step, tree-bisection-and-connection (TBR), and with *Sclerocephalus haeuseri* as the operational outgroup. PAUP* was set to differentiate polymorphisms and partial uncertainty. We tested the matrix with select multistate characters ordered and with all multistate characters unordered. All other parameters were left as the program defaults (*e.g.*, gap states treated as missing data in PAUP*). Bremer decay index was calculated by progressively searching for trees of one step longer and comparing the strict consensus topologies. Bootstrapping was performed with 100,000 fast stepwise addition replicates.

The Bayesian analysis was performed in MrBayes 3.6.2 ([Huelsenbeck & Ronquist, 2001](#); [Ronquist & Huelsenbeck, 2003](#)) with a gamma distribution of rates allowed to vary over 5,000,000 iterations in four simultaneous runs with the first 20% of trees discarded as burn-in. The average standard deviation of split frequencies (ASDSF) between runs was evaluated every 5,000 iterations; convergence was considered to have been achieved when the ASDSF stably dropped below 0.01.

We also sought to investigate possible explanations for the stark differences between topologies recovered by previous studies. Therefore, in addition to our own analysis, we also reassessed the original matrix of [Buffa, Jalil & Steyer \(2019\)](#) and identified a number of scores that should be changed or corrected ([Appendix 3](#)). We then reanalyzed this matrix (NEXUS file appended as [Appendix 4](#)), as well as the original matrix with certain characters ordered ([Appendix 3](#)); the original analysis left all characters as unordered, in contrast to our approach with our own matrix. We also assessed both Bremer decay indices and bootstrap support; only the former was done originally. This part of our study is not meant as a targeted criticism of that particular matrix but rather is intended to address the discrepancies between topologies of that study and that employed by the first author of this study ([Gee, Parker & Marsh, 2019](#)) as the two previous studies that used discrete characters. The same parameters were followed as listed by Buffa, Jalil & Steyer (*e.g.*, simple heuristic search in PAUP* with TBR (reconnection limit = 8) and equal weighting of characters); any unlisted parameters (*e.g.*, polymorphisms treated as ‘unknown’) utilized defaults of the program. Bootstrapping was done with 10,000 replicates and a simple heuristic search. All MPTs from parsimony analyses are included in the Supplemental Information as [Appendix 5](#).

Nomenclatural acts

The electronic version of this article in Portable Document Format (PDF) will represent a published work according to the International Commission on Zoological Nomenclature (ICZN), and hence the new names contained in the electronic version are effectively published under that Code from the electronic edition alone. This published work and the nomenclatural acts it contains have been registered in ZooBank, the online registration system for the ICZN. The ZooBank LSIDs (Life Science Identifiers) can be resolved and the associated information viewed through any standard web browser by appending the LSID to the prefix <http://zoobank.org/>. The LSID for this publication is: urn:lsid:zoobank.org:pub:32E58BF1-B343-4657-91E8-F324D76A7B41. The online version of this work is archived and available from the following digital repositories: PeerJ, PubMed Central SCIE and CLOCKSS.

Systematic Paleontology & Description.

TEMNOSPONDYLI [von Zittel, 1887–1890](#) *sensu* [Schoch, 2013](#)

STEREOSPONDYLI [von Zittel, 1887–1890](#) *sensu* [Yates & Warren, 2000](#)

TREMATOSAUROIDEA [Säve-Söderbergh, 1935](#) *sensu* [Schoch, 2013](#)

METOPOSAURIDAE [Watson, 1919](#) *sensu* [Buffa, Jalil & Steyer, 2019](#)

Buettnererpeton gen. nov.

Diagnosis.—as for the species.

Etymology.—The original name given by [Case \(1922\)](#), *Buettneria*, honored William H. Buettner, a preparator who worked extensively with Case at the UMMP for 40 years. A brief obituary of Mr. Buettner can be found in a publicly accessible University of Michigan report published the year following his death ([University of](#)

[Michigan, 1957](#)). This name remained in usage until 2007, when [Mueller \(2007\)](#) noted that this genus name was already preoccupied by an extant African bush cricket. The type species of *Buettneria*, *B. perfecta*, was then placed within *Koskinonodon*, a genus erected by [Branson & Mehl \(1929\)](#), and was most recently placed within *Anaschisma* [Branson, 1905](#) by [Gee, Parker & Marsh \(2019\)](#). The new proposed genus name for the former *Buettneria bakeri* is *Buettnererpeton*, an available derivation from Mr. Buettner's name that preserves Case's original honoring of his colleague and that is combined with the Greek suffix '-herpeton,' a commonly used nomenclatural term for extinct 'reptiles' and 'amphibians.'

Buettnererpeton bakeri comb. nov.

Buettneria bakeri [Case, 1931](#)

Buettneria bakeri [Romer, 1947](#)

Eupelor fraasi jonesi (in part) [Colbert & Imbrie, 1956](#)

Metoposaurus fraasi jonesi (in part) [Roychowdhury, 1965](#)

Metoposaurus bakeri [Hunt, 1993](#)

Metoposaurus bakeri [Schoch & Milner, 2000](#)

Buettneria bakeri [Sulej, 2002](#)

Koskinonodon bakeri [Brusatte et al., 2015](#)

Holotype.—UMMP 13055, complete skull

Referred specimens.—See [Table 1](#) and the Materials and Methods section for complete listing.

Diagnosis.—The species is diagnosed by the following differential diagnosis. Differentiated from *Anaschisma browni*, *Arganasaurus azerouali*, the three species of *Metoposaurus* (*M. algarvensis*, *M. diagnosticus*, *M. krasiejowensis*), and *Panthasaurus maleriensis* by the exclusion of the lacrimal from the orbital margin. Further differentiated from *An. browni* by: (1) less developed alary process of the premaxilla (suture with the nasal is more shallowly inclined); (2) anterior margin of orbits posterior to anterior margin of interpterygoid vacuities; (3) splenial not contacting the symphyseal surface; (4) presence of sensory groove along posterior region of clavicle. Further differentiated from *P. maleriensis* by: (1) short lacrimal, resulting in maxilla-prefrontal contact; (2) jugal terminating at or just anterior to the anterior margin of the orbits (rather than well anterior to this level). Differentiated from *Arganasaurus* (*A. azerouali*, *A. lyazidi*) by: (1) proportionately short lacrimal; (2) squamosal more pentagonal than triangular in dorsal view. Further differentiated from *Ar. lyazidi* by lacrimal excluded from naris and from *Ar. azerouali* by: (1) maxilla excluded from orbital margin; (2) lacrimal excluded from orbital margin; (3) presence of elongate grooves in growth zones on skull roof. Differentiated from *Dutuitosaurus ouazzoui* by: (1) maxilla excluded from orbital margin; (2) intercentra not elongate. Differentiated from *Apachesaurus gregorii* by: (1) relatively long lacrimal; (2) proportionately deep otic notch framed by a prominent tabular horn.

Description.

The following description is divided by skeletal region. The cranial description follows the structure of [Sulej \(2007\)](#) in which elements are described individually in a more or less anteroposterior order. Each element's description is further

subdivided into two sections: (1) the description of the element in the holotype; and (2) the description of the element based on other specimens. The second section includes comparisons among specimens to capture intraspecific variation. A comparative table of cranial measurements is provided in [Table 3](#) and a composite cranial reconstruction is provided in [Fig. 5](#). Comparisons with the original interpretations of [Case \(1931, 1932\)](#) are noted where appropriate, and it should be noted that there are some slight discrepancies between the illustrated anatomy of those two studies.

Table 3:

Comparative measurements of partial to complete skulls of *Buettnererpeton bakeri*.

Specimen	SL	SW	PrO	PoO	PrP	PoP	EW
UMMP 13055	29.1	21.8	9.4	15.7	23.7	4.8	4.7
UMMP 13820	30.5	24.0	9.5	16.5	24.3	5.6	6.0
UMMP 13822	24.0*	22.8*	7.5	13.2*	18.5*	4.0*	6.0*
UMMP 13823	29.6*	25.4	10.0	15.2*	?	?	5.5
UMMP 13956	?	?	?	?	?	?	4.3
UMMP 14154	?	?	?	?	?	6.1	5.7
YPM VPPU 021742	19.3	17.3	7	9.5	14.9	4.0	?
MCZ 1054	28.7	22.5*	9.1	15.1	22.7	5.0	?

DOI: [10.7717/peerj.14065/table-3](https://doi.org/10.7717/peerj.14065/table-3)

Note:

Asterisk (*) denotes an estimate; all estimates are made only for relatively complete specimens. Abbreviations for measurements: EW, maximum width across exoccipital condyles; PrO, preorbital length; PrP, prepineal length; PoO, postorbital length; PoP, postpineal length; SL, midline skull length from premaxilla to postparietals; SW, maximum skull width. All measurements are in centimeters.

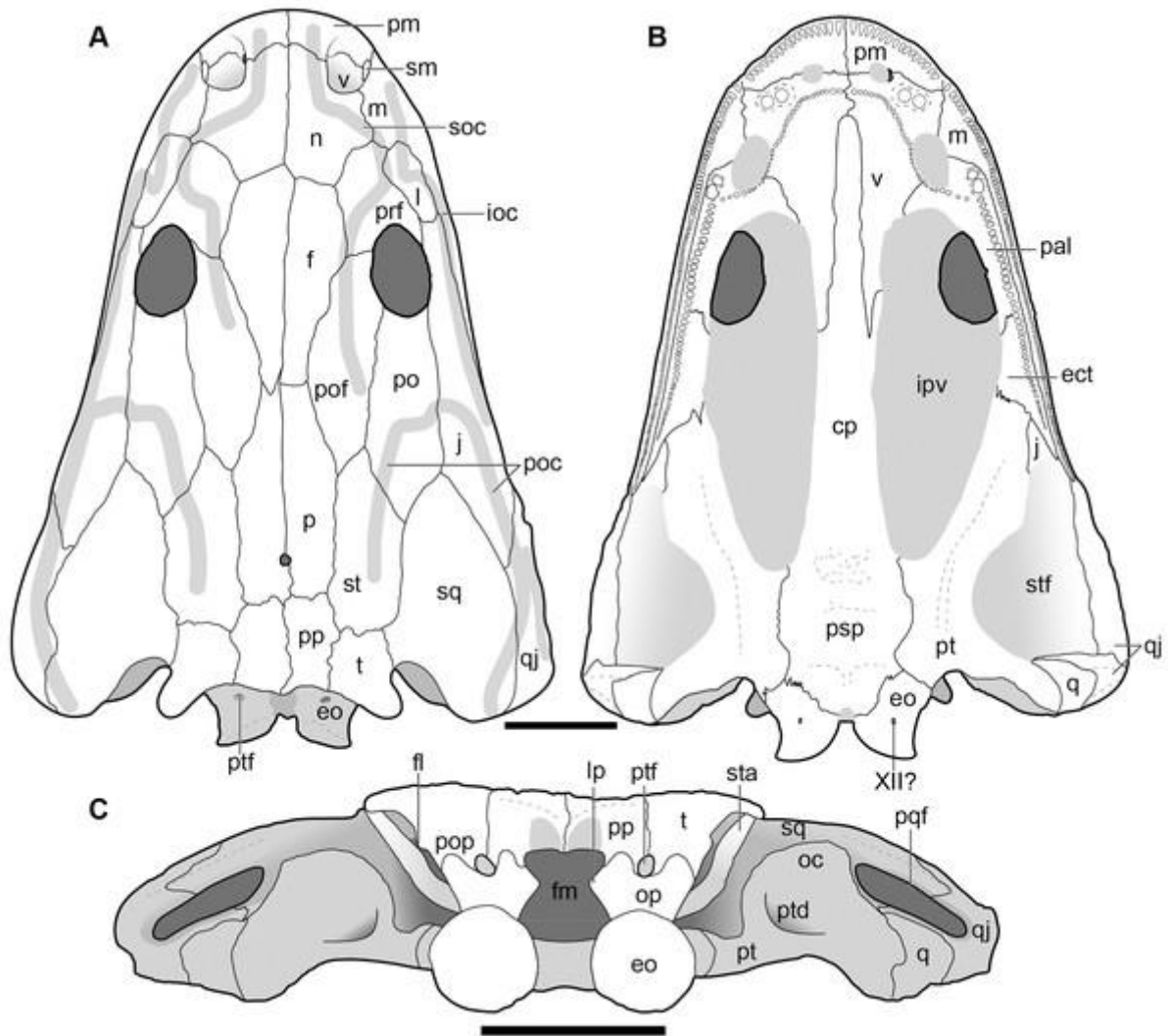


Figure 5: New composite reconstruction of the skull of *Buettnererpeton bakeri*.

(A) Dorsal view; (B) ventral view; (C) occipital view. Fine dashed lines represent topographic details like ridges. Abbreviations: eo, exoccipital; f, frontal; j, jugal; l, lacrimal; m, maxilla; n, nasal; p, parietal; pm, premaxilla; po, postorbital; pof, postfrontal; pp, postparietal; prf, prefrontal; qj, quadratojugal; sq, squamosal; st, supratemporal; t, tabular. Scale bars equal to 5 cm.

[Download full-size image](#)

DOI: [10.7717/peerj.14065/fig-5](https://doi.org/10.7717/peerj.14065/fig-5)

Cranial material.

Overview of cranial material.—The holotype (UMMP 13055) is a complete skull with minimal taphonomic distortion (Figs. 6–8). A number of areas have been infilled with plaster to reconstruct and to stabilize the original fossil material. This is most prominent on the right side of the skull where nearly the entire lateral margin has been reconstructed (Figs. 6 and 7). Both of the temporal regions are damaged posteriorly (squamosal, quadratojugal) and were not reconstructed. Many of the sutures have slightly separated and been infilled with matrix such that their demarcations are accentuated. The orbit is a large oval that is positioned fully posterior to the anterior margin of the interpterygoid vacuity in palatal view (Fig. 7), contrary to *Anaschisma browni* (e.g., Lucas et al., 2016; Gee, Parker & Marsh,

2019; Kufner & Gee, 2021). The naris is slightly smaller and generally circular, although the perfectly circular reconstruction of the right naris is probably more cosmetic than it is accurate.

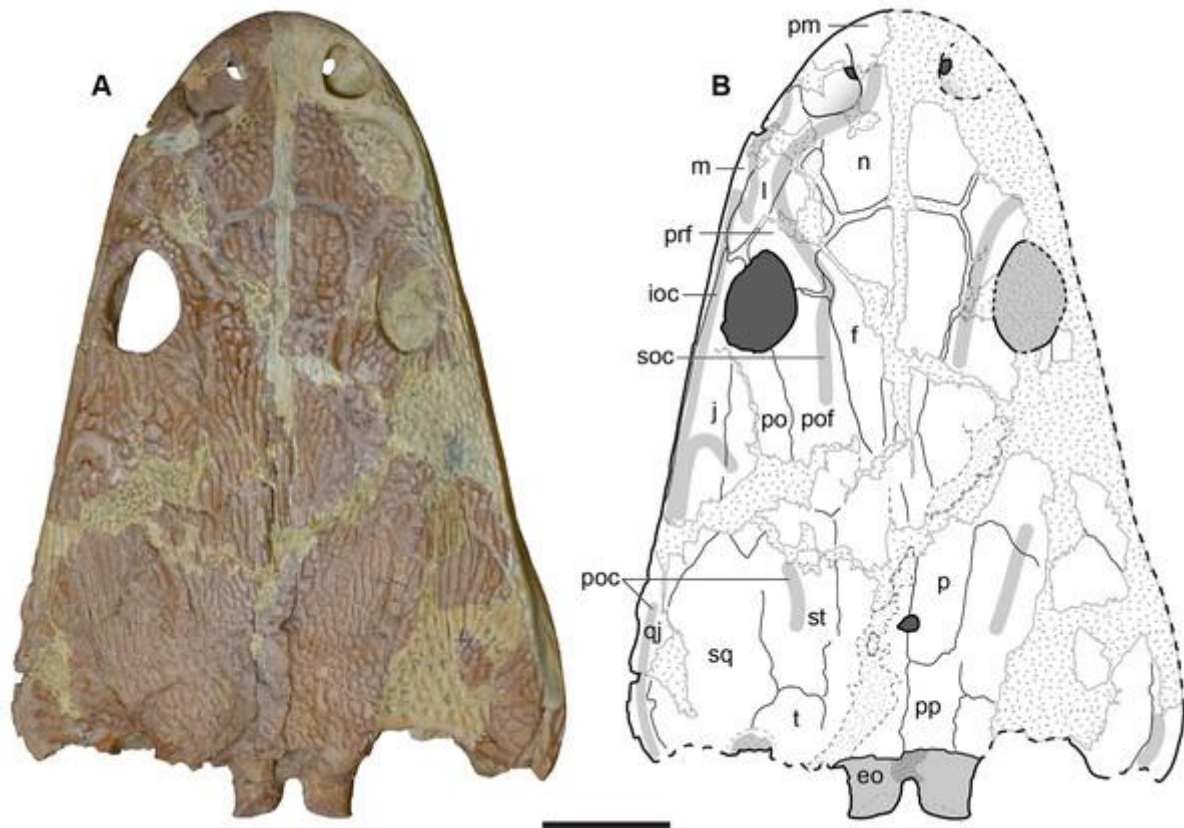


Figure 6: Dorsal view of the holotype skull of *Buettnererpeton bakeri*, UMMP 13055. (A) Photograph; (B) interpretive line drawing. Hatching represents plaster reconstruction; stippling represents residual matrix; dashed gray lines represent raised contours/ridges. Abbreviations: f, frontal; ioc, infraorbital canal; j, jugal; l, lacrimal; m, maxilla; n, nasal; p, parietal; pm, premaxilla; po, postorbital; poc, postorbital canal; pof, postfrontal; pp, postparietal; prf, prefrontal; qj, quadratojugal; soc, supraorbital canal; sq, squamosal; st, supratemporal; t, tabular. Scale bar equal to 5 cm.

[Download full-size image](#)

DOI: [10.7717/peerj.14065/fig-6](https://doi.org/10.7717/peerj.14065/fig-6)

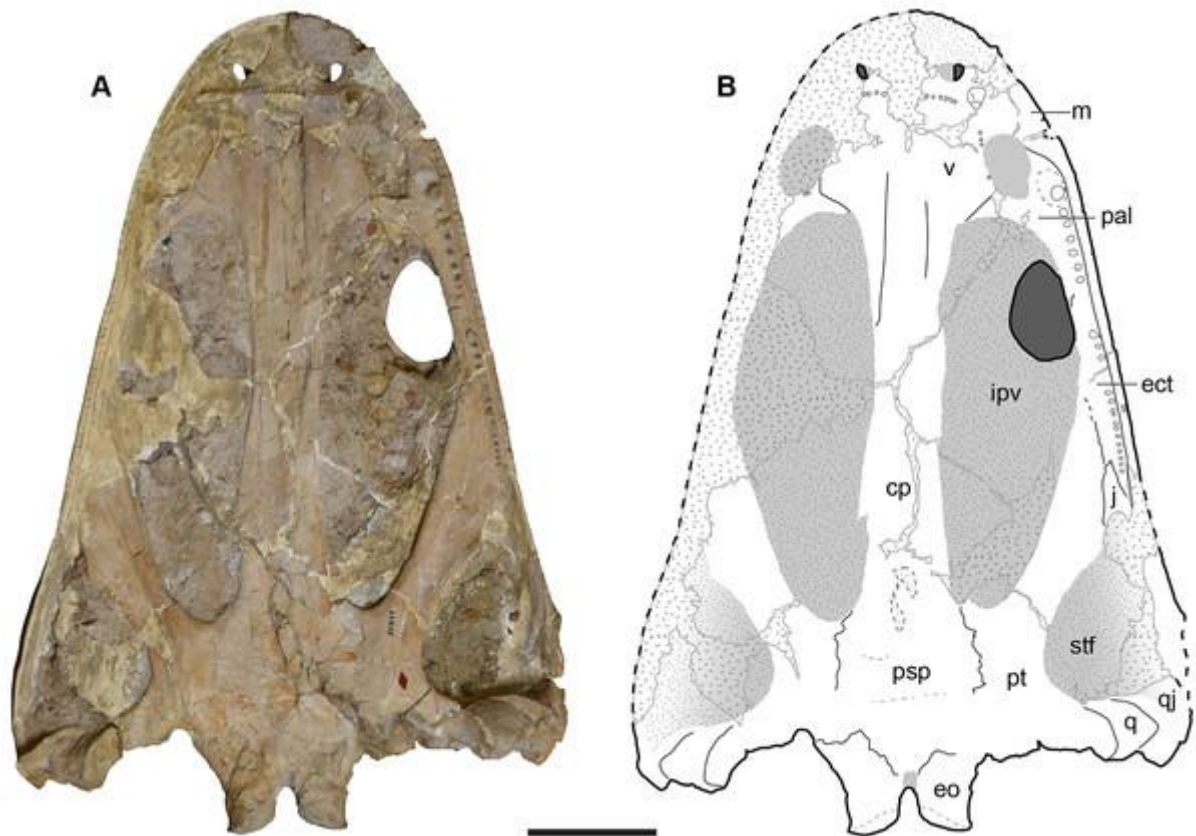


Figure 7: Ventral view of the holotype skull of *Buettnererpeton bakeri*, UMMP 13055.

(A) Photograph; (B) interpretive line drawing. Hatching represents plaster reconstruction; stippling represents residual matrix; dashed gray lines represent raised contours/ridges.

Abbreviations: cp, cultriform process; ect, ectopterygoid; eo, exoccipital; ipv, interpterygoid vacuity; m, maxilla; pal, palatine; psp, parasphenoid; pt, pterygoid; q, quadrate; qj, quadratojugal; stj, subtemporal fenestra; v, vomer. Scale bar equal to 5 cm.

[Download full-size image](#)

DOI: [10.7717/peerj.14065/fig-7](https://doi.org/10.7717/peerj.14065/fig-7)

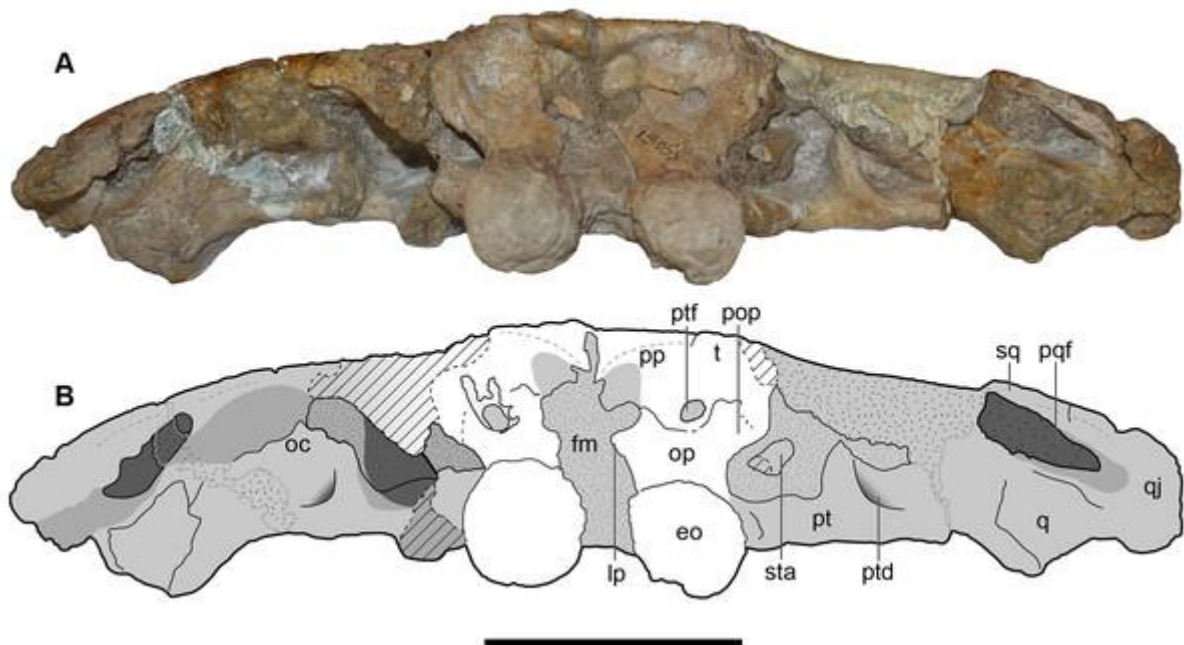


Figure 8: Occipital view of the holotype skull of *Buettnererpeton bakeri*, UMMP 13055.

(A) Photograph; (B) interpretive line drawing. Hatching represents plaster reconstruction; stippling represents residual matrix; dashed gray lines represent raised contours/ridges; diagonal lines represent broken surfaces. Abbreviations: eo, exoccipital; fl, flange on the parotic process of the tabular; oc, oblique crest of the pterygoid; op, occipital pillar; pop, parotic process of the tabular; pp, postparietal; pqf, paraquadrato foramen; pt, pterygoid; ptd, pterygoid depression; ptf, posttemporal foramen; q, quadrate; qj, quadratojugal; sq, squamosal; sta, stapes; t, tabular. Scale bar equal to 5 cm.

[Download full-size image](#)

DOI: [10.7717/peerj.14065/fig-8](https://doi.org/10.7717/peerj.14065/fig-8)

UMMP 13820 is a complete skull figured in dorsal, palatal, and occipital views (Figs. 9–11). The roofing sutures are extremely well-defined, providing a better guide to the full cranial osteology than the holotype, due to many sutures having been infilled by sediments, although they have not separated to the degree observed in the holotype (Figs. 9A and 9B).

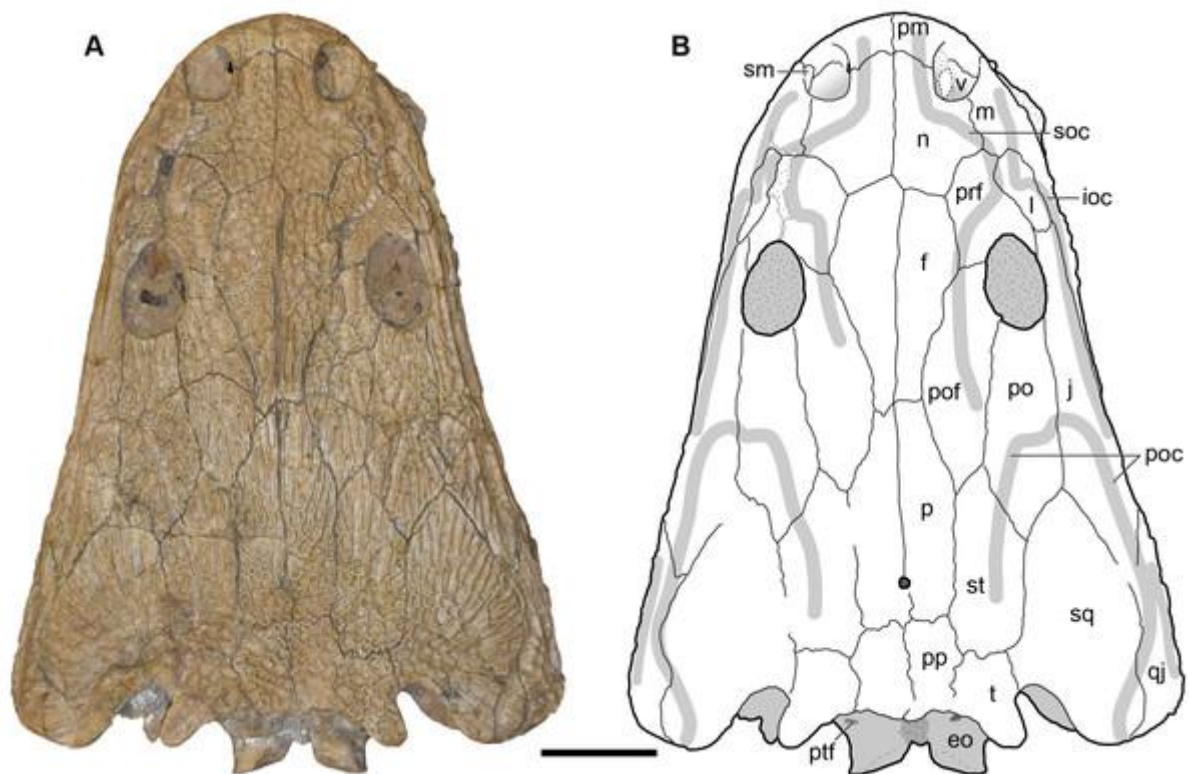


Figure 9: Dorsal view of a referred skull of *Buettnererpeton bakeri*, UMMP 13820.

(A) Photograph; (B) interpretive line drawing. Stippling represents residual matrix; dashed gray lines represent raised contours/ridges. Abbreviations: eo, exoccipital; f, frontal; ioc, infraorbital canal; j, jugal; l, lacrimal; m, maxilla; n, nasal; p, parietal; pm, premaxilla; po, postorbital; poc, postorbital canal; pof, postfrontal; pp, postparietal; prf, prefrontal; ptf, posttemporal foramen; qj, quadratojugal; sm, septomaxilla; soc, supraorbital canal; sq, squamosal; st, supratemporal; t, tabular; v, vomer;. Scale bar equal to 5 cm.

[Download full-size image](#)

DOI: [10.7717/peerj.14065/fig-9](https://doi.org/10.7717/peerj.14065/fig-9)

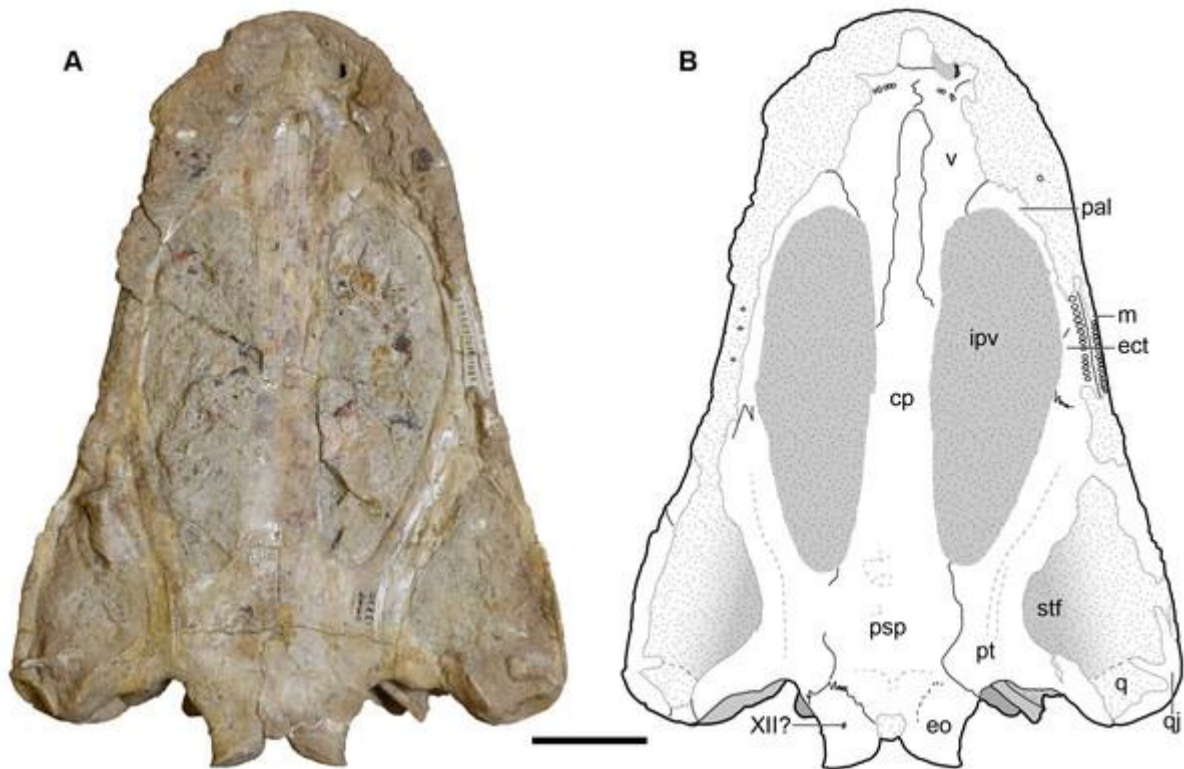


Figure 10: Ventral view of a referred skull of *Buettnererpeton bakeri*, UMMP 13820.

(A) Photograph; (B) interpretive line drawing. Stippling represents residual matrix; dashed gray lines represent raised contours/ridges. Abbreviations: cp, cultriform process; ect, ectopterygoid; eo, exoccipital; ipv, interpterygoid vacuity; j, jugal; m, maxilla; pal, palatine; psp, parasphenoid; pt, pterygoid; ptf, posttemporal foramen; q, quadrate; qj, quadratojugal; stj, subtemporal fenestra; v, vomer; XII?, foramen for cranial nerve XII?. Scale bar equal to 5 cm.

[Download full-size image](#)

DOI: [10.7717/peerj.14065/fig-10](https://doi.org/10.7717/peerj.14065/fig-10)

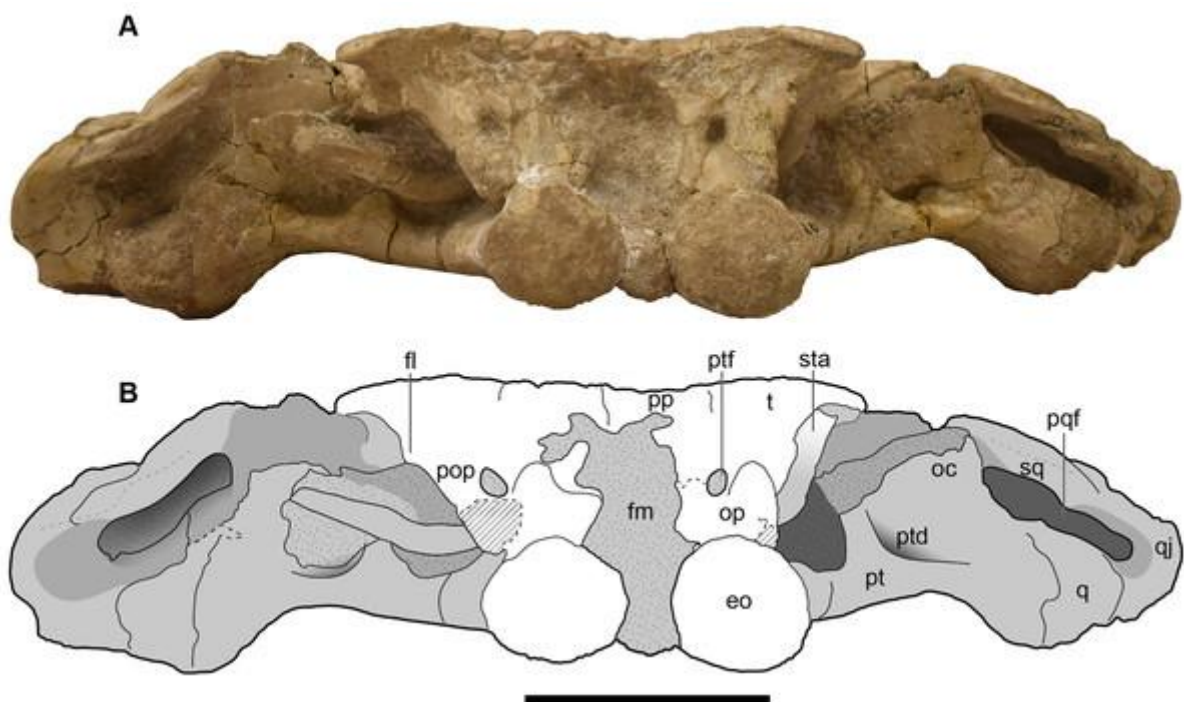


Figure 11: Occipital view of a referred skull of *Buettnererpeton bakeri*, UMMP 13820.

(A) Photograph in occipital view; (B) interpretive line drawing of the same. Stippling represents residual matrix; dashed gray lines represent raised contours/ridges; diagonal lines represent broken surfaces. Abbreviations: eo, exoccipital; fl, flange on the parotic process of the tabular; fm, foramen magnum; oc, oblique crest of the pterygoid; op, occipital pillar; pop, parotic process of the tabular; pp, postparietal; pqf, paraquadrangle foramen; pt, pterygoid; ptd, pterygoid depression; ptf, posttemporal foramen; q, quadrate; qj, quadratojugal; sq, squamosal; sta, stapes; t, tabular. Scale bar equal to 5 cm.

[Download full-size image](#)

DOI: [10.7717/peerj.14065/fig-11](https://doi.org/10.7717/peerj.14065/fig-11)

UMMP 13822 is a half skull split nearly perfectly down the midline, with the left side preserved (Figs. 12–15). Like in the holotype, the orbits are entirely exposed through the interpterygoid vacuity and are set posterior to the anterior margin of the vacuity (Figs. 13A and 13B).

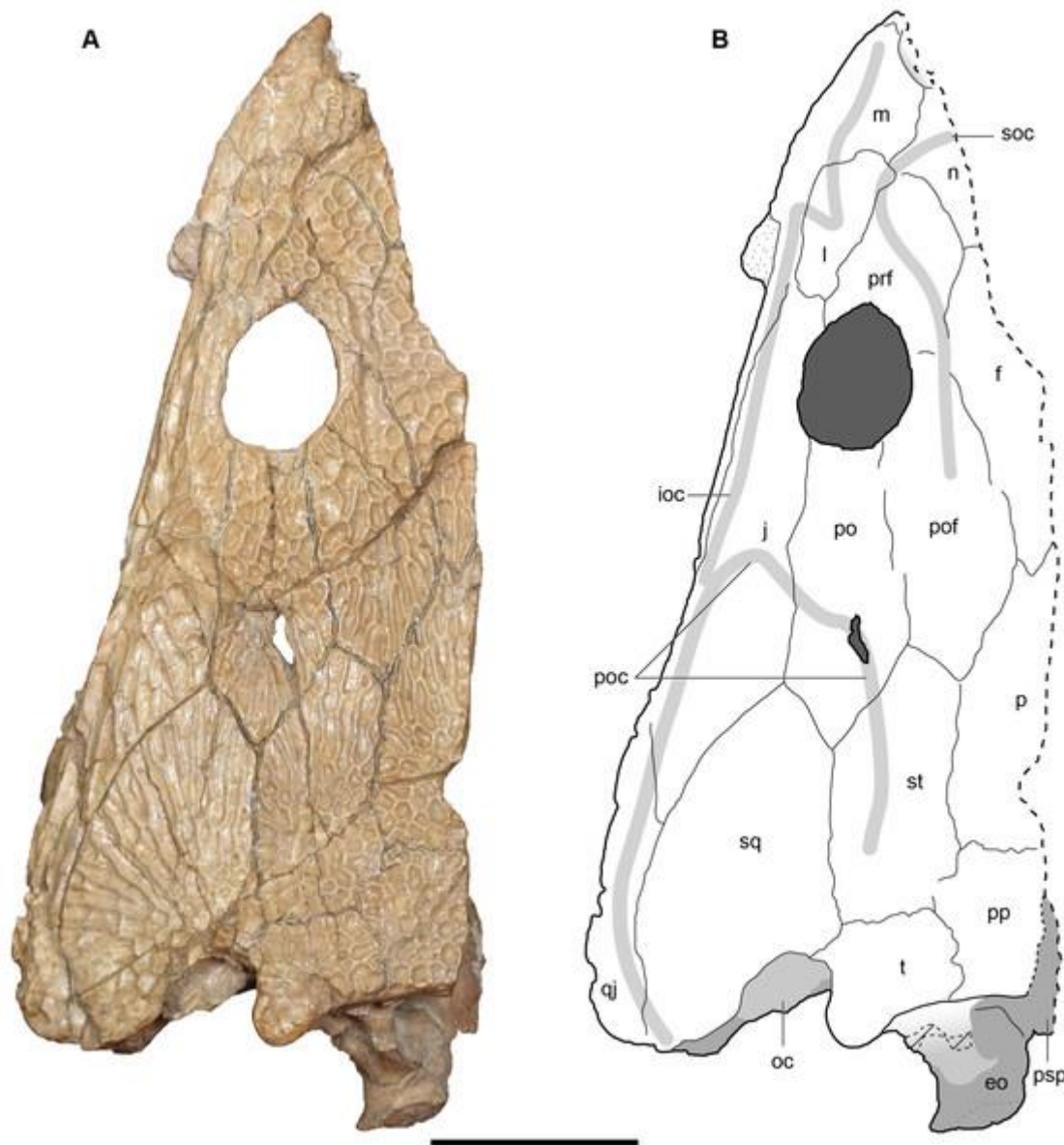


Figure 12: Dorsal view of a referred partial left skull of *Buettnererpeton bakeri*, UMMP 13822.

(A) Photograph; (B) interpretive line drawing. Stippling represents residual matrix; dashed gray lines represent raised contours/ridges; diagonal lines represent broken surfaces. Abbreviations: eo, exoccipital; f, frontal; ioc, infraorbital canal; j, jugal; l, lacrimal; m, maxilla; n, nasal; oc, oblique crest of the pterygoid; p, parietal; po, postorbital; poc, postorbital canal; pof, postfrontal; pp, postparietal; prf, prefrontal; psp, parasphenoid; qj, quadratojugal; soc, supraorbital canal; sq, squamosal; st, supratemporal; t, tabular. Scale bar equal to 5 cm.

[Download full-size image](#)

DOI: [10.7717/peerj.14065/fig-12](https://doi.org/10.7717/peerj.14065/fig-12)

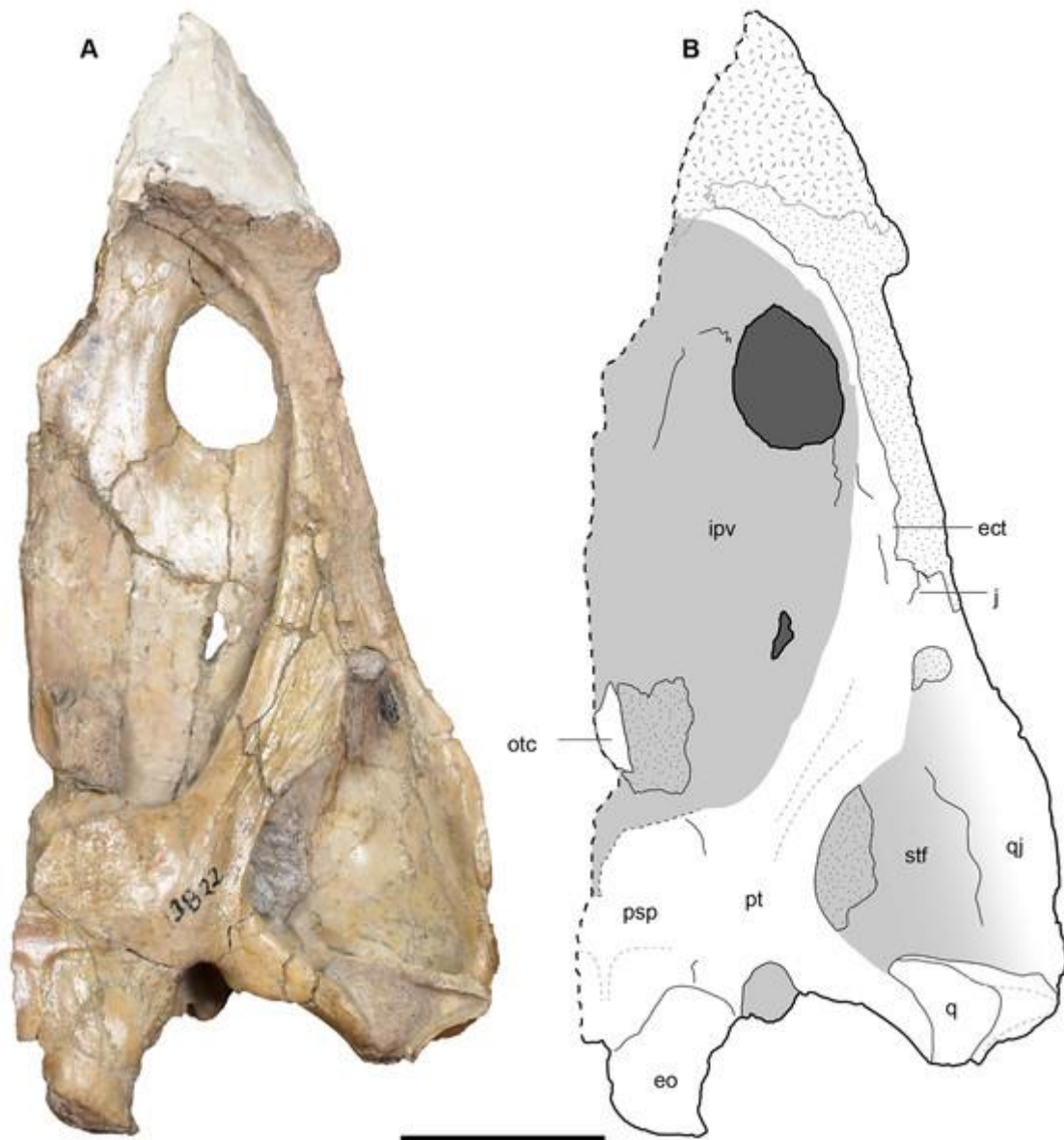


Figure 13: Ventral view of a referred partial left skull of *Buettnerpeton bakeri*, UMMP 13822.

(A) Photograph; (B) interpretive line drawing. Stippling represents residual matrix; dashed gray lines represent raised contours/ridges; diagonal lines represent broken surfaces. Abbreviations: ect, ectopterygoid; eo, exoccipital; ipv, interpterygoid vacuity; j, jugal; otc, orbitotemporal crest; psp, parasphenoid; pt, pterygoid; q, quadrate; qj, quadratojugal; stf, subtemporal fenestra. Scale bar equal to 5 cm.

[Download full-size image](#)

DOI: [10.7717/peerj.14065/fig-13](https://doi.org/10.7717/peerj.14065/fig-13)

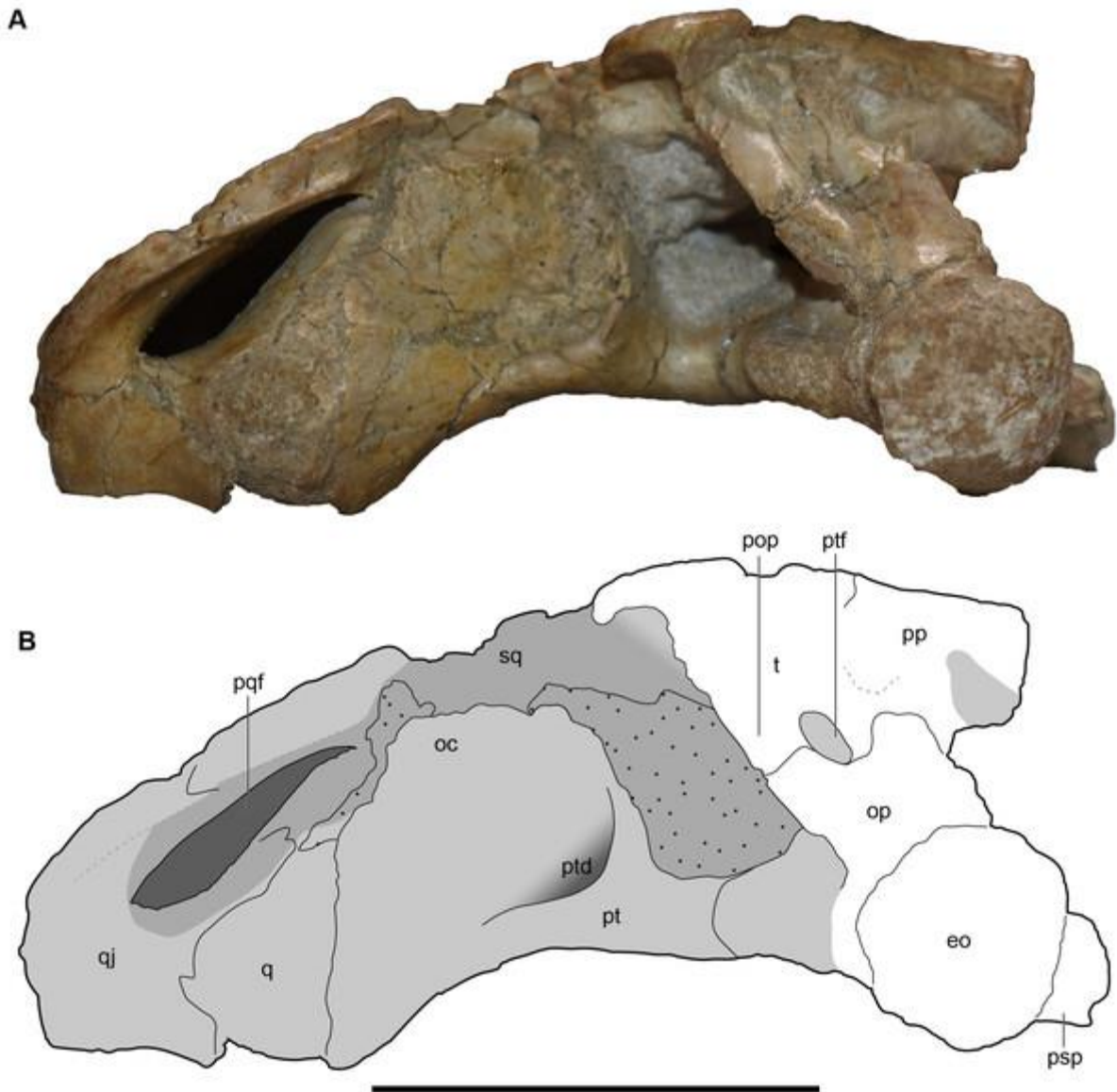


Figure 14: Occipital view of a referred partial left skull of *Buettnererpeton bakeri*, UMMP 13822.

(A) Photograph; (B) interpretive line drawing. Stippling represents residual matrix; dashed gray lines represent raised contours/ridges. Abbreviations: eo, exoccipital; oc, oblique crest of the pterygoid; op, occipital pillar; pop, parotic process of the tabular; pp, postparietal; pqf, paraquadrate foramen; psp, parasphenoid; pt, pterygoid; ptd, pterygoid depression; ptf, posttemporal foramen; q, quadrate; qj, quadratojugal; sq, squamosal; t, tabular. Scale bar equal to 5 cm.

[Download full-size image](#)

DOI: [10.7717/peerj.14065/fig-14](https://doi.org/10.7717/peerj.14065/fig-14)



Figure 15: Lateral and medial views of a referred partial left skull of *Buettnererpeton bakeri*, UMMP 13822.

(A) Photograph in left lateral view; (B) photograph in medial view. Abbreviation: epi, epipterygoid. 'Clay' indicates a small amount of putty that was used to position the skull for photography. Scale bar equal to 5 cm.

[Download full-size image](#)

DOI: [10.7717/peerj.14065/fig-15](https://doi.org/10.7717/peerj.14065/fig-15)

UMMP 13823 is a complete skull, but the dorsal surface has been fully embedded in plaster, probably as a stabilizer given the prominent fracturing on the exposed surfaces, and it was never previously figured or described in this profile ([Fig. 16](#)).

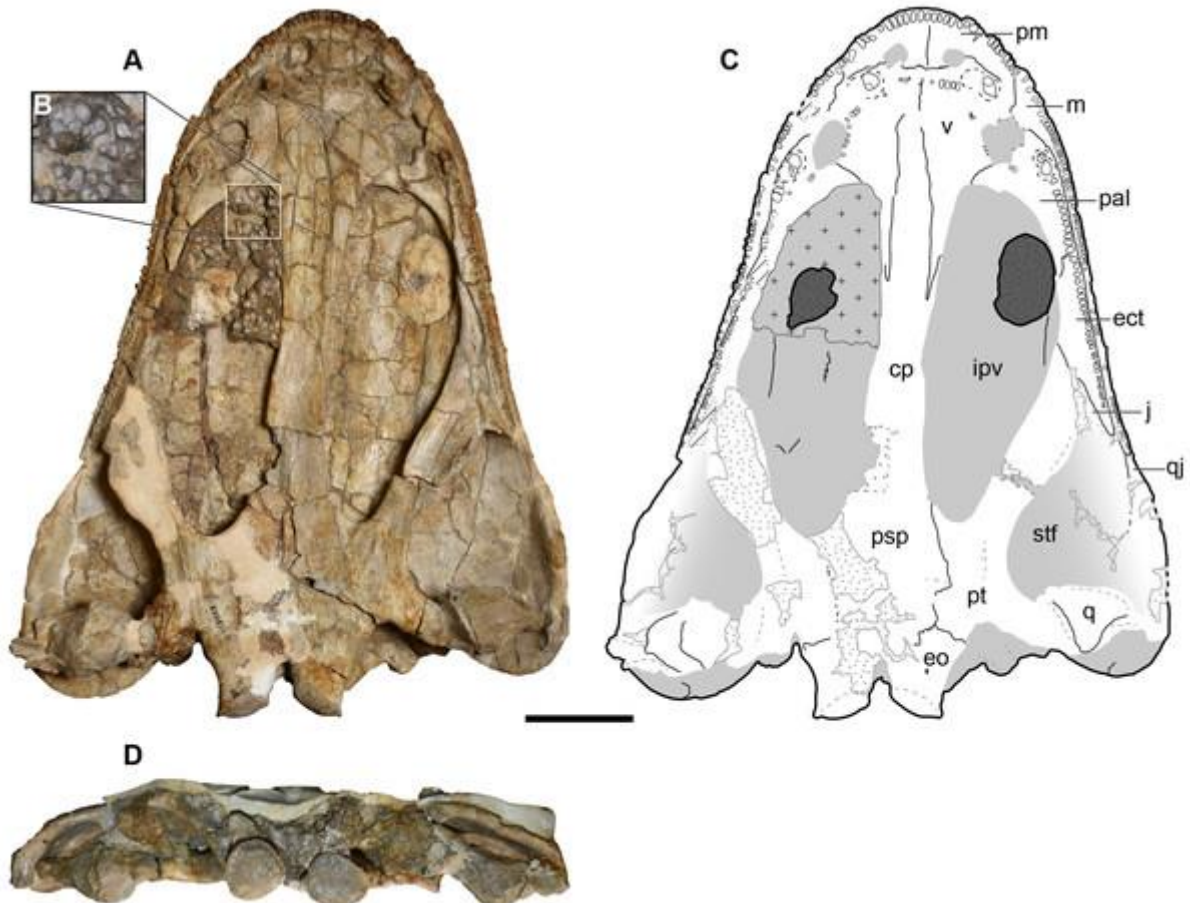


Figure 16: Ventral and occipital views of a referred partial left skull of *Buettnererpeton bakeri*, UMMP 13823.

(A) Photograph in ventral view; (B) inset showing close-up image of the palatal plates in the interpterygoid vacuities; (C) interpretive line drawing in ventral view; (D) photograph in occipital view. Abbreviations: cp, cultriform process; ect, ectopterygoid; eo, exoccipital; ipv, interpterygoid vacuity; j, jugal; m, maxilla; pm, premaxilla; psp, parasphenoid; pt, pterygoid; q, quadrate; qj, quadratojugal; stf, subtemporal fenestra; v, vomer. Scale bar equal to 5 cm.

[Download full-size image](#)

DOI: [10.7717/peerj.14065/fig-16](https://doi.org/10.7717/peerj.14065/fig-16)

UMMP 13956 is an occiput, preserved as far anteriorly as the anterior margin of the squamosal and with two additional fragments of the skull roof of an uncertain position ([Fig. 17](#)). As a nomenclatural note, the physical specimen bears the number '13596,' which is what this specimen was published as by [Case \(1932\)](#), but the specimen card bears the number '13956.' The first number is not registered in the UMMP database as belonging to any specimen, so the official catalogue number is considered to be UMMP 13956 (A. Rountrey, 2019, personal communication). It is slightly more laterally extensive than UMMP 14154 (see further below), at least the portion that is exposed dorsally. The dorsal surface has mostly been left unprepared such that sutures are not well-defined, although the same ornamentation found in the postorbital skull of other specimens is discernible ([Fig. 17A](#)). The conglomeratic matrix is also present within the internal spaces of the skull such that when viewed anteriorly, the broken exposure confers no additional information. The two fragments of the skull roof do not fit with the larger block, but both show a mixture of circular pits and more elongate grooves. Assuming that there was some rationale for associating them with the larger cranial block, they would most likely be part of the postorbital or the postfrontal.

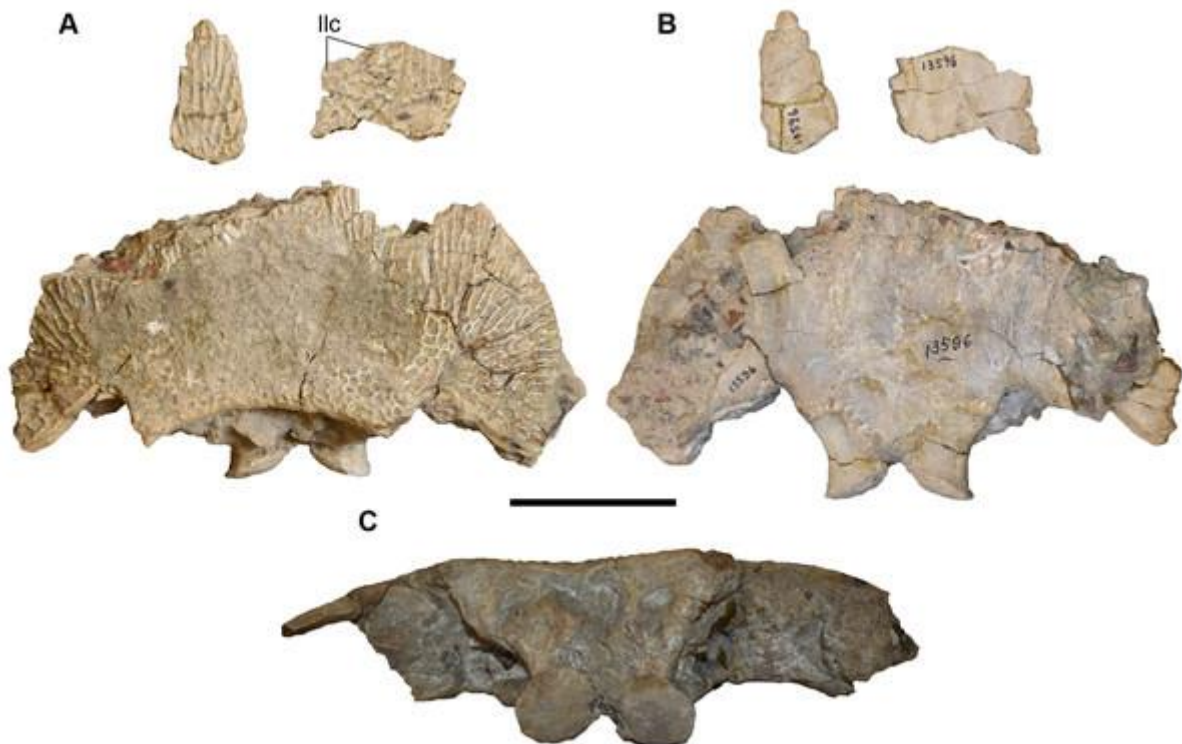


Figure 17: Photographs of a referred posterior skull of *Buettnererpeton bakeri*, UMMP 13956.

(A) Dorsal view; (B) ventral view; (C) occipital view. Scale bar equal to 5 cm.

[Download full-size image](#)

DOI: [10.7717/peerj.14065/fig-17](https://doi.org/10.7717/peerj.14065/fig-17)

UMMP 14098 is a series of fragments from the posterior right side of the skull, without major articulated palatal or occipital elements and with the underside of the roofing elements mostly covered by matrix (Figs. 18–20). The largest fragment is a block of the posterior skull roof, with some of the matrix still present on the underside in addition to a dislodged stapes (Figs. 18A and 18B).

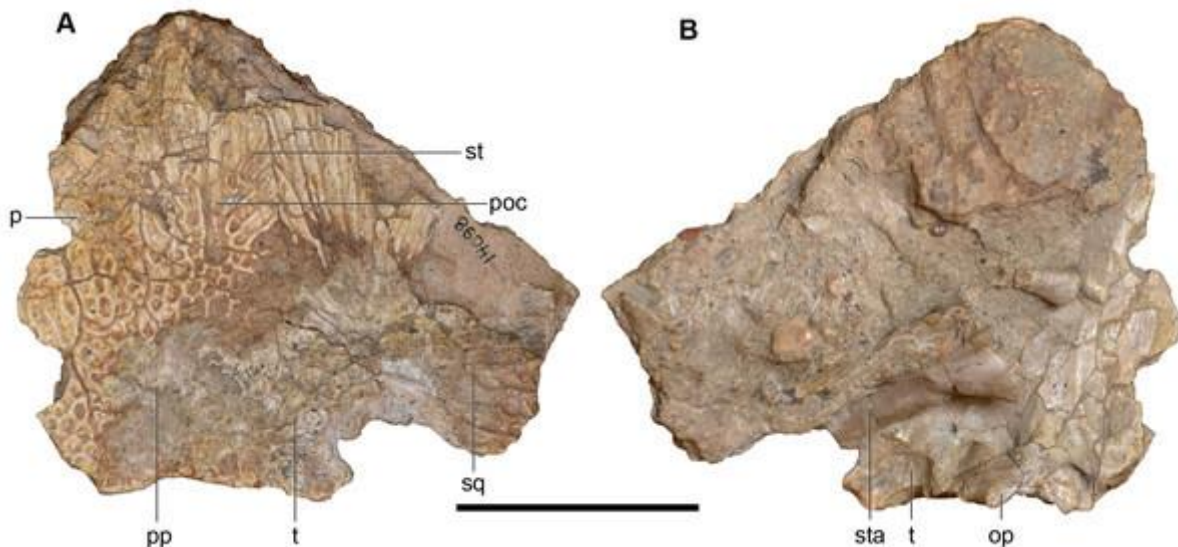


Figure 18: Photographs of the skull roof of a referred partial posterior right skull of *Buettnererpeton bakeri*, UMMP 14098.

(A) Photograph in dorsal view; (B) photograph in ventral view. Abbreviations: op, occipital pillar; p, parietal; poc, postorbital canal; pp, postparietal; sq, squamosal; st, supratemporal; sta, stapes; t, tabular. Scale bar equal to 5 cm.

[Download full-size image](#)

DOI: [10.7717/peerj.14065/fig-18](https://doi.org/10.7717/peerj.14065/fig-18)

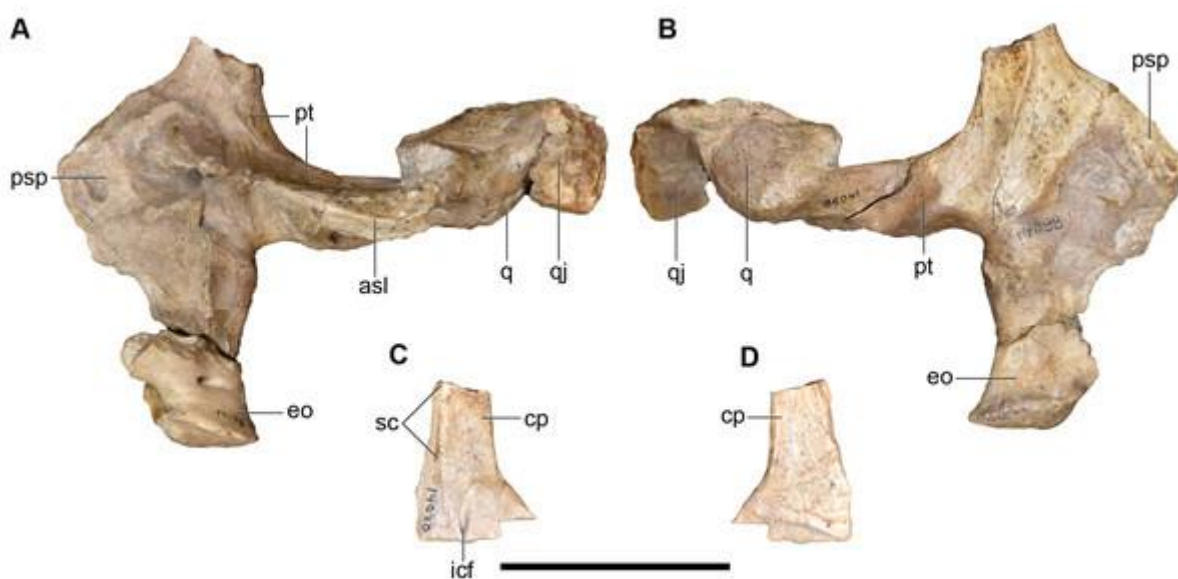


Figure 19: Photographs of the palate and occiput of a referred partial posterior right skull of *Buettnererpeton bakeri*, UMMP 14098.

(A) Palate and occiput in dorsal view; (B) palate and occiput in ventral view; (C) cultriform process in dorsal view; (D) cultriform process in ventral view. Abbreviations: asl, ascending lamina of the pterygoid; cp, cultriform process of the parasphenoid; eo, exoccipital; icf, internal carotid foramen; psp parasphenoid; pt, pterygoid; q, quadrate; qj, quadratojugal; sc, sphenethmoidal crest. Scale bar equal to 5 cm.

[Download full-size image](#)

DOI: [10.7717/peerj.14065/fig-19](https://doi.org/10.7717/peerj.14065/fig-19)

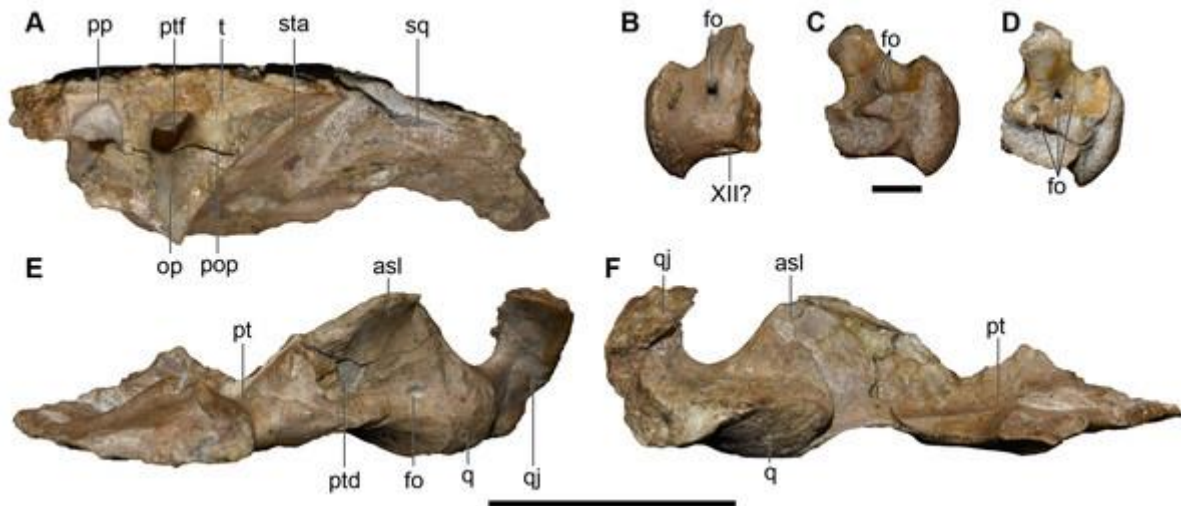


Figure 20: Photographs of the skull roof, palate, and occiput of a referred partial posterior right skull of *Buettnererpeton bakeri*, UMMP 14098.

(A) Skull roof in occipital view; (B) exoccipital in lateral view; (C) the same in medial view; (D) the same in oblique posterodorsal view; (E) palate with exoccipital removed in occipital view; (F) partial palate in anterior view. Abbreviations: asl, ascending lamina of the pterygoid; cp, cultriform process of the parasphenoid; fo, foramen; op, occipital pillar; pop, parotic process of the tabular; pp, postparietal; psp parasphenoid; pt, pterygoid; ptd, pterygoid depression; q, quadrate; qj, quadratojugal, ptf, posttemporal foramen; sq, squamosal; sta, stapes; t, tabular; XII?, foramen for cranial nerve XII?. All elements to same scale. Scale bars under (A, E and F) equal to 5 cm; scale bar under (B–D) equal to 1 cm.

[Download full-size image](#)

DOI: [10.7717/peerj.14065/fig-20](https://doi.org/10.7717/peerj.14065/fig-20)

UMMP 14154 is a partial occiput, including the posteromedial cranial and palatal elements (Figs. 21–23). The right side of the skull roof has been ventrally shifted such that the right median roofing elements lie about a centimeter below the complementary elements of the left side (Fig. 23). A second fragment of this specimen, embedded in plaster dorsally and without ventral expression of sutures, probably includes parts of the postorbital and the postfrontal as well; this fragment is not shown in dorsal view (Figs. 21A and 21B) because it could only be securely rearticulated with the other fragment for photography in ventral view (Figs. 22A and 22B). This was evidently an intentional break, as Case (1931:190) indicated that parts of the roof had been removed to expose the braincase, and the plaster was thus likely used to hold it together.

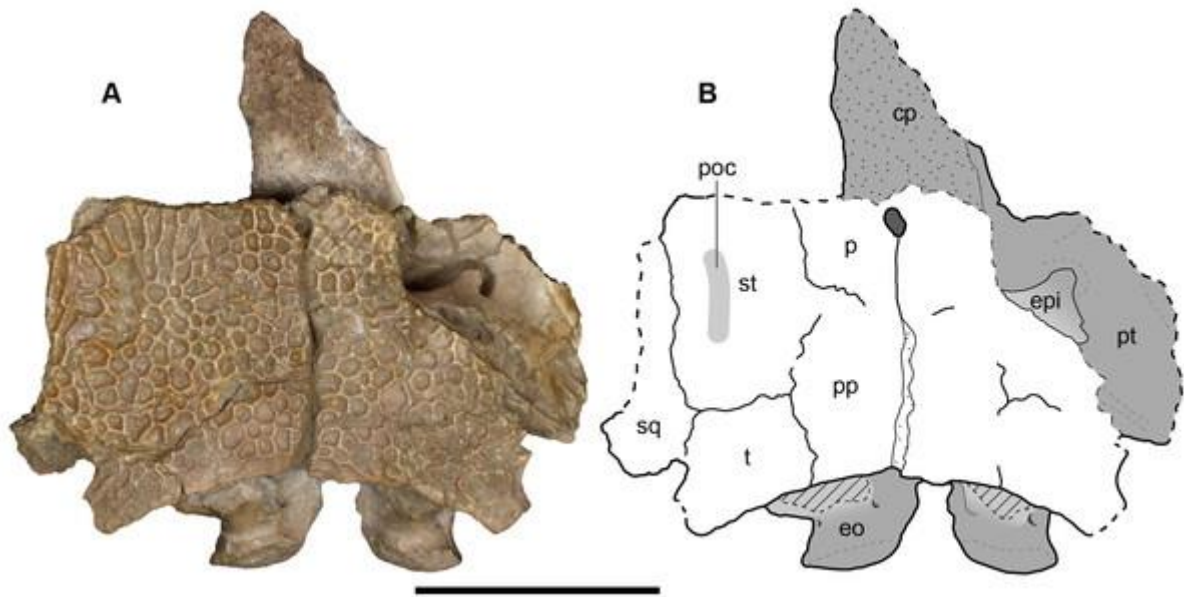


Figure 21: Dorsal view of a referred occiput and posterior skull roof of *Buettnererpeton bakeri*, UMMP 14154.

(A) Photograph; (B) interpretive line drawing. Abbreviations: cp, cultriform process; eo, exoccipital; epi, epipterygoid; p, parietal; poc, postorbital canal; pp, postparietal; psp, parasphenoid; pt, pterygoid; sq, squamosal; st, supratemporal; t, tabular. Scale bar equal to 5 cm.

[Download full-size image](#)

DOI: [10.7717/peerj.14065/fig-21](https://doi.org/10.7717/peerj.14065/fig-21)

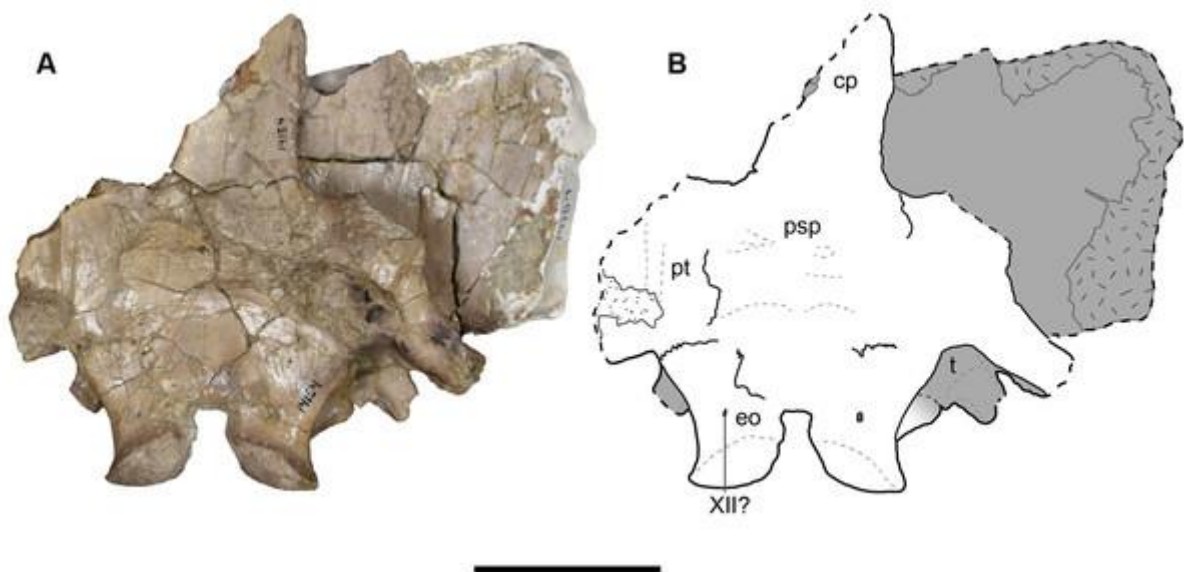


Figure 22: Ventral view of a referred occiput and posterior skull roof of *Buettnererpeton bakeri*, UMMP 14154.

(A) Photograph; (B) interpretive line. Abbreviations: cp, cultriform process; eo, exoccipital; psp, parasphenoid; pt, pterygoid; t, tabular; XII?, foramen for cranial nerve XII?. Scale bar equal to 5 cm.

[Download full-size image](#)

DOI: [10.7717/peerj.14065/fig-22](https://doi.org/10.7717/peerj.14065/fig-22)

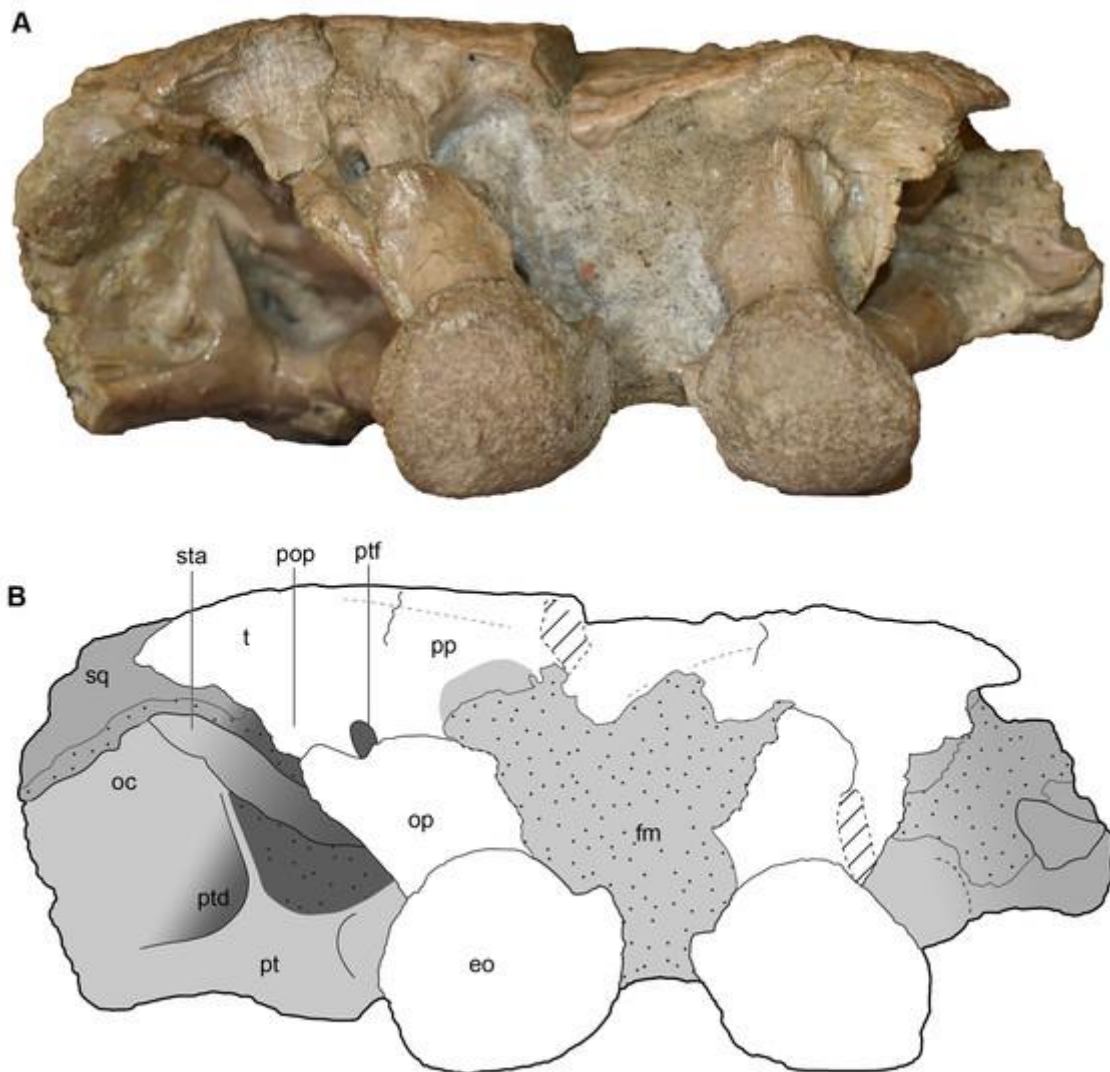


Figure 23: Occipital view of a referred occiput and posterior skull roof of *Buettnererpeton bakeri*, UMMMP 14154.

(A) Photograph; (B) interpretive line drawing. Abbreviations: eo, exoccipital; fm, foramen magnum; oc, oblique crest of the pterygoid; op, occipital pillar; pop, parotic process of the tabular; pp, postparietal; pt, pterygoid; ptd, pterygoid depression; ptf, posttemporal foramen; sq, squamosal; sta, stapes; t, tabular. Scale bar equal to 5 cm.

[Download full-size image](#)

DOI: [10.7717/peerj.14065/fig-23](https://doi.org/10.7717/peerj.14065/fig-23)

UMMP 14262 was reported as the “anterior half of a skull” ([Case, 1932](#):6), but the specimen was never figured, and Case made only one note regarding its morphology – that there was a small median gap between the rows of transvomerine teeth (p. 21 therein). All that remains of the specimen is an unidentifiable fragment embedded in matrix and a few loose fragments ([Fig. 24](#)). No vomer (or teeth) is apparent, and the largest fragment arguably cannot even be proven to belong to a temnospondyl. Collections records give no indication of either an exchange or a loan involving this specimen. There is a specimen in

collections, one number higher (UMMP 14263), that is represented by the anterior half of the skull, but the specimen is listed as being from “Sweetly Cruize,” which [Lucas et al. \(2016\)](#) considered the same as the Rotten Hill locality near Amarillo, TX, that preserves abundant remains of *Anaschisma browni*. The preservation and lithology of UMMP 14263 is consistent with specimens from Rotten Hill and distinct from the sandy conglomerate at the Elkins Place bone bed. UMMP 14263 also does not expose the transvomerine teeth. This conundrum is therefore unlikely to be a typographic error. A catalogue of UMMP fossils that was published by [Case \(1947\)](#) does not list UMMP 14262, but this is an incomplete list based on what we observed. Other specimens that were almost certainly known at the time of the 1932 publication given their catalogue numbers were also not listed in the 1947 publication (e.g., intercentra; many isolated skull bones). [Long & Murry’s \(1995\)](#) appendix of specimens also does not mention UMMP 14262 (for any tetrapod). It should be assumed that this specimen has been lost or transferred without apparent record.



Figure 24: The remaining material associated with UMMP 14262, purportedly the anterior half of a skull of a referred specimen of *Buettnererpeton bakeri*. (A) The largest remaining fragment in three views; (B) vial containing additional fragments. Scale bar equal to 1 cm.

[Download full-size image](#)

DOI: [10.7717/peerj.14065/fig-24](https://doi.org/10.7717/peerj.14065/fig-24)

Finally, there are more than three dozen cranial specimens consisting of largely isolated and fragmentary cranial, palatal, and occipital elements. Their numbering is not repeated in this overview (refer to [Table 1](#)), but they are specifically called out in the following description. Most of these specimens actually comprise multiple elements from multiple individuals, with many seemingly grouped by

which side of the skull they come from (*e.g.*, UMMP 13811 purportedly constitutes four right nasals).

Lateral line grooves.—The lateral line canals are well defined in the holotype ([Fig. 6](#)). The supraorbital canal originates on the premaxilla, medial to the naris and continues posteriorly, curving around the naris. It presumably crosses onto the maxilla and definitively onto the lacrimal before turning back medially onto the prefrontal and the postfrontal, where it terminates. The infraorbital canal is not well-defined anteriorly but is definitively present in the inferred area of the maxilla at the level of the posterior narial margin. It curves medially to closely approach the supraorbital canal on the lacrimal, and then exhibits a marked kink (Z-shaped flexure) where it turns back onto the maxilla and then extends longitudinally down the jugal, where it very nearly contacts the postorbital canal. It is unclear whether the canals contacted along their full length because the relevant region is reconstructed on both sides, but there is a short extent on the left side where they run adjacent to each other. The preserved portion of the postorbital canal is an obliquely oriented line extending from the jugal, across the postorbital, and terminating on the supratemporal. From the point where it parallels the infraorbital canal, there is another groove extending posteriorly onto the quadratojugal that curves slightly medially at the end to extend to the edge of the preserved skull; it is possible that the terminus was either within the squamosal or over the squamosal-quadratojugal suture.

The full course of the lateral line canals is also identified in UMMP 13820 ([Fig. 9](#)). There are no major deviations from the holotype barring the left side of UMMP 13820 in which a groove appears to join the infraorbital and supraorbital canals posterior to the naris. However, this feature is not found on the right side, which lacks the slight damage found on the left side, so it may be an artifact. Minor deviations in this specimen include the clear termination of the postorbital canal on the squamosal (restricted to the quadratojugal in the incompletely preserved region of the holotype) and the more ‘U-shaped’ contour of the postorbital canal along the jugal and the postorbital (*vs* what appears to be a more ‘V-shaped’ contour, incompletely preserved in the holotype). Because the left lacrimal of this specimen is particularly narrow compared to other specimens, the infraorbital canal does not pass onto the lacrimal on this side, but it does pass onto the right lacrimal, which is much wider ([Fig. 9](#)). UMMP 13822 shares the separation of the infraorbital and supraorbital canals posterior to the naris ([Fig. 12](#)), as with the holotype and in contrast to UMMP 13820, further suggesting that the morphology on the left side of UMMP 13820 might be an artifact. UMMP 13822 then shares the more ‘U-shaped’ postorbital canal and the termination of the postorbital canal on the squamosal with UMMP 13820 in contrast to the holotype. The more incomplete UMMP 13956 and UMMP 14154 preserve only short portions of canals that contribute no new information ([Figs. 17, 21](#)). No additional information is available from the limited portions of canals that are preserved on isolated cranial elements.

Ornamentation.—The ornamentation on the skull is similar to that of other metoposaurids, consisting mostly of circular pitting ([Fig. 6](#)). Pitting is more circular to subcircular in the snout region, between the orbits, and posterior to the pineal

foramen on the median elements. Much smaller, shallower pitting is found along the anterior margin of the premaxilla, which is otherwise relatively unornamented. Elongate, radiating grooves that represent zones of more intensive growth are most prominent on the posterior region of the frontal, the pre-pineal region of the parietal, and the squamosal but also occur on most of the postorbital elements at the juncture between the postorbital, the supratemporal, and the squamosal and along the posterolateral margin of the skull on the jugal. The lateral exposure of the maxilla is mostly unornamented but is marked by faint striations.

Ornamentation of the referred specimens, whether as partial and complete skulls or as isolated elements, is identical to that of the holotype (Figs. 9, 12, 17, 21). Among the former, the ornamentation is best preserved in UMMP 13820 in which the entire roof is complete and exposed.

Premaxilla.—The premaxilla is a short element framing the external naris anteriorly that is rectangular in dorsal view (Fig. 6). The suture with the nasal is not clearly defined in the holotype, but Case's (1931, 1932) original interpretation along a transverse crack (not depicted here) is not unreasonable. Based on the original interpretation, an alary process in the form of a distinct posterolateral triangular process would be absent, but the true condition is best left as unknown given the specimen's condition. Eight complete teeth are preserved on the partial left premaxilla but are still largely embedded in matrix; these are slender, conical, and non-recurved. The palatal surface of the premaxilla is otherwise obscured or reconstructed in the holotype, and the posterior suture with the vomer was not identified (Fig. 7). Assuming consistent size and spacing of teeth, the total marginal tooth count is estimated to a range of 110 to 120, although because the premaxilla-maxilla suture is not preserved on either side, the number of positions per element is unknown. This is comparable to *Metoposaurus krasiejowensis*, for which Sulej (2007) estimated 18–20 premaxillary and 83–107 maxillary positions (101–127 total positions).

UMMP 13820 preserves more dorsally complete premaxillae (Fig. 9). They are similar in proportions to the holotype but also preserve the premaxilla-nasal suture, revealing a weakly developed alary process in which the sutural contact is angled posterolaterally rather than straight transversely. However, it is not as developed as in some other metoposaurids like in *Anaschisma browni* (e.g., Lucas et al., 2016), and there is no strongly developed process in which a posteriorly directed triangular process is completely offset from the naris. The palatal surface is obscured by matrix, and a tooth count is not possible (Fig. 10). The only data regarding the palatal exposure comes from UMMP 13823 in which it is fully exposed ventrally. In this specimen, the premaxilla shares a transversely oriented suture with the vomer (Figs. 16A and 16C). There is a shallow median fossa (the fossa subrostralis media of Sulej, 2007, and the anterior palatal fossa of other workers; e.g., Yates & Warren, 2000) between paired perforations (the anterior palatal vacuities/fenestrae). The palatal fenestrae are slightly larger than the circumference of one palatal 'fang' and are more or less round when accounting for slight distortion and do not penetrate through to the skull roof as in some capitosaurids (e.g., Schoch, 1999; Rinehart, Lucas & Schoch, 2015). The fossa bears

only a faint rugose texture compared to other palatal surfaces. The suture between the premaxilla and the maxilla is only tentatively identified on each side (Figs. 16A and 16C), but there appear to have been 18 tooth positions on the premaxilla, within the range for *Metoposaurus krasiejowensis* (Sulej, 2007); Case (1932) positioned the suture more anteriorly than we have here. No teeth are preserved, but the tooth sockets show that the dentition was slightly compressed with the long axis oriented perpendicular to the lateral margin of the skull and that tooth size decreased only very slightly and gradually towards the posterior end of the tooth row. The premaxilla is unknown from the remaining partial to complete skulls and from the suite of isolated elements.

Septomaxilla.—In UMMP 13820 (Fig. 9), it appears that there may be a very thin, plate-like ossification lying on top of the true floor of the left naris, which would be the predicted position of an intranarial septomaxilla, whose occurrence and morphology in metoposaurids remain controversial and very poorly documented (e.g., Roychowdhury, 1965; Chakravorti & Sengupta, 2018; Buffa, Jalil & Steyer, 2019). On the right side, a similar thin plate-like element is suspended in matrix near the middle of the external naris (Fig. 9). If it is not a separate ossification, it would then represent postmortem damage. Positive identification awaits better documentation in other taxa.

Maxilla.—The maxilla is a long, slender element that bears the majority of the marginal dentition in the holotype (Fig. 6). Its dorsal exposure is relatively slender except for a slight medial expansion towards the nasal posterior to the naris, typically separating the lacrimal from the naris. This region is not preserved on either side in the holotype, but a maxilla-nasal contact to exclude the lacrimal from the naris was inferred by Case (1931, 1932). The lateral exposure of the maxilla is dorsoventrally short, underlying the jugal for most of its length and tapering in height posteriorly. On the palatal surface, the maxilla is restricted to the tooth-bearing surface except at the mid-length of the choana, where the maxilla expands medially between the pairs of ‘fangs’ on the vomer and the palatine to contribute to the lateral margin of the opening (Fig. 7). The degree of contribution is not fully resolved in this specimen, but it was at most relatively minor based on the anterior extent of the palatine along the lateral edge of the choana. If it is assumed that all of the exposed tooth sockets pertain to the maxilla (a reasonable inference based on the premaxilla-maxilla suture position in UMMP 13823), there were at least 85 maxillary positions, within the range of 83 to 107 for *Metoposaurus krasiejowensis* (Sulej, 2007).

As with the premaxillae, the maxillae of UMMP 13820 are only completely exposed dorsally (Fig. 9). This specimen confirms the separation of the lacrimal from the naris that was inferred for the holotype – this separation is very wide on each side. The maxilla definitively contacts the prefrontal as well. Only a short portion of the palatal exposure is preserved, with the same tooth socket morphology as the holotype (Fig. 10). The maxilla of UMMP 13822 is also only exposed dorsally (Figs. 12 and 13). Deviating from UMMP 13820, the maxilla does not contact the prefrontal, although it still has a broad contact with the nasal to separate the lacrimal from the naris. Finally, the maxilla in UMMP 13823 confers the most

information regarding the palatal exposure of this element ([Figs. 16A](#) and [16C](#)). Based on the admittedly distorted left choana, the maxilla contributes to about a third of the lateral choanal margin, thereby forming broad contacts with the palatine and the vomer. The suture with the premaxilla can only be inferred. There are at least 104 tooth positions on the left side of UMMP 13823, with two gaps that are too large to reasonably estimate. There are around 120 positions on the right side of the skull, on which the dentition is slightly better preserved. As seen on the left side, the posterior terminus of the maxilla is posterior to both the posterior terminus of the ectopterygoid and the level of the anterior margin of the subtemporal fenestra. The tooth row extends to the end of the maxilla. Isolated maxillae (UMMP 13803) do not confer additional information due to their incompleteness ([Figs. 25C–25E](#)).

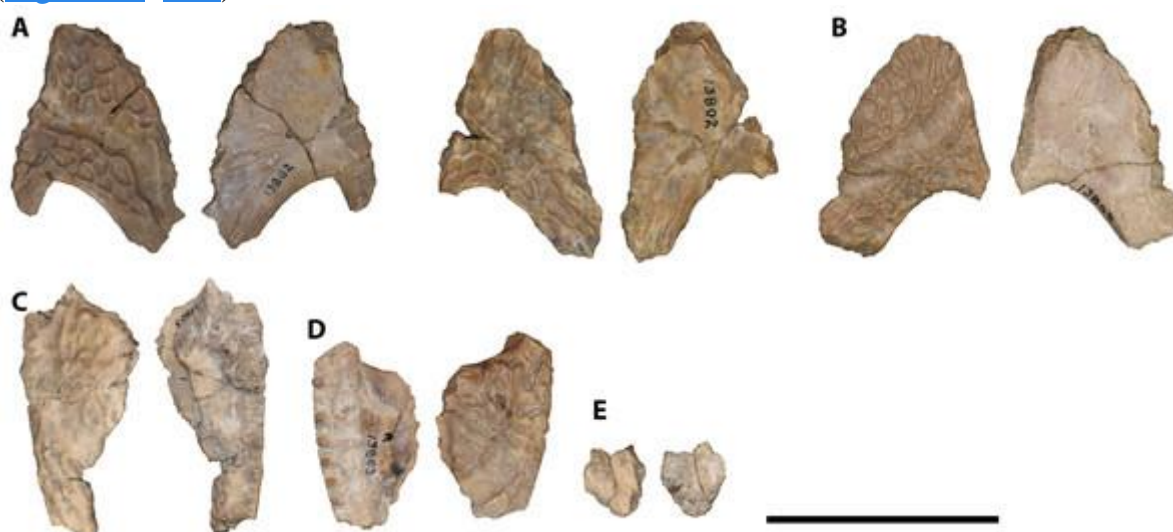


Figure 25: Isolated antorbital elements referred to *Buettnererpeton bakeri*.

(A) UMMP 13802, two left prefrontals in dorsal (left) and ventral (right) views; (B) UMMP 13805, right prefrontal in dorsal (left) and ventral (right) views; (C) UMMP 13803 (in part), partial left maxilla in dorsal (left) and ventral (right) views; (D) UMMP 13803 (in part), partial right maxilla in dorsal (left) and ventral (right) views; (E) UMMP 13803 (in part), maxillary fragment in dorsal (left) and ventral (right) views. Any association between the various parts of UMMP 13803 is not apparent. Scale bar equal to 5 cm.

[Download full-size image](#)

DOI: [10.7717/peerj.14065/fig-25](https://doi.org/10.7717/peerj.14065/fig-25)

Nasal.—The nasal is a polygonal element that frames the naris posteriorly in the holotype; its precise shape is not discernible in this specimen ([Fig. 6](#)). It presumably met the premaxilla anteriorly and definitively contacts the prefrontal laterally and the frontal posteriorly in the holotype. There is no preserved contact with the lacrimal, but the nasal and the lacrimal contact in the vast majority of metoposaurid specimens across taxa (but see an individual of *Metoposaurus krasiejowensis*; [Sulej, 2007](#):fig. 13). Contrary to Case's illustrations ([Case, 1931](#):fig. 1, [1932](#):fig. 2), the posterior narial margin, often formed by the nasal, is not complete, with a small region of plaster where he illustrated the nasal-lacrimal contact. Its morphology is therefore only confidently discernible from the referred specimens.

UMMP 13820 preserves complete nasals (Fig. 9). The lateral margin forms a ‘step’ in which the suture with the prefrontal is angled anterolaterally and then turns into a longitudinal orientation along the contact with the maxilla. This produces a polygonal shape. The nasal contributes to most of the posterior narial margin as well as about half of the medial narial margin. In UMMP 13822 (Fig. 12), the inflection point of the ‘step’ bulges more laterally than in UMMP 13820, which produces the nasal-lacrimal contact in the former. UMMP 13809 represents three isolated left nasals (Fig. 26A), and UMMP 13811 represents three isolated left nasals and one isolated right nasal (Fig. 26B). Most are slightly damaged at the margins but preserve the same polygonal morphology with the stepped lateral margin. There is practically no size difference among them, even though no distinct pairs belonging to one individual can be identified.



Figure 26: Isolated median cranial elements referred to *Buettnererpeton bakeri*. (A) UMMP 13809, three partial left nasals in ventral (left) and dorsal (right) views; (B) UMMP 13811, three isolated left nasals and one isolated right nasal in dorsal (left) and ventral (right) views; (C) UMMP 13814, three right frontals in ventral (left) and dorsal (right)

views; (D) UMMP 13815, two left frontals in dorsal (left) and ventral (right) views; (E) UMMP 13812, three partial right parietals in ventral (left) and dorsal (right) views; (F) UMMP 13813, two partial left parietals in dorsal (left) and ventral (right) views; (G) UMMP 13826, partial right parietal in ventral (left) and dorsal (right) views. All elements are oriented with the anterior face pointing up. Scale bars equal to 5 cm.

[Download full-size image](#)

DOI: [10.7717/peerj.14065/fig-26](https://doi.org/10.7717/peerj.14065/fig-26)

Prefrontal.—The prefrontal, as mostly preserved, has a sub-triangular profile in the holotype as in other metoposaurids and contributes to the anterior and medial orbital margins ([Fig. 6](#)). There is a large patch of plaster anterior to the prefrontal that precludes the confident identification of its anteriormost contacts (some combination of the lacrimal, the maxilla, and the nasal), but the anteriorly tapering morphology, with a defined terminus, suggests that the prefrontal is complete, as with [Case's \(1932\)](#) interpretation. It contacts the lacrimal laterally, the nasal medially, and the jugal posterolaterally. It extends to about the mid-length of the orbit to meet the postfrontal.

The shape of the prefrontal is more rectangular to pentagonal with a blunted anterior terminus in the referred specimens. In UMMP 13820, the anterior margin is essentially squared-off where it contacts the nasal and the maxilla ([Fig. 9](#)). The lateral margin is markedly different on each side on account of the variable lacrimal widths in this specimen. The prefrontal also extends slightly farther down the lateral margin of the orbit but has a more restricted contribution to the medial margin when compared to the holotype. In UMMP 13822, the anterior terminus of the prefrontal is wide but slightly rounded where it contacts the lacrimal and the nasal ([Fig. 12](#)). Its relative contributions to the orbital margins are more like those in the holotype. UMMP 13802 represents two isolated left prefrontals ([Fig. 25A](#)), and UMMP 13805 represents an isolated right prefrontal ([Fig. 25B](#)). All three share a morphology most like that of UMMP 13822 with a wide and gently rounded anterior terminus, but it is difficult to be certain that there has not been some minor damage along the margins. In UMMP 13805 and one of the prefrontals of UMMP 13802, the posteromedial margin is probably incomplete by comparison with those in articulated specimens. The isolated elements clearly show the ventral surface of this element, which is largely smooth except for one or two shallow pits anteromedial to the orbit.

Lacrimal.—The lacrimal is a slender element of the preorbital region ([Fig. 6](#)). In the holotype, it contacts the maxilla laterally, the jugal posteriorly, and the prefrontal medially. It tapers posteriorly, penetrating slightly into the jugal, contrary to the squared-off terminus illustrated by [Case \(1931, 1932\)](#). It is widely excluded from the orbit by the prefrontal and the jugal, a feature separating it from both *Anaschisma* and *Metoposaurus* (*sensu* [Kufner & Gee, 2021](#), and [Brusatte et al., 2015](#), respectively). [Case \(1931, 1932\)](#) interpreted the left lacrimal as being entirely complete and widely excluded from the naris, but there is no clear demarcation of the anterior suture(s) due to plaster reconstruction in this area. The lacrimal is typically shorter in the North American taxa, however, so it is possible that the element is complete and simply without a defined anterior suture.

This inference of the relative length of the lacrimal is validated by UMMP 13820 and UMMP 13822 (Figs. 9, 12), in which it is widely separated from the naris by a gap subequal in length to the total length of the lacrimal. Both specimens also corroborate the interpretation of the holotype as having a lacrimal widely separated from the orbit. The lacrimal varies mainly in its relative width; the left lacrimal of UMMP 13820 is unusually narrow for a metoposaurid (Fig. 9). The right lacrimal of this specimen is more similar to the holotype and to that of UMMP 13822. The unique lacrimal-nasal suture in UMMP 13822 is related to a lateral projection of the nasal rather than to some morphological deviation of the lacrimal.

Frontal.—The frontal is a triangular element forming most of the interorbital region in the holotype (Fig. 6). It sutures to the prefrontal and the postfrontal laterally, to the nasal anteriorly, and to the parietal posteriorly, although the posterior contact is not well-defined in the holotype. The element is broadest anteriorly and then tapers prominently to meet the parietal, although this contact is not preserved except for a minute portion on the right half of the skull (Fig. 6B). The frontal's width in the post-orbital region is less than half that of its width in the pre-orbital region. There is typically minor intraspecific variation in the exact shape of the frontal in metoposaurids (*e.g.*, Sulej, 2007; Lucas et al., 2016), and this is also observed in the material described here. All specimens share a generally triangular profile with the broadest end anteriorly and the narrowest end posteriorly, but the angle of the anterior suture and the longitudinal position of the greatest width vary slightly. In UMMP 13820 and UMMP 13822, the frontal is widest at the prefrontal-postfrontal suture, whereas it is widest anterior to this suture in the holotype (Figs. 9, 12). As seen in UMMP 13820, the orientation of the suture with the nasal ranges from nearly transverse to clearly set at an angle anteromedially. The holotype has an angled suture, whereas that of UMMP 13822 appears to have been transversely oriented. Similarly, the posterior terminus may either be squared-off, as on the right side of UMMP 13820, or it may form a short triangular process wedging into the parietal, as on the left side of this specimen and in UMMP 13822. This variation may also be observed in UMMP 13814, representing three isolated right frontals (Fig. 26C), and in UMMP 13815, representing two isolated left frontals (Fig. 26D). These elements differ by about 10–15% in length between the largest and smallest. The ventral surface of the frontals is mostly smooth, but along the midline in the posterior half, there is a low longitudinal ridge (the orbitotemporal crest of Sulej, 2007), which would extend onto the parietals.

Postfrontal.—The postfrontal is a rectangular element extending from the medial orbital margin, where it meets the prefrontal, to meet the parietal posteromedially, the supratemporal posteriorly, and the postorbital laterally in the holotype (Fig. 6). The contribution of the postfrontal to the medial margin of the orbit is relatively large (> 50% of the margin). Neither the posterior contact with the supratemporal nor that with the parietal is well-preserved, but long contacts occur in all metoposaurids, and there is no reason to presume otherwise here.

The overall profile of the postfrontal is consistent across all specimens, with the referred specimens preserving the long contacts posteriorly with the supratemporal and the parietal that were not fully resolved in the holotype. Variation is primarily

related to the anterior extent along the medial orbital margin. In UMMP 13820, the left postfrontal has a particularly far-reaching anterior terminus that results in the element forming about 80% of the medial orbital margin; the contribution is slightly less on the right side of this specimen (Fig. 9). The contribution is comparatively smaller in UMMP 13822 (Fig. 12), more in line with the holotype. UMMP 13808 represents an isolated left postfrontal (Fig. 27G), and UMMP 13966 represents an isolated right postfrontal (Fig. 27J). UMMP 13970 represents an isolated, articulated set of the left postorbital and the left postfrontal (Fig. 27I); it is only exposed ventrally due to an adhesive sheet used to hold the constituent fragments together that is adhered to the dorsal surface. As preserved, all three had a similar contribution to the orbital margin as the holotype and UMMP 13822. The ventral surface is entirely smooth.

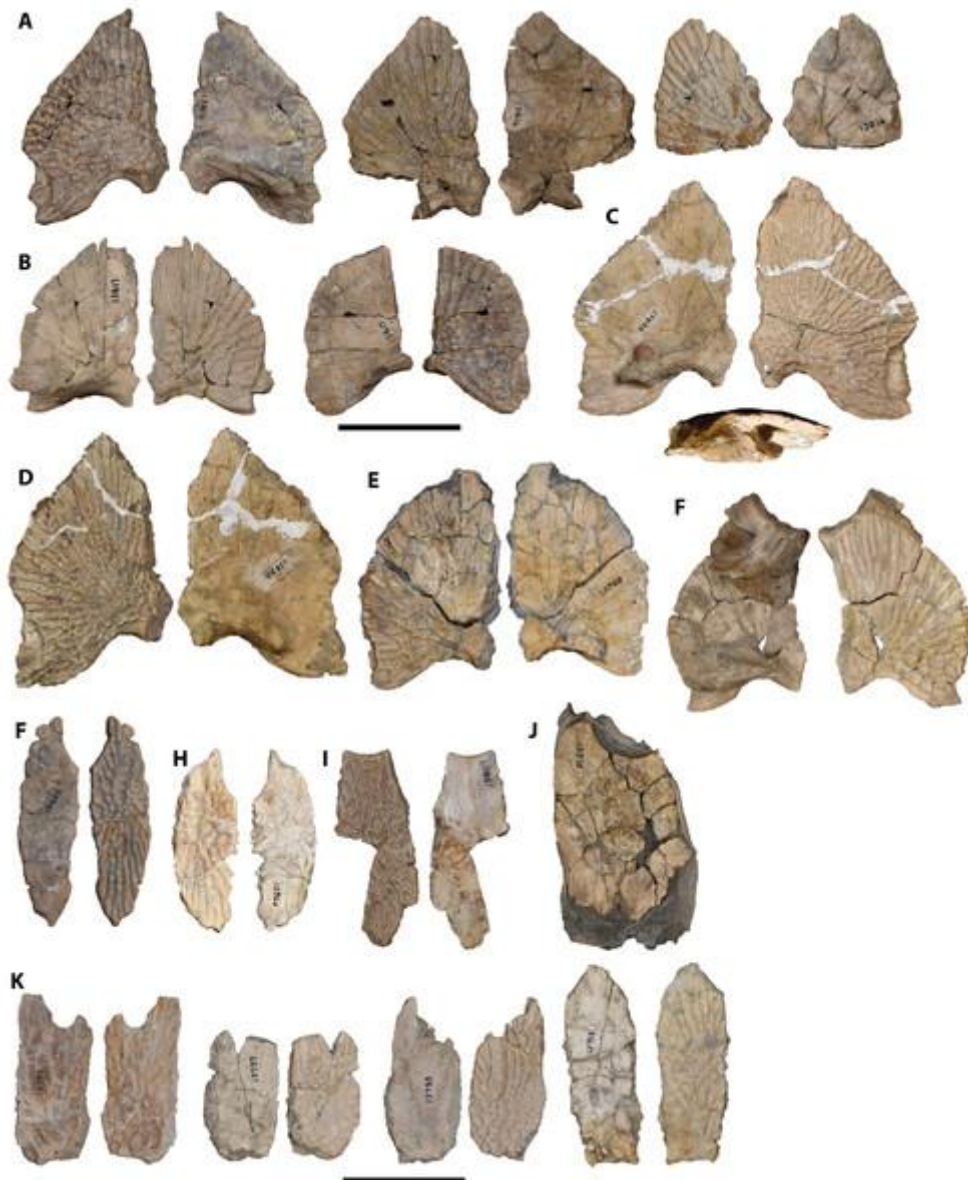


Figure 27: Isolated postorbital cranial elements referred to *Buettnererpeton bakeri*. (A) UMMP 13816, three partial left squamosals in dorsal (left) and ventral (right) views; (B) UMMP 13817, two partial right squamosals in ventral (left) and dorsal (right) views; (C) UMMP 13829, partial right squamosal in ventral (left), dorsal (right), and posterior (bottom)

views; (D) UMMP 13830, partial left squamosal in dorsal (left) and ventral (right) views; (E) UMMP 13968, partial left squamosal in dorsal (left) and ventral (right) views; (F) UMMP 14099 (in part), partial right squamosal in ventral (right) and dorsal (left) views; (G) UMMP 13808, left postfrontal in ventral (left) and dorsal (right) views; (H) UMMP 13807, partial right postorbital in dorsal (left) and ventral (right) views; (I) UMMP 13970, articulated postorbital fragment in ventral view; (J) UMMP 13966, partial right postfrontal in dorsal (left) and ventral (dorsal) views; UMMP 13793, four partial supratemporals in ventral (left) and dorsal (right) views. All elements are oriented with the anterior face pointing up. Scale bars equal to 5 cm.

[Download full-size image](#)

DOI: [10.7717/peerj.14065/fig-27](https://doi.org/10.7717/peerj.14065/fig-27)

Postorbital.—The postorbital is a sub-rectangular element extending from the posterior orbital margin, where it contacts the jugal laterally and the postfrontal medially, to meet the squamosal and the supratemporal posteriorly in the holotype ([Fig. 6](#)). It tapers posteriorly to a point, partially dividing the supratemporal from the squamosal.

The morphology of this element is very consistent across all specimens. The only variation is in the contact with the squamosal, which may be straight as in the holotype and UMMP 13822 or more medially convex, as in UMMP 13820 ([Figs. 9, 12](#)). The overall profile of the postorbitals in UMMP 13820 is still nearly identical. UMMP 13807 represents a partial isolated right postorbital ([Fig. 27H](#)). The ventral surface is entirely smooth.

Supratemporal.—The supratemporal is a pentagonal element that contacts the postfrontal and the postorbital anteriorly, the squamosal laterally, the tabular and the postparietal posteriorly, and the parietal medially in the holotype ([Fig. 6](#)). It has an anterior process wedging between the postfrontal and the postorbital and a squared-off posterior terminus. In the holotype, the sutural relationships are not fully preserved on either side in isolation but can be fully characterized when taken together.

The morphology of this element is very consistent across all specimens. The only notable difference is in the proportions; UMMP 13822, which is the smallest of the partial to complete skulls, has a shorter supratemporal than UMMP 13820, which is the largest of the partial to complete skulls ([Figs. 9, 12](#)). A correlated difference may be the degree to which the anterior terminus is pointed and how sharply it tapers. The posteriorly complete supratemporal of UMMP 14154 does not contribute additional information. UMMP 13793 represents four isolated supratemporals ([Fig. 27K](#)). The supratemporal can typically be sided based on the partial to complete skulls, in which the anterior process is always offset slightly more medially than laterally, but three of the isolated supratemporals are incomplete anteriorly, and the fourth shows no clear asymmetry. A second means of siding is by the postorbital canal, which is closer to the lateral margin in partial to complete skulls. On this basis, all four are left supratemporals. The ventral surface is entirely smooth.

Parietal.—The parietal is a sub-rectangular element that contacts the frontal anteriorly, the postfrontal anterolaterally, the supratemporal laterally, and the postparietal posteriorly in the holotype ([Fig. 6](#)). The parietals are relatively narrow

throughout, although the anterior margins are poorly defined on both sides in the holotype, so it is unclear how constricted the anteriormost region was. The preserved sutures with the supratemporal are variable, the left one being straight and the right one being angled. The circular pineal foramen is situated in the posterior fifth of the parietals.

UMMP 13820 preserves more defined parietals that clearly illustrate the anterior tapering of the parietals (more pronounced on the left side) and the intraspecific variation in the anterior suture with the frontal (interdigitated on the left side, straight transverse on the right side; [Fig. 9](#)). Both lateral margins are straight in this specimen. As with the holotype, the pineal foramen is situated far posterior within the parietals. The left parietal of UMMP 13822 is probably nearly complete, broken along the midline contact given the partial definition of the pineal foramen ([Fig. 12](#)). If complete, the overall element was slightly proportionately wider than in the holotype and UMMP 13820; as with the supratemporal, this may be associated with very minor changes in the precise proportions of the elements throughout ontogeny. Also exposed ventrally is the orbitotemporal crest, which flares laterally around the foramen from the midline. The position of the pineal foramen is, however, the same as the other two specimens. Portions of the parietal are preserved in the partial skulls UMMP 13956, UMMP 14098, and UMMP 14154, but they contribute no additional or conflicting data regarding the overall proportions or sutures. UMMP 13812 represents three isolated right parietals ([Fig. 26E](#)), UMMP 13813 represents two isolated left parietals ([Fig. 26F](#)), and UMMP 13826 represents an isolated right parietal ([Fig. 26G](#)). All of the elements merely confirm the degree of intraspecific variation in the anterior terminus and the contour of the suture with the postorbital where the parietal tapers in width. One of the parietals assigned to UMMP 13812 has a slanted lateral suture with the supratemporal, whereas the others are straight ([Fig. 26E](#)). The pineal foramen is consistent in being in the posterior fifth of the parietals. UMMP 13826 is particularly noteworthy because it is twice as large as the other parietals despite being incomplete ([Fig. 26G](#)). This is the only evidence from the aggregated cranial remains for the presence of much larger individuals than those represented by partial to complete skulls. All isolated parietals are smooth ventrally and show the divergence of the orbitotemporal crest from the midline to contour around the pineal foramen laterally. The crest terminates at or just posterior to the level of the posterior margin of the foramen.

Jugal.—The jugal is an elongate element extending along much of the lateral margin of the skull dorsomedial to the maxilla and lateral to the squamosal and the postorbital; in the holotype, it is only preserved on the left side ([Fig. 6](#)). Here, it terminates at the level of the anterior orbital margin where it meets the lacrimal. The jugal also has a small triangular exposure (the ‘insula jugalis’) on the palate posterior to the termination of the palatal tooth row of the ectopterygoid ([Fig. 7](#)). It therefore separates the ectopterygoid from the subtemporal fenestra. It borders the pterygoid laterally but does not contribute to the palatine ramus.

The jugal is otherwise known from UMMP 13820, UMMP 13822, and UMMP 13823 ([Figs. 9, 12, 13, 16A, 16C](#)). The dorsal exposure, known from UMMP 13820 and UMMP 13822 ([Figs. 9, 12](#)), is essentially identical to that of the

holotype. There is minor variation in the anterior contact with the lacrimal on account of the more pronounced variation in lacrimal shape (especially in UMMP 13822). In both specimens, the jugal extends just anterior to the level of the anterior orbital margin; the right jugal of UMMP 13820 is slightly more anteriorly extensive than the left jugal (Fig. 9). The ventral exposure is known from UMMP 13822 and UMMP 13823 (Figs. 13, 16A, 16C). It is incompletely defined in both and contributes no new or conflicting data relative to the holotype.

Quadratojugal.—The quadratojugal is poorly preserved in the holotype on both sides (Figs. 6–8). In dorsal view, it is a rectangular element sutured to the jugal anteriorly (poorly defined) and to the squamosal laterally (Fig. 6).

More information is available from UMMP 13820 and UMMP 13822. In these specimens, the dorsal sutures are entirely defined (Figs. 9, 12), capturing the undulating nature of the lateral suture with the supratemporal and the tapering anterior contact with the jugal. In ventral view, also seen in UMMP 13823 (Figs. 10, 13, 16A, 16C), the quadratojugal's posterolateral suture with the quadrate is well-defined. In lateral and occipital view, the quadratojugal's curvature is most apparent, forming a gentle dorsally convex surface (Figs. 8, 11, 14–16). In occipital view, the suture with the squamosal extends down the occiput to meet the large paraquadrate foramen, which forms an elongate oval slit (Figs. 11, 14, 16D). Variation in the precise contours of the foramen is undoubtedly due largely to taphonomic distortion. The quadratojugal itself frames the lateral half of the foramen and excludes the quadrate from this opening. No accessory paraquadrate foramina like those identified in *Metoposaurus krasiejowensis* were identified here, but it should be emphasized that only a very thin lamina separates the main paraquadrate foramen from the accessory foramen in that taxon (e.g., Sulej, 2007:fig. 1D), and it is not found in all specimens of *M. krasiejowensis* (Sulej, 2007:41). Given that the Elkins Place bone bed material was prepared more than 90 years ago, there is good reason to suspect that the dividing lamina could have been misidentified as a loose bone chip and been prepared away, or that it was never preserved to begin with, if it was present at all. Largely isolated quadratojugals are known from UMMP 13806 (two isolated right elements; Fig. 28H), UMMP 13818 (three isolated right elements; Fig. 28I), UMMP 13969 (two isolated left elements; Fig. 28G), and UMMP 14098, in which it is articulated with the palatal fragment and separate from the main fragment consisting of the skull roof and occiput (Fig. 20). The isolated quadratojugals are variably complete but are consistent in preserving the smoothly rounded lateral margin of the paraquadrate foramen, with no indication of an accessory paraquadrate foramen. In these specimens, the lateral margin of the paraquadrate foramen is smooth and continuous and of a consistent curvature between specimens, supporting the attribution of variation in more complete specimens to taphonomy. Several also preserve the ventral portion of the quadratojugal that sutures with the quadrate. This articulation is borne by a distinct facet, wider than long, that is covered in unfinished bone (e.g., UMMP 13804; Fig. 28J).



Figure 28: Isolated posterior cranial elements referred to *Buettnererpeton bakeri*.

(A) UMMP 13797, fragment with mostly complete postparietals and articulated fragments of the parietal in dorsal (left) and ventral (right) views; (B) UMMP 13798, two partial left postparietals in dorsal (left), ventral (middle), and posterior (right) views; (C) UMMP 13799, one partial left postparietal and one partial left tabular (association unclear) in dorsal (left) and ventral (right) views; (D) UMMP 13800, right postparietal and tabular in dorsal (left), ventral (right), and posterior (bottom) views; (E) UMMP 13801, two partial right postparietals in dorsal (left), ventral (middle), and posterior (right) views; (F) UMMP 13967, left postparietal and tabular in dorsal (left), ventral (middle), and posterior (right) views; (G) UMMP 13969, two partial left quadratojugals in dorsal (left), ventral (right), and posterior (bottom) views; (H) UMMP 13806, two partial right quadratojugals in dorsal (left), ventral (right), and posterior (bottom) views; (I) UMMP 13818, three partial right quadratojugals in dorsal (left), ventral (right), and posterior (bottom) views; (J) UMMP 13804, ventral process of a left quadratojugal in dorsal (left) and ventral (right) views. All elements are oriented with the anterior face pointing up. Scale bars equal to 5 cm.

[Download full-size image](#)

DOI: [10.7717/peerj.14065/fig-28](https://doi.org/10.7717/peerj.14065/fig-28)

Squamosal.—The squamosal is a large pentagonal element that contributes to the posterior skull margin and to the otic notch, neither of which is complete on either side of the holotype ([Fig. 6](#)). It tapers anteriorly where it meets the postorbital and the jugal and is broadest posteriorly where it meets the quadratojugal laterally and the tabular medially. The occipital portion is very poorly defined in this specimen. As with the quadratojugal, more information on the dorsal and occipital exposures of the squamosal is available from UMMP 13820 and UMMP 13822 ([Figs. 9, 11, 12, 14](#)). The element is nearly completely defined in UMMP 13820 and entirely so on the left side of UMMP 13822. They confirm the general pentagonal shape, although there is some variation with respect to the lateral margin that may be ontogenetic in nature. In UMMP 13820, the largest of the partial to complete skulls, the lateral suture with the quadratojugal is undulating but overall oriented longitudinally. The suture then turns anteromedially just posterior to the contact with the jugal, resulting in a semi-distinct kink in the suture and giving an overall pentagonal shape. This is particularly pronounced on the left side but less so on the right. The incompletely known squamosals of the holotype appear to share this general profile. In UMMP 13822, the lateral suture is far less undulating and forms a more continuous curve with no kink (also observed in UMMP 13956, which is also on the lower end of the known size range; [Fig. 17](#)). The curvature still produces a more pentagonal shape than the sub-triangular shape seen in *Arganasaurus lyazidi*. Our hypothesis of a possible ontogenetic influence is somewhat supported by examination of UMMP 13816 (three isolated left squamosals; [Fig. 27A](#)), UMMP 13817 (two isolated right squamosals; [Fig. 27B](#)), UMMP 13829 (one isolated right squamosal; [Fig. 27C](#)), UMMP 13830 (one isolated left squamosal; [Fig. 27D](#)), UMMP 13968 (one isolated left squamosal; [Fig. 27E](#)), and UMMP 14099 (disarticulated squamosal associated with occipital fragments; [Fig. 27F](#)). The largest specimens (UMMP 13829, UMMP 13830) have clearly undulating margins. This is then variable in medium-sized specimens (UMMP 13816, UMMP 13868, UMMP 14099), and the smallest specimens (UMMP 13817) have continuously curved margins. The isolated squamosals also reveal the presence of an underplating flange on the posterolateral corner. This would underlie the quadratojugal and might explain why the latter is frequently detached from the skull roof, presenting either as an isolated element ([Figs. 28G–28I](#)) or as the only element absent from the posterior skull roof in a partial or complete specimen (UMMP 13956, UMMP 14098; [Figs. 17, 18, 20](#)). The squamosal also forms most of the otic notch, and the various referred specimens confirm the presence of a relatively deep, circular notch. The ventral surface of the squamosal is nearly smooth, but there is a developed transverse ridge at the posterior margin just anterior to the otic notch; this was termed the base of the lamina descendens by [Sulej \(2007\)](#). Finally, the squamosal forms the medial half of the paraquadrata foramen on the occiput; this is best preserved in UMMP 13820 and UMMP 13822 ([Figs. 11, 14](#)). The descending lamina lies mostly dorsal and slightly anterior to the ascending lamina of the pterygoid (best seen in UMMP 13820), but due to compression and damage to the thin dorsal margin of the latter, this contact is not well-defined in an undistorted state in any one specimen.

Tabular.—The tabular is a square element at the posterior margin of the skull but is not well-preserved in the holotype (Fig. 6). It sutures to the squamosal laterally, to the supratemporal anteriorly, and to the postparietal medially. A tabular horn is not preserved in the holotype, but there are distinctly broken surfaces where the horn would have been, and a deep otic notch is well-defined on the left side. That it has an occipital exposure is clear, but the suture with the postparietal medially is unclear (Fig. 8). Ventrally it sutures with the exoccipital. In this specimen, the oval posttemporal foramen is apparently entirely framed by the postparietal and the tabular, with no exoccipital contribution, but the sutural contacts are not entirely clear (Fig. 8).

More information on the tabular is gleaned from the referred specimens. Complete tabulars are preserved in UMMP 13820, UMMP 13822, UMMP 14098, and UMMP 14154 (Figs. 9, 12, 18, 21). Those of UMMP 13823 and UMMP 13956 have damage to the tabular horn distally. There is some variation in the proportions of the main body of the tabular; in UMMP 13820 (Fig. 9), it is at best equant or perhaps slightly longer than it is wide, whereas in UMMP 13822 and UMMP 14154 (Figs. 12, 21), it is distinctly wider than long. This probably correlates with the slight proportional differences observed in other postorbital elements, and by correlation with the relative sizes of these specimens, may be an ontogenetic difference. The tabular horn is also slightly longer in the relatively large UMMP 13820, but the orientation and lack of curvature are consistent throughout. The suture with the postparietal is slightly better defined in UMMP 13820 and UMMP 14154 than the holotype, but the ventral extent along the occiput is unclear (although a straight suture is found in other metoposaurids and could be reasonably inferred). Under this assumption, the posttemporal foramen is then framed by the tabular, the postparietal, and the exoccipital (the last of which has no apparent contribution in the holotype) in UMMP 13820, UMMP 13822, and UMMP 14154 (Figs. 11, 14, 20). The shape and orientation of the longitudinal axis of the foramen is somewhat variable between specimens, but this is likely attributable to taphonomic distortion. In addition to a pair of isolated left tabulars (UMMP 13798; Fig. 28B), UMMP 13800 represents an articulated tabular-postparietal isolate from the right side (Fig. 28D), UMMP 13967 represents a disarticulated but associated tabular-postparietal isolate from the left side (Fig. 28F), and UMMP 13799 represents a tentatively identified, disarticulated, but associated tabular-postparietal isolate from the left side (Fig. 28C). Most of the tabulars are too incomplete to confidently determine their proportions, and the tabular horn is incomplete or lost in all the isolated specimens. UMMP 13800 is the only one that can reasonably be inferred to have a complete base, which is equant. These tabulars also provide data on the ventral surface, which fully exposes the parotic process that descends ventrally to form the posttemporal foramen with the postparietal. In UMMP 13800 (the most complete; Fig. 28D), this opening is almost entirely framed by the preserved portions, with only the exoccipital's contribution missing. As can be seen in several specimens, from the base of the process extend two thin crests. The posterolaterally extending external tabular crest (*sensu* Sulej, 2007) extends beneath the tabular horn to buttress it; this is also visible in the occipital

view of well-preserved specimens like UMMP 13820 ([Fig. 11](#)). The internal tabular crest (*sensu* [Sulej, 2007](#)) extends anteriorly towards the sutural junction between the tabular, the squamosal, and the supratemporal.

Postparietal.—The postparietal is a rectangular element, longer than wide on at least the right side of the holotype, at the posterior margin of the skull ([Fig. 6](#)). It sutures to the parietal anteriorly, to the supratemporal anterolaterally, and to the tabular laterally. The occipital surface is smooth and presumably represents a combination of the tabular and the postparietal, but the suture cannot be traced for most of the presumed ventral extent, and therefore the relative contributions to the posttemporal foramen are unclear ([Fig. 8](#)). Typically, the postparietal's contribution is formed by the supraoccipital process (*sensu* [Sulej, 2007](#)). Towards the midline on the occipital surface, there is a distinct pit or depression that causes the ornamented roofing portion of the postparietal to protrude over the occipital portion. This is most apparent on the right side of the holotype and is accentuated by a slight posterior bulging of the roofing portion along the midline ([Fig. 6](#)). The postparietal of the referred specimens has a similar shape to the holotype, and UMMP 13820 and UMMP 14154 further confirm the rectangular proportions ([Figs. 9, 21](#)). The lateral and medial sutures are straight in most specimens, but that of UMMP 13822 has a step anteriorly to produce a discontinuous margin with the supratemporal and thus a slightly wider postparietal ([Fig. 12](#)); this might correlate with the observations made for other postorbital elements' relative proportions in this specimen. Also noteworthy is that most of the partial to complete crania lack the posterior bulging of the roofing portion along the midline at the margin of the skull; other than the holotype, this is only apparent in UMMP 13820 and UMMP 14098 ([Figs. 9, 18A](#)). In addition to the aforementioned tabular-postparietal isolates (UMMP 13697, UMMP 13799, UMMP 13800), there are an articulated pair of postparietals (UMMP 13797; [Fig. 28A](#)) and a pair of isolated postparietals that are tentatively attributed to the right side (UMMP 13801; [Fig. 28E](#)). Both of the latter specimens appear more or less complete and thus confirm the long rectangular profile. UMMP 13797 also appears to have the posterior bulge of the roofing portion. Ventrally, the postparietal is smooth except for the supraoccipital process, which forms a ventrally descending column that frames the posttemporal foramen along the medial side ([Figs. 11, 14, 23](#)). In the isolated postparietals, the process is insufficient to determine the overall shape of the foramen. In all specimens described here, the descending column has a circular or oval cross-section profile rather than the teardrop shape described in small- and medium-sized individuals of *Metoposaurus krasiejowensis* ([Sulej, 2007](#)).

Parasphenoid.—The parasphenoid is a large element formed by a pentagonal basal plate and a flat, anteriorly directed cultriform process in the holotype ([Fig. 7](#)). It sutures laterally to the pterygoid, posteriorly to the exoccipitals, and anteriorly to the vomers, although all of these sutures are incompletely defined in the holotype. The basal plate merges with the cultriform process anteriorly, has straight lateral sutures with the pterygoids, and then narrows posteriorly between the exoccipitals. Whether the exoccipitals meet or are separated by the basal plate is unclear in the holotype. There is faint ornamentation on the basal plate consisting of shallowly

developed ridges, but the center of the plate has been damaged. There is no indication that the ornamentation extended onto the cultriform process. Two shallowly developed fossae, presumably for muscle attachments, are present on the posterior half, being framed anteriorly by a short but distinct ridge (the ‘muscular crest’ of [Sulej, 2007](#), or the ‘crista muscularis’ of various other workers; *e.g.*, [Schoch, 1999](#); [Buffa, Jalil & Steyer, 2019](#)). The cultriform process is flat throughout and of a nearly consistent width throughout. It narrows only slightly along its mid-length at around the level of the orbits before widening again slightly in the anterior half. A shorter anterior extension separates the vomers for most of their length, although the extent is unclear in the holotype. In metoposaurids, the parasphenoid’s ventral exposure terminates in a fossa (the fodina intervomeris), which may be represented by a crushed region just posterior to the transvomerine teeth of the vomer. This anterior extension is noticeably angled (in palatal view) such that it is increasingly elevated above the plane of the vomers (depressed when viewed ventrally) along their contact.

A few additional details can be gleaned from UMMP 13820, UMMP 13822, UMMP 13823, and UMMP 14154. These mostly confirm inferences based on the holotype, such as that the exoccipitals are divided by the parasphenoid (UMMP 13822; [Fig. 13](#)); the anteriormost extent of the parasphenoid lies well anterior to the interpterygoid vacuities, thereby prominently dividing the vomers for most of their length (UMMP 13820, UMMP 13823; [Figs. 10, 16](#)); the longitudinal orientation of the parasphenoid-pterygoid suture (UMMP 13820, UMMP 13823; [Figs. 10, 16](#)); and the narrowing at the mid-length of the cultriform process (UMMP 13820 and UMMP 13823; [Figs. 10, 16](#)). It is difficult to determine any variability in the ornamentation of the basal plate because it is variably damaged (either fractured or weathered) in the holotype, UMMP 13823, UMMP 13956, and UMMP 14154, but there is at least no evidence that some specimens legitimately lacked such ornamentation. In UMMP 13820 and UMMP 13823, there are very faint striations oriented longitudinally along the cultriform process for most of its length ([Figs. 10, 16](#)); as these are not bounded by ridges, grooves, pits, or other features of ornamentation found on the basal plate, we do not consider this to be an extension of the ornamentation proper. The same feature appears in a small fragment associated with UMMP 14098 that we tentatively identify as part of the parasphenoid ([Figs. 19C and 19D](#)); a foramen on the unornamented side of this fragment may be the internal carotid artery foramen. The dorsal surface of the parasphenoid is otherwise only visible in the partial parasphenoid associated with the palatal fragments of UMMP 14098 ([Fig. 19A](#)); based on the preserved region, only the lateralmost extent of the basal plate is preserved. There is a socket-like fossa located ventromedial to the pterygoid depression that opens anteromedially; this is the facet for the epipterygoid. While the parasphenoid-pterygoid suture relative to the fossa is not clear, a laterally facing foramen posterior to this fossa and just anterior to the pterygoid-exoccipital suture likely represents the foramen for the internal carotid artery, which is always enclosed within the parasphenoid. The artery is mostly covered by a transverse parapterygoid crest. The partial basal

plates of UMMP 13956 and UMMP 14098 (separate from the above fragment of this specimen) confer no additional details.

Pterygoid.—The pterygoid is a complex element with two discrete processes, the palatine and quadrate rami, in the holotype ([Fig. 7](#)). The element is sutured to the basal plate of the parasphenoid medially with a prominent interdigitating suture. This contact is anteroposteriorly long, and there is no discrete basipterygoid process, as with most stereospondyls. In contrast to many other stereospondyls, however, the metoposaurid parasphenoid-ptyerygoid suture is distinctly shorter than the length of the basal plate of the parasphenoid, being truncated posteriorly by the exoccipital extending to contact the pterygoid. From the basicranial suture, the palatine ramus extends anterolaterally to meet the jugal and the ectopterygoid, and the quadrate ramus extends posterolaterally to meet the quadrate. Both jointly frame the sub-triangular subtemporal fenestra, which is widest posteriorly between the rami. The palatine ramus is mostly flat but thickens along its medial edge where it frames the interptyerygoid vacuity. Along the lateral edge, it expands slightly to form a posterolaterally convex transverse flange. The edge of this flange curves ventrally. There is faint ridging on the right palatine ramus that is oriented parallel to its long axis. The quadrate ramus is unornamented and without developed features. It is also flat and slightly narrower than the palatine ramus when compared at the base or in their greatest widths. It sheaths the medial surface of the quadrate. The pterygoid also has an ascending lamina that extends along most of the dorsal surface of the quadrate ramus; this is visible in occipital view, although it is fractured and broken on both sides. The oblique crest that projects posteriorly from this lamina is broken off dorsally. Ventral to the oblique crest and at about the same height as the dorsal margin of the occipital condyle is a deep, posterolaterally facing depression termed the ‘ptyerygoid depression’ by [Sulej \(2007\)](#). The referred specimens contribute little additional data regarding the ventral exposure of the pterygoid. UMMP 13822 and UMMP 13823 preserve the most developed transverse flanges with the posteroventrolaterally descending edge ([Figs. 13, 16](#)). UMMP 13822 preserves the most distinctive ornamentation, but all specimens with a sufficiently complete palatine ramus preserve at least some ridging. UMMP 13820, UMMP 13822, and UMMP 14154 have the most complete and undistorted pterygoids in occipital view ([Figs. 11, 14, 23](#)). These specimens all preserve a more complete ascending lamina with a distinct oblique crest that is roughened along its dorsal margin. These specimens also show the dorsal contact of the ascending lamina with the squamosal such that there is no palatoquadrate fissure, as well as the broad contact laterally with the pterygoid. The pterygoid-squamosal suture is often difficult to discern, whether due to fracturing, incomplete preparation, or a tight contact. This contact is largely obscured in occipital view by the oblique crest. Features of the dorsal surface of the pterygoid are best identified from the partial palate of UMMP 14098 ([Fig. 19A](#)), from the isolated associated pterygoid of UMMP 14099 ([Fig. 29E](#)), from an isolated pair of partial pterygoids (UMMP 12969; [Fig. 30G](#)), and from a series of isolated partial right pterygoids (UMMP 13771, UMMP 13794, UMMP 13795, UMMP 13796; [Figs. 29A–29D](#)). A large conical recess facing anteromedially along the parasphenoid-ptyerygoid suture

is for articulation with the epipterygoid (Figs. 19A, 29), which remains distinct except in very large (presumably mature) specimens (Sulej, 2007). The cross section of the ascending lamina is elongate and teardrop-shaped, being wider laterally and narrowing towards the parasphenoid. A dorsoventrally short and mediolaterally narrow ridge extends posteriorly along the short posteromedial process of the pterygoid that abuts the exoccipital; the ridge then continues onto the exoccipital (Figs. 19A; 30F–30J). In UMMP 14098, a large foramen is present near the distal end of the quadrate ramus on the posterior surface and ventrolateral to the oblique crest that was not exposed in other specimens (Fig. 20E).

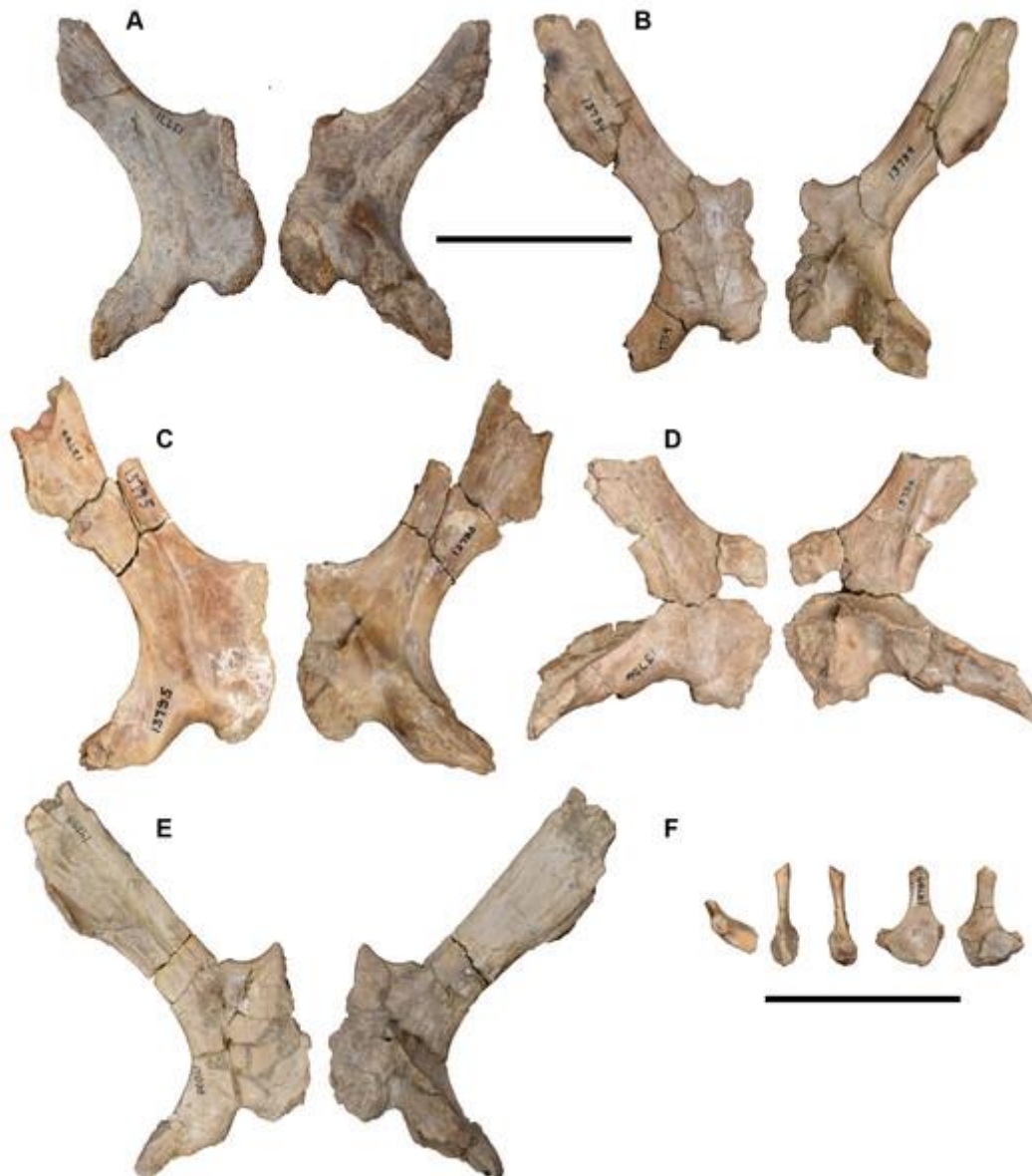


Figure 29: Isolated right pterygoids and left epipterygoid referred to *Buettnererpeton bakeri*.

(A) UMMP 13771 in ventral (left) and dorsal (right) view; (B) UMMP 13794 in ventral (left) and dorsal (right) view; (C) UMMP 13795 in ventral (left) and dorsal (right) view; (D) UMMP 13796 in ventral (left) and dorsal (right) view; (E) UMMP 14099 in ventral (left) and dorsal (right) view; (F) UMMP 13787 in dorsal, anteromedial, posterolateral, anterolateral, and posteromedial view from left to right. Scale bars equal to 5 cm.

[Download full-size image](#)

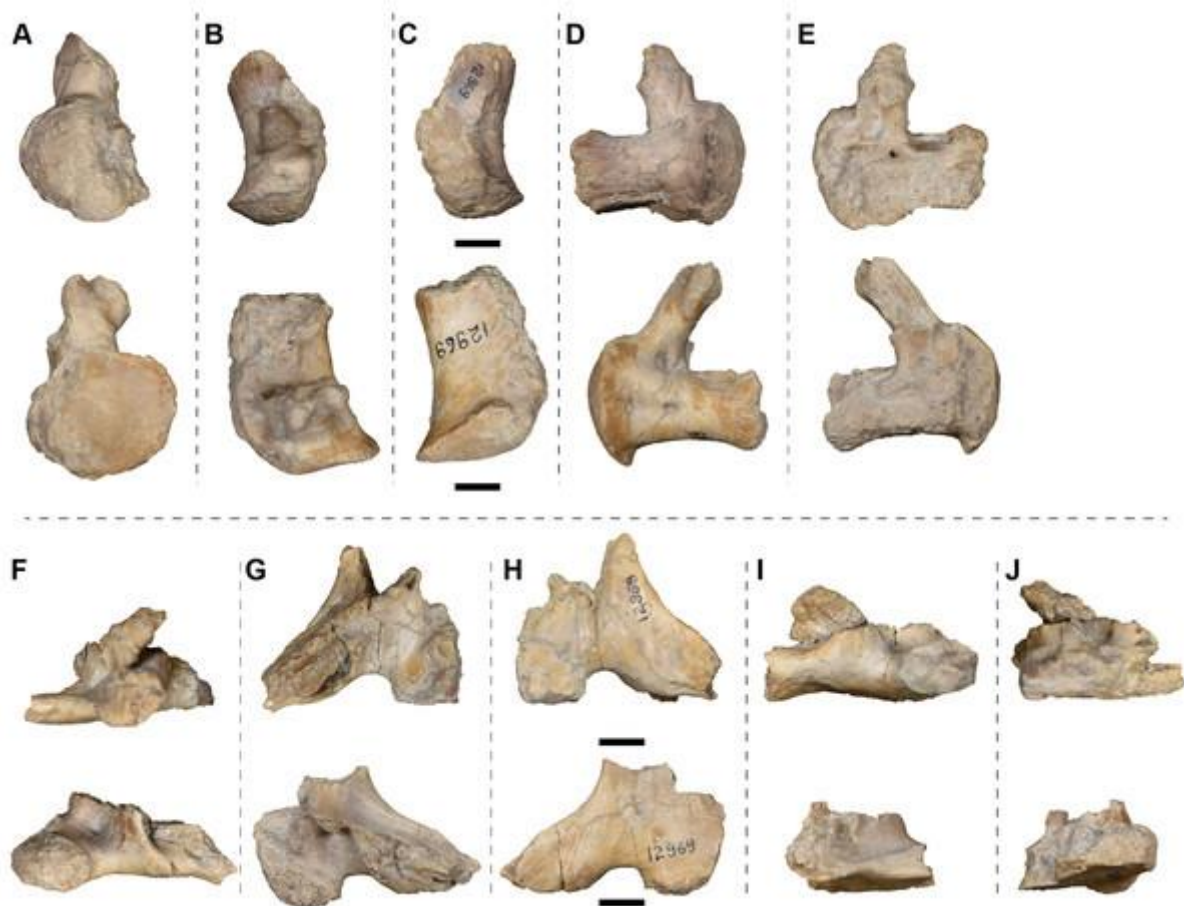


Figure 30: Isolated posterior cranial elements (exoccipitals and partial pterygoids) referred to *Buettnererpeton bakeri*, UMMP 12969.

(A) Partial exoccipitals in posterior view; (B) the same in dorsal view; (C) the same in ventral view; (D) the same in lateral view; (E) the same in medial view; (F) partial pterygoids and exoccipitals in posterior view; (G) the same in dorsal view; (H) the same in ventral view; (I) the same in lateral view; (J) the same in medial view. For parts A–E, the left exoccipital is on the top row, and the right exoccipital (not necessarily of the same individual) is on the bottom row. The same siding applies to parts F–J. The same element is imaged in different views horizontally. Scale bars equal to 1 cm.

[Download full-size image](#)

DOI: [10.7717/peerj.14065/fig-30](https://doi.org/10.7717/peerj.14065/fig-30)

Vomer.—The vomer is a large, subtriangular element that forms most of the palate in the snout region in the holotype ([Fig. 7](#)). In this specimen, it is incomplete anteriorly and laterally on both sides, and the posterior process that extends along the cultriform process, partially excluding the latter from the anteromedial margin of the interpterygoid vacuities, is only fully defined on the ventral left side. The vomer is largely excluded from the anterior margin of the interpterygoid vacuity by a medial process of the palatine. It has a broad contribution to the medial margin of the choana; its extent anterior to the opening and its relationship to the maxilla are uncertain. Its relation to the anterior palatal fenestra is also unclear in this specimen. The vomer has two sockets for ‘fangs’ anterior to the choana. A single row of small parachoanal teeth curves along the medial margin of the choana

toward the palatine. The parachoanal row is mostly continuous, but there are gaps medial and posterior to the ‘fangs’ that separate it from the transvomerine row. Although tooth sockets can be vaguely identified, the preservation is not sufficient to count the parachoanal positions. The transverse transvomerine row of teeth that extends between the pairs of vomerine ‘fangs’ just anterior to the fodina intervomeris is not complete on either side, but there is room for at least nine positions in the row on the left vomer.

Only UMMP 13820 and UMMP 13823 contribute additional data on the vomer ([Figs. 10, 16](#)). UMMP 13820 is preserved similarly to the holotype, with the lateral margins being unknown, but it does preserve the anterior contact with the premaxillae, demonstrating that the vomers contribute to framing the anterior palatal fenestrae ([Fig. 10](#)). There is room for at least five positions in the transvomerine row on each side; there is a wide gap along the midline that lacks teeth or evidence of sockets. In UMMP 13823, the sutures of the vomer are essentially fully defined ([Fig. 16](#)). The vomer can be seen to have a broad contribution to the anterior margin of the choana, where it shares a long contact with the maxilla. Minor asymmetry in the posterior extent of the posterior processes is observed. The right parachoanal row, which can be clearly seen to extend onto the palatine in this specimen, preserves room for at least 25 tooth positions, including two adjacent to the vomerine ‘fangs’; teeth in this position are not found in other specimens or on the left side of this specimen. There are five to six positions on each side of the transvomerine row, with a gap around the midline; this gap is narrower than in UMMP 13820.

Palatine.—The palatine is a ‘Y-shaped’ element that is broadest anteriorly, where it forms much of the anterior margin of the interpterygoid vacuity and the posterior and lateral margins of the choana in the holotype ([Fig. 7](#)). Along the anterolateral margin is a pair of sockets for two ‘fangs.’ A broken ‘fang’ is found in the more posterior socket. The posterior suture with the ectopterygoid is not fully resolved because there are several transverse breaks that occur in this general region and that could plausibly have occurred along the suture. [Case \(1931\)](#) figured the suture at about the level of the mid-length of the orbit, which does correspond to an existing crack. This agrees with the position of the suture in other metoposaurids (e.g., [Sulej, 2007](#); [Lucas et al., 2016](#)), and if it is assumed that this is the correct interpretation ([Fig. 7](#)), then there are around 14 tooth positions (posterior to the ‘fang’ sockets) on the palatine. The posterior margin of the choana is damaged in the holotype, but a slight elevation in this region suggests that the parachoanal tooth row that begins on the vomer also extends onto the palatine.

UMMP 13823 is the only referred specimen with an equally complete palatine ([Fig. 16](#)). The sutures are fully resolved in this specimen and interestingly show a palatine-ectopterygoid suture that is not continuously transverse but instead stepped, with a posteromedial process extending along the anteromedial edge of the ectopterygoid; this feature is common in lydekkerinids (e.g., [Hewison, 1996, 2007](#); [Shishkin, Rubidge & Kitching, 1996](#)). The longitudinal position of the suture is essentially in the same position as the holotype (the mid-length of the orbit). This specimen also confirms the continuation of the parachoanal tooth row

onto the palatine. The right palatine preserves 12 tooth positions posterior to the ‘fang’ pair, similar to the estimated 14 positions in the holotype. The palatine is barely uncovered in UMMP 13820 and UMMP 13822 and confers no additional data in those specimens.

Ectopterygoid.—The ectopterygoid is a narrow rectangular element that carries much of the palatal tooth row and that frames the interpterygoid vacuity laterally in the holotype ([Fig. 7](#)). It is longer than the palatine and of a similar width throughout. It ends in a tapering terminus that partially divides the palatal exposures of the maxilla and the jugal. The pterygoid-ectopterygoid suture is not fully resolved, but as preserved, the ectopterygoid does not contribute to the palatine ramus and has a broad contribution to the interpterygoid vacuity. Following the above assumption regarding the palatine-ectopterygoid suture in the holotype, there would be approximately 40 tooth positions on the ectopterygoid. There are no ectopterygoid ‘fangs,’ although dentition is not preserved in the anteriormost region of the ectopterygoid in this specimen.

As with the palatine, only the ectopterygoid of UMMP 13823 contributes substantial data ([Fig. 16](#)) – those of UMMP 13820 and UMMP 13822 are barely uncovered. UMMP 13823 substantiates the observations made in the holotype and corroborates the inferences of an ectopterygoid that contributes to the interpterygoid vacuity margin but not to the palatine ramus. There are at least 38 tooth positions on the ectopterygoid, similar to the estimated 40 positions in the holotype, and the absence of ectopterygoid ‘fangs’ is verified. Small foramina on the lingual side of the teeth are noted on the ectopterygoid.

Quadrate.—The quadrate is a robust element that is incompletely ossified in the holotype ([Figs. 7](#) and [8](#)). It is framed laterally by a ventral process of the quadratojugal that forms a cup-like socket. Medially it is sheathed by the quadrate ramus of the pterygoid. The descending lamina of the squamosal typically frames the quadrate from above, but this is not well-preserved on either side, although it can be concluded that the quadrate did not contribute to the paraquadrate foramen. In ventral view, the quadrate is triangular, expanding medially. The ventral surface is mostly covered in unfinished bone and is very slightly convex along the sagittal axis. The posterior (occipital) surface of the quadrates is damaged in this specimen, but it is posteriorly convex and largely unfinished ventrally and then forms an anterodorsally directed sheet of bone towards the squamosal and other roofing elements. Whether a supratrochlear tubercle (the ‘hyoid tubercle’ in many early diverging stereospondyls) was present is not discernible given the damage, but this appears to become more distinctive in specimens of *Metoposaurus krasiejowensis* that are both larger than those described here and relatively large within the known sample ([Sulej, 2007](#):fig. 16) and may be a late-stage ontogenetic feature.

The quadrate of UMMP 13820 is mostly obscured ventrally ([Fig. 10](#)), but its occipital profile is similar to that of the holotype in being posteriorly convex and covered by unfinished bone ([Fig. 11](#)). No supratrochlear tubercle is apparent. The lateral suture with the quadratojugal and the medial suture with the pterygoid are mostly resolved in this view, but the suture with the squamosal is not. UMMP

13822 has a well-preserved and ventrally exposed quadrate that shows the proportions, sutures, and textured unfinished surface (Fig. 13). The sutures on the occipital surface are most apparent from this specimen (Fig. 14) and do not conflict with those of other specimens. No supratrochlear tubercle is apparent. The quadrates of UMMP 13823 are slightly damaged, and the occipital exposure is not well-differentiated with respect to sutures, but the left quadrate does preserve what appears to be a supratrochlear tubercle just lateral to the contact with the quadrate ramus (Fig. 16). This is not the largest specimen described here, but it is on the higher end of the documented size range of partial to complete skulls. The quadrate of the articulated palatal fragments associated with UMMP 14098 can be viewed in all profiles (Figs. 19A, 19B, 20E, 20F), but the ventral and occipital surfaces are in agreement with other specimens, and the lateral and medial surfaces are largely obscured by the quadratojugal and the pterygoid, respectively. The dorsal and anterior surface are largely smooth and without notable features like foramina or ornamentation.

Epipterygoid.—An epipterygoid is not clearly identified in the holotype. There is a structure recessed within the posterior skull (visible posterolaterally, not shown here), ventral to the tabular and dorsal to the medial origin of the quadrate ramus of the pterygoid that is in the correct position to be a slightly dislodged epipterygoid. However, diagnostic features of an epipterygoid are not identified.

An epipterygoid is exposed in UMMP 13822, which can be viewed medially due to the incompleteness of the specimen (Fig. 15B). It sits below the supratemporal and above the base of the palatine ramus of the pterygoid. It has been dislodged on account of the compression of the skull such that the dorsal process projects nearly horizontally and medially, and the base is therefore largely obscured. The epipterygoid is more clearly exposed in UMMP 14154, also on account of the incompleteness of the specimen, as both of them are preserved and in articulation (Fig. 21). They comprise a transversely broad base that tapers into a blade-like dorsal stem. Based on the left side of the specimen, it does not appear that the epipterygoid contacted the skull roof. The most information on the epipterygoid comes from UMMP 13787, an isolated element (Fig. 29F). Based on this specimen, the epipterygoid is rather simple, being flat and with only two regions, a fan-shaped expanded base and a narrow dorsal stem. One side of the base is thicker than the other, producing two roughened surfaces that face ventrally; these do not form distinct facets *per se* but also do not form a continuous surface. The only other notable feature is a foramen that pierces the center of the base.

Stapes.—The dorsal stem of the right stapes is visible in the right otic region of the holotype when viewed posteriorly (Fig. 8). It is long and slender, with an oval cross-section, but it has been dislodged to project posteriorly and is not exposed proximally. No other elements of the otic capsule were identified.

Articulated stapedes are also found in UMMP 13820 (on both sides; Fig. 11), UMMP 13823 (on the right side; Fig. 16), UMMP 14098 (on the right side; Figs. 18B, 20A), and UMMP 14154 (both sides; Fig. 23). Those of UMMP 13820 and UMMP 13823 are only exposed distally and confer no additional information. The footplate can be observed in UMMP 14098 and UMMP 14154 on account of the

incompleteness of these specimens. In UMMP 14098, the stapes has been dislodged against the skull roof but is otherwise in the approximate natural position. The morphology of the stapes comprises an expanded base without any apparent stapedia foramen that tapers into a dorsal stem that has a narrow oval cross-sectional profile. There is no groove on the posterior surface of the dorsal stem, but the surface is shallowly troughed in this region. In UMMP 14154, the left stapes is articulated and fully exposed, and the posterior surface of the stem bears a distinct longitudinal groove that deepens proximally and medially. The stapes is also known from two isolated stapedes (UMMP 13777; [Fig. 31](#)). Neither is complete, but they permit characterization of the proximal portion in all views. The partially divided base is evident and marked by two disparately sized roughened articular facets. Some workers (*e.g.*, [Sulej, 2007](#)) consider only the larger of the facets (the dorsal one) to be the footplate. This process is not as developed in UMMP 13777 as in *Metoposaurus krasiejowensis*, in which it is substantially larger than the other process and prominently projects outward. The posterior groove that is prominent in UMMP 14154 is barely developed here. As with the holotype, no other elements of the otic capsule were identified in articulation or in isolation.

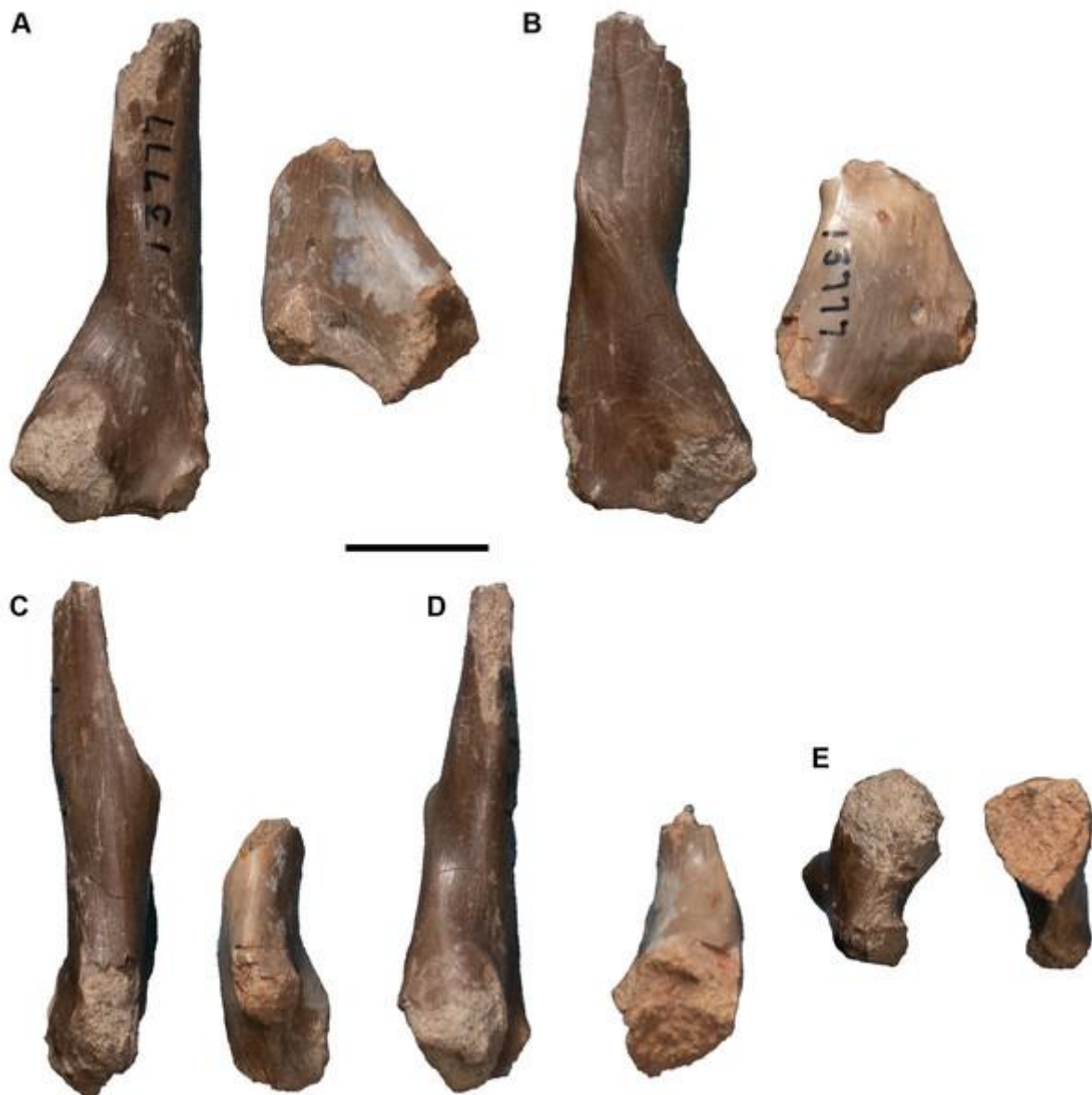


Figure 31: Isolated stapedes referred to *Buettnererpeton bakeri*, UMMP 13777.

(A) Photograph in view 1; (B) photograph in view 2 (rotated 180 degrees relative to A); (C) photograph in view 3 (rotated 90 degrees relative to B); (D) photograph in view 4 (rotated 180 degrees relative to C); (E) photograph in proximal view. Scale bar equals to 1 cm.

[Download full-size image](#)

DOI: [10.7717/peerj.14065/fig-31](https://doi.org/10.7717/peerj.14065/fig-31)

Exoccipital.—The exoccipital is a stout element with two processes, a posteriorly directed one to form the occipital condyle and an anterodorsally directed one to frame the foramen magnum in the holotype (Figs. 7 and 8). Ventrally, the exoccipital sutures to the parasphenoid and probably to the pterygoid, but the latter is not defined in the holotype (Fig. 7). Whether the exoccipitals met medially or were separated by the basal plate of the parasphenoid is also uncertain. In occipital view, the exoccipital forms a dorsally ascending column that abuts the postparietal and the tabular (Fig. 8). The left side is badly distorted, but the right side appears to show that the exoccipital does not contribute to the posttemporal foramen. The foramen magnum is distorted but was originally subdivided by a medially

projecting lamellose process at the mid-height; this process is more complete on the right side. The posteriorly convex occipital condyle is circular in posterior profile and with an unfinished bone surface. The columnar occipital pillars of the exoccipitals are angled posteroventrally such that they have a noticeable exposure in dorsal view, but the posttemporal foramina and the foramen magnum are not exposed. Weathering has obscured any smaller nerve foramina that are typically present.

The exoccipitals are preserved in articulation in UMMP 13820, UMMP 13822, UMMP 13823, UMMP 13956, and UMMP 14154 ([Figs. 10, 11, 13, 14, 16, 17, 22, 23](#)). Most of these preserve a clear suture with the pterygoid in ventral view. UMMP 13822 appears to show a separation of the exoccipitals medially by the parasphenoid ([Fig. 13](#)). Some distortion has occurred in the occipital region of all of these specimens such that the foramen magnum is not symmetrical and is poorly defined in some cases. The least distorted foramen magnum is preserved in UMMP 13956 in which it appears that the dorsal portion was at least wider, and perhaps larger in total surface area, than the ventral portion ([Fig. 17C](#)). Compression in UMMP 13822 and UMMP 13823 also appears to have pushed the exoccipitals more posterior such that their dorsal exposure is greater than in the other specimens ([Figs. 12, 16](#)). The overall morphology of the element is the same as in the holotype, but UMMP 13822 and UMMP 14154 differ in that they show a clear contribution of the exoccipital to the margin of the posttemporal foramen ([Figs. 14, 23](#)). Two sets of isolated exoccipitals are present, UMMP 12969 (in part; [Figs. 30A–30E](#)) and UMMP 13819 ([Fig. 32](#)). Similar to the partial to complete skulls ([Figs. 8, 11, 14, 16, 17, 23](#)), the profile of the occipital condyle is slightly variable, ranging from a more oblate shape to a more circular shape ([Figs. 30A–30E, 32](#)). The partial or isolated elements contribute the most data regarding the passage of nerves and/or blood vasculature. In UMMP 13820, a foramen is visible on the ventral surface of the right exoccipital ([Fig. 10](#)), which may represent one exit for the hypoglossal nerve (XII). A foramen in the same position was only identified in UMMP 14154 (on both sides; [Fig. 22](#)) but may be absent in other specimens due to fracturing in this region. Nerve foramina that may represent other exits for this nerve are also commonly found on the lateral and medial surface of the base of the ascending column of the exoccipital (UMMP 12969, UMMP 13819, UMMP 13956, UMMP 14098, UMMP 14154; [Figs. 19A, 20B–20D, 21, 30D, 30E, 32D, 32E](#)). The foramen that is consistently found on the lateral surface of the base can be seen to continue through to a medial exit (*e.g.*, UMMP 14098; [Figs. 20B, 20C](#)). In UMMP 14098, in addition to the foramina on the medial and lateral surface of the base, there are two other foramina on the medial surface ([Fig. 20C](#)). A small one is positioned posterior to the nerve foramen, and a larger one is positioned anterior to the nerve foramen; these could well represent additional exits for the nerve but could alternately be for vasculature. Two pierce the base of the column, the larger of the two being more laterally positioned and directed posteroventrally. The third is oriented anteroposteriorly and enters the condyle at the center of its cross-section. Some other specimens have additional foramina ventral to this position (*e.g.*, UMMP 13819; [Fig. 32E](#)), whereas

others exhibit no foramina despite being well-preserved (e.g., UMMP 12969; [Fig. 30E](#)). Finally, foramina are also consistently identified on the anterior face of the occipital pillar at its base, which can be seen in dorsal view when the pillar is damaged (e.g., UMMP 14098; [Fig. 20D](#)). This foramen apparently connects with any foramina on the lateral surface below the one at the base of the pillar, as well as with any foramen that has shifted to be positioned along the ventral surface and with a longitudinal canal that extends as far anteriorly as the element is preserved.



Figure 32: Isolated exoccipitals referred to *Buettnererpeton bakeri*, UMMP 13819.

(A) Posterior view; (B) dorsal view; (C); ventral view; (D) lateral view; (E) medial view. The same element is imaged in different views horizontally. Scale bars equal to 1 cm.

[Download full-size image](#)

DOI: [10.7717/peerj.14065/fig-32](https://doi.org/10.7717/peerj.14065/fig-32)

We consider it highly likely that at least one foramen within the exoccipital is for the hypoglossal nerve (XII) based on other temnospondyls (e.g., [Säve-Söderbergh, 1936](#); [Sawin, 1941, 1945](#); [Wilson, 1941](#); [Romer & Witter, 1942](#); [Shishkin & Sulej, 2009](#); [Maddin, Reisz & Anderson, 2010](#); [Witzmann et al., 2012](#)), but the maximum

number of exits and whether this might be variable is unclear. [Case \(1932:fig. 12\)](#) depicted the course of two canals, but this was based on an exoccipital of *Anaschisma browni* from Rotten Hill whose taphonomic damage exposes the entire course of the canals. Whether both canals identified by [Case \(1932\)](#) are for the hypoglossal nerve is unclear, especially if they are fully separated as Case argued. [Sulej \(2007\)](#) suggested that both canals might be for veins in *Metoposaurus krasiejowensis*. At least one could alternatively be for the vagus nerve (X; [Dutuit, 1976](#)), and there is always the possibility that multiple nerves and/or blood vessels (e.g., the jugular vein) passed through a single foramen (e.g., [Case, 1931](#)). Resolving the neurology further requires tomographic analysis to clearly map the canals in 3D and to ascertain their connectivity (e.g., [Arbez, Dahoumane & Steyer, 2017](#); [Gee, 2020a](#)).

Other neurocranial ossifications.—Additional ossifications of the braincase, like the sphenethmoid, were not apparent in any of the specimens, as with most other metoposaurids. If the sphenethmoid ossified in this taxon, it likely would only have done so at a much larger size based on *Anaschisma browni* ([Wilson, 1941](#)) and *Dutuitosaurus ouazzoui* ([Dutuit, 1976](#)). There is also no evidence for an ossified basioccipital or an ossified synotic tectum (the ‘supraoccipital’ in crown amniotes); the absence of the latter results in the keyhole-shaped foramen magnum. *Palatal plates.*—A notable feature in UMMP 13823 is the presence of more than 50 small plates in the anterior right interpterygoid vacuity ([Figs. 16A and 16B](#)). [Case \(1932\)](#) identified these as scleral ossicles, a reasonable conclusion since they occur near the orbit, but there is a distinct variability in size and shape of these plates ([Fig. 16B](#)). This variability is not often found in scleral ossicles, but it is found in palatal plates that would have filled the interpterygoid vacuities (as documented in metoposaurids by [Sulej, 2007](#), and as summarized in temnospondyls by [Gee, Haridy & Reisz, 2017](#)). Given the count of the plates (which is also quite high for the scleral ossicles of a single eye), it might be predicted that these plates occurred throughout the vacuity but were accidentally removed during preparation in this specimen. The same might be true in other specimens, but alternatively, the relatively coarse sediment suggests sufficient energetics to dislodge loose elements prior to preservation (as with the scleral ossicles). No true scleral ossicles were identified by us.

Mandibular material. There are eight hemimandibles only one of which was associated with a skull (UMMP 13823), in addition to MCZ 1054, a specimen that was exchanged in the 1930s and that we did not personally examine. [Case \(1932\)](#) also listed a complete hemimandible (UMMP 13946) that we could not physically locate. Examination of collections records revealed that this specimen was exchanged with the Museum of Comparative Zoology (MCZ) in May 1932 and now bears the number MCZ 1056; likely, it was part of the same exchange as UMMP 13821 (= MCZ 1054) and was unnoted in Case’s publication. The description follows the general structure of the cranial description with the caveat that there is no lower jaw associated with the holotype, so all specimens are described in a single section per element.

The hemimandible is typical for metoposaurids, which otherwise exhibit very little variation in morphology and dentition (Brusatte et al., 2015). Complete hemimandibles are represented by UMMP 13823, UMMP 13944, and UMMP 13947 (Figs. 33–35). Case (1932:figs. 21, 22) figured UMMP 13823 as his representative of the lower jaw, likely because it is the only hemimandible associated with a skull, but the specimen currently has a large patch of plaster adhered to the labial side of the tooth row. This was not figured by Case, who did not figure the labial surface, so the plaster was likely added later to stabilize the specimen. The lingual surface is also heavily fractured and the Meckelian foramen is not so perfectly oblate, two features that were not figured by Case. There is plaster infilling on the lingual surface near the symphysis, possibly interrupting the adsymphyseal tooth row. The fractures seem to be taphonomic rather than recent, so Case’s original figures should be regarded more as reconstructions than as specimen illustrations. The remaining five hemimandibles are incomplete (Fig. 36).

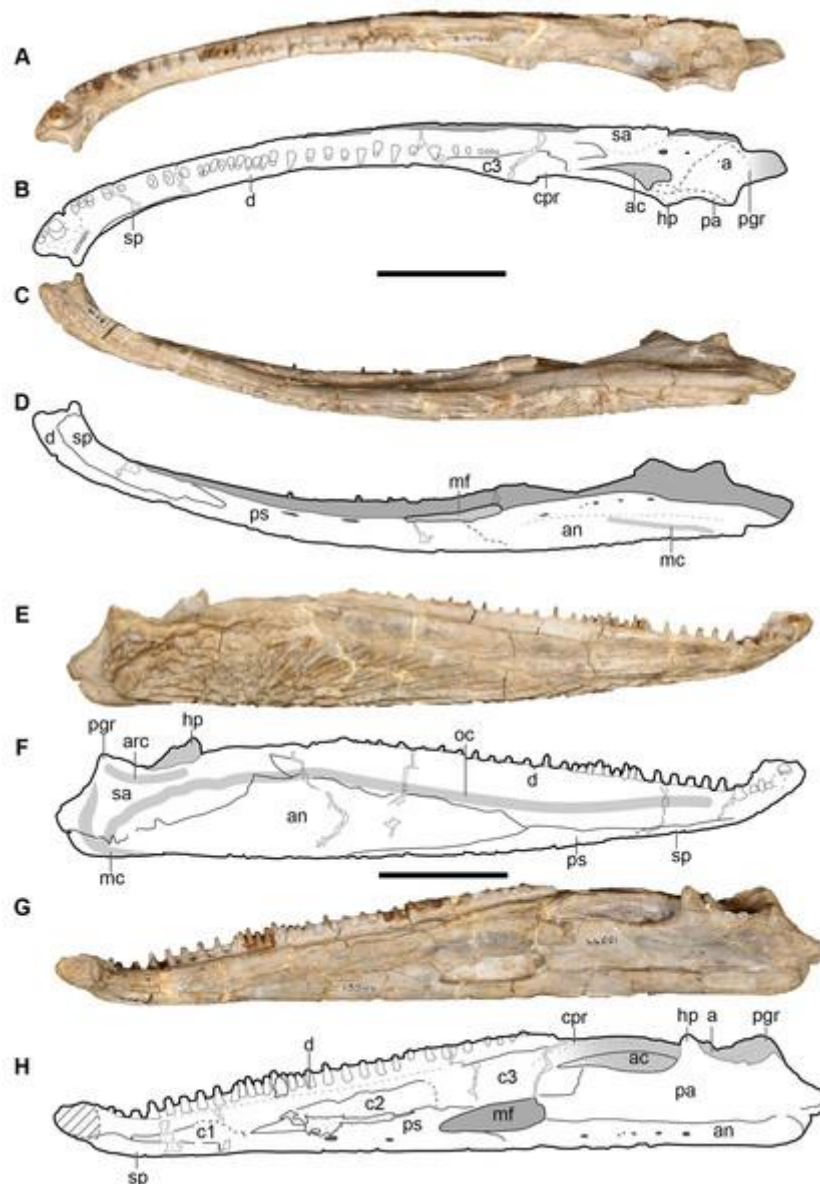


Figure 33: Right hemimandible referred to *Buettnererpeton bakeri*, UMMP 13944.

(A) Photograph in dorsal view; (B) interpretive drawing of the same; (C) photograph in ventral view; (D) interpretive drawing of the same; (E) photograph in labial view; (F) interpretive drawing of the same; (G) photograph in lingual view; (H) interpretive drawing of the same. Abbreviations: a, articular; ac, adductor chamber; amf, anterior Meckelian foramen; an, angular; c1, first coronoid (“precoronoid”); c2, second coronoid (“intercoronoid”); c3, third coronoid (“coronoid”); cpr, coronoid process; d, dentary; hp, hamate process; mf, Meckelian foramen; pa, prearticular; ps, postsplenial; sa, surangular; sp, splenial. Scale bars equal to 5 cm.

[Download full-size image](#)

DOI: [10.7717/peerj.14065/fig-33](https://doi.org/10.7717/peerj.14065/fig-33)

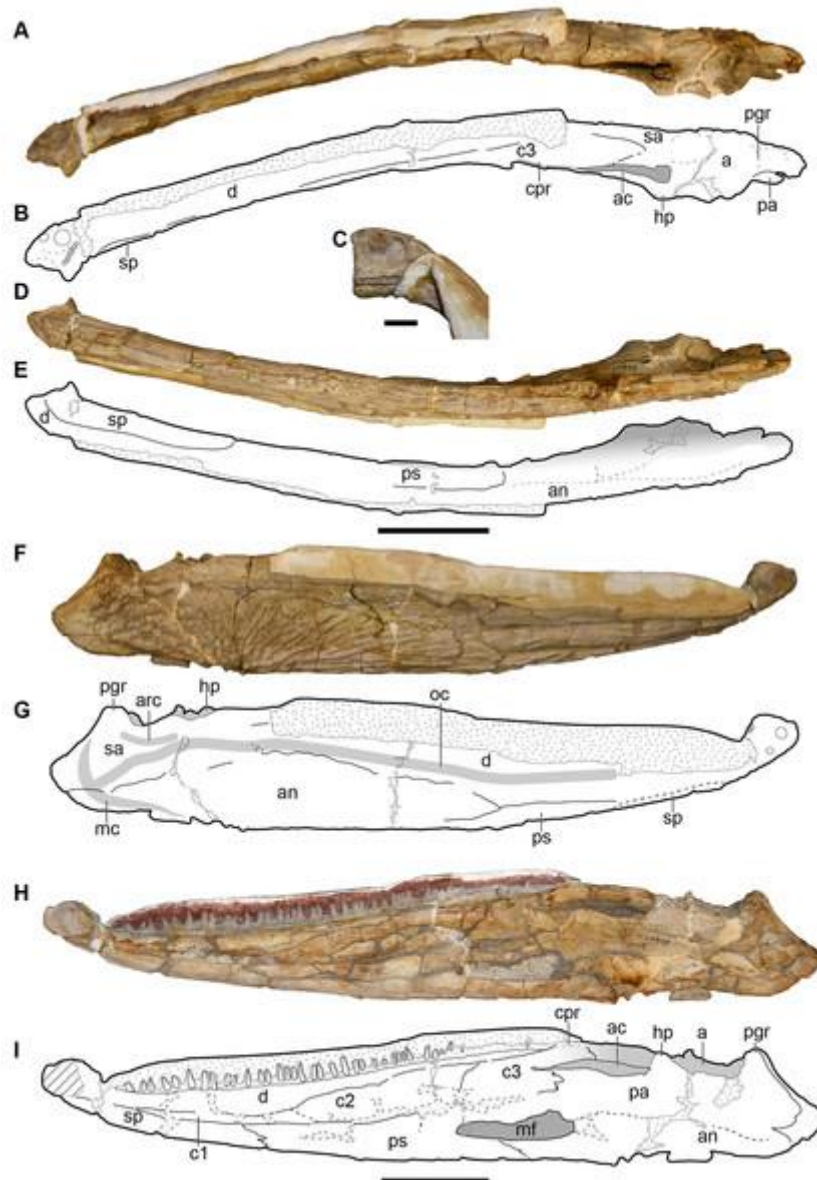


Figure 34: Right hemimandible referred to *Buettnererpeton bakeri*, UMMP 13823.

(A) Photograph in dorsal view; (B) interpretive drawing of the same; (C) photograph in ventral view; (D) interpretive drawing of the same; (E) photograph in labial view; (F) interpretive drawing of the same; (G) photograph in lingual view; (H) interpretive drawing of the same. Abbreviations: a, articular; ac, adductor chamber; an, angular; c1, first coronoid (“precoronoid”); c2, second coronoid (“intercoronoid”); c3, third coronoid (“coronoid”); cpr, coronoid process; d, dentary; hp, hamate process; mf, Meckelian foramen; pa, prearticular; ps,

postsplenial; sa, surangular; sp, splenial. Note that this hemimandible is associated with the skull in [Fig. 12](#). Scale bars equal to 5 cm.

[Download full-size image](#)

DOI: [10.7717/peerj.14065/fig-34](https://doi.org/10.7717/peerj.14065/fig-34)

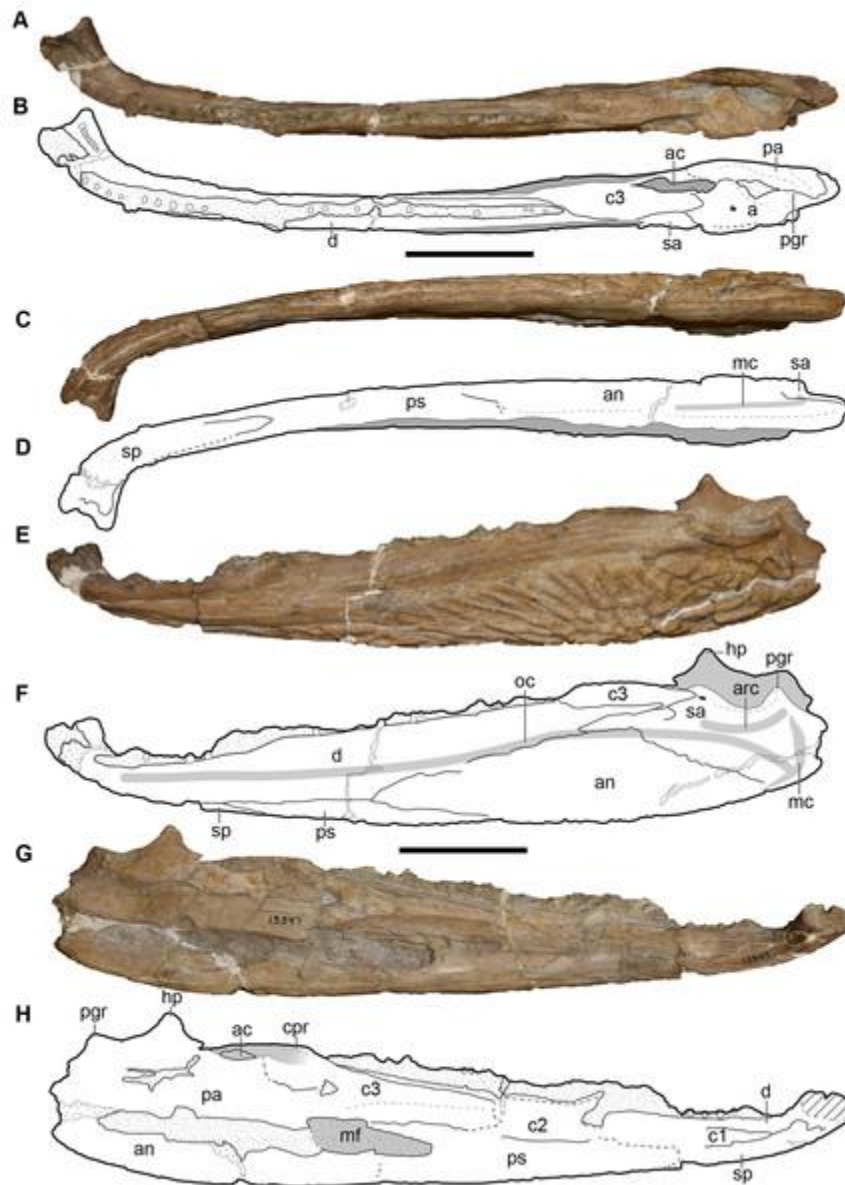


Figure 35: Left hemimandible referred to *Buettnererpeton bakeri*, UMMP 13947.

(A) Photograph in dorsal view; (B) interpretive drawing of the same; (C) photograph in ventral view; (D) interpretive drawing of the same; (E) photograph in labial view; (F) interpretive drawing of the same; (G) photograph in lingual view; (H) interpretive drawing of the same. Abbreviations: a, articular; ac, adductor chamber; an, angular; c1, first coronoid (“precoronoid”); c2, second coronoid (“intercoronoid”); c3, third coronoid (“coronoid”); cpr, coronoid process; d, dentary; hp, hamate process; mf, Meckelian foramen; pa, prearticular; ps, postsplenial; sa, surangular; sp, splenial. Scale bars equal to 5 cm.

[Download full-size image](#)

DOI: [10.7717/peerj.14065/fig-35](https://doi.org/10.7717/peerj.14065/fig-35)



Figure 36: Partial hemimandibles in dorsal, ventral, lingual, and labial views (top to bottom) referred to *Buettnererpeton bakeri*.

(A) UMMP 13975, nearly complete left hemimandible; (B) UMMP 13827, partial right surangular; (C) UMMP 13828, partial left surangular; (D) UMMP 13949, partial posterior left hemimandible; (E) UMMP 13948, partial posterior right hemimandible; (F) UMMP 12970, partial anterior left hemimandible; (G) UMMP 13945, partial anterior left hemimandible. Scale bars equal to 5 cm.

[Download full-size image](#)

DOI: [10.7717/peerj.14065/fig-36](https://doi.org/10.7717/peerj.14065/fig-36)

The overall morphology of the hemimandible of *Buettnererpeton bakeri* aligns with the conserved morphology among other metoposaurids. It has a slight curvature along the longitudinal axis that becomes more pronounced towards the symphysis, which curves slightly upward as it turns medially (Figs. 33A–33D, 35A–35D, 36A, 36F, 36G). The symphyseal region curves slightly upward as well such that the symphyseal surface faces dorsomedially. The hemimandible increases in height posteriorly to the termination of the tooth row, where the dorsal margin of the labial wall of the adductor chamber forms a low, dorsally convex coronoid

process ([Figs. 33E–33H, 34F–34I, 35E–35H](#)). The labial wall is thus higher than the lingual wall ([Figs. 33G, 33H, 34H, 34I](#)). The glenoid is an obliquely angled facet, more transverse than longitudinal; it is framed anterolingually by the hamate process of the prearticular and by the postglenoid ridge posteriorly. The postglenoid area (PGA) forms a short boss with a squared-off posterior end ([Figs. 33–35](#)). Ornamentation is primarily found along the ventral margin and on the posterolabial surface (primarily the angular). Circular pitting radiates outward into grooves dorsally from the ventral margin. A prominent oral canal is also found on the labial surface, extending anteriorly from the PGA for much of the length ([Figs. 33E, 33F, 34F, 34G, 35E, 35F](#)). It joins with a short mandibular canal on the labial surface of the postglenoid region. A shorter and disconnected articular canal is found on the labial surface just below the postglenoid ridge and dorsal to the oral canal.

Dentary.—The dentary is the only tooth-bearing element in the metoposaurid hemimandible ([Figs. 33–35](#)). It has a long and tall labial and ventral exposure, which is ornamented towards the ventral margin of the hemimandible, and a shorter lingual exposure. It overlies the splenial, the postsplenial, and the angular on the labial surface and the splenial and all three coronoids on the lingual surface. Like the upper dentition, the mandibular teeth are conical, non-pedicellate, and monocuspid. Faint external striations marking the plicidentine can sometimes be noted. There are 36 partial teeth preserved with room for at least an additional 22 teeth in UMMP 13944 ([Fig. 33](#)); this is more positions (58) than was suggested by Case based on the hemimandible associated with UMMP 13823 (45 positions; [Fig. 34](#)). One symphyseal ‘fang’ is partially preserved with a large socket for a second ‘fang’ in UMMP 13944 ([Fig. 33](#)). In this specimen, the ‘fangs’ intercede into the marginal tooth row such that there are two positions at the end of the symphysis and the rest of the tooth row on the other side of the ‘fangs’ ([Figs. 26A and 26B](#)). At least eight adsymphyseal tooth positions are identified on the lingual surface of the symphysis. This tooth row is somewhat variable; UMMP 13823 has 10 positions in the adsymphyseal row, whereas UMMP 13944 and UMMP 13947 may have as few as eight. One other source of variation in the dentition is in the number of marginal teeth anterior to the symphyseal ‘fangs’; there may be room for three positions in UMMP 13944 compared to two positions in UMMP 13823. Features suggested by Case to be diagnostic of this species among metoposaurids, like the presence of an adsymphyseal row, are no longer diagnostic ([Konietzko-Meier & Wawro, 2007](#)).

Coronoid series.—There are three coronoids, as with almost all temnospondyls, although this is only discernible when all of the data are taken together because complete sutures between all three are not preserved in any single specimen ([Figs. 33G, 33H, 34H, 34I, 35G, 35H](#)). [Case \(1932\)](#) only identified two (with his ‘coronoid I’ encompassing the middle and the posterior coronoids), but his identification is refuted by the defined suture between the middle and the posterior coronoids in UMMP 13823 ([Figs. 34H and 34I](#)). No teeth are present on any of the coronoids in any specimen, as with all other metoposaurids.

Splénial.—The splénial is a short element at the front of the hemimandible with a narrow labial exposure and a broader lingual exposure, ventral to the dentary and anterior to the postsplénial (Figs. 33–35). The splénial does not contribute to the symphysis (Figs. 33C, 33D, 35C, 35D), a feature shared only with *Arganasaurus azerouali* and *Dutuitosaurus ouazzoui* (Buffa, Jalil & Steyer, 2019).

Postsplénial.—The postsplénial is a more elongate element with a similarly narrow labial exposure and a broader lingual exposure (Figs. 33–35). It underlies the coronoids and appears to have contacted all three, although only the middle coronoid shares a substantial contact. The postsplénial contributes to the anterior margin of the Meckelian foramen (sometimes the Meckelian window), an elongate oval that tapers anteriorly to a rounded tip; it appears undistorted in UMMP 13944 (Figs. 33G and 33H) but is slightly distorted in the other specimens (Figs. 34H, 34I, 35G, 35H). Anteriorly within the postsplénial are two small foramina, not fully prepared out, the more anterior of these is usually termed the anterior Meckelian foramen.

Prearticular.—The prearticular is a long element that is only exposed lingually (Figs. 33G, 33H, 34H, 34I, 35G, 35H). It forms the posterior margin of the Meckelian foramen, ventral to the posterior coronoid and dorsal to the angular. It also forms most of the lingual wall of the adductor chamber, including the prominent dorsally projecting hamate process, as well as the lingual edge of the glenoid. Posteriorly, it frames the chorda tympanic foramen, which is frequently distorted in these specimens and in metoposaurid hemimandibles in general.

Angular.—The angular is a long element with a broad labial and ventral exposure (Figs. 33–35). Labially, it sutures to the surangular posterodorsally, to the dentary anterodorsally, and to the postsplénial anteriorly. It bears most of the ornamentation on the labial surface but only a small portion of the oral canal (Figs. 33E, 33F, 34F, 34G, 35E, 35F). On the lingual surface, it forms the posteroventral margin of the Meckelian foramen, suturing to the postsplénial anteriorly and to the prearticular dorsally (Figs. 33G, 33H, 34H, 34I, 35G, 35H).

Surangular.—The surangular has a broad triangular labial exposure, forming most of the labial wall of the adductor chamber and extending to the posterior end of the hemimandible (Figs. 33E, 33F, 34F, 34G, 35E, 35F). It wedges anteriorly between the dentary and the angular and expands in height posteriorly to form the labial surface of the PGA.

Postcranial material.

Axial material.—The vertebral column is represented by one atlas (UMMP 13792, Fig. 37) isolated intercentra (UMMP 12945, UMMP 118525, UMMP 118526, UMMP 118527, Figs. 38–43), neural arches (UMMP 13870; UMMP 14205, Figs. 44A–44C), and haemal arches (UMMP 13779, Figs. 44D and 44E). Case (1932:27) described 45 intercentra as having been scattered within the bonebed, but he did not indicate any specimen number(s) and photographed an apparently random set of only nine (in presumed anterior view). During our visit, we identified 41 intercentra (in addition to one complete atlas, two isolated pairs of neural arches, and one pair of isolated chevrons) in a single drawer, divided between four boxes. One box with 13 intercentra was catalogued as

UMMP 12945 and is associated with the Elkins bone bed ([Figs. 38, 40–43](#)). The other three boxes (with five, six, and seventeen intercentra) contained intercentra of the same size and preservation as UMMP 12945 but had no specimen numbers or collections information at the time of our examination. However, we were able to tentatively identify intercentra in the uncatalogued boxes among those figured by [Case \(1932:pl. IV, fig. 3\)](#), confirming that they are from the locality. The discrepancy between the 41 intercentra that we examined and Case's purported 45 might lie in the four non-intercentra vertebral specimens noted above. There is no apparent organization among the four boxes (*e.g.*, by inferred region of the axial column or by inferred association to a single individual). For example, UMMP 12945 includes at least one postcervical intercentrum, three presacral intercentra, two perisacral intercentra, and four postsacral intercentra. Specimen numbers have thus been assigned for the three boxes that previously lacked any (UMMP 118525, UMMP 118526, and UMMP 118527; [Figs. 38–43](#)), rather than assigning all of the material to UMMP 12945.

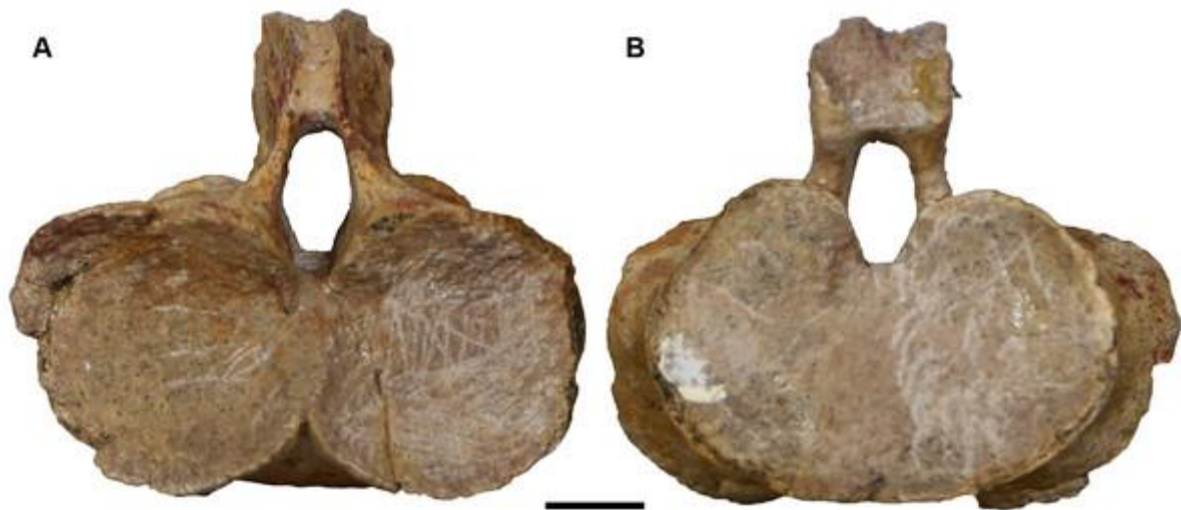


Figure 37: Isolated atlas referred to *Buettnererpeton bakeri*, UMMP 13792. (A) Anterior view; (B) posterior view. Scale bar equal to 1 cm.

[Download full-size image](#)

DOI: [10.7717/peerj.14065/fig-37](https://doi.org/10.7717/peerj.14065/fig-37)



Figure 38: Isolated possible axis (A) and postcervical (B–F) intercentra in anterior, posterior, dorsal, ventral, and left lateral views (left to right) referred to *Buettnererpeton bakeri*.

(A, C, F) UMMP 118525 (in part); (B) UMMP 12945 (in part); (D) UMMP 118527 (in part); (E) UMMP 118526 (in part). For dorsal and ventral views, anterior is facing up. Scale bars equal to 1 cm.

[Download full-size image](#)

DOI: [10.7717/peerj.14065/fig-38](https://doi.org/10.7717/peerj.14065/fig-38)



Figure 39: Isolated anterior dorsal (A–E) and mid-dorsal (F–H) intercentra in anterior, posterior, dorsal, ventral, and left lateral views (left to right) referred to *Buettnererpeton bakeri*.

(A–F, H) UMMP 118525 (in part); (G) UMMP 118526 (in part). For dorsal and ventral views, anterior is facing up. Scale bars equal to 1 cm.

[Download full-size image](#)

DOI: [10.7717/peerj.14065/fig-39](https://doi.org/10.7717/peerj.14065/fig-39)



Figure 40: Isolated presacral intercentra in anterior, posterior, dorsal, ventral, and left lateral views (left to right) referred to *Buettnererpeton bakeri*.

(A, C, E) UMMP 12945 (in part); (B, D) UMMP 118527 (in part); (F–H) UMMP 118525 (in part). For dorsal and ventral views, anterior is facing up. Scale bars equal to 1 cm.

[Download full-size image](#)

DOI: [10.7717/peerj.14065/fig-40](https://doi.org/10.7717/peerj.14065/fig-40)



Figure 41: Isolated perisacral intercentra in anterior, posterior, dorsal, ventral, and left lateral views (left to right) referred to *Buettnererpeton bakeri*.

(A, C) UMMP 12945 (in part); (B, D) UMMP 118526 (in part); (E) UMMP 118525 (in part). For dorsal and ventral views, anterior is facing up. Scale bars equal to 1 cm.

[Download full-size image](#)

DOI: [10.7717/peerj.14065/fig-41](https://doi.org/10.7717/peerj.14065/fig-41)



Figure 42: Isolated anterior caudal (postsacral) (A–D), caudal (E), and small indeterminate position (F–G) intercentra in anterior, posterior, dorsal, ventral, and left lateral views (left to right) referred to *Buettnererpeton bakeri*.

(A, B, D, F) UMMP 12945 (in part); (C) UMMP 118525 (in part); (E, G) UMMP 118527 (in part). For dorsal and ventral views, anterior is facing up. Scale bars equal to 1 cm.

[Download full-size image](#)

DOI: [10.7717/peerj.14065/fig-42](https://doi.org/10.7717/peerj.14065/fig-42)



Figure 43: Indeterminate intercentra in anterior, posterior, dorsal, ventral, and left lateral views (left to right) referred to *Buettnererpeton bakeri*.

(A, B, E) UMMP 12945 (in part); (C) UMMP 118525 (in part); (D) UMMP 118526 (in part); (F) UMMP 118527 (in part). For dorsal and ventral views, anterior is facing up. Scale bars equal to 1 cm.

[Download full-size image](#)

DOI: [10.7717/peerj.14065/fig-43](https://doi.org/10.7717/peerj.14065/fig-43)



Figure 44: Isolated neural arches (A–C) and haemal arches (D, E) in (A) dorsal, ventral, anterior, posterior, and left lateral views (left to right) and (B–E) in dorsal, ventral, lateral, and medial views (left to right) referred to *Buettnererpeton bakeri*. (A) UMMP 14205; (B) left caudal neural arch, UMMP 13780 (in part); (C) partial right caudal neural arch, UMMP 13780 (in part); (D) partial right haemal arch, UMMP 13779 (in part); (E) partial right haemal arch, UMMP 13779 (in part). In dorsal and ventral views, anterior is facing up. Scale bars equal to 1 cm.

[Download full-size image](#)

DOI: [10.7717/peerj.14065/fig-44](https://doi.org/10.7717/peerj.14065/fig-44)

The atlas is complete and relatively undistorted (Fig. 37). The posterior surface of the intercentrum is a single face, indented dorsally for the notochordal canal. The anterior face is divided into the two facets for the occipital condyles, which meet medially. There are no diapophyses on the co-ossified neural arch or parapophyses on the lateral surface of the intercentrum. The ventral surface is smooth except at the anterior midline below the union of the two facets. The co-ossified neural arch has a short neural spine that projects posterodorsally at a steep angle. Vertical ridges along the anterior face of the spine are barely developed.

One intercentrum is tentatively identified as an axis intercentrum (Fig. 38A). In anterior view, this intercentrum is more dorsoventrally short than the others giving it a more quadrangular appearance. It bears a broad parapophysis on the lateral surface that is confluent with both the anterior and the posterior faces. The body of the intercentrum is opisthocoealous with a strongly convex anterior condyle and a concave posterior cotyle. A notochordal pit is present on the dorsal aspect of both the anterior and the posterior face.

Given the lack of articulated axial columns of North American metoposaurids, the following identifications are based on those of Dutuit (1976) and Sulej (2007) and should be viewed as tentative assignments to general axial regions (Figs. 38–42).

Nearly all of the intercentra form dorsally-closed discs as is typical for metoposaurids with one exception described below. Six intercentra could not be confidently assigned to an axial position due to poor preservation of the

parapophyses, arguably the most definitive feature for determining the position in presacral intercentra (Fig. 43).

The postcervical and anterior dorsal intercentra were identified based on the broad, unfinished parapophyses on the posterior aspect of the lateral surface (Fig. 38). Postcervical intercentra differ from anterior dorsal intercentra in the angle of the parapophysis with the former being more vertical, however, gradational changes between intercentrum types can make assignment to a given region problematic. As noted previously, one postcervical intercentrum is included in UMMP 12945 (Fig. 38B), three are included in UMMP 118525 (Figs. 38A, 38C, 38E), one in UMMP 118526 (Fig. 38E), and one in UMMP 118527 (Fig. 38D). Five anterior dorsal intercentra are included in UMMP 118525 (Figs. 39A–39E). The postcervical and anterior dorsal intercentra all have a sometimes-faint indentation on the dorsal aspect of the anterior and posterior face for the notochord. There are only three mid-dorsal intercentra identified based on a single, short parapophysis, with one included in UMMP 118525 (Figs. 39F and 39H) and another in UMMP 118526 (Fig. 39G). A notochordal pit is also present on the anterior and posterior face of the mid-dorsal intercentra.

Presacral (Fig. 40) and perisacral (Fig. 41) intercentra are by far the most common vertebral elements recovered from the Elkins bone bed, making up about one third of the recovered intercentra. The presacral intercentra can be identified by the presence of an anterior parapophysis and rounded posterior parapophysis (Fig. 40) as opposed to the more pointed posterior parapophysis of perisacral (Fig. 41) and anterior caudal intercentra (Figs. 42A–42D). Three presacral intercentra are included in UMMP 12945 (Figs. 40A, 40C, 40E), two are included in UMMP 118527 (Figs. 40B and 40D), and three are included in UMMP 118525 (Figs. 40F–40H). The perisacral intercentra are identified by a broad anterior parapophysis and a broad, pointed posterior parapophysis (Fig. 41). The unfinished surfaces of the anterior and the posterior parapophyses of the perisacral intercentra contact one another. Two perisacral intercentra are included in UMMP 12945 (Figs. 41A and 41C), two are included in UMMP 118526 (Figs. 41B and 41D), and one is included in UMMP 118525 (Fig. 41E).

Anterior caudal (“postsacral”) intercentra lacking co-ossified haemal arches are also present and primarily identified by the broad, pointed and ventrally placed posterior parapophyses (Figs. 42A–42D). The anterior caudal intercentra can also be tentatively identified by a slightly more dorsoventrally oblong shape in anterior view. Two anterior caudal intercentra are confidently identified in UMMP 12945 (Figs. 42A and 42B), one is tentatively identified in UMMP 12945 (Fig. 42D), and one is tentatively identified in UMMP 118525 (Fig. 42C). Among these intercentra, the indentation on the anterior and posterior faces for the notochord is variably present with no clear pattern in size or axial position.

One caudal intercentrum of UMMP 118527 (Fig. 42E) was previously identified as such by Case (1932:pl. IV, fig. 3) with broken haemapophyses co-ossified on the ventral surface. The intercentrum is wedge-shaped in lateral view and dorsally open unlike all of the other intercentra present. This is the only putative caudal intercentrum from the Elkins bone bed. Two small, probable pre- to “postsacral”

intercentra of UMMP 12945 ([Fig. 42F](#)) and UMMP 118527 ([Fig. 42G](#)) are difficult to assign to an axial region due to poorly defined parapophyses. These two intercentra are noteworthy in being anteroposteriorly shorter than their transverse width like most large metoposaurid intercentra (with the exception of *Dutuitosaurus*) and unlike the elongate intercentra of the small-bodied *Apachesaurus*.

UMMP 14205 is identified as a mid-dorsal to anterior caudal (“postsacral”) neural arch ([Fig. 44A](#)) based on the size and position of the prezygapophyses in comparison with examples of *Metoposaurus krasiejowensis* described by [Sulej \(2007:figs. 32, 37\)](#). The spine is short and unossified dorsally where the two halves meet. The prezygapophyses are short and anteriorly directed. A shallow anteroposterior groove is present on the underside of each descending flank of the neural arch.

UMMP 13780 is a pair of partial caudal neural arches ([Figs. 44B](#) and [44C](#)) previously identified by [Case \(1932:p. 28–29\)](#) as possible haemapophyses. The ventral margin is convex and unossified. There is a small protuberance, here identified as the prezygapophysis, anteriorly from the dorsal region. The dorsal extension of the neural spine is incomplete in both arches. These caudal neural arches are essentially indistinguishable from those of *Metoposaurus krasiejowensis* ([Sulej, 2007:figs. 34–35](#)).

UMMP 13779 is two partial right haemal arches consisting of the articular surfaces with the ventral intercentrum and missing the more distal portion where the chevron tapers to a cylindrical rod ([Figs. 44D](#) and [44E](#)).

Nineteen isolated ribs are also identified. Two sets of ribs with no clear association (UMMP 13776 and UMMP 13788) and two large individual ribs (UMMP 13778 and UMMP 13783) are present in the collection. Most of the ribs are essentially complete with both the proximal and distal ends preserved, but a few are incomplete, missing one or both ends. [Sulej \(2007\)](#) categorized metoposaurid ribs by ‘type’, and those ‘types’ are tentatively identified here. One issue noted by [Sulej \(2007:80\)](#) is an overlap between ontogenetic change and differences in adjacent rib positions. Because of this, all identifications apart from a cervical rib (‘type A’) and an anterior caudal rib (‘type J’) should be viewed as generalized morphological assignments and not necessarily reflective of axial position.

A single putative cervical rib or ‘type A rib’ is present in UMMP 13788 ([Fig. 45A](#)). This identification is based on the fully distinct tuberculum and capitulum. This rib is very sharply curved and bears a well-defined ridge on the dorsal surface extending and widening distally with furrows along the anterior and posterior sides. The anterior margin of the shaft forms a blade-like edge. There is a shallow depression on the ventral surface of the proximal end.



Figure 45: Isolated cervical (type A) and anterior dorsal (type C) ribs in anterior, dorsal, posterior, and ventral views (left to right) and on the far right, in proximal and distal views (top to bottom) referred to *Buettnererpeton bakeri*, UMMP 13788 (in part). (A) left rib; (B and C) right ribs. (A) type A rib; (B) type C rib; (C) partial, proximal type C rib. Scale bars equal to 1 cm.

[Download full-size image](#)

DOI: [10.7717/peerj.14065/fig-45](https://doi.org/10.7717/peerj.14065/fig-45)

Two partial ‘type C’ ribs are present and identified by a broad distal expansion ([Fig. 45B](#)) or oval proximal end with a modestly differentiated capitulum and tuberculum ([Fig. 45C](#)). The proximal end of one rib is broken, but a shallow furrow can be seen along the length of the ventral surface. On the other rib, a furrow extends to the proximal end on both the dorsal and ventral surface ([Fig. 45C](#)). The distal end is like a flattened comma in cross-section. However, this rib lacks the distinct bend at the midpoint of other ‘type C’ ribs (*e.g.*, [Sulej, 2007:fig. 38D₂](#)) but has a gradual curve instead.

UMMP 13778 is a single rib of a large individual in two pieces ([Case, 1932:30](#), expressed some uncertainty; [Fig. 46A](#)). This rib is mostly straight and with a massively expanded proximal end that is damaged but that appears to have a similar cross-section to that of UMMP 13783. The distal end is not expanded with an oblate cross-section. It appears to be a ‘type E’ or ‘type F,’ with a ridge on the proximal end extending to about the mid-shaft. The crest is however not well-defined. The size discrepancy is such that it could conceivably be proposed to be an ontogenetic variation. Additional potential ‘type E/F’ ribs are similar in size, but often missing one or both ends ([Figs. 46B](#) and [46C](#)).



Figure 46: Isolated left, mid-dorsal (type E or F) ribs in anterior, dorsal, posterior, and ventral views (left to right) and on the far right, in proximal and distal views (top to bottom) referred to *Buettnererpeton bakeri*.

(A) UMMP 13778; (B and C) UMMP 13788 (in part). B is incomplete on the proximal end and D is incomplete on the distal end. Scale bars equal to 1 cm.

[Download full-size image](#)

DOI: [10.7717/peerj.14065/fig-46](https://doi.org/10.7717/peerj.14065/fig-46)

At least five ‘type H’ ribs are present in the collection with three of similar or transitional morphology between rib types adjacent to ‘type H’. Each of these ribs is relatively straight with little curvature and with a broadly expanded proximal end. UMMP 13783 is a single rib of a large individual (Fig. 47A). It is relatively straight and without uncinata processes, closely resembling the ‘type H’ or ‘type I’ of Sulej (2007). The proximal end has a distinct division of the tuberculum and the capitulum, forming a kidney-bean-shaped cross-section. This is notably different from the subtriangular cross-section of the ‘type H’ ribs, but this rib is about twice the size of the same rib types described by Sulej (2007:fig. 38L). The distal end is not expanded and has an oblate cross-section. A sharp crest extends for most of the length of the shaft. One border also had a thicker ridge that extends for most of the length of the rib. Two of the remaining ribs (Figs. 47B and 47C) have a flattened comma-like cross-section of the proximal end with a very modest curvature. This may be a transition between the oval cross-section of ‘type G’ ribs and the more exaggerated comma of ‘type H’ ribs. The cross-section of the proximal end of the remaining ribs (Figs. 47D–47H) resembles the more typical comma shape of Sulej’s ‘type H’ ribs. Each of the smaller ribs (Figs. 47B–47H) tapers to a slight constriction at the distal end of the shaft. There is some variation in the curvature, which may have been compressed in one direction.

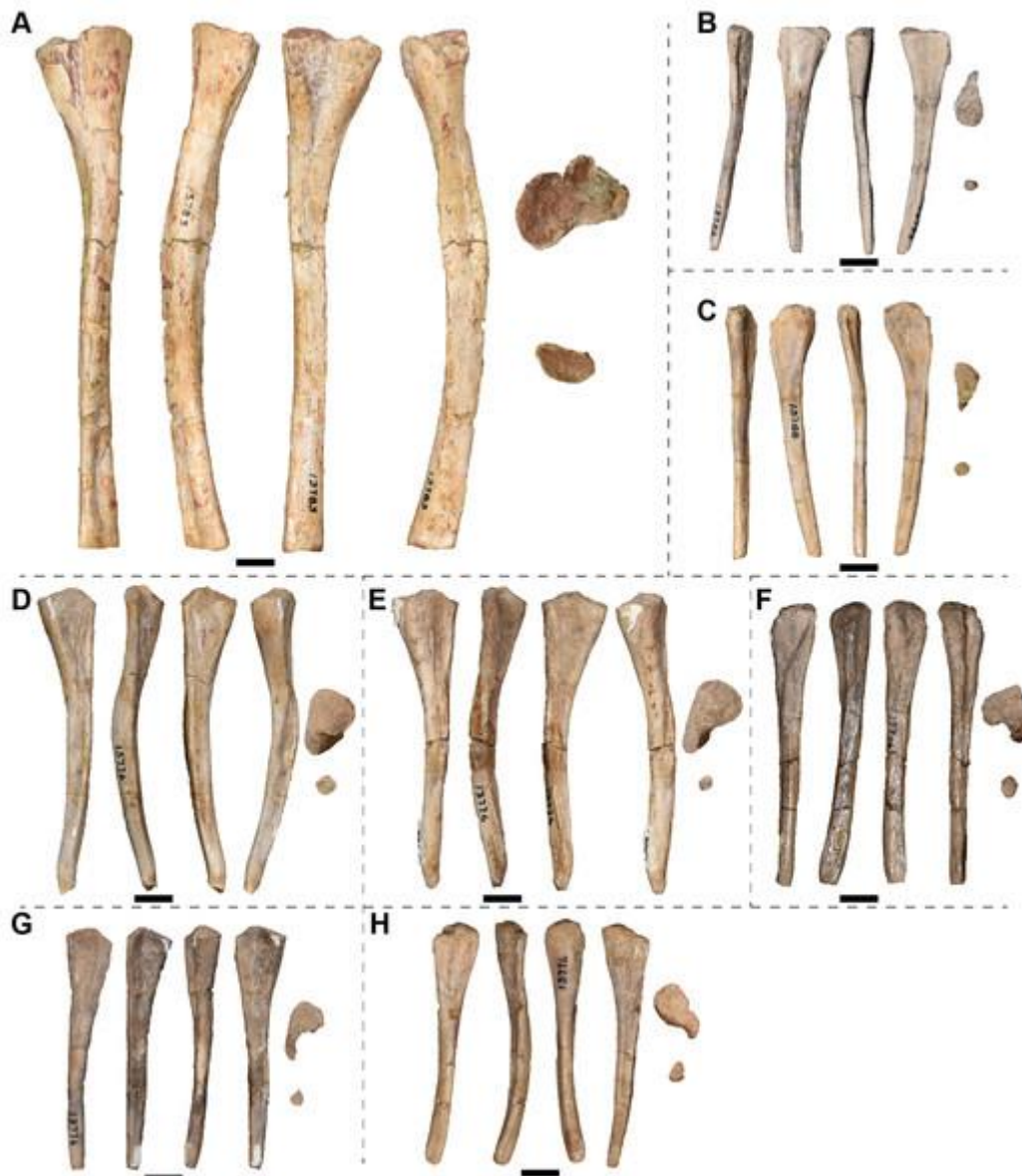


Figure 47: Isolated posterior dorsal (types G and H or H/I) ribs in anterior, dorsal, posterior, and ventral views (left to right) and on the far right, in proximal and distal views (top to bottom) referred to *Buettnererpeton bakeri*.

(A–D, F, H) Left ribs; (E, G, I–K) right ribs. (A) Type H/I rib; (B and C) type G/H ribs; (D–H) type H ribs. (A) UMMP 13783; (B and C) UMMP 13788 (in part); (D–H) UMMP 13776 (in part). Scale bars equal to 1 cm.

[Download full-size image](#)

DOI: [10.7717/peerj.14065/fig-47](https://doi.org/10.7717/peerj.14065/fig-47)

The five remaining ribs are likely perisacral or caudal in origin, being relatively short and straight and with a greatly expanded proximal end. One rib of UMMP 13788 ([Fig. 48A](#)) appears to be a large ‘type I’ or ‘type J’ rib with the proximal end subcircular in cross-section and with a slight extension that may represent the attachment of the capitulum. The distal end of this rib is incomplete, but a prominent ridge extends down the ventral surface. There is a slight bend just prior to the mid-length and a modest curvature in the rib shaft at the distal end. Two putative ‘type I’ ribs are present under UMMP 13788 ([Figs. 48B](#) and [48C](#)). These

ribs are exceptionally short, although it is not clear if the distal end is entirely complete in the shortest one (Fig. 48B). The cross-section of each of these is flattened with a pronounced anterior and posterior expansion. The prominent ridge of one rib (Fig. 48D) missing both the proximal and distal end is similar to that of the putative large ‘type I/J’ rib, but this identification is tentative due to a lack of informative morphology. A single ‘type J’ rib was identified under UMMP 13776 (Fig. 48E). This rib has the comma-shaped cross-section of the proximal end and tapers to a point in the distal shaft. The curvature of the ‘type J’ rib appears greater than the perisacral ribs with the possible exception of the ‘type I/J’ rib (Fig. 48A). A ridge extends down one edge of the ‘type J’ rib (Fig. 48E).



Figure 48: Isolated perisacral (type I) or anterior caudal (type J) ribs in anterior, dorsal, posterior, and ventral views (left to right) and on the far right, in proximal and distal views (top to bottom) referred to *Buettnererpeton bakeri*.

(A, D and E) Right ribs; (B and C) left ribs. (A) Large type I/J rib; (B and C) type I ribs; (E and F) type J ribs. (A–D) UMMP 13788 (in part); (E) UMMP 13776 (in part). A is incomplete on the distal end and D is incomplete on the proximal and distal ends. Scale bars equal to 1 cm.

[Download full-size image](#)

DOI: [10.7717/peerj.14065/fig-48](https://doi.org/10.7717/peerj.14065/fig-48)

Pectoral girdle material.—UMMP 13786 is a fragmentary element identified as a ‘puboischium?’ by Case (1932). However, an ossified pubis has never been identified in a metoposaurid, and it probably remained cartilaginous along with the carpals and tarsals. The ischium is a simple wedge-shaped element without many distinctive features (*e.g.*, Sulej, 2007). It is relatively narrow. Crucially, most of the margins of the element appear damaged, which suggests that the wedge-shaped profile, somewhat superficially similar to the metoposaurid ischium, is not reflective of the true shape. We propose here that this is not a largely complete ‘puboischium’ (reiterating that there is no evidence for an ossified or co-ossified pubis in metoposaurids) but that this is instead a partial scapula, mostly damaged ventrally, that was incorrectly oriented and misidentified, likely because of the post-mortem damage. Firstly, a clearly broken, squared-off surface that would have

to be the dorsally facing articular surface for the ilium under Case's interpretation is actually the part of the scapula dorsal to the supraglenoid foramen. This is supported by the observation that there is a bifurcation along this surface, with a ridge deviating from the main axis of the element (Fig. 49C); in a complete element, this would continue to diverge to form a broad glenoid. A groove divides the bifurcation, with a small foramen nestled inside. The supraglenoid foramen is large in metoposaurids (e.g., Sulej, 2007:fig. 47), so it is not surprising that the element would fracture in that region. The only definitively undamaged margin of smooth, finished bone is a short concave surface that leads into this bifurcation. Under Case's interpretation, this would be adjacent to the acetabulum and thus either the anterior or posterior margin of the 'puboischium,' but under our interpretation, it would represent the dorsal portion of the posterior margin of the scapula (and is consistent with that of other metoposaurids in this regard). The opposing surface (the ventral margin of Case's 'puboischium') is then the anterior margin of the scapula, and the roughened, uneven margin reflects the articulation with the cleithrum (see also Sulej, 2007). A convex surface of unfinished bone that joins the anterior and posterior margins would be the muscular crest of the scapula. In summation, the element was incorrectly oriented by Case, leading to his misinterpretation of the element as a wedge-shaped 'puboischium'; the element instead possesses all the expected features of an incomplete scapula. The scapula is rare among North American taxa – for example, none were reported from the Rotten Hill bonebed (Lucas et al., 2016) – so it is unsurprising that a fragmentary one was misidentified by Case. UMMP 13786 represents the only scapula from this locality.

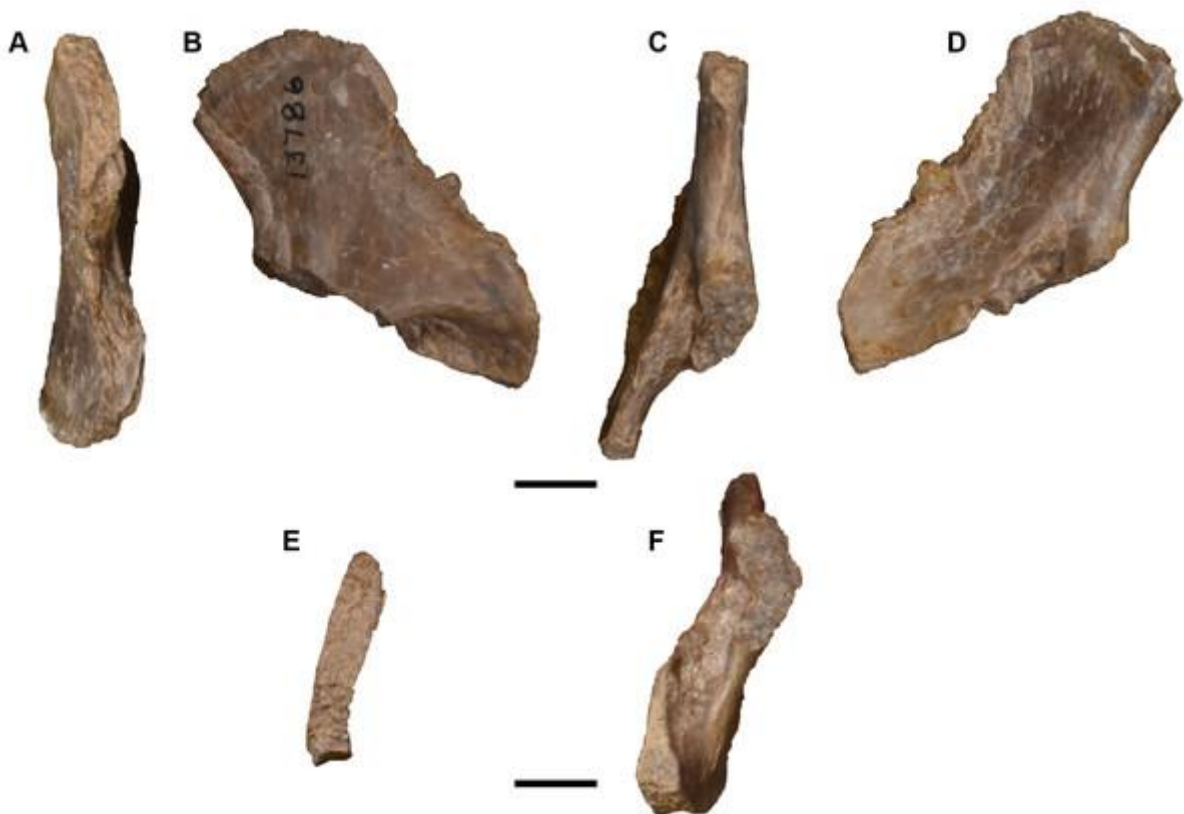


Figure 49: Photographs of partial left scapula referred to *Buettnererpeton bakeri*, UMMP 13786.

(A) Anterior view; (B) medial view; (C) posterior view; (D) lateral view; (E) dorsal view; (F) ventral view. Scale bars equal to 1 cm.

[Download full-size image](#)

DOI: [10.7717/peerj.14065/fig-49](https://doi.org/10.7717/peerj.14065/fig-49)

There are two cleithra, one mistakenly catalogued in an assortment of ribs (UMMP 13788; [Fig. 50B](#)) and a second catalogued with a seemingly random assortment of predominantly cranial fragments (UMMP 14099; [Fig. 51A](#)). They are mainly identified on the basis of the developed rugosities, marked by strong ridges, and a smooth area for articulation with the clavicle that is bounded by an elevated longitudinal ridge and that tapers to a point. The other end is flat and rounded with a short longitudinal ridge (the scapular crest).



Figure 50: Photographs of isolated cleithra referred to *Buettnererpeton bakeri*.

(A) UMMP 14099 (in part), complete right cleithrum in anterior, medial, posterior, and lateral views (left to right); (B) UMMP 13788 (in part), partial left cleithrum in anterior, medial, posterior, and lateral views (left to right). Scale bar equal to 1 cm.

[Download full-size image](#)

DOI: [10.7717/peerj.14065/fig-50](https://doi.org/10.7717/peerj.14065/fig-50)

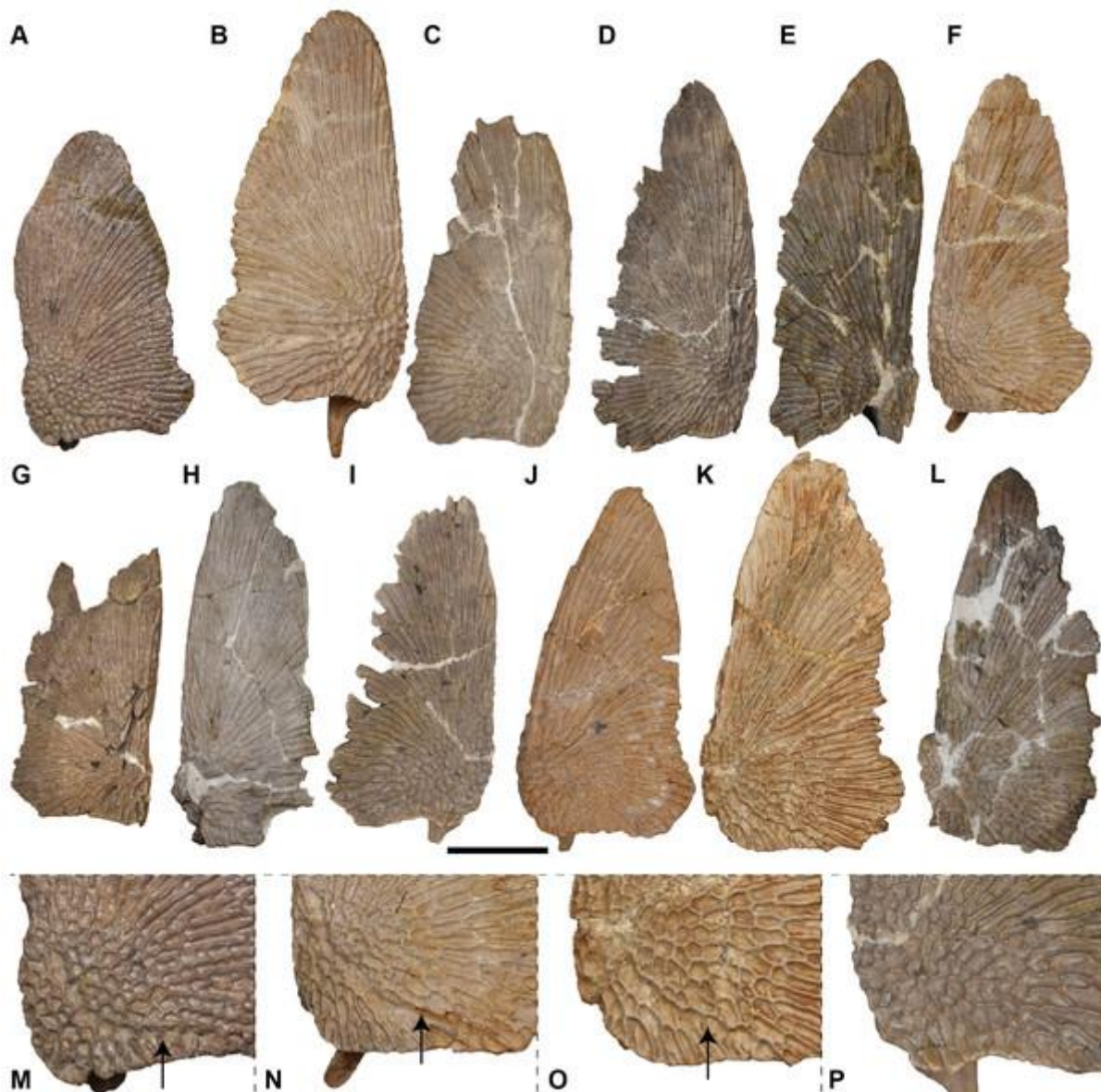


Figure 51: Ventral view of isolated clavicles referred to *Buettnererpeton bakeri*. (A) UMMP 13028; (B) UMMP 13824; (C) UMMP 13825; (D) UMMP 13896; (E) UMMP 13897; (F) UMMP 13898; (G) UMMP 13899; (H) UMMP 13900; (I) UMMP 13901; (J) UMMP 13902; (K) UMMP 13903; (L) UMMP 13904; (M) close-up of sensory groove in UMMP 138028; (N) close-up of sensory groove in UMMP 13898; (O) close-up of sensory groove in UMMP 13902; (P) close-up of equivalent region in UMMP 13901 (reflected for a consistent view) showing the absence of a groove. All elements are oriented with the anterior face pointing up. Arrows in parts M–O point to the sensory groove. Scale bar equal to 5 cm.

[Download full-size image](#)

DOI: [10.7717/peerj.14065/fig-51](https://doi.org/10.7717/peerj.14065/fig-51)

There are a total of twelve clavicles, six left and six right and most entirely complete (Figs. 51–54). Several have the dorsal surface embedded in plaster and thus can only be studied from the ventral and lateral surfaces. The anatomy is very consistent throughout, in line with the relatively minimal variation among metoposaurids at large with the exception of the size of the region marked by circular pitting along the posterolateral corner. UMMP 13824 is utilized as a representative of the clavicles described here as it is complete and fully exposed.

The ventral portion of the clavicle is flat and ornamented along the ventral surface (Fig. 51). Ornamentation consists of circular pitting near the posterolateral corner that radiates outward into elongate grooves. Also of note is the presence of a longitudinal sensory groove in the posterolateral region, demarcated by the interruption of the ornamentation pattern. The dorsal surface is mostly smooth but bears striations along the medial edge where it would meet the interclavicle (Fig. 52). A tall ascending process forms a blade-like structure with the posterodorsally directed process for the cleithrum (Figs. 53, 54A–54I); this entire feature is typically lost during preservation in North American taxa. The ascending process is mostly straight but deflects slightly medially (Figs. 52, 54J–54Q). There is a distinct fossa on the lateral surface and a curved posterior margin below the dorsal process (Fig. 53). The primary source of biological variation among the clavicles is with respect to an indentation found along the posteromedial border. In some specimens (UMMP 13824, UMMP 13898, UMMP 13903; Figs. 51B, 51F, 51K), the indentation is deep and thus the margin forms a step. In other specimens (*e.g.*, UMMP 13902; Fig. 51J), the indentation is shallow, forming a slightly angled margin, while in others (*e.g.*, UMMP 13825, UMMP 13899; Figs. 51C and 51G), it is practically nonexistent and could be readily confused for slight taphonomic damage, not uncommon in clavicles. Because this margin articulates with the interclavicle, the degree of indentation might prove useful for making tentative associations between the ornamented girdle elements, although this was not attempted here. The degree to which the sensory groove is developed is also variable. In this sample, it is most apparent in UMMP 13898, in which it curves around the posterolateral corner (Figs. 51F and 51N), and is least apparent in UMMP 13901 (Figs. 51I and 51P).

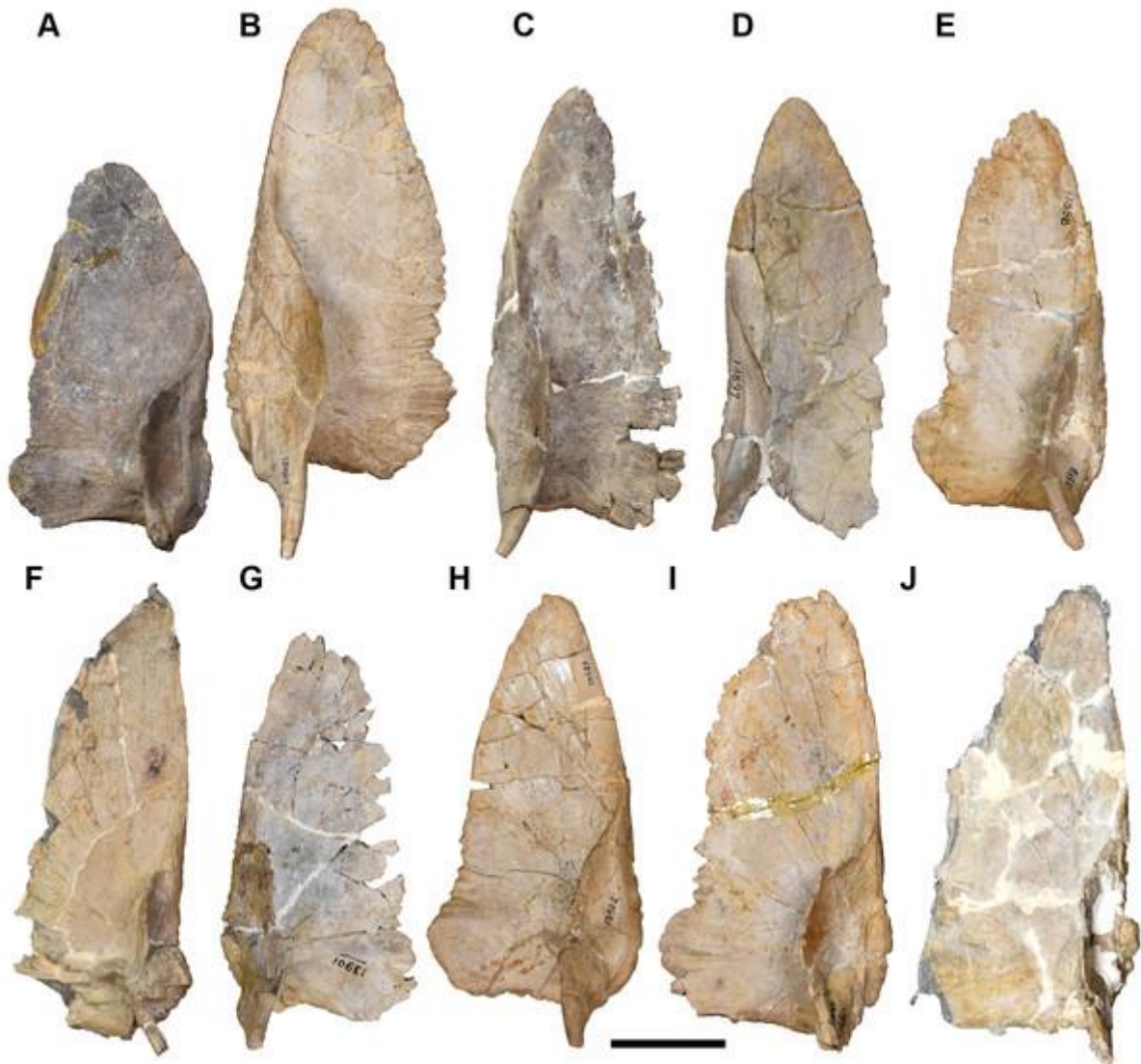


Figure 52: Dorsal view of isolated clavicles referred to *Buettnererpeton bakeri*. (A) UMMP 13028; (B) UMMP 13824; (C) UMMP 13896; (D) UMMP 13897; (E) UMMP 13898; (F) UMMP 13900; (G) UMMP 13901; (H) UMMP 13902; (I) UMMP 13903; (J) UMMP 13904. All elements are oriented with the anterior face pointing up. Scale bar equal to 5 cm.

[Download full-size image](#)

DOI: [10.7717/peerj.14065/fig-52](https://doi.org/10.7717/peerj.14065/fig-52)



Figure 53: Lateral view of isolated clavicles referred to *Buettnererpeton bakeri*. (A–F) right clavicles; (G–L) left clavicles. (A) UMMP 13028; (B) UMMP 13898; (C) UMMP 13900; (D) UMMP 13902; (E) UMMP 13903; (F) UMMP 13904; (G) UMMP 13824; (H) UMMP 13825; (I) UMMP 13896; (J) UMMP 13897; (K) UMMP 13899; (L) UMMP 13901. Scale bar equal to 5 cm.

[Download full-size image](#)

DOI: [10.7717/peerj.14065/fig-53](https://doi.org/10.7717/peerj.14065/fig-53)

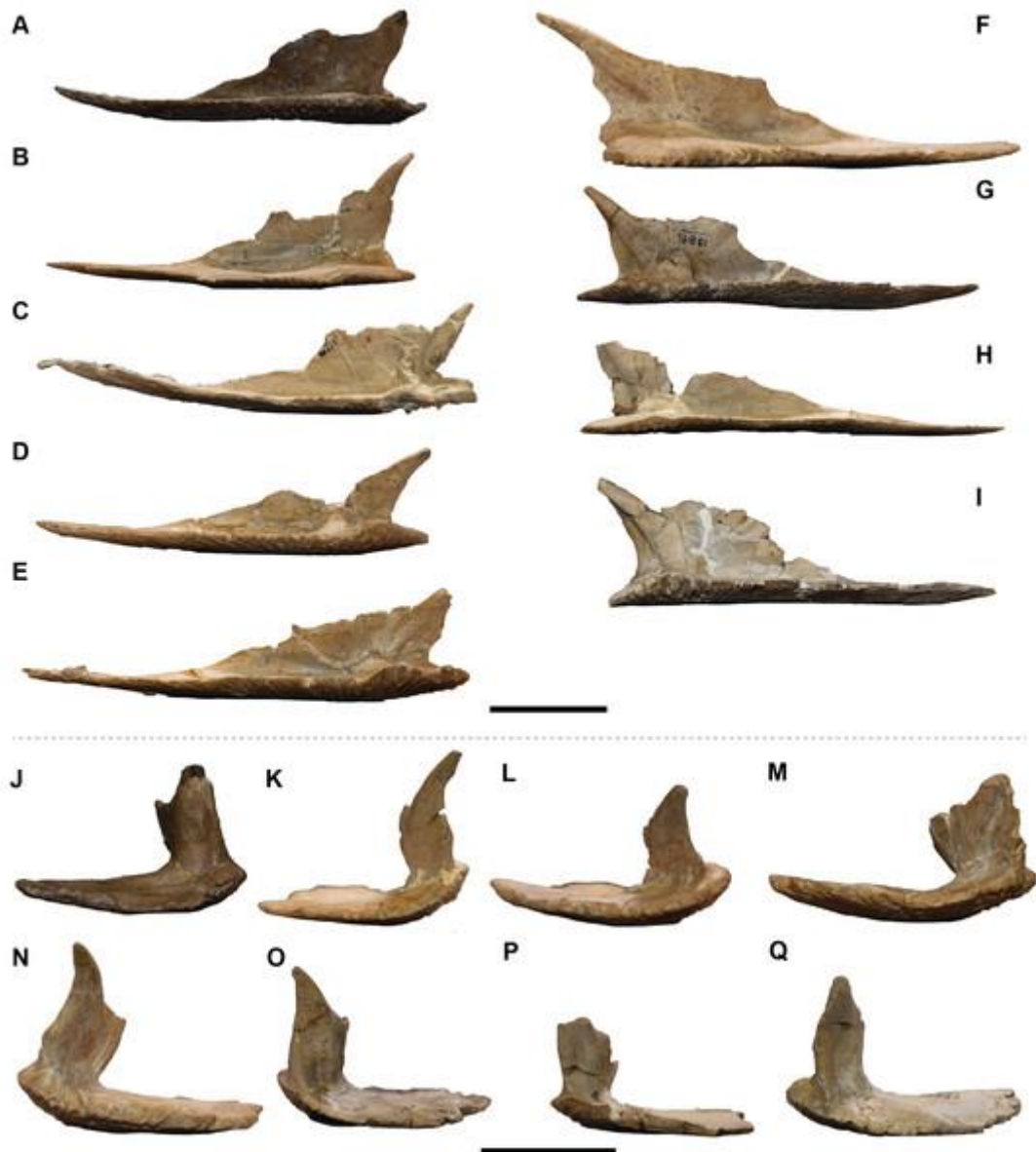


Figure 54: Medial and posterior views of isolated clavicles referred to *Buettnererpeton bakeri*.

(A–E) right clavicles in medial view; (F–I) left clavicles in medial view; (J–M) right clavicles in posterior view; (N–Q) left clavicles in posterior view. (A) UMMP 13028; (B) UMMP 13898; (C) UMMP 13900; (D) UMMP 13902; (E) UMMP 13903; (F) UMMP 13824; (G) UMMP 13896; (H) UMMP 13897; (I) UMMP 13901; (J) UMMP 13028; (K) UMMP 13898; (L) UMMP 13902; (M) UMMP 13903; (N) UMMP 13824; (O) UMMP 13896; (P) UMMP 13897; (Q) UMMP 13901. Scale bars equal to 5 cm.

[Download full-size image](#)

DOI: [10.7717/peerj.14065/fig-54](https://doi.org/10.7717/peerj.14065/fig-54)

There are 12 interclavicles, many of which are relatively complete ([Figs. 55–57](#)). As with the clavicles, a few specimens are embedded in plaster on the dorsal surface, while a few others are held together partially by what appears to be rice paper. Also like the clavicles, there is relatively little biological variation among them, and UMMP 13027 is described as a representative for its completeness and clear exposure in dorsal and ventral view. The ventral surface is largely marked by the typical pits and grooves found on the interclavicle of metoposaurids ([Figs.](#)

[55](#) and [56](#)). The region of circular pitting is concentrated at the center and then radiates outwards into elongate grooves, especially anteriorly. Unornamented facets for the clavicles bear faint striations. The dorsal surface is largely smooth and flat, but there are prominent buttresses extending anterolaterally below the articulation facets for the clavicles (the ‘trabecula clavicularis’ of [Sulej, 2007](#); [Fig. 57](#)). These join at the center, more or less below the central pitted region, to form a single longitudinal ridge (the ‘eminencia centralis’ of [Sulej, 2007](#); [Fig. 57](#)) that extends towards the posterior margin. The lattermost ridge may terminate in a visible rugosity, as in UMMP 13915 ([Fig. 57F](#)). The anterior process tapers in width to form a narrow stylus, while the posterior margin is a bluntly convex curve. There are three sources of intraspecific variation noted here. The first is the size of the region of circular pitting ([Table 4](#)). This has conventionally been utilized as a taxonomic differentiator between North American and European taxa, but at least two specimens here (UMMP 13029, UMMP 13911; [Figs. 55B](#) and [56A](#)) have very small regions of circular pitting, more like that observed in the European taxa (the incomplete UMMP 13914 may also have almost no pitting; [Fig. 56D](#)). The second source of variation follows that noted for the clavicle and corresponds to the contacting edge between these elements. The ornamented surface extending anteriorly can have straight lateral margins (*e.g.*, UMMP 13027, UMMP 13912; [Figs. 55A](#) and [56B](#)), a slightly stepped margin (*e.g.*, UMMP 13905, UMMP 13914; [Figs. 55D](#) and [56D](#)), or a prominently stepped margin (*e.g.*, UMMP 13029; UMMP 13910; [Fig. 55B](#) and [55G](#)). The final source of variation is in the posterolateral margins of the interclavicle. In some specimens, the margin is more or less straight for its entirety (*e.g.*, UMMP 13905, UMMP 13907; [Figs. 55C](#) and [55E](#)), whereas in others, there is a prominent step posterior to the clavicular facet (*e.g.*, UMMP 13906, UMMP 13908; [Figs. 55D](#) and [55F](#)). This variability does not have a clear connection to the clavicular variation.

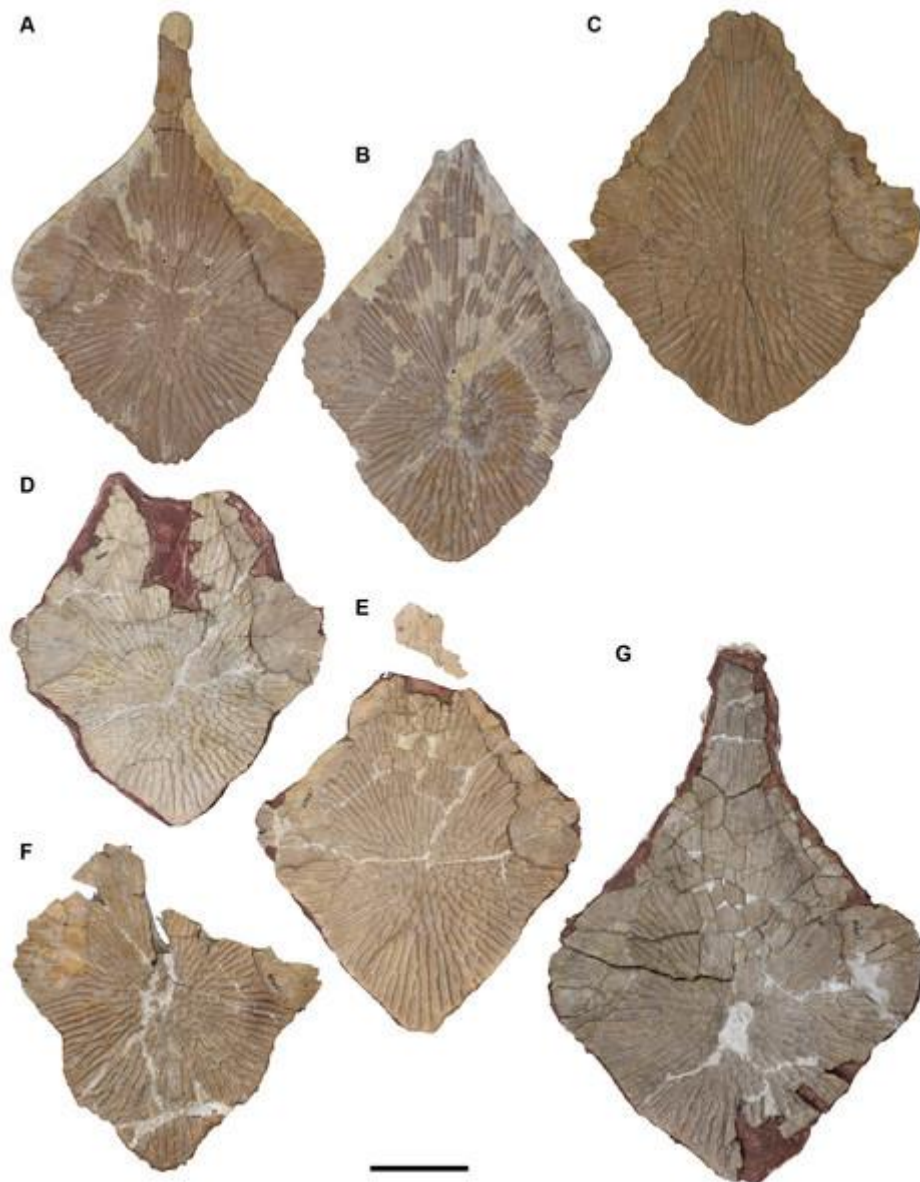


Figure 55: Ventral view of isolated interclavicles referred to *Buettnererpeton bakeri*. (A) UMMP 13027; (B) UMMP 13029; (C) UMMP 13029; (D) UMMP 13906; (E) UMMP 13907; (F) UMMP 13908; (G) UMMP 13910. All elements are oriented with the anterior margin pointing up. Scale bar equal to 5 cm.

[Download full-size image](#)

DOI: [10.7717/peerj.14065/fig-55](https://doi.org/10.7717/peerj.14065/fig-55)

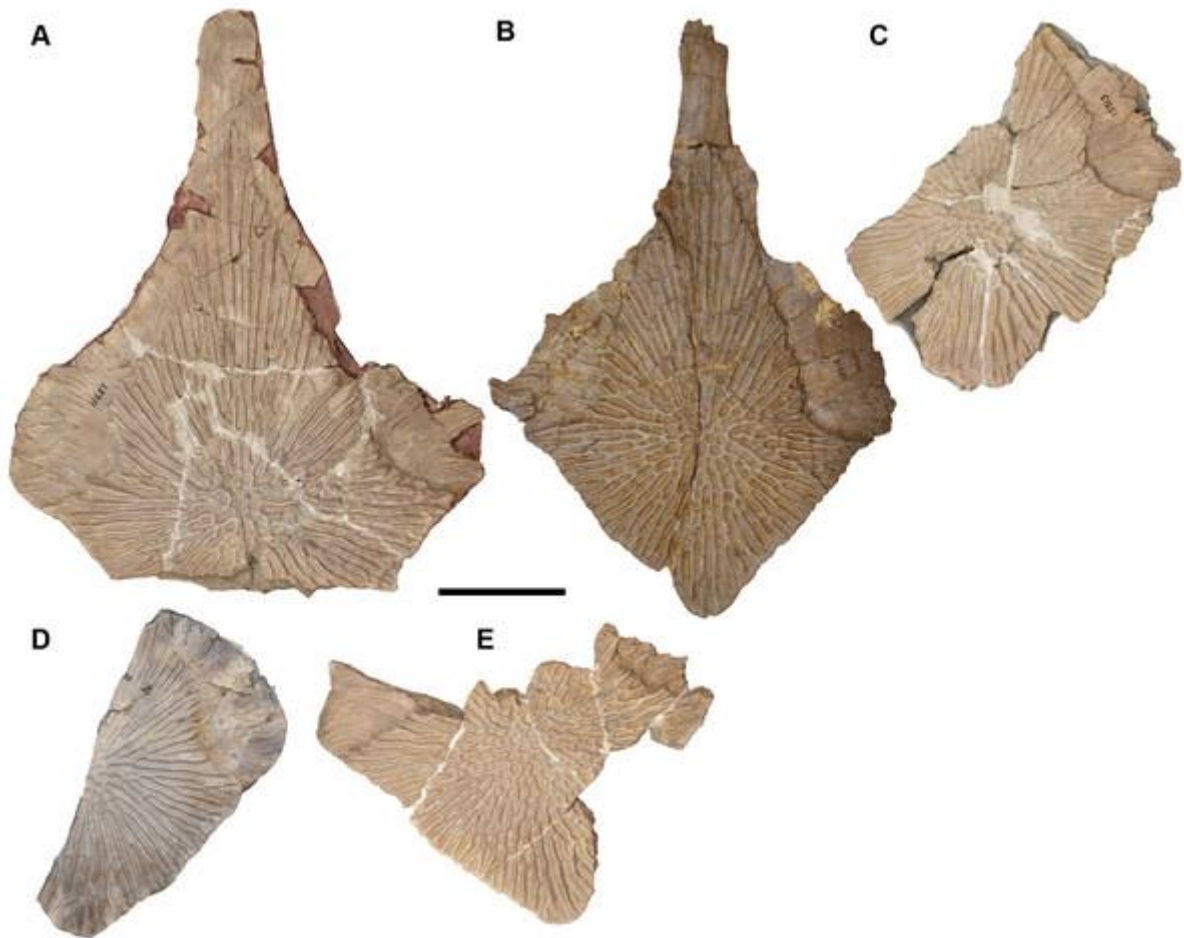


Figure 56: Ventral view of isolated interclavicles referred to *Buettnererpeton bakeri*. (A) UMMP 13911; (B) UMMP 13912; (C) UMMP 13913; (D) UMMP 13914; (E) UMMP 13915. All elements are oriented with the anterior margin pointing up. Scale bar equal to 5 cm.

[Download full-size image](#)

DOI: [10.7717/peerj.14065/fig-56](https://doi.org/10.7717/peerj.14065/fig-56)

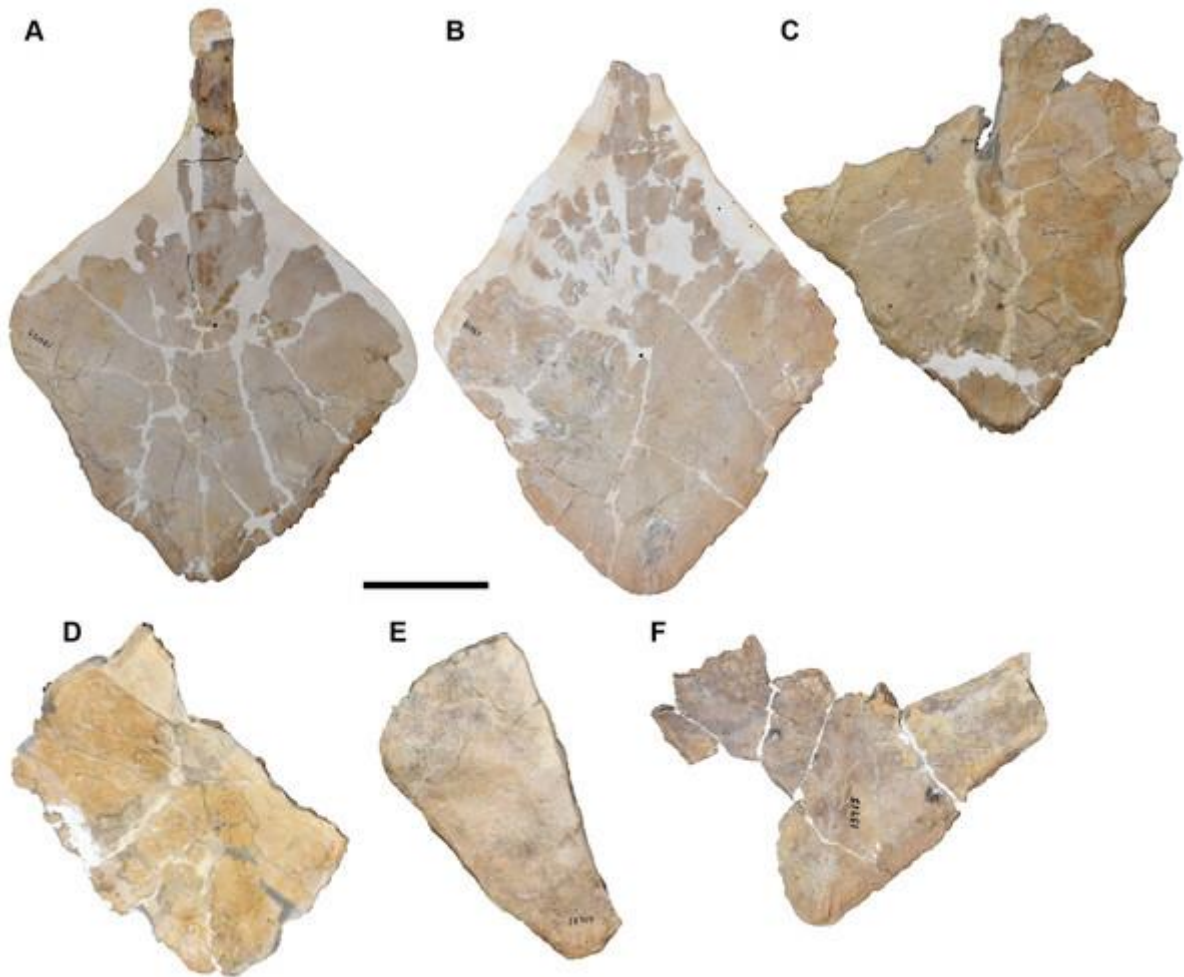


Figure 57: Dorsal view of isolated interclavicles referred to *Buettnererpeton bakeri*. (A) UMMP 13027; (B) UMMP 13029; (C) UMMP 13908; (D) UMMP 13913; (E) UMMP 13914; (F) UMMP 13915. All elements are oriented with the anterior margin pointing up. Scale bar equal to 5 cm.

[Download full-size image](#)

DOI: [10.7717/peerj.14065/fig-57](https://doi.org/10.7717/peerj.14065/fig-57)

Table 4:
Comparative measurements of partial to complete interclavicles of *Buettnererpeton bakeri*.

Specimen	IL	IW	PW	PW:IW
UMMP 13027	23.0	16.0	4.3	0.27
UMMP 13029	21.7*	16.1	< 3.5	< 0.22
UMMP 13905	21.3*	18.0	5.5	0.31
UMMP 13906	17.8*	16.3	4.7	0.29
UMMP 13907	18.3*	16.7	5.1	0.31
UMMP 13908	16.8*	16.1	5.0	0.31
UMMP 13910	26.6	19.3	6.1	0.32

Specimen	IL	IW	PW	PW:IW
UMMP 13911	23.3	18.8	4.4	0.23
UMMP 13912	23.6	16.1	4.2	0.26
UMMP 13913	14.4*	15.4	2.8	0.18
UMMP 13914	12.9*	15.6	1.6	0.10
UMMP 13915	11.8*	17.1	5.6	0.33

DOI: [10.7717/peerj.14065/table-4](https://doi.org/10.7717/peerj.14065/table-4)

Note:

Abbreviations for measurements: IL, maximum interclavicle length; IW, maximum interclavicle width; PW, maximum width of region of circular pitting. Note that for practically all specimens, the maximum length represents an incomplete total length; any measurement that is not considered to be a close approximation of the true length is marked with an asterisk (*). Estimates derived from a half-measurement and an assumption of symmetry are indicated by italics.

Forelimb material.—Two humeri are documented from the site ([Fig. 58](#)). UMMP 13775 is a complete left humerus. The proximal and distal ends are broadly expanded and relatively compressed with unossified ends. The supinator process is a small protrusion on the distal end above the ectepicondyle ([Figs. 58B](#) and [58D](#)). It is noticeably less developed and less protruding than in other taxa such that the gap between the process and the proximal head is much larger than that seen in other taxa. In this regard, it is quite similar to *Dutuitosaurus ouazzoui* ([Dutuit, 1976:fig. 58](#)). There is also no development of the attachment for the adductor musculature; in *M. krasiejowensis*, this forms a discrete ridge-like projection from the ventral margin on the proximal head ([Sulej, 2007](#)). In UMMP 13775, it is entirely smooth in this region. The deltopectoral crest protrudes laterally from the proximal end of the shaft and bears rugosities on its anterior and posterior surfaces. The rugose area on the posterior surface of the deltopectoral crest has previously been interpreted to be for insertion of the *m. biceps brachii* ([Ochev, 1972](#)) or the *m. pectoralis major* ([Dutuit, 1976](#)), and the rugose area on the anterior surface has been interpreted to be for insertion of the *m. deltoideus* ([Ochev, 1972](#); [Dutuit, 1976](#)). Other features and proportions are in line with those of other metoposaurids. UMMP 13772 is a partial left humerus and is longer than UMMP 13775 by about 20%. The shaft and most of the proximal head are preserved, but most of the ventral region of the distal end is lost. Excepting taphonomic damage, there are no differences from UMMP 13775.



Figure 58: Isolated left humeri referred to *Buettnererpeton bakeri*, UMMP 13772 (right) and UMMP 13775 (left).

(A) Anterior view; (B) medial view; (C) posterior view; (D) lateral view; (E) proximal view; (F) distal view. Abbreviations: dpc, deltopectoral crest; ec, ectepicondyle; ent, entepicondyle; md; insertion for the *m. deltoideus*; mi, insertion for the *m. biceps brachii* or the *m. pectoralis major*; sup, supinator process. Scale bars equal to 1 cm.

[Download full-size image](#)

DOI: [10.7717/peerj.14065/fig-58](https://doi.org/10.7717/peerj.14065/fig-58)

[Case \(1932:fig. 38\)](#) figured three putative ulnae (UMMP 13774). However, these elements are actually more similar to the tibiae of *Dutuitosaurus ouazzoui* ([Dutuit, 1976:fig. 69](#)) and *Metoposaurus krasiejowensis* ([Sulej, 2007:figs. 65–66](#)) than to the ulnae of these taxa ([Dutuit, 1976:fig. 60](#); [Sulej, 2007:figs. 56–57](#)). Features more consistent with the tibia include an asymmetrically expanded proximal end, resulting in a markedly concave anterior surface; proximal and distal cross-sections of a similar oblate profile (rather than markedly disparate profiles); and the presence of a rugose area for muscle attachment on the extensor surface of the

proximal end. UMMP 13774 does resemble the ulnae of *Anaschisma browni* as figured by [Sawin \(1945: fig. 10e-f\)](#) and [Lucas et al. \(2016:fig. 66\)](#). While this could be regarded as a taxonomic differentiator, it should also be considered that these elements may have been confused for each other by some previous workers (see also [Warren & Snell, 1991:60](#)). We consider the identifications and characterizations of [Dutuit \(1976\)](#) and [Sulej \(2007](#), which was based on Dutuit) to be more reliable since Dutuit based his identifications on the articulated skeletons of *D. ouazzoui*, whereas all other descriptions have been based on isolated bonebed material. [Lucas et al. \(2016\)](#) refer to [Sawin \(1945\)](#) in their comparative description and thus probably based their identifications largely on Sawin's study of entirely disarticulated material. If Sawin's interpretation was informed by Case's misinterpretation, this would account for the discrepancies between the 'ulna' and 'tibia' in North American taxa compared to other metoposaurids. Therefore, UMMP 13774 is reinterpreted as a trio of tibiae. It is worth noting that these bones were originally interpreted as tibiae, as indicated by strikethrough text on the collections card. These tibiae are figured and described in additional detail further below in the 'Hindlimb' section.

UMMP 13782, originally described by Case as a tibia, is therefore an ulna ([Fig. 59](#)). In UMMP 13782, the proximal end is massively expanded to have a large circular cross-sectional profile. This would represent the olecranon, although there is no development of the olecranon process, similar to other metoposaurids (*e.g.*, *Metoposaurus krasiejowensis*; [Sulej, 2007:fig. 56d](#)). The proximal expansion is symmetrical when viewed in anterior or posterior view, unlike the asymmetrical proximal expansion (greater anteriorly) of the tibia. This results in a proximodistally straight element, rather than one that appears slightly curved. The shaft is constricted, more so than in *M. krasiejowensis*, and then expands into a more oblate distal end. The distal expansion, while less than the proximal expansion, is prominent compared to the shaft ([Figs. 59B and 59D](#)), one feature separating it from tibiae (which are essentially unexpanded distally). The distal end is also greatly compressed anteroposteriorly to form an oblate cross-section at the end ([Fig. 59F](#)); this too differs from the circular profile of the uncompressed tibia. There are two partially defined facets on the distal surface, presumably for the ulnare and for the intermedium, which are unknown in metoposaurids and which were probably cartilaginous. A ridge down the proximal surface is a weakly developed extensor keel. The only other feature of note is a shallow crest along the posterior surface (the posterior ulnar keel of [Pawley & Warren, 2006](#)) that extends down to the distal end (termed the 'crista musculi extensoris carpi ulnaris' by [Sulej, 2007](#) following [Ochev, 1972](#)). The cross-sectional profiles of the ends align closely with those of *M. krasiejowensis* ([Sulej, 2007](#)). The element would represent a right ulna.

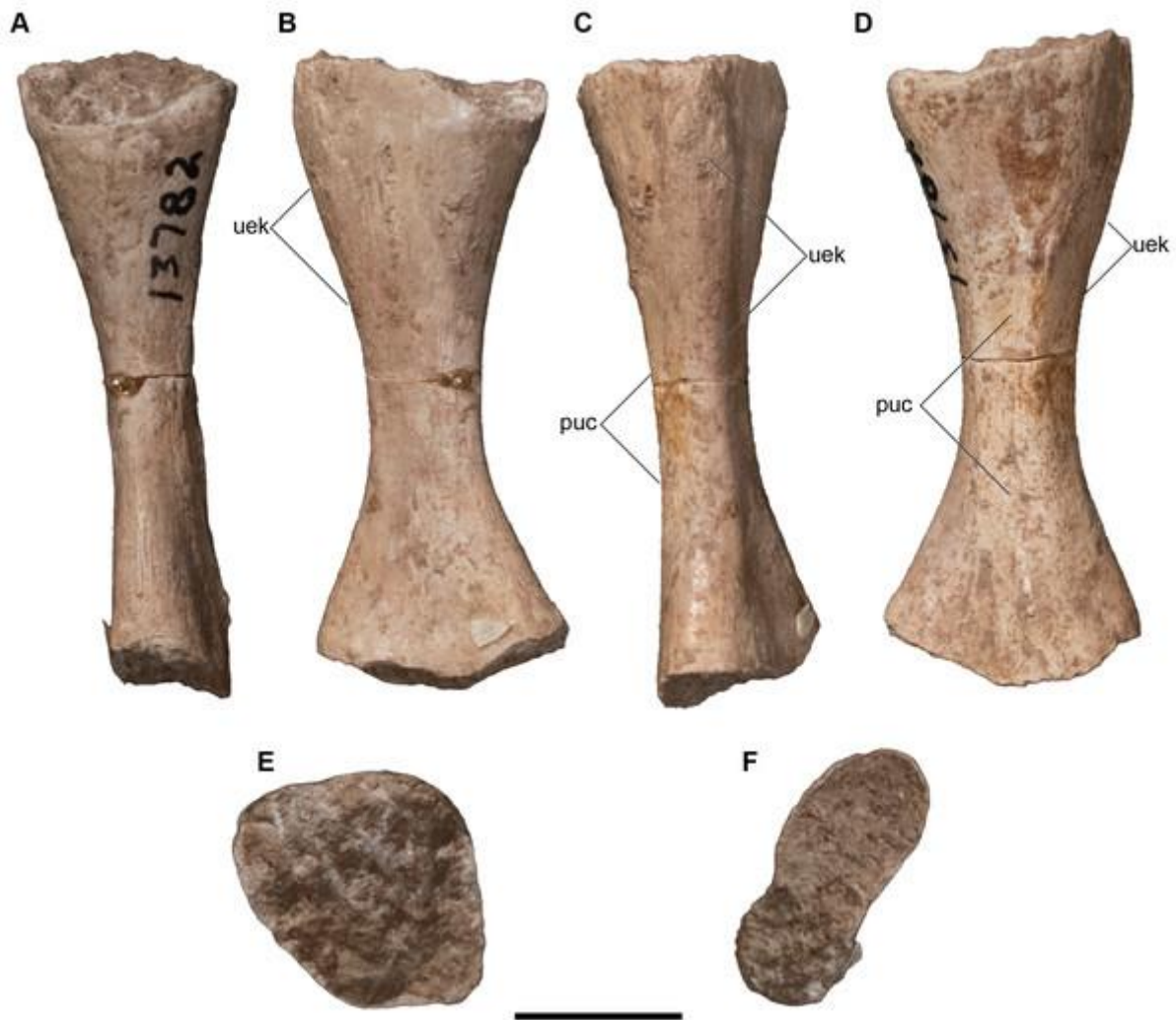


Figure 59: Isolated right ulna referred to *Buettnererpeton bakeri*, UMMP 13782. (A) Anterior view; (B) medial view; (C) posterior view; (D) lateral view; (E) proximal view; (F) distal view. Abbreviations: puc, posterior ulnar keel; uek, ulnar extensor keel. Scale bars equal to 1 cm.

[Download full-size image](#)

DOI: [10.7717/peerj.14065/fig-59](https://doi.org/10.7717/peerj.14065/fig-59)

A probable radius was originally misidentified as a femur in a set of three putative femora, UMMP 13773 (Fig. 60). The element is long and slender. The proximal and distal cross sections are similar to the radius of *Metoposaurus krasiejowensis* with a circular proximal cross section and a subtriangular distal cross section (Sulej, 2007:fig. 55). It is likely that Case's misidentification was made due to the presence of the proximal tubercle on the laterally facing surface ('anterior tuberculum' of Sulej, 2007); this projection somewhat resembles the trochanter of the femur described in more detail below. However, the tubercle in UMMP 13773 forms a narrow and gently convex ridge, not an expanded rugose projection (as with the femoral trochanter). While similar in overall morphology to the femur, this element lacks the distinct dorsal (intercondylar) and ventral (popliteal) fossae on the distal surface of the femur with instead a weak medial ridge and a convex lateral surface. Consequently, the cross-sectional profiles of the proximal and distal ends are also markedly different; the proximal end is circular,

and the distal end is triangular (Figs. 60E and 60F). In femora, the development of more asymmetrical condyles and fossa dividing them produces more complex profiles (see Sulej, 2007:fig. 64g). Additionally, the tubercle forms only a very shallow continuation with a proximodistal ridge on the lateral surface, compared to the ‘crista aspera’ of the femur.



Figure 60: Isolated right radius referred to *Buettnererpeton bakeri*, UMMP 13773 (in part).

(A) Anterior view; (B) medial view; (C) posterior view; (D) lateral view; (E) proximal view; (F) distal view. Abbreviations: mr, medial ridge; ptu, proximal tubercle. Scale bars equal to 1 cm.

[Download full-size image](#)

DOI: [10.7717/peerj.14065/fig-60](https://doi.org/10.7717/peerj.14065/fig-60)

UMMP 13784 consists of four elements previously identified as radii (Figs. 61A and 61C). The identity of these elements should be treated skeptically because they are simple in form, with a straight and slender shaft and ends that are slightly expanded and with oval cross-sections. There are no diagnostic features on any of the four elements, which could be attributed to relative immaturity, and it is obvious that they do not represent other limb elements. The radius is typically sided by the asymmetrical position of a proximal tubercle that descends into a ridge along the ventral surface, but no such feature is present in any of these elements. The

surfaces are smooth and without ridges, crests, or grooves. The only real structural feature is the presence of some foramina and striations near the ends. The cross-sectional profiles are elongate ovals, whereas the proximal end of the radius in *Metoposaurus krasiejowensis* is circular where it would meet the correspondingly large articular facet of the humerus, and there does not appear to be any compression in UMMP 13784. Therefore, it must be considered whether they represent metapodials much larger than a pair of phalanges (UMMP 13785; [Figs. 61B](#) and [61D](#)) and that their identification was made on the assumption that there must be radii present in the locality because virtually all other skeletal elements are confidently represented. The presence of rare, isolated elements of much larger individuals indicates that size alone cannot be used to identify these elements. These elements are entirely within the range of proportions for the manual phalanges of *M. krasiejowensis* ([Sulej, 2007](#)). Considering that the material at this locality is entirely disarticulated, that isolated elements of much larger individuals occasionally occur (*e.g.*, [Fig. 26G](#)) and that some skeletal elements are represented by only one specimen (*e.g.*, ulna, ischium), there was no reason to assume that radii are definitively present (but see reidentified radius above). We therefore identify UMMP 13784 as a set of large metapodial elements. The two previously identified phalanges (UMMP 13785) were specifically associated with the pes, although the justification for this placement is unknown. They are both short and slightly expanded at the ends (more so in the larger one). They are otherwise flat and lack any distinctive features like UMMP 13784.



Figure 61: Isolated autopodial elements referred to *Buettnererpeton bakeri*, UMMP 13784 (metapodials) and UMMP 13785 (phalanges).

(A) UMMP 13784 in view 1; (B) UMMP 13784 in view 2; (C) UMMP 13785 in view 1; (D) UMMP 13785 in view 2. The different views are not specified by anatomical profile because it is not possible to determine dorsal and ventral based on the preserved anatomy. Scale bar equal to 1 cm.

[Download full-size image](#)

DOI: [10.7717/peerj.14065/fig-61](https://doi.org/10.7717/peerj.14065/fig-61)

Pelvic girdle material.—Following the reidentification of UMMP 13786 as a scapula, the only pelvic elements are several ilia (Fig. 62). All six ilia from the site are catalogued under a single number, UMMP 13789, four from the left side and two from the right; there is no indication that any confidently form a pair from a single individual. The largest of these is about 25% longer than the smallest, but their morphology is conserved overall and is similar to that of other metoposaurids. There is a dorsal shaft, oval in cross-section and with an unfinished dorsal surface. The dorsal end appears to be slightly wider in the largest specimen, as

with *Metoposaurus krasiejowensis* (Sulej, 2007). The anterior margin of the shaft is very slightly convex near its base and is otherwise straight in larger specimens, forming a very slightly sinusoidal margin that is more like the condition observed in *Anaschisma browni* than in *M. krasiejowensis*. The two smallest left ilia have an essentially straight margin, despite being about the same size as the two right ilia. The medial and lateral surface of the shaft bear the internal oblique crest and the external oblique crest ('linea obliqua' of Sulej, 2007), respectively, that are expressed as elevated ridges extending down the medial and lateral sides (Figs. 62E and 62F). When viewed anteriorly, the shaft is more medially deflected in smaller specimens and is essentially in line with the ventral base in larger specimens. The base is broadly expanded anteroposteriorly and more slightly transversely. It forms a triangular cross-section that is broadest anteriorly. The acetabulum is a large, roughened area that becomes increasingly less well-defined in lateral view in larger specimens. The orientation of the acetabular face also becomes more vertical in larger specimens, as Sulej (2007) noted for *M. krasiejowensis*. Along the anterior margin is a shallow groove of variable development across the specimens that is deeper in larger specimens. The ventrolateral surface is largely smooth, although there is a shallow depression opposite the position of the acetabulum.

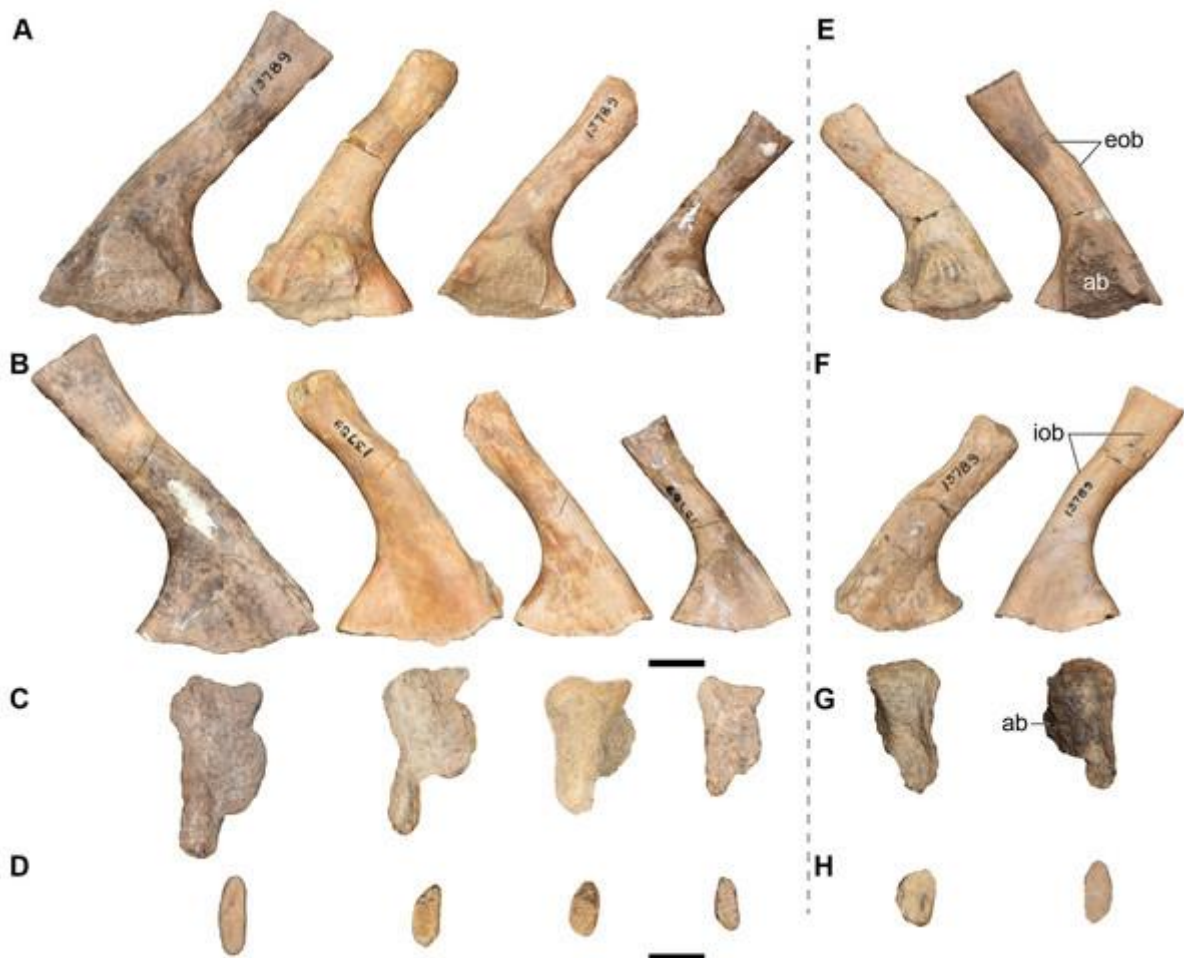


Figure 62: Isolated ilia referred to *Buettnererpeton bakeri*, UMMP 13789.

Four ilia are from the left side of the body, and two ilia are from the right side. (A) Lateral view; (B) medial view; (C), ventral view; (D) dorsal view. Abbreviations: ab, acetabulum; eob, external oblique crest; iob, internal oblique crest. Scale bars equal to 1 cm.

[Download full-size image](#)

DOI: [10.7717/peerj.14065/fig-62](https://doi.org/10.7717/peerj.14065/fig-62)

Hindlimb material.—There are four femora, one left and three right (Figs. 63 and 64). Two of these, UMMP 12946 and UMMP 12947 are much larger and would correspond to an individual of a much larger size than is represented by the partial to complete skulls and hemimandibles (Fig. 63). UMMP 12946 was labeled as a left femur, and UMMP 12947 as labeled as a right femur, but this siding is reversed, which is assessed by the asymmetrical position of the trochanter and by the condyles for the tibia and the fibula. In flexor profile, there is a deep, narrow groove (the intertrochanteric fossa) extending down the proximal head of UMMP 12946. It lies adjacent to the trochanter, which has been partially weathered. No such groove is apparent in UMMP 12947, but the external surfaces of the proximal end have been weathered in this specimen. Extending from the trochanter is a smooth ridge, the adductor crest (alternatively the ‘crista aspera’ of some workers; e.g., Sulej, 2007). It is not particularly pronounced and merges gradually into the mid-shaft. There is a thin groove adjacent to it on the ventral surface. The popliteal fossa is a shallow depression on the distal end. The anterior surface bears no major features, although some small, elongate foramina are visible on the distal end of UMMP 12946. In extensor view, the intercondylar fossa is well defined as a shallow trough extending up the distal head. At least two foramina, mostly distally facing, are present near the distal end. Sulej (2007) described a depression for the ilium on the proximal end in *Metoposaurus krasiejowensis*, but this surface is nearly flat in these specimens. The posterior surface also bears no major features beyond small foramina distally. One feature that differentiates these femora is that the anterodistal region proximal to the smaller condyle is outwardly swollen in UMMP 12947, thus creating a convex margin when viewed in the flexor profile compared to the straight margin of UMMP 12946. This might represent a pathological condition, as the margin is straight in specimens of other metoposaurids (e.g., Sulej, 2007:fig. 63), but a confident assessment would require examination of the internal microanatomy and histology. The other two femora (UMMP 13773; Fig. 64) are less than 50% of the length of these large specimens, being more in line with the size class of most elements in the bonebed. These femora do not differ greatly from the larger specimens, although the articular surfaces are more amorphous in shape, and the intercondylar fossa is much shallower. Both of these femora bear a rugosity on the posterior surface of the proximal end (Fig. 64C) that may correspond to the insertion of *m. ischiotrochantericus* (sensu Pawley & Warren, 2006:fig. 9.4), but this is not as apparent on the larger femora (Figs. 64E and 64F) probably due to weathering on the external surface. A third putative femur catalogued under UMMP 13773 is actually a radius and was described above.

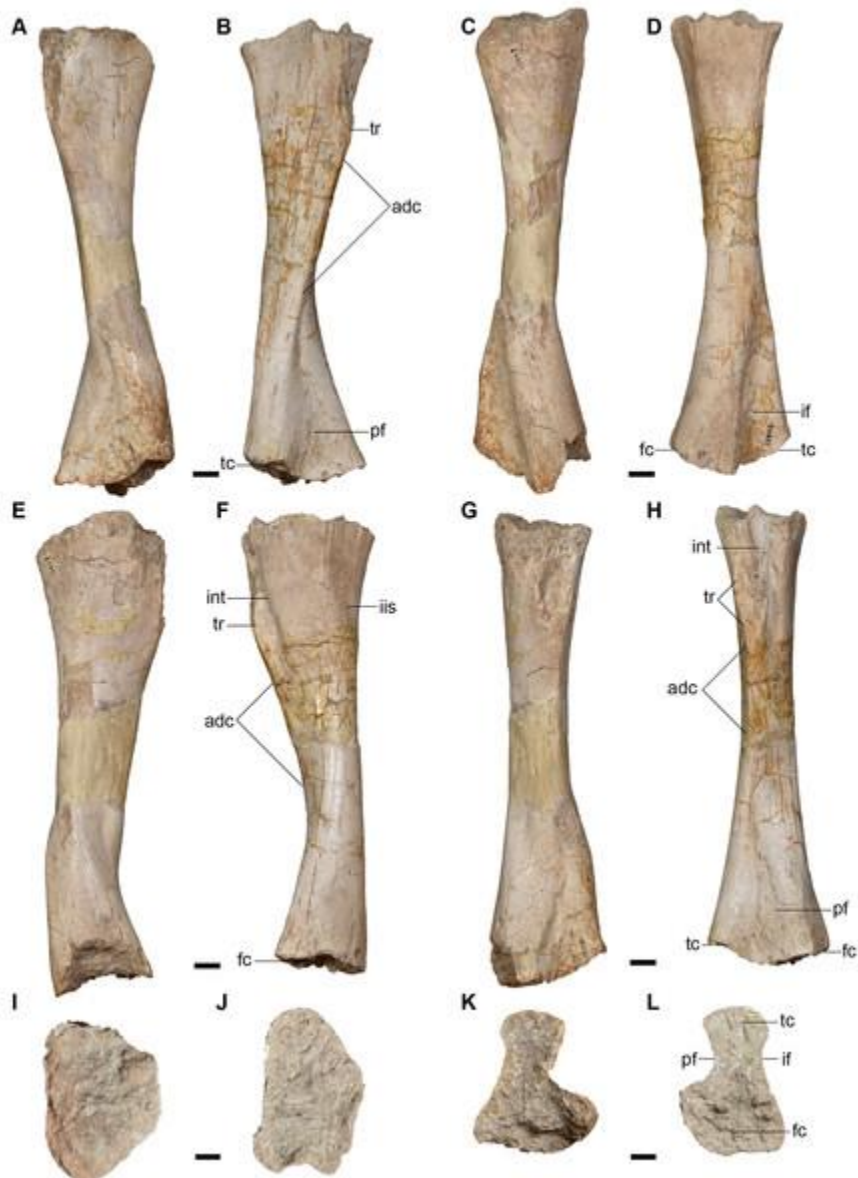


Figure 63: Large, isolated femora referred to *Buettnererpeton bakeri*, UMMP 12946 (right femur) and UMMP 12947 (left femur).

(A) UMMP 12947 in anterior view; (B) UMMP 12946 in the same view; (C) UMMP 12947 in dorsal (extensor) view; (D) UMMP 12946 in the same view; (E) UMMP 12947 in posterior view; (F) UMMP 12946 in the same view; (G) UMMP 12947 in ventral (flexor) view; (H) UMMP 12946 in the same view; (I) UMMP 12947 in proximal view; (J) UMMP 12946 in the same view; (K) UMMP 12947 in distal view; (L) UMMP 12946 in the same view.

Abbreviations: adc, adductor crest; fc, fibular condyle; if, intercondylar fossa; int, intertrochanteric fossa; iis, insertion of *m. ischiotrochantericus*; pf, popliteal fossa; tc, tibial condyle; tr, trochanter. For I–L, anterior is facing up. Scale bars equal to 1 cm.

[Download full-size image](#)

DOI: [10.7717/peerj.14065/fig-63](https://doi.org/10.7717/peerj.14065/fig-63)

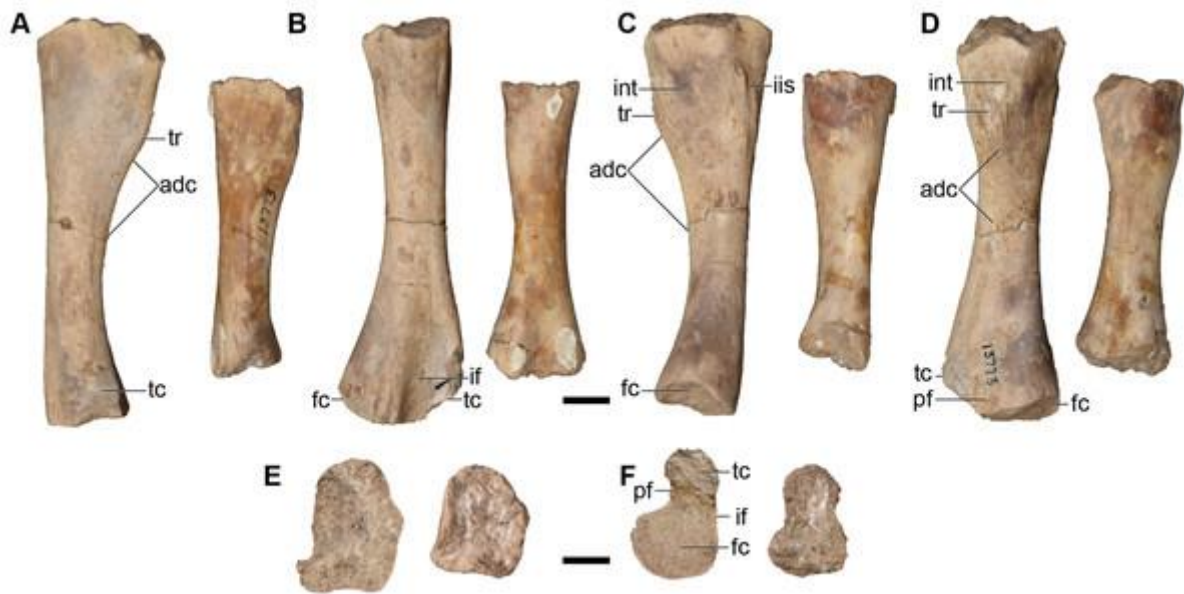


Figure 64: Photographs of isolated small right femora referred to *Buettnererpeton bakeri*, UMMP 13773 (in part).

(A) Anterior view; (B) dorsal (extensor) view; (C) posterior view; (D) ventral (flexor) view; (E) proximal view; (F) distal view. Abbreviations: adc, adductor crest; fc, fibular condyle; if, intercondylar fossa; iis, insertion of the *m. ischiotrochantericus*; int, intertrochanteric fossa; pf, popliteal fossa; tc, tibial condyle; tr, trochanter. For (E and F), anterior is facing up. Scale bars equal to 1 cm.

[Download full-size image](#)

DOI: [10.7717/peerj.14065/fig-64](https://doi.org/10.7717/peerj.14065/fig-64)

Two fibulae are catalogued under UMMP 13781 ([Fig. 65](#)) and were identified as such by [Case \(1932:fig. 40\)](#). The smaller one pertains to the right side, and the larger one pertains to the left side. The distal end is greatly expanded. There is a weakly developed ridge on the posterior margin of this end that is more apparent in the larger of the two fibulae. In flexor view, there is a shallow groove near the anterior margin of the distal end; [Pawley & Warren \(2006\)](#) termed this the ‘fibular sulcus’ in *Eryops megacephalus*. It extends from the anterior margin toward the distal margin but does not contact the intermedial facet ([Fig. 65B](#)). No such feature is present in the smaller fibula. The other surfaces are essentially smooth, without pronounced ridges or depressions. The cross-sections of the ends are slender, elongate ovals. These elements are very similar to those of *Metoposaurus krasiejowensis* ([Sulej, 2007](#)) and *Dutuitosaurus ouazzoui* ([Dutuit, 1976](#)) but are markedly different from those of *Anaschisma browni* figured by [Sawin \(1945:fig. 10k–l\)](#) in which the proximal end is nearly circular in cross-sectional view. However, the profiles shown for *A. browni* by [Lucas et al. \(2016:fig. 72\)](#) are consistent with those of other metoposaurids, and these data are considered to be more valid here.



Figure 65: Isolated fibulae referred to *Buettnererpeton bakeri*, UMMP 13781.

(A) Anterior view; (B) medial (flexor) view; (C) posterior view; (D) lateral (extensor) view; (E) proximal view; (F) distal view. Abbreviations: fs, 'fibular sulcus'; imf, intermedial facet. For (E and F), anterior is facing up. Scale bars equal to 1 cm.

[Download full-size image](#)

DOI: [10.7717/peerj.14065/fig-65](https://doi.org/10.7717/peerj.14065/fig-65)

As noted for the forelimb, the tibia and the ulna appear to have been confused for each other in [Case's \(1932\)](#) original publication. There are therefore three tibiae (two left, one right), all catalogued under UMMP 13774 ([Fig. 66](#)). In these elements, the proximal end is markedly expanded from the shaft and is asymmetrically expanded in the anterior direction to form a markedly concave margin. In contrast, the distal end is essentially unexpanded compared to the shaft (very slight expansion anteriorly to form a slightly convex articular surface). Both ends have oblate cross-sectional profiles. There is a distinct trough (the cnemial trough) on the extensor surface of the proximal end; this is bordered on the anterior edge by a shallowly defined ridge (the cnemial crest). There is a slightly roughened

region on the flexor surface (Fig. 66B) that would correspond to the tibial tuberosities identified by Sulej (2007) that lies adjacent to a longitudinal ridge that would represent the ‘cristae anterior tibiae’ of Sulej. The cross-sections of the ends are more elongate than those of *Metoposaurus krasiejowensis*, but the overall morphology is not appreciably different (Figs. 66E and 66F).



Figure 66: Isolated tibiae referred to *Buettnererpeton bakeri*, UMMP 13774.

One tibia is from the left side and two are from the right side. (A) Anterior view; (B) medial (extensor view); (C) posterior view; (D) lateral (flexor) view; (E) proximal view; (F) distal view. Abbreviations: cn, cnemial crest; cnt, cnemial trough; cat, ‘crista anterior tibiae’; imf, intermedial facet. Scale bars equal to 1 cm.

[Download full-size image](#)

DOI: [10.7717/peerj.14065/fig-66](https://doi.org/10.7717/peerj.14065/fig-66)

Indeterminate material. There is a large box with a collection of various fragments that lack a specimen number or any collections tag. A note in the drawer suggests that they might either belong to UMMP 13822 (Figs. 12–15) or to UMMP 9716 (a specimen of *Anaschisma browni*, not from the Elkins bone bed, that was cursorily mentioned by Case, 1932). There is no reason to strongly associate these fragments with any particular specimen. For example, one is a large hemimandible that does not even appear to belong to a temnospondyl and that is markedly distinct in preservation from the Elkins bone bed material, and another is a distinctly smaller and fragmentary skull in many pieces. A number of other fragments do appear very similar in preservation to the Elkins bone bed material, but there is no associated locality information that would allow them to be catalogued in

confidence and associated with the bonebed. They are also not sufficiently complete to be clearly matched with specimens described and figured by [Case \(1931, 1932\)](#) that were documented without specimen numbers (in contrast to the several dozen intercentra; see above). These fragments are noted here in description only: two pterygoid fragments; fragments of a purportedly extremely small skull (with a label of ‘Snyder 31’); assorted ornamented fragments; tooth-bearing fragments; the posterior end of a left hemimandible still largely embedded in matrix; an isolated tabular; and other unidentifiable fragments.

Phylogenetic analysis

Novel matrix employed in this study. The PAUP* analysis of our matrix recovered nine MPTs with a length of 623 steps (distributed across two tree islands; CI = 0.501; RI = 0.551; HI = 0.705; [Fig. 67A](#)). The topology is most similar to that of [Buffa, Jalil & Steyer \(2019\)](#) among previously published topologies. Metoposauridae is monophyletic, and the three European species of *Metoposaurus* form a clade. The sister group to *Metoposaurus* is the pairing of *Buettnererpeton bakeri* and *Anaschisma browni*, which form an intuitive geographic grouping that contradicts phenetic placement of *B. bakeri* in *Metoposaurus*. *Panthesaurus maleriensis* is the sister taxon to this clade, contradicting [Lucas’ \(2021\)](#) supposition that it also belongs in *Metoposaurus*. The Moroccan taxa then form a clade, with *Arganasaurus* recovered as monophyletic. *Apachesaurus* is recovered as the earliest diverging metoposaurid. The relationships of the non-metoposaurids are less resolved. *Sclerocephalus*, *Rhineceps*, and *Lydekkerina* form successively diverging branches at the base. This is followed by a trichotomy of Capitosauria (*Cyclotosaurus*, *Eocyclotosaurus*, *Quasicyclotosaurus*, *Mastodonsaurus*), *Benthosuchus*, and all remaining temnospondyls. In tree island 1 (MPTs 1–6), *Benthosuchus* diverges before Capitosauria, whereas this is reversed in tree island 2 (MPTs 7–9). Nominal trematosaurids never form a clade, inclusive or exclusive of Metoposauridae ([Figs. 68A](#) and [68B](#)). In tree island 1 ([Fig. 68A](#)), *Callistomordax*, *Lyrocephaliscus*, and *Trematolestes* form a clade, with *Trematosaurus* as the sister group to a trichotomy of this clade, Metoposauridae, and a clade of remaining temnospondyls (*Almasaurus*, Brachyopoidea, *Chinlestegophis*, *Gerrothorax*, *Rileymillerus*). In tree island 2 ([Fig. 68B](#)), these four trematosaurids form a grade between *Benthosuchus* and remaining temnospondyls in this order: *Lyrocephaliscus*, *Callistomordax* + *Trematolestes*, and *Trematosaurus*. The final clade is formed by *Almasaurus*, Brachyopoidea, *Chinlestegophis*, *Gerrothorax*, and *Rileymillerus*, and the topology is the same across both tree islands. *Gerrothorax* is the sister taxon to Brachyopoidea, and this trio forms a trichotomy with *Chinlestegophis* and *Rileymillerus*. *Almasaurus* is the earliest diverging taxon in this clade.

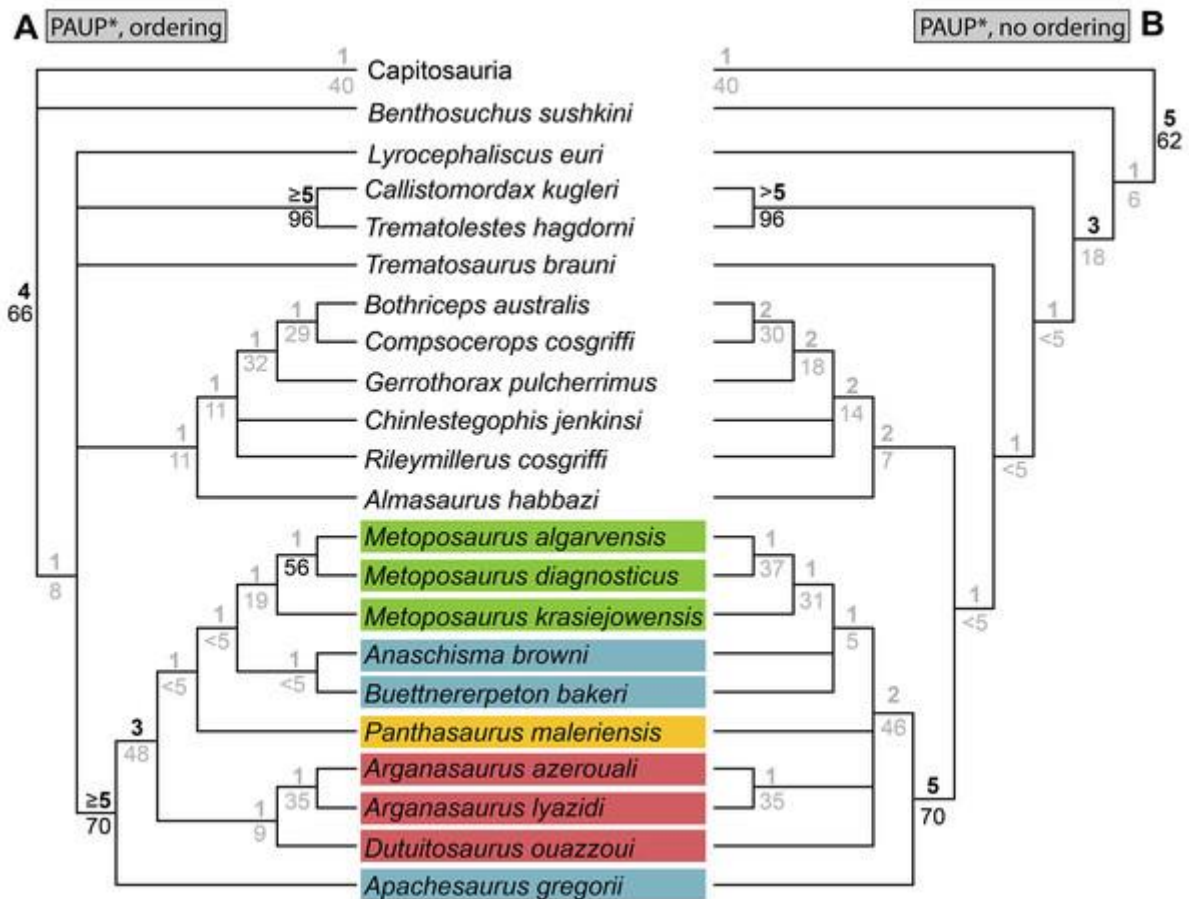


Figure 67: Comparison of topologies recovered with different parsimony analyses of the matrix of this study.

(A) Strict consensus recovered from analysis in PAUP* with certain multistate characters ordered; (B) strict consensus recovered from analysis in PAUP* with all multistate characters unordered. Topologies are restricted to higher stereospondyls (post-*Lydekkerina*). Bremer values are above the line, and bootstrap values are below. All values not considered to meet standard thresholds for ‘strong support’ (Bremer index ≥ 3 ; bootstrap value $\geq 50\%$) are in gray text.

[Download full-size image](#)

DOI: [10.7717/peerj.14065/fig-67](https://doi.org/10.7717/peerj.14065/fig-67)

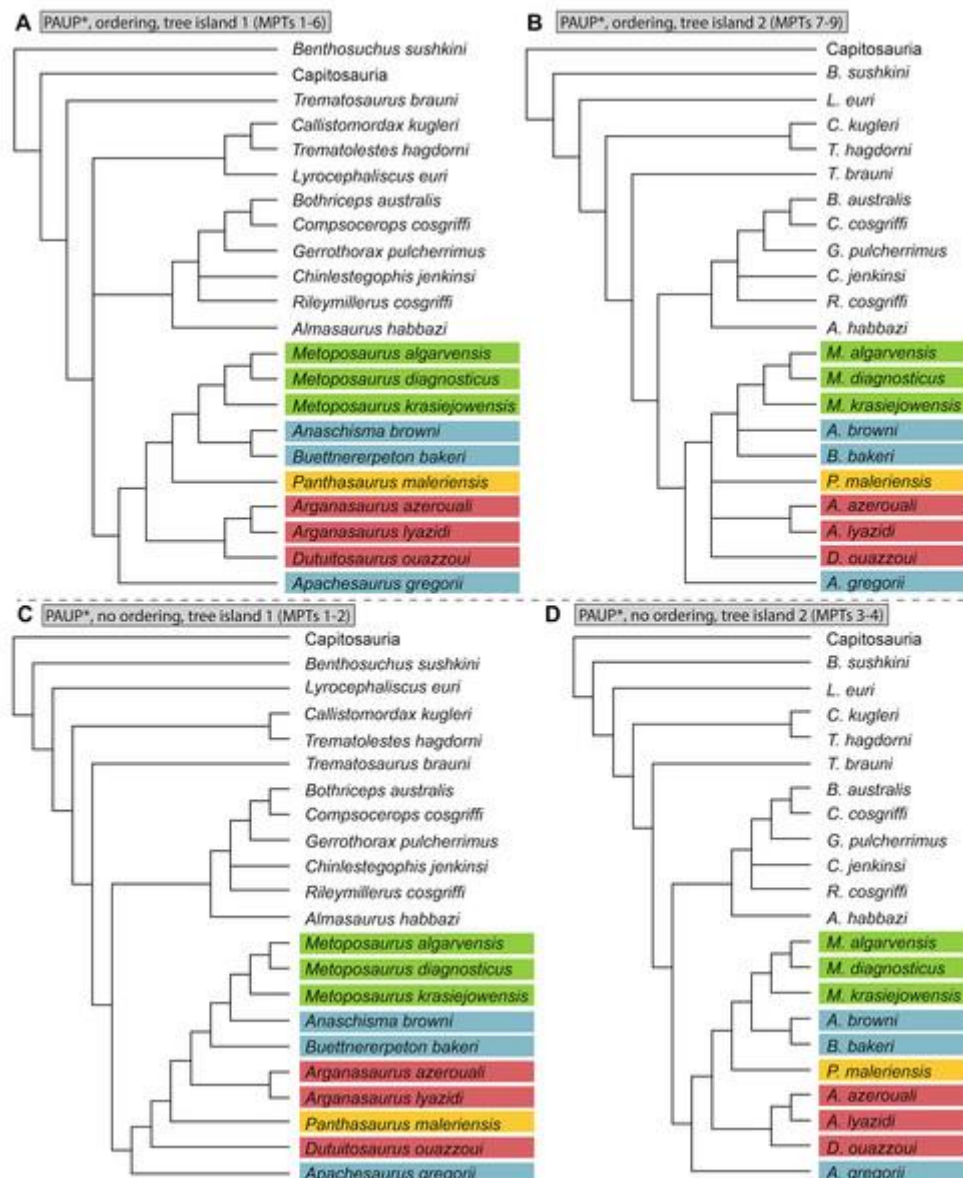


Figure 68: Comparison of tree islands recovered with different parsimony analyses of the matrix of this study.

(A) Strict consensus of tree island 1 from the analysis with certain multistate characters ordered; (B) strict consensus of tree island 2 from the analysis with certain multistate characters ordered; (C) strict consensus of tree island 1 from the analysis with all multistate characters unordered; (D) strict consensus of tree island 2 from the analysis with all multistate characters unordered. Topologies are restricted to higher stereospondyls (post-*Lydekkerina*).

[Download full-size image](#)

DOI: [10.7717/peerj.14065/fig-68](https://doi.org/10.7717/peerj.14065/fig-68)

We also tested whether leaving all characters unordered, as with [Buffa, Jalil & Steyer \(2019\)](#), would affect the topology. The same analysis in PAUP* recovered four MPTs with a length of 604 steps (distributed across two tree islands; CI = 0.507; RI = 0.550; HI = 0.695) and with a slightly different strict consensus ([Fig. 67B](#)). In this iteration, the strict consensus is more (fully) resolved with respect to non-metoposaurids but less resolved with respect to metoposaurids. The base of the tree is the same as in the iteration with ordering. Non-metoposaurid trematosaurids then form a grade after Capitosauria in this order: *Benthosuchus*, *Lyrocephaliscus*,

Callistomordax + *Trematolestes*, and *Trematosaurus*. The clade formed by *Almasaurus*, *Brachyopoidea*, *Chinlestegophis*, *Gerrothorax*, and *Rileymillerus* has the same topology as the previous iteration. Regarding *Metoposauridae*, in the strict consensus, *Metoposauridae*, *Metoposaurus* (*sensu* [Brusatte et al., 2015](#), and the previous iteration), and *Arganasaurus* were recovered as monophyletic. *Apachesaurus* was again recovered as the earliest diverging taxon. Resolution has been lost elsewhere. *Anaschisma browni* and *Buettnererpeton bakeri* are no longer exclusive sister taxa but instead form individual branches of a trichotomy with *Metoposaurus*. *Panthasaurus* is not the exclusive sister taxon to this clade and instead forms one branch of a polytomy with branches for *Dutuitosaurus* and *Arganasaurus* (the Moroccan taxa do not form a single clade). Tree island 1 (MPTs 1–2; [Fig. 68C](#)) recovers *An. browni* as the sister taxon to *Metoposaurus*. The progressively earlier diverging sister taxa that bridge this clade to *Apachesaurus* at the base are, in this order: *B. bakeri*, *Arganasaurus*, *Panthasaurus*, and *Dutuitosaurus*. Tree island 2 (MPTs 3–4; [Fig. 68D](#)) recovers the same topology as the previous iteration. These results therefore also support generic differentiation of *B. bakeri*.

The MrBayes analysis of our matrix with select character ordering recovered a less resolved topology, either when examining the 50%-majority-rule consensus at face value or when applying a more stringent threshold for ‘strong’ posterior probabilities (> 70%; [Fig. 69A](#)). Nodes that were recovered in the majority-rule consensus are largely compatible with those recovered by the equivalent parsimony analysis. Interestingly, *Almasaurus habbazi*, not *Chinlestegophis jenkinsi*, is the exclusive sister taxon to *Rileymillerus cosgriffi*. The all-clades-compatible consensus, which forces resolution at every node, recovered low posterior support (mostly < 30%) for nodes not recovered in the 50%-majority-rule consensus; this consensus is thus not depicted here for either treatment. Only *Metoposauridae* and two nodes within *Metoposaurus* were recovered, with the same relationships between the three species of *Metoposaurus* as in the parsimony analyses. The topology was not substantially different when all multistate characters were left unordered ([Fig. 69B](#)), but the relationships of the small-bodied taxa changed drastically, with *C. jenkinsi* and *R. cosgriffi* now forming the sister clade to *Brachyopoidea*, exclusive of *A. habbazi*. However, it should be noted that in both analyses, the posterior probabilities for the nodes of these small-bodied taxa were always below 70%.

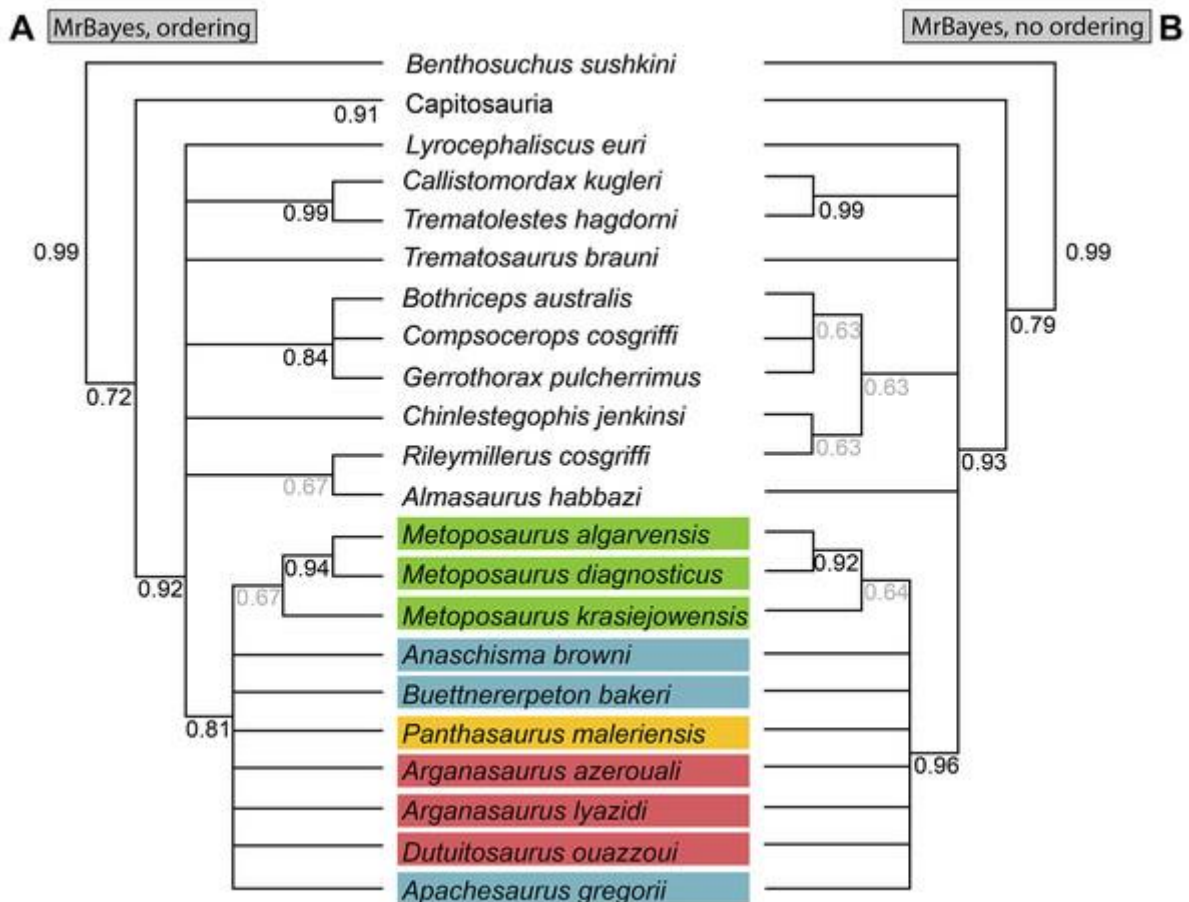


Figure 69: Comparison of topologies recovered with different Bayesian analyses of the matrix of this study.

(A) 50%-majority-rule consensus recovered from analysis in MrBayes with certain multistate characters ordered; (B) 50%-majority-rule consensus recovered from analysis in MrBayes with all multistate characters unordered. Topologies are restricted to higher stereospondyls (post-*Lydekkerina*). Posterior probabilities are below the line and italicized. All values not considered to meet standard thresholds for ‘strong support’ (posterior probability $\geq 70\%$) are in gray text.

[Download full-size image](#)

DOI: [10.7717/peerj.14065/fig-69](https://doi.org/10.7717/peerj.14065/fig-69)

Reanalysis of the matrix of [Buffa, Jalil & Steyer \(2019\)](#). Reanalysis of the original matrix of [Buffa, Jalil & Steyer \(2019\)](#) with ordering of seven characters that we believe occur along a morphocline recovered 12 MPTs with length 149 steps (CI = 0.517; RI = 0.589; HI = 0.483; [Fig. 70B](#)). The strict consensus is mostly incongruent with the original topology recovered by [Buffa, Jalil & Steyer \(2019\)](#) ([Fig. 70A](#)). Only three nodes are shared between them: Metoposauridae; all metoposaurids to the exclusion of *Dutuitosaurus ouazzoui*; and a polytomy of the three European *Metoposaurus* species. All nodes, including Metoposauridae, lack strong Bremer support (> 2), but some nodes (e.g., *Metoposaurus*) are strongly supported by bootstrapping ($> 50\%$).

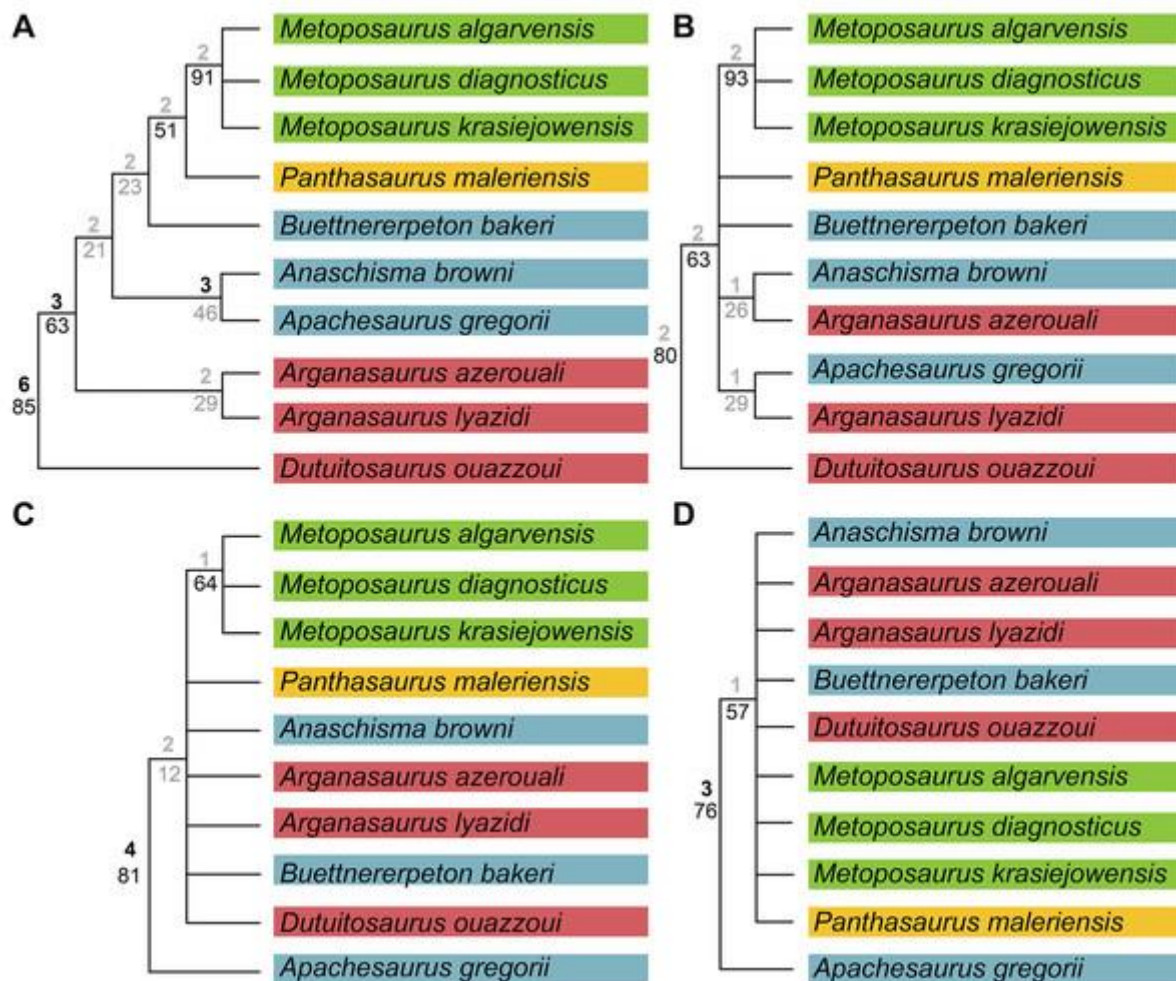


Figure 70: Comparison of topologies recovered with different analyses of the matrix of Buffa, Jalil & Steyer (2019).

(A) Original strict consensus with newly reported bootstrap and Bremer values; (B) strict consensus recovered when seven characters were ordered (Appendix 3) but scores were otherwise left unchanged; (C) strict consensus recovered with scoring modifications and no ordering of any characters; (D) strict consensus recovered with scoring modifications and seven ordered characters. Bremer values are above the line; bootstrap values are below. All values not considered to meet standard thresholds for 'strong support' (Bremer index ≥ 3 ; bootstrap value $\geq 50\%$) are in gray text.

[Download full-size image](#)

DOI: [10.7717/peerj.14065/fig-70](https://doi.org/10.7717/peerj.14065/fig-70)

Analysis with the scoring modifications listed in Appendix 2 and all characters unordered recovered nine MPTs with a length of 160 steps (one tree island; CI = 0.600; RI = 0.579; HI = 0.525; Fig. 70C). This analysis recovers a topology that is largely incongruent with the original analysis by Buffa, Jalil & Steyer.

Metoposauridae is largely unresolved. The only nodes recovered within Metoposauridae are (1) all metoposaurids to the exclusion of *Apachesaurus gregorii*; and (2) a monophyletic *Metoposaurus sensu Brusatte et al. (2015)*. Only Metoposauridae has both strong Bremer and bootstrap support; *Metoposaurus* has only strong bootstrap support, and the clade of all non-*Apachesaurus* metoposaurids has neither.

Analysis with the scoring modifications and ordering of the seven characters listed in [Appendix 2](#) recovered 34 MPTs with a length of 164 steps (one tree island; CI = 0.591; RI = 0.568; HI = 0.537; [Fig. 70D](#)). The strict consensus is practically unresolved within Metoposauridae, with *Apachesaurus gregorii* recovered as the earliest diverging taxon and all other taxa recovered in a polytomy. Bremer support for Metoposauridae is strong, but the node for all post-*Apachesaurus* metoposaurids is only strongly supported by bootstrapping.

Discussion

Intra-locality ontogenetic assessment

Most localities with many individuals of a given taxon will likely preserve some range of variably sized individuals, as is the case with the Elkins Place bone bed. Assessing such variation is important for phylogenetic work, especially when an OTU is constructed from many specimens, and even when producing a composite reconstruction like our [Fig. 5](#). Among the partial to complete skulls, there is little range in size variation; the smallest specimen, UMMP 13822, is estimated to a midline length around 24 cm, and the largest, UMMP 13820, is just over 30 cm (~20% longer; [Table 3](#)). Despite the incompleteness of UMMP 13822, a comparison with UMMP 13820 as endmembers of the known ontogenetic range from this site (based on skulls) does not indicate any clear ontogenetic differences beyond very minor proportional differences that are hard to confidently determine given the limited sample. There are no differences in sutural relationships, no measurable difference in suture morphology exceeding a reasonable range for intraspecific variation in other taxa (*e.g.*, [Sulej, 2007](#); [Lucas et al., 2016](#)), no differences in proportions of major qualitative features (*e.g.*, tabular horn length, orbit position), and no apparent difference in the relative degree of ossification. Nearly all isolated cranial, palatal, and occipital elements are in line with the range bracketed by partial to complete skulls except for UMMP 13826 ([Fig. 26G](#)), a parietal that is twice as large as any articulated within a skull. This element exhibits no clear differences that are attributable to ontogeny.

The hemimandibular and postcranial data present a similar narrative. All lower jaws are of a similar size and are entirely consistent with the partial to complete skulls from the locality. There is a small size range in certain postcranial elements (*e.g.*, fibulae, ilia; [Figs. 62, 65](#)), but there are few differences between them, practically none of which have phylogenetic import in any study. A pair of very large femora ([Fig. 63](#)) likely correspond to an individual of a similar size to UMMP 13826, but otherwise, all postcrania are in line with the relative size expected for specimens with the skull lengths found in the partial to complete skulls (based on the proportions established by [Sawin, 1945](#), [Dutuit, 1976](#), and [Sulej, 2007](#)). These femora are proportionately longer than smaller femora ([Fig. 64](#)), but the relative degree of development is similar (*e.g.*, unfinished condylar ends, pronounced trochanter).

In summation, there is undoubtedly a very wide size range, which presumably correlates with some measure of ontogenetic variation, at the Elkins Place bone bed. However, nearly all specimens in fact pertain to a very narrow size range (individuals with skull length between 24 and 30 cm), and outliers are represented only by isolated elements that differ in no appreciable fashion from smaller elements. From a functional standpoint, these outliers have no influence on the phenetic comparisons, the phylogenetic analyses, or the resultant taxonomy.

Inter-locality ontogenetic assessment

Proper comparisons also require some assessment of the maturity of specimens of *Buettnererpeton bakeri* from the type locality relative to other metoposaurids, both conspecifics from other localities and different species. Therefore, before proceeding with such comparisons, it is important to establish whether proper comparisons can be made on the ground of relative ontogenetic equivalency. For example, if it was argued that all specimens belonged only to markedly immature individuals, the taxon should probably not be sampled in a phylogenetic analysis to begin with. It would also complicate phenetic comparisons with taxa only represented from larger individuals (*e.g.*, *Panthesaurus maleriensis*). This is a salient point here because the overwhelming majority of specimens from the Elkins Place bone bed belong to relatively small metoposaurids with skulls less than approximately 30 cm in length ([Table 3](#)). By comparison, the largest known metoposaurids (of *Anaschisma browni* from Texas and *Dutuitosaurus ouazzoui* from Morocco) have skulls exceeding 60 cm. A handful of isolated elements from the type locality suggest that *B. bakeri* reached a size closer to this upper bound ([Figs. 26G, 63](#)); skulls reported by [Martz \(2008\)](#) and [Mueller et al. \(2016\)](#) are also slightly larger than those redescribed here (~35–45 cm range). The most robust means of ontogenetic assessment is bone histology, a method previously applied by the first author. Here, a histological analysis was not an objective of the study and would have many caveats because of the entirely disarticulated nature of material; no postcrania can be confidently associated with a given skull in order to draw a correlation between skeletochronological age and various aspects of external cranial anatomy. Given the variation between metoposaurids from different geographic regions ([Konietzko-Meier & Klein, 2013](#); [Teschner et al., 2020](#)), it would also be difficult to contextualize such results without a large body of histological data for North American taxa, specifically for limb elements; such work is planned by the authors in the future.

What then can be said based on external anatomy? A comparison of YPM VPPU 021742 from Nova Scotia (the smallest known skull of *Buettnererpeton bakeri*; [Fig. 4](#)), our composite reconstruction for the Elkins Place bone bed material (representative of all partial to complete skulls), and TTU P-10530 from the Boren Quarry (larger than any from the Elkins Place bone bed) show practically no differences that can be confidently identified as both biological and ontogenetic ([Fig. 71](#)). YPM VPPU 021742 appears proportionately wider, but it is important to recall that this specimen is a natural 2D mold and therefore some dorsoventral

compression has occurred. This likely accounts for proportionately wider postorbitals, parietals, supratemporals, and jugals in this specimen. By the same token, the very prominent posteriorly projecting exoccipitals of the Boren Quarry specimen shown in [Fig. 71](#) are also likely taphonomic; the larger (more incomplete) specimen figured by [Martz \(2008:fig. 4.2c\)](#) has less protruding exoccipitals. The Boren Quarry material also has a slightly more triangular skull, but there is clear non-ontogenetic intraspecific variation in skull profile in *Anaschisma browni* ([Sawin, 1945](#); [Lucas et al., 2016](#)), which may be exaggerated by taphonomic distortion. The only features that can be confidently interpreted as ontogenetic differences are the position of the pineal foramen and the elements contacted by the infraorbital sensory groove. Regarding the pineal foramen, in YPM VPPU 021742, it is closer to the mid-length of the parietals than to the posterior margin of these elements. Conversely, in the Elkins Place bone bed and Boren Quarry specimens, it is closer to the posterior margin. Regarding the infraorbital groove, the overall contour is the same across size classes, but it does not contact the maxilla in YPM VPPU 021742, barely contacts it in the Elkins Place bone bed specimens, and has a long contact in TTU P-10530. There is no ontogenetic change in the most important features utilized in taxonomy and phylogenetics, such as the lacrimal-orbit relationship, and on balance, the Elkins Place bone bed material that we redescribe here is more similar to the larger and presumably more mature Boren Quarry material.

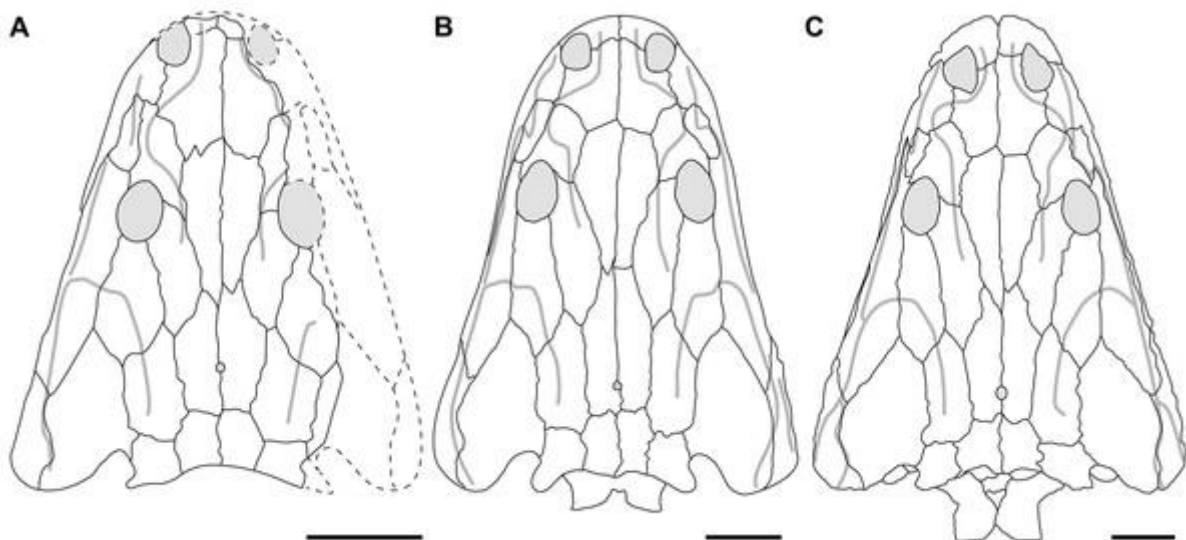


Figure 71: Partial ontogenetic trajectory of *Buettnererpeton bakeri*.

(A) The smallest known partial to complete skull, YPM VPPU 021742; (B) composite reconstruction based on the specimens from the Elkins Place Bonebed; (C) larger specimen from the Boren Quarry, TTU-P 10530 (reproduced from [Martz, 2008:fig. 4.2b](#)). Note that Martz figured a slightly larger but slightly more incomplete skull from the Boren Quarry, but only relatively low-resolution photographs that do not permit an interpretive line drawing to be derived from them were provided. Scale bars equal to 5 cm.

[Download full-size image](#)

DOI: [10.7717/peerj.14065/fig-71](https://doi.org/10.7717/peerj.14065/fig-71)

Postcranial comparisons are more difficult due to disarticulation and the underdeveloped nature of stereospondyl postcrania in general, but nearly every

postcranial element that ossifies in metoposaurids is known from the type locality. The one exception is the ischium, a loosely articulated element that also seems susceptible to taphonomic loss in other bonebeds (*e.g.*, Rotten Hill, with an MNI of 68 preserves only three ischia; [Lucas et al., 2016](#)). Previous work on ossification sequences of temnospondyls with detailed ontogenetic data (*e.g.*, [Schoch, 2004](#); [Witzmann, 2006](#); [Schoch & Witzmann, 2009](#)) also supports an interpretation of relative skeletal maturity. The only other elements absent from the type locality are late-stage ossifications not known to ossify in any metoposaurid, such as the prootic.

Collectively, these comparisons support a hypothesis that the cranial and postcranial anatomy was relatively stable (the ‘adult condition’) by the time a skull length of 30 cm was reached, as in the Elkins Place bone bed specimens. This is in agreement with the very minor changes observed in the only taxon in which features of early ontogeny are definitively known, *M. krasiejowensis*, the smallest (published) skull of which is 27 cm in length ([Sulej, 2007](#):appendix 1). Most of the ontogenetic transformations identified by [Sulej \(2007](#):appendix 2) are also very slight (*e.g.*, the transverse position of the postparietal-tabular suture) compared to more overt ontogenetic changes in other taxa such as marked snout elongation (edopoids, eryopoids, many long-snouted stereospondyls; *e.g.*, [Warren & Hutchinson, 1988](#); [Steyer, 2003](#); [Sequeira, 2003](#); [Schoch, 2021](#)), the appearance or disappearance of lateral exposures of the palatal elements (some dissorophoids; *e.g.*, [Reisz, Schoch & Anderson, 2009](#)), or marked changes to cranial ornamentation (many non-paedomorphic temnospondyls). These conclusions underscore the point that skeletal/somatic maturity and maximum body size need not be treated as correlated; if they were, any specimen less than 60 cm in skull length (almost every specimen) would need to be regarded as immature to some degree. Therefore, we can be reasonably confident that the phylogenetic analysis has not been extremely distorted by ontogenetic immaturity (at least of *Buettnererpeton*) and that it can be properly compared to taxa represented by larger individuals.

Phylogenetic relationships

Our analyses ([Figs. 67–69](#)) recovered different, but fully resolved, topologies depending on whether certain multistate characters were ordered and depending on which optimality criterion was used. The only consensus across both parsimony and Bayesian analyses is that *Metoposaurus sensu* [Brusatte et al. \(2015\)](#), restricted to the three European taxa, is monophyletic and that Metoposauridae is monophyletic. In no analysis did *Metoposaurus* form a clade with exclusively *Buettnererpeton bakeri* and *Panthasaurus maleriensis* (*i.e.*, there is no support for the expansive concept of *Metoposaurus* employed by some workers; *e.g.*, [Lucas, 1998, 2018, 2021](#)). At least based on the parsimony analyses ([Figs. 67](#) and [68](#)), *Anaschisma browni* is as closely related to *Metoposaurus* as *B. bakeri* is. No analysis recovered a sister relationship between *An. browni* and *P. maleriensis*, supporting [Sengupta’s \(2002\)](#) and [Chakravorti & Sengupta’s](#)

(2018) arguments that the Indian metoposaurid is not congeneric with *An. browni*. The third North American taxon, *Apachesaurus gregorii*, was usually recovered in a position distant to *An. browni* and *B. bakeri*, and in the parsimony analyses, it was recovered as the earliest diverging taxon (Figs. 67 and 68). This differs from the Moroccan taxa, which form an exclusive clade in three of the four analyses (Figs. 67A and 69).

The internal conflict among our own analyses underlies broader discord between previous metoposaurid analyses (Fig. 3). Chakravorti & Sengupta (2018) and Gee, Parker & Marsh (2019), using drastically different matrices recovered practically no resolution within Metoposauridae. Conversely, Buffa, Jalil & Steyer (2019) recovered nearly a fully resolved tree, but it is discordant with those that we found except for the monophyly of *Metoposaurus sensu Brusatte et al. (2015)*. Notably, their analysis did recover an exclusive clade of *Metoposaurus*, *Buettnererpeton bakeri*, and *Panthasaurus maleriensis*, lending support to concepts of a more inclusive *Metoposaurus*. They also recovered *Apachesaurus gregorii* as the sister taxon of *Anaschisma browni* and recovered *Arganasaurus* as a clade. These disparities are further compounded when considering the results found upon reanalysis of a modified version of their matrix (Fig. 70).

There are two further complications to consider here. All previous analyses and our own analyses tend to recover weak statistical support (Bremer index < 3, bootstrap frequency < 50%, posterior probability < 70%) for most nodes other than Metoposauridae. As aptly put by Sanderson (1995:299), “without some assessment of reliability, a phylogeny has limited value. It may still function as an efficient summary of available information on character-state distributions among taxa...but it is effectively mute on the evolutionary history of those taxa”. Therefore, any node without strong support under any support metric should not be considered reliable because it may hinge on a single score. Most discrepancies between resolved topologies are found at nodes with weak support. If nodes in either the topology of Buffa, Jalil & Steyer (2019) or in our topologies were collapsed if they did not have at least one metric indicating strong support, almost all nodes would be collapsed (Fig. 72), and the resultant topologies would be nearly identical to each other and nearly identical to the topologies of Chakravorti & Sengupta (2018) and Gee, Parker & Marsh (2019): almost complete polytomies.

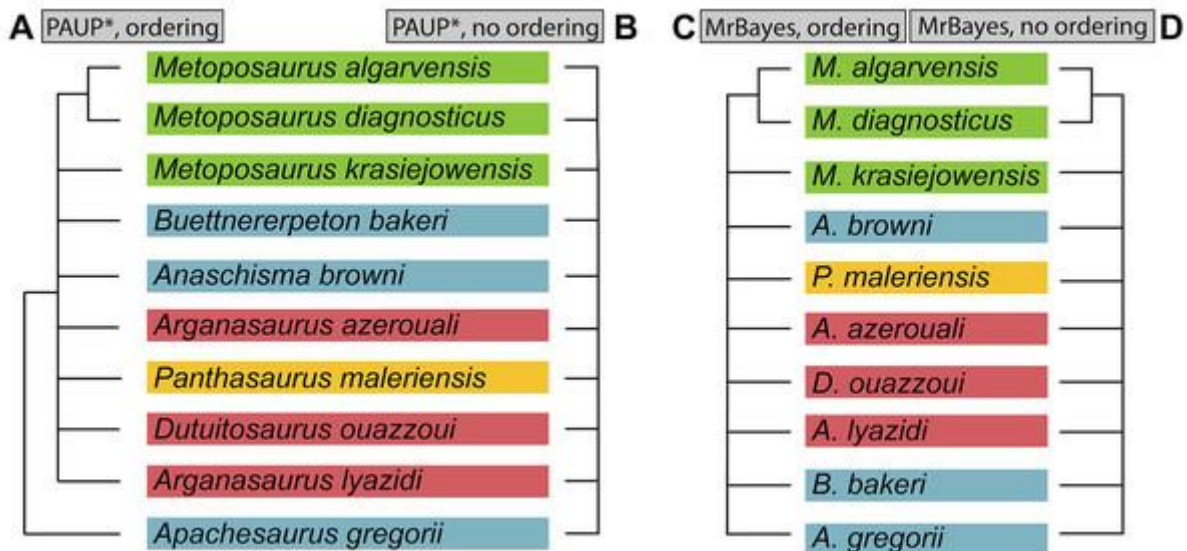


Figure 72: Comparison of topologies recovered with different analyses of the matrix of this study with all nodes that do not meet the standard thresholds for strong support collapsed.

These topologies reflect the only relationships that we feel can be regarded as robust and thus used in broader narratives of metoposaurid evolution. (A) Collapsed strict consensus from the analysis in PAUP* with certain multistate characters ordered; (B) collapsed strict consensus recovered from the analysis in PAUP* with all multistate characters unordered; (C) collapsed 50%-majority-rule consensus from analysis in MrBayes with certain multistate characters ordered; (D) collapsed 50%-majority-rule consensus from analysis in MrBayes with all multistate characters unordered. Thresholds for ‘strong support’ were as follows: Bremer index ≥ 3 ; bootstrap value $\geq 50\%$; posterior probability $\geq 70\%$. A node was collapsed if it did not meet any of these.

[Download full-size image](#)

DOI: [10.7717/peerj.14065/fig-72](https://doi.org/10.7717/peerj.14065/fig-72)

Our reanalysis of the matrix of [Buffa, Jalil & Steyer \(2019\)](#) also underscores the lability of well-resolved topologies. With no scoring changes and only seven multistate characters ordered, the tree largely collapses compared to the original ([Figs. 70A](#) and [70B](#)). Many of the remaining nodes are peculiar (*e.g.*, *Anaschisma browni* + *Arganasaurus azerouali*), although the pairing of *Apachesaurus gregorii* and *Arganasaurus lyazidi* is intriguing because these taxa are known from the smallest specimens among metoposaurids. When scoring changes that we consider to meet a high evidentiary standard were implemented ([Appendix 3](#)), the topology was practically unresolved regardless of character ordering ([Figs. 70C](#) and [70D](#)). We want to again emphasize that our decision to reanalyze this matrix was not out of any personal or professional animus against Buffa, Jalil & Steyer. Instead, it was motivated by our desire to further explore differences between matrices that recovered fully resolved topologies and by the fact that theirs was the only one of three previous studies to recover much resolution at all. Modification of our matrix by other workers may produce similar changes in, or loss of, resolution.

Finally, we briefly discuss other discordant results of our analysis. The closer relationship of brachyopoids, rather than capitosaurids (*e.g.*, [Schoch, 2008](#), and

derivates), to trematosaurids and metoposaurids is not surprising considering that ‘short-faced’ stereospondyls often cluster in other analyses (e.g., [Yates & Warren, 2000](#); [Pawley, 2007](#); [McHugh, 2012](#); [Schoch, 2013](#); [Maganuco, Pasini & Auditore, 2014](#)) – such a similarity sometimes led to phenetic associations between dvinosaurs, brachyopoids, and metoposaurids prior to computer-assisted phylogenetics (e.g., [Romer, 1947](#); [Dutuit, 1976](#)). It is notable that analyses with the broadest taxon samples tend to recover these short-snouted clusters, indicating that taxon inclusion/exclusion contributes to the present discrepancies. Rhytidosteids undoubtedly play a role in further resolution of Stereospondyli given uncertainty over their monophyly (compare topologies of [Dias-da-Silva & Marsicano, 2011](#); [Schoch, 2013](#); [Maganuco, Pasini & Auditore, 2014](#)), and should they not be monophyletic, the ‘true’ position of the most commonly sampled members (e.g., *Laidleria*, *Peltostega*, *Sangaia*).

Finally, a persistent result of the analysis of our expanded matrix is the separation of *Callistomordax kugleri* from Metoposauridae ([Figs. 67–69](#)). This result conflicts with most previous analyses that have sampled both taxa, including [Schoch \(2008\)](#), the original description and analysis of *C. kugleri*; derivates of this matrix ([Schoch, 2011, 2019](#); [Sues & Schoch, 2013](#); [Schoch, Milner & Witzmann, 2014](#)); and other largely independent matrices (e.g., [Schoch, 2013](#); [Buffa, Jalil & Steyer, 2019](#)). In addition to our revision of the matrix of Buffa, Jalil & Steyer, we also examined some of these other matrices in the hopes of identifying additional characters and states that support a sister relationship between Metoposauridae and *C. kugleri* and the inclusion of this clade within Trematosauria. All of the synapomorphies listed by Buffa, Jalil & Steyer, are valid, and we attribute their results in part to the more limited taxon sampling – the only other stereospondyls sampled were the rhinesuchid *Rhineceps nyasaensis* and *Almasaurus habbazi*. Either features or taxa that might favor a closer relationship of *C. kugleri* with another taxon are thus largely unsampled (e.g., the unpaired frontal shared with *Trematolestes hagdorni*, the sister taxon in our analysis or the keeled cultriform process purportedly shared with *A. habbazi*).

Conversely, the family of matrices associated with the matrix of [Schoch \(2008\)](#) has a richer stereospondyl sample, but we also identified several mischaracterizations or overgeneralizations that artificially strengthened the sister relationship of *Callistomordax kugleri* and Metoposauridae. Firstly, there is only one metoposaurid OTU in this family of matrices, so the relationship is really one between *C. kugleri* and a specific metoposaurid. Originally, it was stated to be a composite of *Anaschisma browni*, *Dutuitosaurus ouazzoui*, and *Metoposaurus diagnosticus*, but the scorings do not appear to account for interspecific differences like the pleurocentra ossifications purportedly retained in *D. ouazzoui* and absent in all other metoposaurids ([Dutuit, 1972, 1976](#)); the prefrontal-jugal contact in *D. ouazzoui*, which is not found in any metoposaurid with a lacrimal-orbit contact like *A. browni* and *M. diagnosticus* ([Dutuit, 1976](#); [Sulej, 2002, 2007](#); [Lucas et al., 2016](#)); and the presence of keeled teeth in some specimens of *M. diagnosticus* ([Milner & Schoch, 2004](#)). The metoposaurid OTU was subsequently changed to *M. diagnosticus* in subsequent studies and could represent a chimera

of *M. diagnosticus* and *M. krasiejowensis* in the contemporary framework (the *M. diagnosticus* of [Sulej, 2002](#)). If so, this restriction fails to account for intraspecific variation that is noted particularly from Krasiejów, such as in the prefrontal-jugal relationship and the presence or absence of symphyseal teeth ([Konietzko-Meier & Wawro, 2007](#); [Sulej, 2007](#)). If the OTU is restricted to *M. diagnosticus* in the contemporary framework (*sensu* [Brusatte et al., 2015](#), and subsequent workers), the characterization still fails to account for intraspecific variation in features like the dentition, notwithstanding that the most recent comprehensive description of *M. diagnosticus* is more than 130 years old ([Fraas, 1889](#)).

Some scores for this composite OTU are also erroneous, irrespective of the composition of the OTU. [Schoch \(2008\)](#) listed a vertically oriented iliac shaft (as opposed to a posterodorsally oriented shaft) as a synapomorphy of Trematosauria inclusive of Metoposauridae, but all metoposaurids have strongly inclined iliac shafts (*e.g.*, [Sengupta, 2002](#):fig. 12C; [Sulej, 2007](#):figs. 58–59, 71; [Lucas et al., 2016](#):fig. 67; [Fig. 62](#)), as does *Callistomordax kugleri* ([Schoch, 2008](#):fig. 9c therein, compared with that of *Trematolestes hagdorni* in [Schoch, 2006](#):fig. 6A). A second example is a purported synapomorphy of Metoposauroidea + *Almasaurus habbazi* + *Rileymillerus cosgriffi*: intercentra that are as long as wide in ventral view; this condition is only found in *Apachesaurus gregorii* among metoposaurids. In the same vein, *Ap. gregorii* is the only metoposaurid without intercentra with an anteriorly convex surface, a purported apomorphy for *C. kugleri* + Metoposauridae; those of *Ap. gregorii* are instead concave with a throughgoing notochordal canal, a feature likely to represent relative immaturity ([Gee, Parker & Marsh, 2017](#); [Gee & Parker, 2018](#)). The dense sampling of both metoposaurids and many characters that differentiate them in our matrix undoubtedly further exaggerates the topological disparity because Metoposauridae is not as homogenous as when depicted as a single OTU of a composite nature that does not include all metoposaurids. A final example of a dubious apomorphy of *C. kugleri* + Metoposauridae is the purported presence of ‘long smooth [occipital] blades as long as the dermal portion of the postparietal.’ This feature is genuinely found in *Callistomordax*, but metoposaurids have anteroposteriorly elongated postparietals that are longer than wide (they are wider than long in *Callistomordax*), and the occipital portion (which is not smooth; *e.g.*, [Sulej, 2007](#):37) is clearly much shorter in height than the roofing portion is long (*e.g.*, [Sulej, 2007](#):fig. 1; [Figs. 9, 11, 12, 14, 21, 23](#)).

Erroneous support is then likely compounded by different character sampling – [Schoch \(2008\)](#) does not have a character for the medial edge of the palatine ramus, which is inwardly convex in *Callistomordax kugleri* and *Almasaurus habbazi* but straight in metoposaurids, or any character for coronoid dentition, which is unique in *Callistomordax* in having teeth only on the middle coronoid. We have not re-examined this family of matrices in full and consider a full retesting of it to be beyond the scope of this study, but the above discussion serves as evidence that erroneous or overgeneralized scores have contributed to an artificially strong (or even spurious) sister relationship. In short, the sister relationship of *Callistomordax* with Metoposauridae has probably been overstated to a degree due to a combination of misrepresented apomorphies and limited taxon sampling,

although their general relatedness is not in question here. [Maganuco, Pasini & Auditore \(2014\)](#) recovered *Almasaurus* as the sister taxon to a Metoposauridae comprised of two OTUs (*Anaschisma browni* and *Metoposaurus diagnosticus*) and then *Callistomordax* as the sister taxon to these three taxa; this clade is then allied with brachyopoids and other short-faced temnospondyls and not with other trematosaurids.

Future directions for metoposaurid phylogenetics

It should be apparent that the phylogeny of the metoposaurids remains without even partial consensus and is highly sensitive to both the primary data and to the analytical methods. It is perhaps unsurprising that intrarelationships of this clade remain difficult to resolve considering the exceptional morphological conservatism within the clade. This is perhaps best exemplified by *Metoposaurus krasiejowensis*, which all workers consider valid at the species level (implied by continued usage), but which is differentiated from *Metoposaurus diagnosticus* only by a linear equation for the expansion angle of the sutures separating the parietal from the supratemporal ([Sulej, 2002, 2007](#)).

At present, no topology recovered by a computer-assisted analysis can be used to draw robust conclusions regarding the relationships of metoposaurids, and it is better to derive only conservative claims from well-supported nodes than to overextend the data where support does not exist, creating potentially spurious relationships and narratives. Below, we briefly outline some areas where additional study could improve phylogenetic inference. These pertain only to the primary data and not to certain analytical approaches (*e.g.*, likelihood *vs* parsimony, character weighting and ordering).

Polymorphisms

How polymorphisms (specifically non-ontogenetic intraspecific variations) are treated is directly relevant to all studies because they are part of the primary data. Scoring a taxon for a single state when it displays at least two misrepresents the data. Despite exhibiting non-ontogenetic polymorphism throughout their evolutionary history (*e.g.*, [Langston, 1953](#); [Boy, 1995](#); [Schoch & Rubidge, 2005](#); [Jeannot, Damiani & Rubidge, 2006](#); [Schoch, 2009](#); [Schoch & Witzmann, 2012](#); [Morkovin, 2015](#)), temnospondyls are rarely scored as being polymorphic in phylogenetic analyses. For example, [McHugh's \(2012\)](#) temnospondyl matrix of 99 taxa and 297 characters and [Schoch's \(2013\)](#) temnospondyl matrix of 72 taxa and 212 characters both contain zero polymorphisms. Therefore, polymorphism is widely recognized phenetically among temnospondyls, but it oddly remains overlooked or ignored in phylogenetics. Polymorphisms are pervasive in metoposaurids ([Table 5](#)), and many pertain to phylogenetic characters, but most metoposaurid analyses have not accounted for this variability. This is inherently problematic, both as a conceptual overgeneralization of species-level anatomy, as certain characters will appear more discrete than they are in reality, and as a methodological shortcoming, as previous studies have demonstrated that including

polymorphisms outperforms analysis without them (*e.g.*, [Wiens, 1995, 1998](#); [Wiens & Servedio, 1997](#)). Treatment of polymorphisms has been extensively discussed in the literature (*e.g.*, [Campbell & Frost, 1993](#); [Kornet & Turner, 1999](#); [Wiens, 1999](#)); the underlying point is that there is no strong *a priori* rationale for omitting polymorphisms. Therefore, any future metoposaurid analyses will need to account for these. Of the 49 scoring changes that we made to the matrix of [Buffa, Jalil & Steyer \(2019\)](#), 16 changes (32.6%) involved changing a previously scored cell from a single state to a polymorphism based on the literature, and these likely account for some of the discrepancies in topologies ([Fig. 70](#)).

Table 5:

Summary table of sources of non-ontogenetic intraspecific variation (polymorphism) in features that have been historically utilized in taxonomy and phylogenetic analyses.

Feature	Taxon	Reference
CRANIAL		
Lacrimal-orbit	<i>M. krasiejowensis</i>	Sulej (2007)
Lacrimal contribution to lateral orbital margin	<i>An. browni</i>	Lucas et al. (2016)
Lacrimal-nasal	<i>P. maleriensis</i>	Roychowdhury (1965) , Sengupta (2002)
	<i>B. bakeri</i>	Case (1932) ; this study
Parietal-postorbital	<i>M. krasiejowensis</i>	Sulej (2007)
	<i>An. browni</i>	Lucas et al. (2016)
Prefrontal-maxilla	<i>M. krasiejowensis</i>	Sulej (2007)
Postfrontal contribution to orbit	<i>An. browni</i>	Lucas et al. (2016)
Anterior extent of jugal	<i>An. browni</i>	Lucas et al. (2016)
Occiput (dorsal exposure)	<i>Ap. gregorii</i>	Spielmann & Lucas (2012)
Parasphenoid ornamentation	<i>An. browni</i>	Sawin (1945) , Gee & Jasinski (2021)
	<i>M. krasiejowensis</i>	Sulej (2007)
MANDIBULAR		
Adsymphyseal teeth	<i>M. krasiejowensis</i>	Konietzko-Meier & Wawro (2007)
Chorda tympani foramen	<i>M. krasiejowensis</i>	Sulej (2007)

Feature	Taxon	Reference
Surangular-prearticular	<i>M. krasiejowensis</i>	Sulej (2007)
Relative length of Meckelian foramen	<i>M. krasiejowensis</i>	Sulej (2007)
POSTCRANIAL		
Reticulate ornamentation on interclavicle	<i>An. browni</i>	Lucas et al. (2016)
	<i>Ap. gregorii</i>	Spielmann & Lucas (2012)
Reticulate ornamentation on clavicle	<i>M. krasiejowensis</i>	Antczak & Bodzioch (2018)
Interclavicle (posterolateral margin)	<i>An. browni</i>	Lucas et al. (2016)
	<i>B. bakeri</i>	Case (1932) ; this study
	<i>M. krasiejowensis</i>	Sulej (2007)
Clavicle (anterolateral margin)	<i>P. maleriensis</i>	Roychowdhury (1965) , Sengupta (2002)
Clavicle (anteromedial margin/contact)	<i>M. krasiejowensis</i>	Sulej (2007)
	<i>D. ouazzoui</i>	Dutuit (1976)
Clavicle (posteromedial margin)	<i>B. bakeri</i>	Case (1932) ; this study
	<i>M. krasiejowensis</i>	Sulej (2007)
	<i>An. browni</i>	Lucas et al. (2016)
Humerus (deltopectoral crest/supinator process size)	<i>An. browni</i>	Lucas et al. (2016)
Ilium shaft (sinuosity)	<i>M. krasiejowensis</i>	Sulej (2007)

DOI: [10.7717/peerj.14065/table-5](https://doi.org/10.7717/peerj.14065/table-5)

Note:

This is not an exhaustive list of all previously reported polymorphisms; additional sources of intraspecific variation not related to features typically employed for taxonomy or phylogenetic characters are detailed by [Dutuit \(1976\)](#), [Sulej \(2007: Appendix 2\)](#), and [Lucas et al. \(2016\)](#).

Missing data

Given the incompleteness of the fossil record, there will always be missing data for extinct taxa, which inherently hampers phylogenetic inference. Missing data may

also arise from outdated descriptions, especially when they precede the computer-assisted phylogenetics era in which descriptions may be conformed around phylogenetics with respect to the types of figures and language that are employed. Three metoposaurids would benefit from updated documentation to provide a better anatomical characterization that does not necessitate first-hand observation.

Arganasaurus lyazidi was named and described by [Dutuit \(1976\)](#), but there are no interpretive line drawings or reconstructions. The only figures are three low-resolution photographic plates ([Dutuit, 1976](#): pls. XLVIII-L). The descriptive osteology itself is less than half a page, and Dutuit expressly stated (p. 182 therein) that the material available to him was insufficient to diagnose this taxon. Therefore, essentially the entire anatomy has been derived from the revised (but in fact novel) diagnosis of [Hunt \(1993\)](#) and his corresponding reconstruction of the skull.

Dutuitosaurus ouazzoui was conversely described in painstaking detail by [Dutuit \(1976\)](#), but the photographic plates are also limited, and there are few interpretive figures that permit an assessment of intraspecific variation despite this taxon's large sample size. Recent workers ([Chakravorti & Sengupta, 2018](#); [Buffa, Jalil & Steyer, 2019](#)) have cited personal observations in scoring some characters for this taxon, but its osteology has never been revised, and even recent published photographs are those originally published by Dutuit (e.g., [Rinehart et al., 2013](#):fig. 1; [Khaldoune et al., 2016](#):fig. 14). The question surrounding *D. ouazzoui* is whether Dutuit's characterization is an oversimplification that obscures polymorphisms. The cranial osteology is an oversimplification insofar as it does not account for all of the material. [Dutuit \(1976:41\)](#) himself remarked on the prohibitively large number and varying degree of preparation, which precluded any biometric analysis or characterization of cranial variation. He did provide a summary of variation for most postcranial elements, but the cranial data is of greater import given the skew towards cranial characters in diagnoses and character matrices.

Metoposaurus diagnosticus is characterized from the most dated descriptions among metoposaurids. The most thorough description of this taxon is over 130 years old ([Fraas, 1889](#)). While a reconstruction is ubiquitous throughout the literature, this mostly comprises only the dorsal view of a single skull roof. The only recent figures of *M. diagnosticus* include [Sulej's \(2002\)](#) interpretive line drawing of the holotype; and photographs without line drawings by [Milner & Schoch \(2004\)](#). The palate, occiput, and postcranial anatomy thus remain exceptionally poorly characterized.

The status of “*Metoposaurus*” *bakeri*

As discussed above, phylogenetic inference is unable to confer robust support for the inclusion of this species within *Metoposaurus*, although the topologies are so disparate and poorly supported that there is also no strong support for any other particular hypothesis (e.g., placement in *Anaschisma* vs erection of a novel genus). Therefore, the following section presents a phenetic comparison and rationale for the erection of a novel genus to accommodate this species.

Comparative osteology

Metoposaurid taxonomy has long hinged on a handful of emphasized cranial and postcranial features. The lacrimal is discussed first, as its position and relative length produce the most variation in the skull roof of metoposaurids. *Buettnererpeton bakeri* was originally placed in *Metoposaurus* following historical interpretations that the lacrimal was excluded from the orbit in the latter (e.g., [Hunt, 1993](#)). This was subsequently disproven in the type species by [Sulej \(2002\)](#), and another two species with the lacrimal entering the orbit were named by [Sulej \(2002\)](#) and [Brusatte et al. \(2015\)](#). *Buettnererpeton bakeri* therefore shares a lacrimal excluded from the orbit only with *Apachesaurus gregorii*, *Arganasaurus lyazidi*, and *Dutuitosaurus ouazzoui*, although this occurs very rarely in *M. krasiejowensis*. The lacrimal of *B. bakeri* is intermediate in size, being anteriorly truncated such that it does not reach the naris (allowing a maxilla-nasal contact). The relative length of the lacrimal is evidenced by its anterior extent relative to the prefrontal. It either ends at, or just anterior, to the anteriormost margin of the prefrontal ([Figs. 4, 9, 12](#)), compared to *Ap. gregorii* in which the very short lacrimal ends well posterior to this level. This differs from *Ar. lyazidi* in which an anteriorly extensive lacrimal reaches the naris, fully dividing the maxilla and the nasal, as well as *Panthisaurus maleriensis* in which the lacrimal nearly reaches to the naris from the orbital margin ([Chakravorti & Sengupta, 2018](#)). Some previous comparative reconstructions (e.g., [Hunt, 1993:fig. 4](#); [Spielmann & Lucas, 2012:fig. 13](#)) have depicted a lacrimal-nasal contact, which separates the maxilla and the prefrontal, in *B. bakeri*. This follows [Case's \(1931:fig. 1\)](#) original illustration of the holotype, in which he depicts a point contact between the four elements, which was modified in [Case \(1932:fig. 2\)](#) to a longer lacrimal-nasal suture that definitively separates the maxilla and the prefrontal. However, [Case \(1932:figs. 3–5\)](#) illustrates other specimens without a lacrimal-nasal contact, which we reaffirmed here ([Figs. 4, 9](#)). The holotype is too badly preserved and partially reconstructed in this region to verify his interpretations of this specimen ([Fig. 6](#)), but one referred specimen preserves a broad lacrimal-nasal contact ([Fig. 12](#)). Similar variation in both the presence of the contact and the degree of sutural overlap when present is documented in *Metoposaurus krasiejowensis* in which this may vary within an individual ([Sulej, 2007:fig. 13](#)) and in *Anaschisma browni* ([Lucas et al., 2016](#)). The predominating condition differs between these taxa, however. In *M. krasiejowensis*, the lacrimal and nasal usually contact (as is the only condition in the type species, *M. diagnosticus*, and in *D. ouazzoui*), whereas they are usually separated in *An. browni* (as is the only condition in *Ap. gregorii*).

The only other substantial source of non-ontogenetic interspecific variation among cranial sutures is in the premaxilla-nasal suture. In one referred specimen of *Buettnererpeton bakeri* ([Fig. 9](#)), the suture angles slightly posterolaterally to form an oblique contact (the contact is unknown in all other specimens). The angle is steeper in *Anaschisma browni* ([Lucas et al., 2016](#)) but typically shallower in *Metoposaurus* (e.g., [Sulej, 2002, 2007](#)); the latter has a nearly horizontal contact. *Arganasaurus lyazidi* and *Dutuitosaurus ouazzoui* also have nearly horizontal contacts ([Dutuit, 1976](#); [Hunt, 1993](#)). That of *B. bakeri* is most similar

to *Apachesaurus gregorii* (Hunt, 1993). Some referred specimens of *Panthesaurus maleriensis* have a nearly horizontal contact (Roychowdhury, 1965; Sengupta, 2002), but Chakravorti & Sengupta (2018) illustrate the holotype as having a sinusoidal contact, with a distinct anterior projection of the nasal and a smaller posterior projection of the premaxilla adjacent to the midline. This kind of complexity with a fully defined projection otherwise only appears rarely in *M. krasiejowensis* (Sulej, 2007:fig. 9).

Three qualitative features differentiate *Apachesaurus gregorii* from other metoposaurids but do little for differentiating among the remaining taxa. *Apachesaurus gregorii* has been differentiated from all other metoposaurids by the shallow otic notches without a distinct tabular horn, although these features may reflect ontogenetic immaturity (Gee & Parker, 2018), and *Arganasaurus* also has relatively shallow otic notches (a bit deeper than in *Ap. gregorii*; Buffa, Jalil & Steyer, 2019). The possibility of a correlation with maturity raises the issue of whether ontogenetically non-equivalent units are being compared (further discussed below), but the Nova Scotia specimen of *B. bakeri* is similarly sized to specimens of *Ap. gregorii* and *Ar. lyazidi* and already possesses deep otic notches, so the differentiation from these two taxa on this basis is established. Similarly, the occiput is either not exposed in dorsal view or only very slightly in *Ap. gregorii*, whereas it projects prominently in all other taxa except some examples of *Anaschisma browni* (Kufner & Gee, 2021). Contrary to the revised diagnosis of *Arganasaurus* as being unique in having a posteroventrally sloping occiput (Buffa, Jalil & Steyer, 2019), this feature occurs in all specimens of *B. bakeri* in which the occiput is preserved (Figs. 6, 9, 12, 17) but was not apparent in Case's (1931, 1932) original work. Romer (1947:235) also noted the consistent presence of a sloped occiput in metoposaurids like in brachycephalic stereospondyls. Finally, *Ap. gregorii* has a narrow cultriform process compared to the broad, flat process found in all other metoposaurids; the former is more similar to other stereospondyls.

Emphasized postcranial features have largely related to the clavicle and the interclavicle, as these large, plate-like elements are among the most frequently preserved elements. For both elements, the relative size of regions of reticulate or circular ornamentation was long employed as a means of differentiating North American and European metoposaurids (e.g., Colbert & Imbrie, 1956; Hunt, 1993; Sulej, 2002, 2007). However, Lucas et al. (2016) reported one probable specimen of *Anaschisma browni* from Rotten Hill with a *Metoposaurus*-like interclavicle, and Spielmann & Lucas (2012) documented more evenly distributed variability in *Apachesaurus gregorii*. We also documented variability in the relative size of the region of circular pitting on the interclavicle in *Buettnererpeton bakeri* (Figs. 55 and 56), and it appears that this feature is of little utility in at least the North American taxa. Similar variation occurs in the clavicular ornamentation of *B. bakeri* (Fig. 51) and *M. krasiejowensis* (Antczak & Bodzioch, 2018), and this feature may also be of reduced utility.

Dutuitosaurus ouazzoui has long been diagnosed as having ossified pleurocentra, contrary to all other metoposaurids (Dutuit, 1972, 1976; Hunt, 1993), but Sulej

(2007:118) has pointed out that this occurs only in one of the dozens of known specimens of this taxon and that pleurocentra are not found along the entire presacral column despite the articulation of many specimens. We further discuss this feature in [Appendix 1](#) as rationale for not scoring this taxon for this condition, but the balance of evidence favors Sulej's interpretation of a pathological condition given the sparse distribution in the one taxon known from many articulated skeletons with complete presacral columns. Furthermore, some taxa have no known axial material, and it is inherently difficult to conclude biological absence for taxa represented only by isolated material unless it occurs in great abundance in bonebeds (e.g., *Anaschisma browni*, *Buettnererpeton bakeri*, *Metoposaurus krasiejowensis*). A final feature that one of us has cited ([Gee, Parker & Marsh, 2019](#)) is the contour of the anterodorsal margin of the ilium (more frequently sinusoidal in large individuals of *Metoposaurus* than in *Anaschisma*; e.g., [Sulej, 2007](#):fig. 58; [Lucas et al., 2016](#):fig. 67), but this feature appears intraspecifically variable in at least small individuals of *Buettnererpeton bakeri* ([Fig. 62](#)) and may be similarly so in *A. browni* ([Kufner & Gee, 2021](#)) and in small to medium individuals of *M. krasiejowensis*.

In summary, as with most other metoposaurids, *Buettnererpeton bakeri* lacks distinct autapomorphies and is instead differentially diagnosed by a unique combination of characters. The full diagnosis is not repeated here, but discrete features like the exclusion of the lacrimal from the orbit in all specimens are an immediate differentiator from the other North American taxon known from appreciably sized specimens, *Anaschisma browni*. The intermediate length of the lacrimal in *B. bakeri* separates it from taxa with much longer lacrimals separated from the orbit (sometimes reaching the naris, as in *Arganasaurus lyazidi*) and from taxa with much shorter lacrimals separated from the orbit (*Apachesaurus gregorii*). Other discrete features include the separation of the splenial from the symphysis and the presence of a clavicular sensory groove in at least some individuals (further differentiated from *An. browni*); and the absence of a maxilla-orbit contact (differentiated from *Dutuitosaurus ouazzoui*). Most of the other differential features are gradational rather than discrete (e.g., the development of the alary process or the otic notch), and so while they are considered presently valid, these may prove to be less useful for differentiation as larger sample sizes and their intraspecific variation (both ontogenetic and non-ontogenetic) are characterized.

Rationale for erecting a novel genus

In light of the lack of consensus from phylogenetic analyses, the immediate question is what warrants the placement of *Buettnererpeton bakeri* within a new genus, *Buettnererpeton*. Could this species, acknowledged by all workers to be distinct, belong to either *Metoposaurus* or *Anaschisma*, the two genera (accounting for synonymy and nomenclatural changes of *Anaschisma*) to which it has been previously assigned? The immediate answer is no. Diagnoses of both taxa include a lacrimal that enters the orbit (e.g., [Sulej, 2007](#); [Brusatte et al., 2015](#); [Gee, Parker & Marsh, 2019](#); [Kufner & Gee, 2021](#)).

One option would be to simply remove the lacrimal character from the diagnosis of one of these taxa to create a more inclusive *Anaschisma* or *Metoposaurus*. This could be preferable as an explicit means of acknowledging that the lacrimal-orbit relationship is intraspecifically variable in *M. krasiejowensis* (Sulej, 2007). There is also a precedent for a genus in which the constituent species differ with respect to this character: *Arganasaurus* (Buffa, Jalil & Steyer, 2019). However, this is untenable because in most diagnoses of *Anaschisma* and *Metoposaurus*, the lacrimal-orbit contact is the only diagnostic cranial character (e.g., Hunt, 1993; Schoch & Milner, 2000; Milner & Schoch, 2004; Lucas et al., 2016), unlike for *Arganasaurus*, which is diagnosed by other cranial features (Buffa, Jalil & Steyer, 2019). Other diagnoses either include features susceptible to taphonomic loss (e.g., absence of an opisthotic in *Metoposaurus sensu Brusatte et al., 2015*) or features expressly stated to be intraspecifically variable with a majority condition (e.g., relative anterior extent of the prefrontal and the lacrimal in *Anaschisma sensu Gee, Parker & Marsh (2019)*).

We cannot find an alternative cranial synapomorphy that unites *Buettnererpeton bakeri* with either *Anaschisma* or *Metoposaurus* but not with both (i.e., synonymizing *Anaschisma* with *Metoposaurus* and placing *B. bakeri* in this expanded genus). Therefore, removing the lacrimal-orbit feature from either taxon would eliminate the means of differentiating isolated skulls of *Anaschisma* and *Metoposaurus* because it would render their constituent species as *nomina dubia* as their type specimens (all isolated skulls) would no longer be diagnostic. This conundrum is only exacerbated if the Indian *Panthasaurus maleriensis* is considered to belong to *Metoposaurus* (Roychowdhury, 1965; Lucas, 2021; but see Hunt, 1993; Schoch & Milner, 2000; Sengupta, 2002; Sulej, 2002; Brusatte et al., 2015; Chakravorti & Sengupta, 2018). Therefore, it is also not possible to diagnose a clade comprised of the three European taxa, *Buettnererpeton bakeri*, and *Panthasaurus maleriensis* that excludes *Anaschisma browni* (the most similar in cranial anatomy to the European *Metoposaurus*) if not all other metoposaurids to form a monogeneric family (as with Roychowdhury, 1965, and Dutuit, 1976). Buffa, Jalil & Steyer (2019) did recover three unambiguous synapomorphies uniting this clade of the European *Metoposaurus*, *B. bakeri*, and *P. maleriensis*: an unossified opisthotic, ornamentation of the parasphenoid restricted to basal plate, and small posttemporal foramen. However, two of these features are disputed by other workers. *Panthasaurus maleriensis* purportedly has an ossified opisthotic (Chakravorti & Sengupta, 2018, contra Roychowdhury, 1965). The ornamentation on the parasphenoid is intraspecifically variable in *Metoposaurus krasiejowensis*, being absent in some specimens (Sulej, 2007); Chakravorti & Sengupta also state that ornamentation is absent in *M. diagnosticus*. All five species share a small posttemporal foramen as defined by Buffa, Jalil & Steyer, but it is also found in *Arganasaurus azerouali* and *Anaschisma browni*. This illustrates the difference between an unambiguous synapomorphy of a clade and a diagnostic feature of a clade. Finally, *B. bakeri* lacks the shallow otic notch with “bulge-like” tabular horns and a triangular squamosal that diagnose *Arganasaurus*. It differs from *Panthasaurus maleriensis* in lacking the long lacrimal entering the orbit and

in several of the more qualitative features listed for this taxon by [Chakravorti & Sengupta \(2018\)](#), such as anteroposteriorly short postparietals and the lateral expansion of the parietals anteriorly. There is therefore no basis for accommodating *B. bakeri* within one of these genera.

An alternative approach would be to accommodate *Buettnererpeton bakeri* into an existing genus in which the lacrimal is always excluded from the orbit (*Apachesaurus* or *Dutuitosaurus*). The insistence by some workers on the interpretation of *Apachesaurus* as a diminutive metoposaurid much smaller than other taxa (*e.g.*, [Rinehart & Lucas, 2018](#); [Lucas, 2021](#)) would bar *B. bakeri* from congenericity because there are typically large metoposaurids referred to *B. bakeri* from sites approximately coeval to the Elkins Place bone bed that have a lacrimal excluded from the orbit ([Houle & Mueller, 2004](#); [Martz, 2008](#); [Mueller et al., 2016](#)). If all specimens of *A. gregorii* are considered to be juveniles, numerous features separate similarly sized specimens of *B. bakeri* from those of *A. gregorii* ([Spielmann & Lucas, 2012](#)), including a wide cultriform process, a deep otic notch, a longer lacrimal, and a lacrimal flexure of the supraorbital canal that contacts the lacrimal. In *D. ouazzoui*, the maxilla enters the orbit due to a truncated jugal ([Dutuit, 1976](#); also found in *Arganasaurus azerouali*; [Buffa, Jalil & Steyer, 2019](#)) but not in *B. bakeri*. The intercentra of *D. ouazzoui* are also proportionately longer than in non-*Apachesaurus* metoposaurids, including *B. bakeri*. Therefore, it is also not possible to accommodate *Buettnererpeton bakeri* into either *Apachesaurus* or *Dutuitosaurus*, and we thus erect *Buettnererpeton* to accommodate this species.

Ontogenetic disparity among metoposaurids

A previously noted important consideration in the discussion of metoposaurid osteology and taxonomy, with an eye towards future work, is ontogeny in metoposaurids. These points are not exclusive to *Buettnererpeton bakeri* and are expanded on here for Metoposauridae at large.

Although there is a wealth of histological data assessing skeletochronology (*e.g.*, [Steyer et al., 2004](#); [Konietzko-Meier & Klein, 2013](#); [Konietzko-Meier & Sander, 2013](#); [Gee & Parker, 2017, 2020](#); [Gee, Parker & Marsh, 2017](#); [Teschner, Sander & Konietzko-Meier, 2017](#); [Teschner et al., 2020](#)), these methods remain constrained by gaps in the fossil record and disparity between taxa, and as we noted previously, there is little data for North American taxa. The question of whether *Buettnererpeton bakeri* might only be represented by immature specimens applies to other taxa as well; there is marked size disparity among metoposaurids in general ([Fig. 73](#); Table S2). Presumably, size disparity tracks ontogenetic disparity to a degree (*i.e.*, some taxa are not represented by mature individuals). However, this assumption can be complicated by intraspecific variation and unfounded assumptions about tight correlations between size and maturity (*e.g.*, [Brinkman, 1988](#); [Brochu, 1996](#)). This complicates qualitative comparisons and phylogenetic analyses.

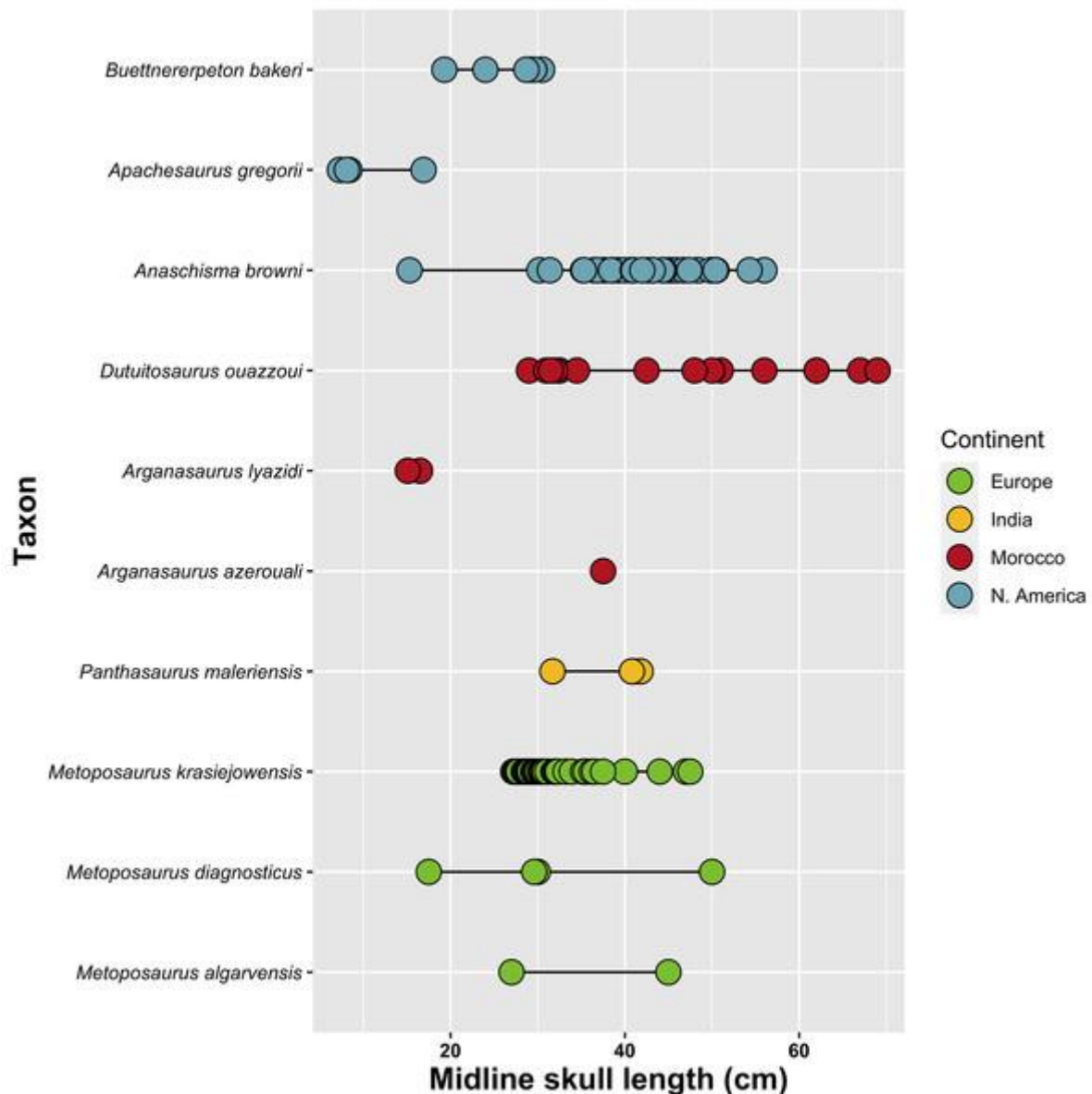


Figure 73: Size chart comparing midline skull lengths between metoposaurids.

Midline skull length is based on the length from the anterior margin of the premaxillae to the posterior margin of the postparietals. Refer to Table S2 for list of measurements and data annotations.

[Download full-size image](#)

DOI: [10.7717/peerj.14065/fig-73](https://doi.org/10.7717/peerj.14065/fig-73)

One taxon worth mentioning is *Arganasaurus lyazidi*, which is known from essentially the same size range as *Apachesaurus gregorii* (both smaller than *Buettnererpeton bakeri*). [Dutuit \(1976\)](#) mentioned the possibility that *Ar. lyazidi* could be a dwarf taxon, but evidence for this has never been provided, and this hypothesis has never been adopted by other workers, suggesting an implied consensus that this taxon is represented only by juveniles. In naming *Ap. gregorii*, [Hunt \(1993:85\)](#) remarked that this taxon “is undoubtedly the smallest metoposaurid – with an adult skull length about half of other metoposaurid [sic].” It is unclear why Hunt and others have not considered *Ar. lyazidi* a possible diminutive taxon as well (or conversely, why they have so forcefully argued

that *Ap. gregorii* is a definitive diminutive taxon). It should be noted that our parsimony analyses recovered *Ar. lyazidi* in an early diverging position (albeit in a clade with other Moroccan taxa, which are represented by larger specimens) after *Ap. gregorii*, the predicted position for taxa represented only by immature specimens (Fig. 67). This is one instance in which an early diverging position could result from both immaturity and genuine phylogeny.

Failure to account for ontogenetic disparity will bias qualitative comparisons, phenetic taxonomy, and phylogenetic analyses. In particular, comparisons with small specimens are difficult because some are interpreted as dwarfed adults (*Apachesaurus gregorii*) while others are implicitly considered as juveniles (*Arganasaurus lyazidi*). Comparison of taxa represented by non-overlapping ranges of specimens (e.g., *Ar. lyazidi* and *Panthesaurus maleriensis*; Fig. 73) must be very careful to avoid overemphasis of gradational differences like the relative size of different features, especially when they are known to be ontogenetically influenced in metoposaurids and/or temnospondyls more broadly (e.g., orbit size scales with negative allometry in tetrapods). Relative size was sometimes employed in taxonomic diagnoses (e.g., Branson & Mehl, 1929; Schoch & Milner, 2000), with variably sized specimens from the same depositional basin serving as the holotypes of taxa now considered to be synonymous (e.g., Gee, Parker & Marsh, 2019; Kufner & Gee, 2021). For *Buettnererpeton bakeri*, proper comparisons with *Apachesaurus gregorii* and *Arganasaurus lyazidi* are best made with the single Nova Scotia specimen, the smallest of *B. bakeri* (Fig. 4).

Ontogenetic disparity remains challenging to address in phylogenetic analyses because juvenile individuals may be recovered in an artificially early diverging position (stemward slippage) because they appear to “retain” plesiomorphies, when in fact they lack apomorphies that only appear at later stages of ontogeny (e.g., Tykoski, 2005; Wiens, Bonett & Chippindale, 2005; Lamsdell & Selden, 2013, 2015; Sansom & Wills, 2013; Tsai & Fordyce, 2014; Woodruff et al., 2018; Carr, 2020; Gee, 2020b; Zietlow, 2020, but see also Mannion, Tschopp & Whitlock, 2021). Most temnospondyls, including metoposaurids, are not known from a sufficiently complete sample to conduct separate analyses grouped by ontogenetic stage (e.g., Steyer, 2000). Given this, the position of the small-bodied metoposaurids must be carefully scrutinized. The recovery of *Apachesaurus gregorii* as the earliest diverging metoposaurid by Chakravorti & Sengupta (2018) and our reanalysis of Buffa, Jalil & Steyer (2019; Figs. 70C and 70D) should be noted in light of the debate over whether this taxon represents a dwarfed metoposaurid or simply one represented solely by juveniles.

Metoposaurid biogeography and biostratigraphy

Our decision to erect a new genus for the species that has most frequently been referred to as “*Metoposaurus*” *bakeri* has implications for the use of metoposaurids in biostratigraphy. Metoposaurids have long been of interest for local and global Late Triassic biostratigraphy because they occur across Laurasia, often in great abundance (e.g., Huber, Lucas & Hunt, 1993; Lucas et al., 2007; Lucas,

1998, 2015, 2021). However, there is substantial controversy regarding global tetrapod biostratigraphic correlations because of concerns over the utility of different index taxa and the delimitation of different zones, chrons, and assemblages (e.g., [Langer, 2005](#); [Lehman & Chatterjee, 2005](#); [Rayfield et al., 2005](#); [Schultz, 2005](#); [Lucas, Spielmann & Hunt, 2007](#); [Rayfield, Barrett & Milner, 2009](#); [Irmis et al., 2010, 2011](#); [Lucas, 2010, 2018](#); [Olsen, Kent & Whiteside, 2010](#); [Parker & Martz, 2010](#); [Desojo & Ezcurra, 2011](#); [Kammerer, Nesbitt & Shubin, 2011](#); [Butler, 2013](#); [Sues & Olsen, 2015](#); [Martz & Parker, 2017](#)). It must be emphasized that taxonomy does not exist for the sake of biostratigraphy. While there are many species concepts utilized by neontologists and paleontologists (e.g., [Simpson, 1951](#); [Mayr, 1976](#); [Donoghue, 1985](#); [Nixon & Wheeler, 1990](#); [Wiley & Mayden, 2000](#); [Hausdorf, 2011](#)), one based strictly on geographic or stratigraphic distribution is not among them. The most common definition used by paleontologists is to define species as monophyletic groups. Other workers have also criticized proponents of a global tetrapod biostratigraphic framework for utilizing selective taxonomic schemes that maintain the utility of their framework (e.g., [Rayfield, Barrett & Milner, 2009](#); [Irmis et al., 2010](#)), and these account for countless discrepancies in taxonomy from that employed by other tetrapod workers (e.g., [Milner & Schoch, 2004](#); [Butler, 2013](#)). The unsupported more exclusive concept of *Metoposaurus* also obscures the fact that *Metoposaurus* would only be an index taxon of the Otischalkian in North America, as the Krasiejów locality (*M. krasiejowensis*) is likely within the Adamanian or Revueltian ([Milner & Schoch, 2004](#); [Lucas, 2015](#); [Szulc et al., 2015](#); [Buffa, Jalil & Steyer, 2019](#); contra [Lucas, Spielmann & Hunt, 2007](#)). Finally, there is the so-called issue of ‘generification’ (see [Hendricks et al., 2014](#), and references therein) in which paleontologists prefer to work with genera for numerous reasons (e.g., easier to differentiate higher taxa, greater representation of higher taxa in the fossil record) even though it is the species that represents the ‘true’ evolutionary unit.

Global scale.—*Metoposaurus* has long been utilized for global biostratigraphy because it has been argued to occur on more than one continent (e.g., [Roychowdhury, 1965](#); [Dutuit, 1976](#); [Hunt, 1993](#)), and it is considered to be an index taxon of the Otischalkian by some workers (e.g., [Lucas, 1998, 2018, 2021](#)). Since [Hunt \(1993\)](#), *Metoposaurus* has been considered to definitively occur in western Europe, where the type species, *M. diagnosticus*, occurs. *Metoposaurus* has sometimes also included the North American “*Metoposaurus*” *bakeri* (e.g., [Hunt, 1993](#); [Lucas, 2021](#)), the Indian “*Metoposaurus*” *maleriensis* (e.g., [Sulej, 2007](#); [Lucas, 2018](#)), and the non-diagnostic Malagasy “*Metoposaurus hoffmani*” ([Fortuny et al., 2019](#)). When *Metoposaurus* is conceived of as including the North American and Indian taxa, it becomes an extremely useful index taxon because it allows correlation between three of the four major metoposaurid-bearing regions. However, the overwhelming majority of workers do not consider *Metoposaurus* to be found in all three of Europe, India, and North America (e.g., [Hunt, 1993](#); [Schoch & Milner, 2000](#); [Sulej, 2002, 2007](#); [Milner & Schoch, 2004](#); [Brusatte et al., 2015](#); [Chakravorti & Sengupta, 2018](#); [Buffa, Jalil & Steyer, 2019](#); [Gee, Parker & Marsh, 2019](#)), nor is this concept supported by phylogenetic analyses (e.g., [Buffa,](#)

[Jalil & Steyer, 2019](#)) or by phenetic comparisons (e.g., [Case, 1931, 1932](#); [Colbert & Imbrie, 1956](#); [Brusatte et al., 2015](#); this study). The more exclusive concept of a strictly European distribution employed by most workers (e.g., [Sulej, 2002, 2007](#); [Brusatte et al., 2015](#); [Chakravorti & Sengupta, 2018](#); [Buffa, Jalil & Steyer, 2019](#); [Gee, Parker & Marsh, 2019](#); [Fortuny et al., 2019](#))

renders *Metoposaurus* unavailable for global tetrapod biostratigraphy.

Consequently, it is not surprising that advocates of global biostratigraphy insist on the more inclusive concept of *Metoposaurus* (e.g., [Lucas, 1998, 2018, 2021](#)) despite the overwhelming consensus that this concept does not reflect best taxonomic practices or evolutionary relationships. However, as advocated by us and by most other workers, there is no metoposaurid genus that occurs on more than one continent and consequently no basis for the use of metoposaurids in global tetrapod biostratigraphy

Regional scale.—The utility of metoposaurids in North American biostratigraphy is greatly hindered by a paucity of well-documented, diagnostic specimens with precisely constrained stratigraphy, which are inherently necessary for robust biostratigraphic work. Recent studies that depict temporal or stratigraphic ranges have not provided the primary data (voucher specimens) or the primary literature to justify them (e.g., [Buffa, Jalil & Steyer, 2019](#); [Lucas, 2021](#)). This casts doubt on the nuances of the long ranges of *Anaschisma browni* (Otischalkian-Revueltian) and *Apachesaurus gregorii* (Adamanian-Apachean), especially when there are discrepancies between studies (as in the two cited above).

Biostratigraphy inherently requires specimens with both well-characterized anatomy (and confident identifications) and well-constrained stratigraphy. Most descriptive work on North American metoposaurids is either historical (e.g., [Case, 1922, 1931](#); [Branson & Mehl, 1929](#); [Sawin, 1945](#); [Colbert & Imbrie, 1956](#)) or based on redescription of historical material (e.g., [Lucas et al., 2016](#); [Gee & Jasinski, 2021](#); [Kufner & Gee, 2021](#)). However, most historical material is very poorly constrained stratigraphically (below the formation level) and spatially; consequently, much of this material holds poor prospects for refinement using modern methods and frameworks unless historical localities can be relocated, or sufficient detail can be gleaned from historical notes. Given the sheer number of metoposaurid-bearing localities, this is a daunting task. Conversely, newer material is often more precisely situated stratigraphically, but there is little descriptive work because this is largely viewed as redundant since the osteology of metoposaurids is both well-established and highly conserved. Collectively, this means that across tens of thousands of specimens from hundreds of localities, only a very small subset of specimens has both well-characterized anatomy and well-constrained stratigraphy. The need for both is a shortcoming of compendia like [Long & Murry \(1995\)](#), who provided comprehensive lists of metoposaurid specimens and localities with member-level stratigraphic precision but very few photos and no descriptions. At the time of that publication, over 95% of the listed metoposaurid specimens had never been described or figured in any capacity, so it was (is) not possible to assess whether they can indeed be referred to a particular taxon without firsthand observation or whether identifications were merely based on non-

diagnostic features like relative size or stratigraphic occurrence. This ambiguity is especially poignant because most elements are not diagnostic, merely differential, and many of these identifications may be based on circular logic (*e.g.*, all small-bodied material belongs to *Apachesaurus gregorii*, even in isolation and without association with more diagnostic material; [Irmis, 2005](#); [Martz et al., 2012](#)). The stratigraphic resolution of Long & Murry is also hindered by subsequent, frequent revision to the stratigraphy of the North American Late Triassic deposits (*e.g.*, [Martz, 2008](#); [Parker & Martz, 2010](#); [Rasmussen et al., 2020](#)).

These issues cast doubt on the upper and lower bounds of the ranges of *Anaschisma browni* and *Apachesaurus gregorii*. For example, the highest occurrences of *Anaschisma* are based on large isolated postcranial bones (*e.g.*, [Hunt & Lucas, 1993a, 1993b](#); [Long & Murry, 1995](#); [Zeigler, Heckert & Lucas, 2003](#); [Heckert et al., 2005](#); [Spielmann, Lucas & Heckert, 2007](#)). However, there are no postcranial autapomorphies for *Anaschisma*, only a few features that differentiate it from a select few other metoposaurids (*e.g.*, relative size of reticulate ornamentation on the interclavicle compared to *Metoposaurus*; [Colbert & Imbrie, 1956](#); [Lucas et al., 2016](#); [Gee, Parker & Marsh, 2019](#); [Kufner & Gee, 2021](#)). The highest tentative report of the monospecific *Anaschisma* (as ‘*cf. Buettneria* sp.’) is large isolated intercentra from the Owl Rock Member (Revueltian Estimated Holochronozone) of the Chinle Formation in Arizona ([Spielmann, Lucas & Heckert, 2007](#)). It is therefore only accurate to state that large-bodied metoposaurids occur at the end of the Revueltian. If only occurrences of *An. browni* that are based on published, diagnostic cranial remains are considered, then the highest occurrence of this taxon is at Lamy (lower portion of the Garita Creek Formation; [Lucas et al., 2010](#)) or Rotten Hill (estimated here to be around the middle portion of the Tecovas Formation based on the age estimate of 220–225 Ma by [Lucas et al., 2016](#)). This is much lower than the depicted youngest occurrence at the Revueltian-Apachean boundary ([Lucas, 2021](#); [Fig. 74](#)).

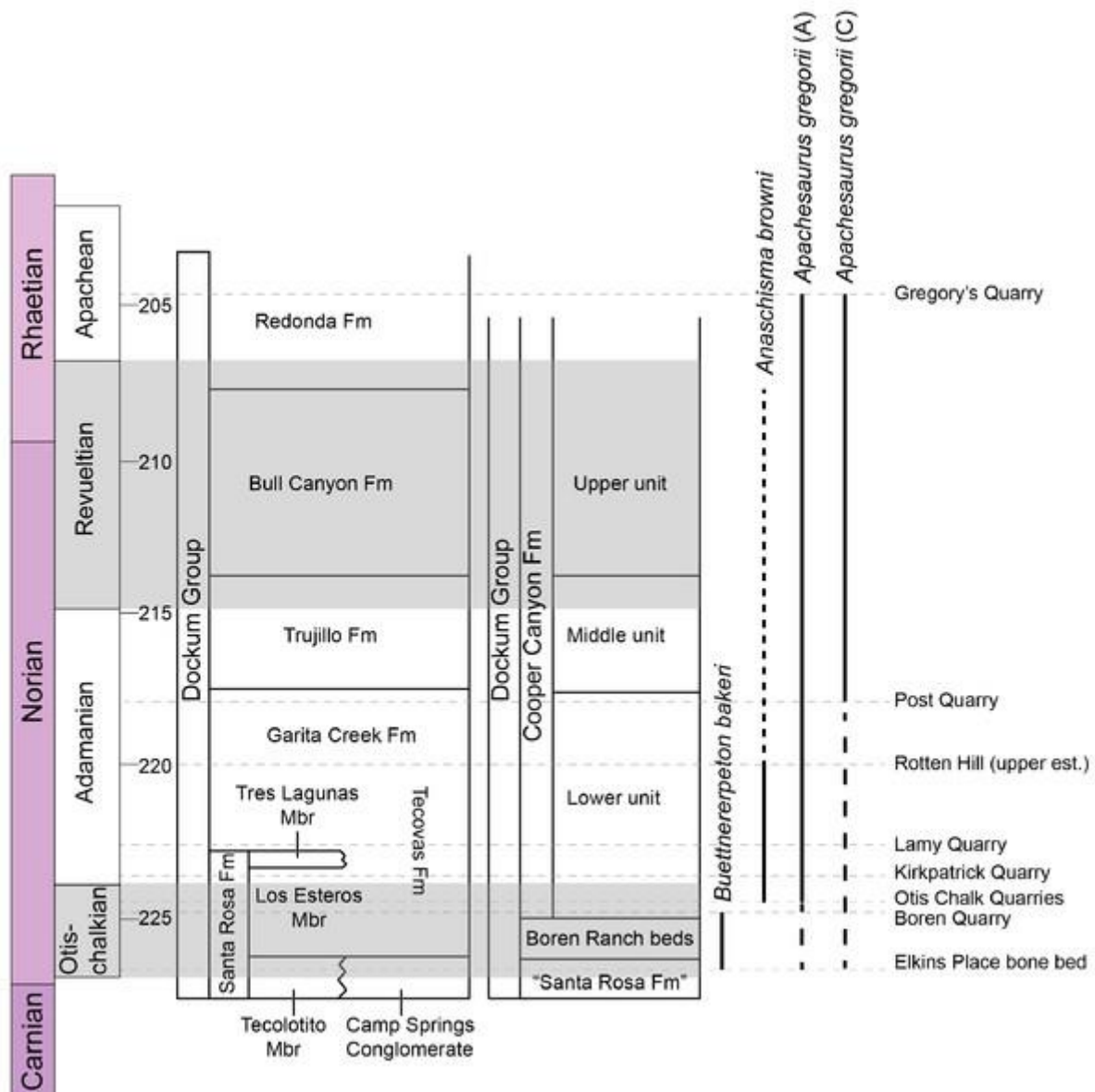


Figure 74: Comparison of stratigraphic ranges of the North American metoposaurids.

Ranges are based on diagnostic voucher specimens from localities with established stratigraphic position. The lowest occurrence of *Buettnererpeton bakeri* is the Elkins Place bone bed (Case, 1931, 1932; Lehman & Chatterjee, 2005; this study), while the highest occurrence is the Boren Quarry (Martz, 2008). The lowest occurrence of *Anaschisma browni* is the Otis Chalk Quarries (Sawin, 1945), while the highest occurrence is probably Rotten Hill (Lucas et al., 2016). *Anaschisma browni*'s range may be extended considerably to higher stratigraphic units if specimens currently lacking published documentation or apomorphies (e.g., large, isolated intercentra) are included. The lowest occurrence of *Apachesaurus gregorii*, if all referred material (A) is considered (following Spielmann & Lucas, 2012; Rinehart & Lucas, 2018), is the Otis Chalk quarries, whereas if only diagnostic cranial material (C) is considered (Gee & Parker, 2020), this bound is the Post Quarry. Either range may be extended lower by the cranial material from Collier's Ranch (uncertain position in the Tecovas Formation). The highest occurrence is Gregory's Quarry.

[Download full-size image](#)

DOI: [10.7717/peerj.14065/fig-74](https://doi.org/10.7717/peerj.14065/fig-74)

Regarding *Apachesaurus gregorii*, [Spielmann & Lucas \(2012\)](#) stated that all Otischalkian and Adamanian records of *A. gregorii* are from isolated intercentra, but at least one partial skull, known mostly from figures (TTU-P 9237; [Davidow-Henry, 1987, 1989](#); [Long & Murry, 1995](#); [Spielmann & Lucas, 2012](#)), occurs at Collier's Ranch (10 miles SE of Crosbyton, Crosby Co., TX). This site is allegedly low in the Tecovas Formation ([Chatterjee, 1991](#):281, 283) but has never been situated more precisely. It could be roughly equivalent to the better constrained Kirkpatrick Quarry (MOTT 3628; 12 km SW of Crosbyton), as both occur in a thin carbonate nodule layer within mudstone beds ([Chatterjee, 1991](#); [Lehman & Chatterjee, 2005](#)). The Kirkpatrick Quarry is just above the Otischalkian-Adamanian boundary (*e.g.*, [Lehman & Chatterjee, 2005](#); [Lessner et al., 2018](#)). The next highest occurrence of cranial material of *A. gregorii* is TTU-P 9216 from the Post Quarry (Adamanian; [Martz et al., 2012](#)).

These quandaries underscore the importance of reporting voucher specimens with detailed stratigraphic data and sufficient anatomical documentation to justify taxonomic identifications and to permit other workers to assess them without requiring personal observation. Poor documentation of specimens is only exacerbated by uncertainty in the stratigraphic relationship of localities to each other, which is particularly acute for historical localities in Texas. The Otis Chalk quarries represent the lowest definitive occurrence of *Anaschisma browni* and perhaps the lowest occurrence of *Apachesaurus gregorii* ([Fig. 74](#)), but these sites have been famously difficult to place (*e.g.*, [Lucas & Anderson, 1993, 1994](#); [Lehman, 1994](#); [Martz, 2008](#)). They may be close to the level of the Boren Quarry, the highest occurrence of *Buettnererpeton bakeri* ([Martz, 2008](#)). These issues are further compounded in trying to relate different depositional basins (*e.g.*, the Chugwater Group in the Rocky Mountain Region with the Dockum Group in primarily New Mexico and Texas). There are inherently different narratives that emerge from interpretations of stratigraphic ranges (*e.g.*, co-occurrence/competition *vs* succession/anagenesis), which places a premium on publishing diagnostic specimens, with defensible rationale and constrained stratigraphy, in order to refine our concepts of temporal and stratigraphic ranges of these taxa.

Supplemental Information

Text-based appendices containing character lists and modifications, scoring modifications, other comments on the phylogenetic analyses, and measurement data for Figure 59.

DOI: [10.7717/peerj.14065/supp-1](https://doi.org/10.7717/peerj.14065/supp-1)

[Download](#)

Character matrix for the phylogenetic matrix used in this study.

DOI: [10.7717/peerj.14065/supp-2](https://doi.org/10.7717/peerj.14065/supp-2)

[Download](#)

Modified character matrix from [Buffa, Jalil & Steyer \(2019\)](#).

DOI: [10.7717/peerj.14065/supp-3](https://doi.org/10.7717/peerj.14065/supp-3)

[Download](#)

MPTs recovered from parsimony analyses.

TRE (.tre) files containing all sets of MPTs recovered from the parsimony analysis of the novel matrix used in this study and the reanalysis of the matrix used by [Buffa, Jalil & Steyer \(2019\)](#).

DOI: [10.7717/peerj.14065/supp-4](https://doi.org/10.7717/peerj.14065/supp-4)

[Download](#)

Additional Information and Declarations

Competing Interests

The authors declare that they have no competing interests.

Author Contributions

[Bryan M. Gee](#) conceived and designed the experiments, performed the experiments, analyzed the data, prepared figures and/or tables, authored or reviewed drafts of the article, and approved the final draft.

[Aaron M. Kufner](#) conceived and designed the experiments, performed the experiments, analyzed the data, prepared figures and/or tables, authored or reviewed drafts of the article, and approved the final draft.

Data Availability

The following information was supplied regarding data availability:

The phylogenetic matrix with the sets of trees recovered by parsimony analyses are available in the [Supplemental Files \(Appendix 5\)](#).

New Species Registration

The following information was supplied regarding the registration of a newly described species:

Publication LSID: urn:lsid:zoobank.org:pub:32E58BF1-B343-4657-91E8-F324D76A7B41.

Buettnererpeton gen. nov. genus LSID: urn:lsid:zoobank.org:act:97CA64A0-E13B-4FAD-A1C1-23452D01F83E.

Funding

Bryan M. Gee was supported by graduate student funding from the University of Toronto and by NSF ANT-1947094 (to Christian Sidor). Aaron Kufner was supported by a Geological Society of America Graduate Student Research Grant (12497-19). The funders had no role in study design, data collection and analysis, decision to publish, or preparation of the manuscript.

Acknowledgements

Thanks to Jeff Wilson, Adam Rountrey, and Kelsey Wiggins for facilitating collections access and to Adam Rountrey for assistance sorting out discrepancies in historical collections records. Thanks to Hans-Dieter Sues for sharing a high-resolution photograph of the Nova Scotia specimen of *Buettnererpeton bakeri* and to Dhurjati Sengupta and Sanjukta Chakravorti for sharing photographs of material from the Natural History Museum London. Thanks to Tomasz Sulej, an anonymous reviewer, and Claudia Marsicano for comments on the first submission of this manuscript, and to Valentin Buffa and Andy Farke for comments on this version.

Institutional abbreviations

MCZ

Museum of Comparative Zoology, Harvard University, Cambridge, MA

MOTT

Museum of Texas Tech Locality

TMM

Texas Memorial Museum, Austin, TX

TTU-P

Texas Tech University, Lubbock, TX

UMMP (=UMMNH)

University of Michigan Museum of Paleontology, Ann Arbor, MI

YPM VPPU

Yale Peabody Museum, Ithaca, NY

References

- **Antczak M, Bodzioch A. 2018.** [Ornamentation of dermal bones of *Metoposaurus krasiejowensis* and its ecological implications.](#) *PeerJ* **6**:e5267
- **Arbez T, Dahoumane A, Steyer J-S. 2017.** [Exceptional endocranium and middle ear of *Stanocephalosaurus* \(Temnospondyli: Capitosauria\) from the Triassic of Algeria revealed by micro-CT scan, with new functional interpretations of the hearing system.](#) *Zoological Journal of the Linnean Society* **180**(4):910-929
- **Baird D. 1986.** [Some upper Triassic reptiles, footprints, and amphibians from New Jersey.](#) *The Mosasaur* **3**:125-153

- **Baird D, Olsen PE. 1983.** [Late Triassic herpetofauna from the Wolfville Fm. of the Minas Basin \(Funday Basin\) Nova Scotia, Canada](#) *Geological Society of America, Abstract with Program* **15**:122
- **Bolt JR, Chatterjee S. 2000.** [A new temnospondyl amphibian from the Late Triassic of Texas](#). *Journal of Paleontology* **74**(4):670-683
- **Boy JA. 1995.** [Über die Micromelerpetontidae \(Amphibia: Temnospondyli\). 1. Morphologie und Paläoökologie des *Micromelerpeton credneri* \(Unter-Perm; SW-Deutschland\)](#) *Paläontologische Zeitschrift* **69**(3-4):429-457
- **Branson EB. 1905.** [Structure and relationships of American Labyrinthodontidae](#). *The Journal of Geology* **13**(7):568-610
- **Branson EB, Mehl MG. 1929.** [Triassic amphibians from the Rocky Mountain region](#). *The University of Missouri Studies* **4**:154-253
- **Brinkman D. 1988.** [Size-independent criteria for estimating relative age in *Ophiacodon* and *Dimetrodon* \(Reptilia, Pelycosauria\) from the Admiral and lower Belle Plains formations of west-central Texas](#). *Journal of Vertebrate Paleontology* **8**(2):172-180
- **Brochu CA. 1996.** [Closure of neurocentral sutures during crocodylian ontogeny: implications for maturity assessment in fossil archosaurs](#). *Journal of Vertebrate Paleontology* **16**(1):49-62
- **Broom R. 1915.** [On the Triassic stegocephalians, *Brachyops*, *Bothriceps*, and *Lydekkerina*, gen. nov.](#) *Proceedings of the Zoological Society of London* **1915**:363-368
- **Brusatte SL, Butler RJ, Mateus O, Steyer JS. 2015.** [A new species of *Metoposaurus* from the Late Triassic of Portugal and comments on the systematics and biogeography of metoposaurid temnospondyls](#). *Journal of Vertebrate Paleontology* **35**(3):e912988
- **Buffa V, Jalil NE, Steyer J-S. 2019.** [Redescription of *Arganasaurus \(Metoposaurus\) azerouali* \(Dutuit\) comb. nov. from the Upper Triassic of the Argana Basin \(Morocco\), and the first phylogenetic analysis of the Metoposauridae \(Amphibia, Temnospondyli\)](#) *Papers in Palaeontology* **5**(4):699-717
- **Butler RJ. 2013.** [Francosuchus' trauthi is not Paleorhinus: implications for Late Triassic vertebrate biostratigraphy](#). *Journal of Vertebrate Paleontology* **33**(4):858-864
- **Campbell JA, Frost DR. 1993.** [Anguid lizards of the genus *Abronia*: revisionary notes, descriptions of four new species, a phylogenetic analysis, and key](#). *Bulletin of the American Museum of Natural History* **216**:1-128
- **Carr TD. 2020.** [A high-resolution growth series of *Tyrannosaurus rex* obtained from multiple lines of evidence](#). *PeerJ* **8**(12):e9192
- **Case EC. 1920.** [On a very perfect thoracic shield of a large labyrinthodont in the geological collections of the University of Michigan](#). *Occasional Papers of the Museum of Zoology* **82**:1-3
- **Case EC. 1922.** [New reptiles and stegocephalians from the Upper Triassic of western Texas](#). *Carnegie Institute of Washington* **321**:7-84
- **Case EC. 1931.** [Description of a new species of *Buettneria*, with a discussion of the brain case](#). *Contributions from the Museum of Paleontology, University of Michigan* **3**:187-206
- **Case EC. 1932.** [A collection of stegocephalians from Scurry County, Texas](#). *Contributions from the Museum of Paleontology, University of Michigan* **4**:1-56
- **Case EC. 1947.** [Catalogue of the type and figured specimens of vertebrate fossils in the Museum of Paleontology, University of Michigan](#). *Contributions from the Museum of Paleontology, University of Michigan* **6**:319-336

- **Chakravorti S, Sengupta DP. 2018.** [Taxonomy, morphometry and morphospace of cranial bones of *Panthisaurus* gen. nov. *maleriensis* from the Late Triassic of India.](#) *Journal of Iberian Geology* **45**(2):317-340
- **Chatterjee S. 1991.** [Cranial anatomy and relationships of a new Triassic bird from Texas.](#) *Philosophical Transactions of the Royal Society of London. Series B: Biological Sciences* **332**:277-346
- **Colbert E, Imbrie J. 1956.** [Triassic metoposaurid amphibians.](#) *Bulletin of the American Museum of Natural History* **110**:399-452
- **Cope ED. 1868.** [Synopsis of the extinct Batrachia of North America.](#) *Proceedings of the Academy of Natural Sciences of Philadelphia* **1868**:208-221
- **Datta D, Kumar N, Ray S. 2019.** [Taxonomic identification of isolated phytosaur \(Diapsida, Archosauria\) teeth from the Upper Triassic of India and their significances.](#) *Historical Biology* **33**:272-282
- **Davidow-Henry B. 1987.** [New metoposaurs from the southwestern United States and their phylogenetic relationships.](#) M. Sc. Thesis, Texas Tech University
- **Davidow-Henry B. 1989.** [Small metoposaurid amphibians from the Triassic of western North America and their significance.](#) In: Lucas SG, Hunt AP, eds. *Dawn of the Age of Dinosaurs in the American Southwest*. Albuquerque: New Mexico Museum of Natural History and Science. 278-292
- **Desojo JB, Ezcurra MD. 2011.** [A reappraisal of the taxonomic status of *Aetosauroides* \(Archosauria, Aetosauria\) specimens from the Late Triassic of South America and their proposed synonymy with *Stagonolepis*.](#) *Journal of Vertebrate Paleontology* **31**(3):596-609
- **Dias-da-Silva S, Marsicano C. 2011.** [Phylogenetic reappraisal of Rhytidosteidae \(Stereospondyli: Trematosauria\), temnospondyl amphibians from the Permian and Triassic.](#) *Journal of Systematic Palaeontology* **9**(2):305-325
- **Donoghue MJ. 1985.** [A critique of the biological species concept and recommendations for a phylogenetic alternative.](#) *Bryologist* **88**(3):172-181
- **Dutuit J-M. 1972.** [Decouverte des pleurocentres dans les vertèbres de stégocéphales métoposauridés.](#) *Comptes Rendu de l'Academie des Sciences. Paris D* **274**:536-537
- **Dutuit J-M. 1976.** [Introduction à l'étude paléontologique du Trias continental marocain. Description des premiers stegocephales recueillis dans le couloir d'Argana \(Atlas occidental\)](#) *Memoires du Museum National d'Histoire Naturelle, Paris Series C* **36**:1-253
- **Dutuit J-M. 1978.** [Description de quelques fragments osseux provenant de la région de Folakara \(Trias supérieur malgache\)](#) *Bulletin du Muséum National d'Histoire Naturelle, Paris 3e sér., 516, Sciences de la Terre* **69**:79-89
- **Fortuny J, Arbez T, Mujal E, Steyer J-S. 2019.** [Reappraisal of '*Metoposaurus hoffmani*' Dutuit, 1978, and description of new temnospondyl specimens from the Middle-Late Triassic of Madagascar \(Morondava Basin\)](#) *Journal of Vertebrate Paleontology* **39**(1):e1576701
- **Fraas E. 1889.** [Die Labyrinthodonten der schwäbischen Trias.](#) In: *Palaeontographica*. Stuttgart: Schweizerbart. **36**:1-158
- **Fröbisch NB, Schoch RR. 2009.** [Testing the impact of miniaturization on phylogeny: paleozoic dissorophoid amphibians.](#) *Systematic Biology* **58**(3):312-327
- **Gee BM. 2020a.** [Ecology, ontogeny, and taxonomy of the diverse early Permian dissorophoid assemblage from Richards Spur, Oklahoma.](#) D. Phil. Thesis, University of Toronto

- **Gee BM. 2020b.** [Size matters: the effects of ontogenetic disparity on the phylogeny of Trematopidae \(Amphibia: Temnospondyli\)](#) *Zoological Journal of the Linnean Society* **190**(1):79-113
- **Gee BM, Haridy Y, Reisz RR. 2017.** [Histological characterization of denticulate palatal plates in an Early Permian dissorophoid.](#) *PeerJ* **5**(1):e3727
- **Gee BM, Jasinski SE. 2021.** [Description of the metoposaurid *Anaschisma browni* from the New Oxford Formation of Pennsylvania.](#) *Journal of Paleontology* **95**(5):1061-1078
- **Gee BM, Makovicky PJ, Sidor CA. 2022.** [Upside down: ‘*Cryobatrachus*’ and the lydekkerinid record from Antarctica.](#) *Journal of Paleontology* **96**(3):658-683
- **Gee BM, Parker WG. 2017.** [A juvenile *Koskinonodon perfectus* \(Temnospondyli, Metoposauridae\) from the Upper Triassic of Arizona and its implications for the taxonomy of North American metoposaurids.](#) *Journal of Paleontology* **91**:1047-1059
- **Gee BM, Parker WG. 2020.** [Morphological and histological description of small metoposaurids from Petrified Forest National Park, AZ, USA and the taxonomy of *Apachesaurus*.](#) *Historical Biology* **32**:203-233
- **Gee BM, Parker WG. 2018.** [A large-bodied metoposaurid from the Revueltian \(late Norian\) of Petrified Forest National Park \(Arizona, USA\)](#) *Neues Jahrbuch für Geologie und Paläontologie-Abhandlungen* **287**:61-73
- **Gee BM, Parker WG, Marsh AD. 2017.** [Microanatomy and paleohistology of the intercentra of North American metoposaurids from the Upper Triassic of Petrified Forest National Park \(Arizona, USA\) with implications for the taxonomy and ontogeny of the group.](#) *PeerJ* **5**:e3183
- **Gee BM, Parker WG, Marsh AD. 2019.** [Redescription of *Anaschisma* \(Temnospondyli: Metoposauridae\) from the Late Triassic of Wyoming and the phylogeny of the Metoposauridae.](#) *Journal of Systematic Palaeontology* **18**:233-258
- **Goldfuß A. 1847.** [Beiträge zur vorweltlichen Fauna des Steinkohlengebirges.](#) Bonn: Henry & Cohen.
- **Grand A, Corvez A, Duque Velez LM, Laurin M. 2013.** [Phylogenetic inference using discrete characters: performance of ordered and unordered parsimony and of three-item statements.](#) *Biological Journal of the Linnean Society* **100**(4):914-930
- **Gregory JT. 1980.** [The otic notch of metoposaurid labyrinthodonts.](#) In: Jacobs LL, ed. *Aspects of Vertebrate History*. Flagstaff: Museum of Northern Arizona. 125-135
- **Haughton SH. 1927.** [On Karroo vertebrates from Nyasaland.](#) *South African Journal of Geology* **29**:69-83
- **Hausdorf B. 2011.** [Progress toward a general species concept.](#) *Evolution* **65**(4):923-931
- **Heckert AB, Jenkins HS, Lucas SG, Hunt AP. 2013.** [Mandibles of juvenile phytosaurs \(Archosauria: Crurotarsi\) from the Upper Triassic Chinle Group of Texas and New Mexico, USA.](#) *New Mexico Museum of Natural History & Science Bulletin* **61**:228-236
- **Heckert AB, Lucas SG, Sullivan RM, Hunt AP, Spielmann JA. 2005.** [The vertebrate fauna of the Upper Triassic \(Revueltian: early-mid Norian\) Painted Desert Member \(Petrified Forest Formation: Chinle Group\) in the Chama Basin, northern New Mexico.](#) *New Mexico Geological Society Guidebook* **56**:302-318
- **Hendricks JR, Saupe EE, Myers CE, Hermsen EJ, Allmon WD. 2014.** [The generification of the fossil record.](#) *Paleobiology* **40**(4):511-528
- **Hewison RH. 1996.** [The skull of *Deltacephalus whitei*, a lydekkerinid temnospondyl amphibian from the Lower Triassic of Madagascar.](#) *Palaeontology* **39**(2):305-321

- **Hewison RH. 2007.** [The skull and mandible of the stereospondyl *Lydekkerina huxleyi*, \(Tetrapoda: Temnospondyli\) from the Lower Triassic of South Africa, and a reappraisal of the family Lydekkerinidae, its origin, taxonomic relationships and phylogenetic importance.](#) *Journal of Temnospondyl Palaeontology* **1**:1-80
- **Hewison RH. 2008.** [The sacral region, pelvis and hind limb of the stereospondyl *Lydekkerina huxleyi* \(Tetrapoda: Temnospondyli\) from the Lower Triassic of South Africa.](#) *Journal of Temnospondyl Palaeontology* **2**:1-26
- **Hopson JA. 1984.** [Late Triassic traversodont cynodonts from Nova Scotia and southern Africa.](#) *Palaeontologia Africana* **25**:181-201
- **Houle M, Mueller B. 2004.** [A new occurrence of *Buettneria bakeri* \(Temnospondyli: Metoposauridae\) from the Norian \(Cooper Canyon Formation, Dockum Group\) of west Texas.](#) *Journal of Vertebrate Paleontology* **24**(sup003):73A
- **Huber P, Lucas SG, Hunt AP. 1993.** [Vertebrate biochronology of the Newark Supergroup Triassic, eastern North America.](#) *New Mexico Museum of Natural History and Science Bulletin* **3**:179-186
- **Huelsenbeck JP, Ronquist F. 2001.** [MRBAYES: Bayesian inference of phylogenetic trees.](#) *Bioinformatics* **17**(8):754-755
- **Hunt AP. 1993.** [Revision of the Metoposauridae \(Amphibia: Temnospondyli\) and description of a new genus from western North America.](#) *Museum of Northern Arizona Bulletin* **59**:67-97
- **Hunt AP, Lucas SG. 1993a.** [Taxonomy and stratigraphic distribution of late Triassic metoposaurid amphibians from Petrified Forest National Park, Arizona.](#) *Journal of the Arizona-Nevada Academy of Science* **27**:89-96
- **Hunt AP, Lucas SG. 1993b.** [Triassic vertebrate paleontology and biochronology of New Mexico.](#) *New Mexico Museum of Natural History and Science Bulletin* **2**:49-60
- **Huxley TH. 1859.** [On some amphibian and reptilian remains from South Africa and Australia.](#) *Quarterly Journal of the Geological Society* **15**(1-2):642-658
- **Irmis RB. 2005.** [The vertebrate fauna of the Upper Triassic Chinle Formation in northern Arizona.](#) *Mesa Southwest Bulletin* **9**:63-88
- **Irmis RB, Martz JW, Parker WG, Nesbitt SJ. 2010.** [Re-evaluating the correlation between Late Triassic terrestrial vertebrate biostratigraphy and the GSSP-defined marine stages.](#) *Albertiana* **38**:40-52
- **Irmis RB, Mundil R, Martz JW, Parker WG. 2011.** [High-resolution U-Pb ages from the Upper Triassic Chinle Formation \(New Mexico, USA\) support a diachronous rise of dinosaurs.](#) *Earth and Planetary Science Letters* **309**(3-4):258-267
- **Jaeger GF. 1828.** [Über die fossile Reptilien, welche in Württemberg aufgefunden worden sind.](#) Stuttgart: J. B. Metzler.
- **Jeannot AM, Damiani R, Rubidge BS. 2006.** [Cranial anatomy of the Early Triassic stereospondyl *Lydekkerina huxleyi* \(Tetrapoda: Temnospondyli\) and the taxonomy of South African lydekkerinids.](#) *Journal of Vertebrate Paleontology* **26**:822-838
- **Kammerer CF, Nesbitt SJ, Shubin NH. 2011.** [The first silesaurid dinosauriform from the Late Triassic of Morocco.](#) *Acta Palaeontologica Polonica* **57**(2):277-284
- **Khaldoune F, Jalil N-E, Germain D, Steyer J-S. 2016.** [Les vertébrés du Permien et du Trias du Maroc \(bassin d'Argana, Haut-Atlas occidental\): une fenêtre ouverte sur l'évolution autour de la grande crise finipaléozoïque.](#) *Mémoires de la Société Géologique de France* **180**:103-167

- **Konietzko-Meier D, Klein N. 2013.** [Unique growth pattern of *Metoposaurus diagnosticus krasiejowensis* \(Amphibia, Temnospondyli\) from the Upper Triassic of Krasiejów, Poland.](#) *Palaeogeography, Palaeoclimatology, Palaeoecology* **370**(3):145-157
- **Konietzko-Meier D, Sander PM. 2013.** [Long bone histology of *Metoposaurus diagnosticus* \(Temnospondyli\) from the Late Triassic of Krasiejów \(Poland\) and its paleobiological implications.](#) *Journal of Vertebrate Paleontology* **33**(5):1003-1018
- **Konietzko-Meier D, Wawro K. 2007.** [Mandibular dentition in the Late Triassic temnospondyl amphibian *Metoposaurus*.](#) *Acta Palaeontologica Polonica* **52**:213-215
- **Kornet DJ, Turner H. 1999.** [Coding polymorphism for phylogeny reconstruction.](#) *Systematic Biology* **48**(2):365-379
- **Kufner AM, Gee BM. 2021.** [Reevaluation of the holotypes of *Koskinonodon princeps* Branson and Mehl, 1929, and *Borborophagus wyomingensis* Branson and Mehl, 1929 \(Temnospondyli, Metoposauridae\)](#) *Journal of Vertebrate Paleontology* **41**(1):e1922067
- **Kuhn O. 1961.** [Die Familien der Rezenten und Fossilen Amphibien und Reptilien.](#) Bamberg: Meisenbach.
- **Lamsdell JC, Selden PA. 2013.** [Babes in the wood—a unique window into sea scorpion ontogeny.](#) *BMC Evolutionary Biology* **13**(1):1-46
- **Lamsdell JC, Selden PA. 2015.** [Phylogenetic support for the monophyly of proetide trilobites.](#) *Lethaia* **48**(3):375-386
- **Langer MC. 2005.** [Studies on continental Late Triassic tetrapod biochronology. II. The Ischigualastian and a Carnian global correlation.](#) *Journal of South American Earth Sciences* **19**(2):219-239
- **Langston W. 1953.** [Permian amphibians from New Mexico.](#) In: *University of California Publications in Geological Sciences.* Berkeley: University of California Press. **29**:349-416
- **Lehman TM. 1994.** [The saga of the Dockum Group and the case of the Texas/New Mexico boundary fault.](#) *New Mexico Bureau of Mines & Mineral Resources Bulletin* **150**:37-51
- **Lehman T, Chatterjee S. 2005.** [Depositional setting and vertebrate biostratigraphy of the Triassic Dockum Group of Texas.](#) *Journal of Earth System Science* **114**(3):325-351
- **Lessner EJ, Parker WG, Marsh AD, Nesbitt SJ, Irmis RB, Mueller BD. 2018.** [New insights into Late Triassic dinosauromorph-bearing assemblages from Texas using apomorphy-based identifications.](#) *PaleoBios* **35**:P9351039960
- **Long RA, Murry PA. 1995.** [Late Triassic \(Carnian and Norian\) Tetrapods from the Southwestern United States.](#) In: *New Mexico Museum of Natural History and Science Bulletin.* Albuquerque: New Mexico Museum of Natural History and Science. **4**:1-254
- **Loughney KM, Fastovsky DE, Parker WG. 2011.** [Vertebrate fossil preservation in blue paleosols from the Petrified Forest National Park, Arizona, with implications for vertebrate biostratigraphy in the Chinle Formation.](#) *Palaios* **26**(11):700-719
- **Lucas SG. 1998.** [Global Triassic tetrapod biostratigraphy and biochronology.](#) *Palaeogeography, Palaeoclimatology, Palaeoecology* **143**(4):347-384
- **Lucas SG. 2010.** [The Triassic timescale based on nonmarine tetrapod biostratigraphy and biochronology.](#) *Geological Society, London, Special Publications* **334**(1):447-500
- **Lucas SG. 2015.** [Age and correlation of Late Triassic tetrapods from southern Poland.](#) *Annales Societatis Geologorum Poloniae* **85**:627-635
- **Lucas SG. 2018.** [Late Triassic terrestrial tetrapods: Biostratigraphy, biochronology and biotic events.](#) In: Tanner L, ed. *The Late Triassic World.* Cham: Springer. 351-405

- **Lucas SG. 2021.** [Biochronology of Late Triassic Metoposauridae \(Amphibia, Temnospondyli\) and the Carnian pluvial episode](#). *Annales Societatis Geologorum Poloniae* **90**:409-418
- **Lucas SG, Anderson OJ. 1993.** [Stratigraphy of the Permian-Triassic boundary in southeastern New Mexico and west Texas](#). *New Mexico Geological Society Guidebook* **44**:219-230
- **Lucas SG, Anderson OJ. 1994.** [The Camp Springs Member, base of the Late Triassic Dockum Formation in West Texas](#). *West Texas Geological Society Bulletin* **34**:1-15
- **Lucas SG, Hunt AP. 1993.** [Tetrapod biochronology of the Chinle Group](#). *New Mexico Museum of Natural History and Science Bulletin* **3**:327-329
- **Lucas SG, Hunt AP, Heckert AB, Spielmann JA. 2007.** [Global Triassic tetrapod biostratigraphy and biochronology: 2007 status](#). *New Mexico Museum of Natural History and Science Bulletin* **41**:229-240
- **Lucas SG, Rinehart LF, Heckert AB, Hunt AP, Spielmann JA. 2016.** [Rotten Hill: a Late Triassic bonebed in the Texas Panhandle, USA](#). Albuquerque: New Mexico Museum of Natural History and Science Bulletin. **72**:1-97
- **Lucas SG, Rinehart LF, Krainer K, Spielmann JA, Heckert AB. 2010.** [Taphonomy of the Lamy amphibian quarry: a Late Triassic bonebed in New Mexico, USA](#). *Palaeogeography, Palaeoclimatology, Palaeoecology* **298**(3-4):388-398
- **Lucas SG, Spielmann JA, Hunt AP. 2007.** [Biochronological significance of Late Triassic tetrapods from Krasiejów, Poland](#). *New Mexico Museum of Natural History and Science Bulletin* **41**:248-258
- **Lydekker R. 1889.** [Note on the occurrence of a species of *Bothriceps* in the Karoo system of South Africa](#). *Journal of Natural History* **4**(24):475-476
- **Lydekker R. 1890.** [Catalogue of the fossil Reptilia and Amphibia in the British Museum \(Natural History\). Part IV](#). London: British Museum of Natural History.
- **Maddin HC, Reisz RR, Anderson JS. 2010.** [Evolutionary development of the neurocranium in Dissorophoidea \(Tetrapoda: Temnospondyli\), an integrative approach](#). *Evolution & Development* **12**(4):393-403
- **Maddison WP, Maddison DR. 2018.** [Mesquite: a modular system for evolutionary analysis, version 3.6](#).
- **Maganuco S, Pasini G, Auditore M. 2014.** [A revision of the short-faced stereospondyls *Mahavisaurus dentatus* and *Lyrosaurus australis* from the Lower Triassic of Madagascar: cranial anatomy, ontogenetic remarks, palaeoecology and rhytidosteid phylogeny](#). *Memori della Società Italiana di Scienze Naturali e del Museo Civico di Storia Naturale di Milano* **39**:1-64
- **Mannion PD, Tschoop E, Whitlock JA. 2021.** [Anatomy and systematics of the diplodocoid *Amphicoelias altus* supports high sauropod dinosaur diversity in the Upper Jurassic Morrison Formation of the USA](#). *Royal Society Open Science* **8**(6):210377
- **Martz JW. 2008.** [Lithostratigraphy, chemostratigraphy, and vertebrate biostratigraphy of the Dockum Group \(Upper Triassic\) of southern Garza County, West Texas](#). D. Phil. Thesis, Texas Tech University
- **Martz JW, Mueller B, Nesbitt SJ, Stocker MR, Parker WG, Atanassov M, Fraser N, Weinbaum J, Lehane JR. 2012.** [A taxonomic and biostratigraphic re-evaluation of the Post Quarry vertebrate assemblage from the Cooper Canyon Formation \(Dockum Group, Upper](#)

[Triassic\) of southern Garza County, western Texas](#). *Earth and Environmental Science Transactions of the Royal Society of Edinburgh* **103**(3–4):339-364

- **Martz JW, Parker WG. 2017.** [Revised formulation of the Late Triassic Land Vertebrate Faunachrons of western North America: recommendations for codifying nascent systems of vertebrate biochronology](#). In: Ziegler KE, Parker W, eds. *Terrestrial Depositional Systems*. Amsterdam: Elsevier. 39-125
- **Mayr E. 1976.** [Species concepts and definitions](#). In: Grene M, Mendelsohn E, eds. *Topics in the Philosophy of Biology*. Dordrecht: Springer. 353-371
- **Mazin JM, Janvier P. 1983.** [L'anatomie de *Lyrocephaliscus euri* \(WIMAN\), trématosauré du Trias Inférieur du Spitsberg: arrière-crâne, squelette axial et ceinture scapulaire](#). *Palaeovertebrata* **13**:13-31
- **McHugh JB. 2012.** [Temnospondyl ontogeny and phylogeny, a window into terrestrial ecosystems during the Permian-Triassic mass extinction](#). D. Phil. Thesis, University of Iowa
- **Milner AR, Schoch RR. 2004.** [The latest metoposaurid amphibians from Europe](#). *Neues Jahrbuch für Geologie und Paläontologie – Abhandlungen* **232**(2–3):231-252
- **Milner AR, Schoch RR. 2013.** [Trimerorhachis \(Amphibia: Temnospondyli\) from the Lower Permian of Texas and New Mexico: cranial osteology, taxonomy and biostratigraphy](#). *Neues Jahrbuch für Geologie und Paläontologie – Abhandlungen* **270**(1):91-128
- **Morkovin BI. 2015.** [On the development of surface ornamentation of skull bones in the ontogeny of Early Triassic benthosuchids \(Amphibia, Temnospondyli\)](#) *Paleontological Journal* **49**(1):57-69
- **Moulton JM. 1974.** [A description of the vertebral column of *Eryops* based on the notes and drawings of A. S. Romer](#). *Breviora* **428**:1-44
- **Mueller BD. 2007.** [Koskinonodon Branson and Mehl, 1929, a replacement name for the preoccupied temnospondyl *Buettneria* Case, 1922](#). *Journal of Vertebrate Paleontology* **27**:225
- **Mueller B, Martz JW, Hungerbühler A, Nesbitt SJ. 2016.** [A diverse Late Triassic \(Norian\) tetrapod fauna and taphonomy of MOTT VPL 3869 from the Tecovas Formation \(Dockum Group\) in Garza County, Texas, USA](#).
- **Nixon KC, Wheeler QD. 1990.** [An amplification of the phylogenetic species concept](#). *Cladistics* **6**(3):211-223
- **Ochev VG. 1972.** [Capitosauroid Labyrinthodonts from the Southeast of European part of the USSR](#). Izdatel'stvo Saratovskogo Universiteta, Saratov. 269 [Russian]
- **Olsen PE, Kent DV, Whiteside JH. 2010.** [Implications of the Newark Supergroup-based astrochronology and geomagnetic polarity time scale \(Newark-APTS\) for the tempo and mode of the early diversification of the Dinosauria](#). *Earth and Environmental Science Transactions of the Royal Society of Edinburgh* **101**(3–4):201-229
- **Pardo JD, Small BJ, Huttenlocker AK. 2017.** [Stem caecilian from the Triassic of Colorado sheds light on the origins of Lissamphibia](#). *Proceedings of the National Academy of Sciences of the United States of America* **114**(27):E5389-E5395
- **Parker WG, Martz JW. 2010.** [The Late Triassic \(Norian\) Adamanian-Revuelian tetrapod faunal transition in the Chinle Formation of Petrified Forest National Park, Arizona](#). *Earth and Environmental Science Transactions of the Royal Society of Edinburgh* **101**(3–4):231-260
- **Pawley K. 2007.** [The postcranial skeleton of *Trimerorhachis insignis* Cope, 1878 \(Temnospondyli: Trimerorhachidae\): a plesiomorphic temnospondyl from the Lower Permian of North America](#). *Journal of Paleontology* **81**(5):873-894

- **Pawley K, Warren A. 2005.** [A terrestrial stereospondyl from the Lower Triassic of South Africa: the postcranial skeleton of *Lydekkerina huxleyi* \(Amphibia: Temnospondyli\)](#) *Palaeontology* **48**(2):281-298
- **Pawley K, Warren A. 2006.** [The appendicular skeleton of *Eryops megacephalus* Copoe, 1877 \(Temnospondyli: Eryopoidea\) from the Lower Permian of North America.](#) *Journal of Paleontology* **80**:561-580
- **Rasmussen C, Mundil R, Irmis RB, Geisler D, Gehrels GE, Olsen PE, Kent DV, Lepre C, Kinney ST, Geissman JW+1 more. 2020.** [U-Pb zircon geochronology and depositional age models for the Upper Triassic Chinle Formation \(Petrified Forest National Park, Arizona, USA\): implications for Late Triassic paleoecological and paleoenvironmental change.](#) *GSA Bulletin* **133**(3–4):539-558
- **Ray S, Bhat MS, Mukherjee D, Datta PM. 2016.** [Vertebrate fauna from the Late Triassic Tiki Formation of India: new finds and their biostratigraphic implications.](#) *The Palaeobotanist* **65**:47-59
- **Rayfield EJ, Barrett PM, McDonnell RA, Willis KJ. 2005.** [A geographical information system \(GIS\) study of Triassic vertebrate biochronology.](#) *Geological Magazine* **142**(4):327-354
- **Rayfield EJ, Barrett PM, Milner AR. 2009.** [Utility and validity of Middle and Late Triassic ‘land vertebrate faunachrons’.](#) *Journal of Vertebrate Paleontology* **29**(1):80-87
- **Reisz RR, Schoch RR, Anderson JS. 2009.** [The armoured dissorophid *Cacops* from the Early Permian of Oklahoma and the exploitation of the terrestrial realm by amphibians.](#) *Naturwissenschaften* **96**(7):789-796
- **Rineau V, Grand A, Zaragüeta R, Laurin M. 2015.** [Experimental systematics: sensitivity of cladistic methods to polarization and character ordering schemes.](#) *Contributions to Zoology* **8**(2):129-148
- **Rineau V, Zaragüeta i Bagils RZ, Laurin M. 2018.** [Impact of errors on cladistic inference: simulation-based comparison between parsimony and three-taxon analysis.](#) *Contributions to Zoology* **87**(1):25-40
- **Rinehart LF, Lucas SG. 2016.** [Eocyclotosaurus appetolatus, a Middle Triassic amphibian: osteology, life history, and paleobiology.](#) Albuquerque: New Mexico Museum of Natural History and Science Bulletin. **70**:1-118
- **Rinehart LF, Lucas SG. 2018.** [Description of a juvenile specimen of the Late Triassic amphibian *Apachesaurus gregorii*: developmental and relative growth.](#) *New Mexico Museum of Natural History and Science Bulletin* **79**:565-583
- **Rinehart LF, Lucas SG, Schoch RR. 2015.** [Eocyclotosaurus appetolatus, a new cyclotosaurid amphibian from the Middle Triassic \(Perovkan\) Moenkopi Formation of New Mexico, USA.](#) *Journal of Vertebrate Paleontology* **35**(3):e929140
- **Rinehart LF, Lucas SG, Tanner LH, Spielmann JA. 2013.** [The functional morphology of dermal bone ornamentation in temnospondyl amphibians.](#) *New Mexico Museum of Natural History and Science* **61**:524-532
- **Romer AS. 1947.** [Review of the Labyrinthodontia.](#) *Bulletin of the Museum of Comparative Zoology* **99**:1-368
- **Romer AS, Witter RV. 1942.** [Edops, a primitive rhachitomous amphibian from the Texas red beds.](#) *The Journal of Geology* **50**(8):925-960
- **Ronquist F, Huelsenbeck JP. 2003.** [MrBayes 3: Bayesian phylogenetic inference under mixed models.](#) *Bioinformatics* **19**(12):1572-1574

- **Roychowdhury T. 1965.** [A new metoposaurid amphibian from the Upper Triassic Maleri Formation of Central India.](#) *Philosophical Transactions of the Royal Society of London B: Biological Sciences* **250**(761):1-52
- **Sanderson MJ. 1995.** [Objections to bootstrapping phylogenies: a critique.](#) *Systematic Biology* **44**(3):299-320
- **Sansom RS, Wills MA. 2013.** [Fossilization causes organisms to appear erroneously primitive by distorting evolutionary trees.](#) *Scientific Reports* **3**(1):1-5
- **Säve-Söderbergh G. 1935.** [On the dermal bones of the head in labyrinthodont stegocephalians and primitive Reptilia.](#) *Meddelelser om Grønland* **98**:1-211
- **Säve-Söderbergh G. 1936.** [On the morphology of Triassic stegocephalians from Spitsbergen, and the interpretation of the endocranium in the Labyrinthodontia.](#) In: *Kunglik Svensk Vetenskapsakademiens Handlingar*. Stockholm: Almqvist & Wiksell. **16**:1-181
- **Sawin HJ. 1941.** [The cranial anatomy of *Eryops megacephalus*.](#) *Bulletin of the Museum of Comparative Zoology* **88**:407-463
- **Sawin HJ. 1945.** [Amphibians from the Dockum Triassic of Howard County, Texas.](#) *University of Texas Publication* **4401**:361-399
- **Schoch RR. 1999.** [Comparative osteology of *Mastodonsaurus giganteus* \(Jaeger, 1828\) from the Middle Triassic \(Lettenkeuper: Longobardian\) of Germany \(Baden-Württemberg, Bayern, Thüringen\)](#) *Stuttgarter Beiträge zur Naturkunde Serie B* **278**:1-175
- **Schoch RR. 2000.** [The status and osteology of two new cyclotosaurid amphibians from the Upper Moenkopi Formation of Arizona \(Amphibia: Temnospondyli; Middle Triassic\)](#) *Neues Jahrbuch für Geologie und Paläontologie – Abhandlungen* **216**(3):387-411
- **Schoch RR. 2004.** [Skeleton formation in the Branchiosauridae: a case study in comparing ontogenetic trajectories.](#) *Journal of Vertebrate Paleontology* **24**(2):309-319
- **Schoch RR. 2006.** [A complete trematosaurid amphibian from the Middle Triassic of Germany.](#) *Journal of Vertebrate Paleontology* **26**:29-43
- **Schoch RR. 2008.** [A new stereospondyl from the German Middle Triassic, and the origin of the Metoposauridae.](#) *Zoological Journal of the Linnean Society* **152**(1):79-113
- **Schoch RR. 2009.** [Life-cycle evolution as response to diverse lake habitats in Paleozoic amphibians.](#) *Evolution* **63**(10):2738-2749
- **Schoch RR. 2011.** [A trematosauroid temnospondyl from the Middle Triassic of Jordan.](#) *Fossil Record* **42**(2):119-127
- **Schoch RR. 2013.** [The evolution of major temnospondyl clades: an inclusive phylogenetic analysis.](#) *Journal of Systematic Palaeontology* **11**(6):673-705
- **Schoch RR. 2019.** [Osteology of the temnospondyl *Trematosaurus brauni* Burmeister, 1849 from the Middle Buntsandstein of Bernburg, Germany.](#) *Palaeodiversity* **12**(1):41-63
- **Schoch RR. 2021.** [The life cycle in late Paleozoic eryopid temnospondyls: developmental variation, plasticity and phylogeny.](#) *Fossil Record* **24**(2):295-319
- **Schoch RR, Milner AR. 2000.** [Handbook of Paleoherpertology Part 3B. Stereospondyli.](#) München: Verlag Dr. Friedrich Pfeil.
- **Schoch RR, Milner AR, Witzmann F. 2014.** [Skull morphology and phylogenetic relationships of a new Middle Triassic plagiosaurid temnospondyl from Germany, and the evolution of plagiosaurid eyes.](#) *Palaeontology* **57**(5):1045-1058
- **Schoch RR, Rubidge BS. 2005.** [The amphibamid *Micropholis* from the Lystrosaurus assemblage zone of South Africa.](#) *Journal of Vertebrate Paleontology* **25**:502-522

- **Schoch RR, Witzmann F. 2009.** [Osteology and relationships of the temnospondyl genus *Sclerocephalus*](#). *Zoological Journal of the Linnean Society* **157**(1):135-168
- **Schoch RR, Witzmann F. 2012.** [Cranial morphology of the plagiosaurid *Gerrothorax pulcherrimus* as an extreme example of evolutionary stasis](#). *Lethaia* **45**(3):371-385
- **Schultz CL. 2005.** [Biostratigraphy of the non-marine Triassic: is a global correlation based on tetrapod faunas possible?](#) In: Koutsoukos EAM, ed. *Applied Stratigraphy*. New York: Springer. 123-145
- **Sengupta DP. 1995.** [Chigutisaurid temnospondyls from the Late Triassic of India and review of the family Chigutisauridae](#). *Palaeontology* **38**:313-339
- **Sengupta DP. 2002.** [Indian metoposaurid amphibians revised](#). *Paleontological Research* **6**:41-65
- **Sequeira SE. 2003.** [The skull of *Cochleosaurus bohemicus* Frič, a temnospondyl from the Czech Republic \(Upper Carboniferous\) and cochleosaurid interrelationships](#). *Earth and Environmental Science Transactions of the Royal Society of Edinburgh* **94**(1):21-43
- **Shishkin MA, Sulej T. 2009.** [The Early Triassic temnospondyls of the Czatkowice 1 tetrapod assemblage](#). *Palaeontologia Polonica* **65**:31-77
- **Shishkin MA, Rubidge BS, Kitching JW. 1996.** [A new lydekkerinid \(Amphibia, Temnospondyli\) from the lower Triassic of South Africa: implications for evolution of the early capitosauroid cranial pattern](#). *Philosophical Transactions of the Royal Society of London Series B: Biological Sciences* **351**:1635-1659
- **Simpson GG. 1951.** [The species concept](#). *Evolution* **5**:285-298
- **Slowinski JB. 1993.** [Unordered versus ordered characters](#). *Systematic Biology* **42**(2):155-165
- **Spielmann JA, Lucas SG. 2012.** [Tetrapod fauna of the Upper Triassic Redonda Formation east-central New Mexico: the characteristic assemblage of the Apachean land-vertebrate faunachron](#). *New Mexico Museum of Natural History and Science Bulletin* **55**:1-119
- **Spielmann JA, Lucas SG, Heckert AB. 2007.** [Tetrapod fauna of the Upper Triassic \(Revueltian\) Owl Rock Formation, Chinle Group, Arizona](#). *New Mexico Museum of Natural History and Science Bulletin* **41**:371-383
- **Steyer J-S. 2000.** [Ontogeny and phylogeny in temnospondyls: a new method of analysis](#). *Zoological Journal of the Linnean Society* **130**(3):449-467
- **Steyer J-S. 2003.** [A revision of the early Triassic capitosauroids \(Stegocephali, Stegospondyli\) from Madagascar, with remarks on their comparative ontogeny](#). *Journal of Vertebrate Paleontology* **23**(3):544-555
- **Steyer J-S, Laurin M, Castanet J, de Ricqlès A. 2004.** [First histological and skeletochronological data on temnospondyl growth: palaeoecological and palaeoclimatological implications](#). *Palaeogeography, Palaeoclimatology, Palaeoecology* **206**(3-4):193-201
- **Stocker MR. 2012.** [A new phytosaur \(Archosauriformes, Phytosauria\) from the Lot's Wife beds \(Sonsela Member\) within the Chinle Formation \(Upper Triassic\) of Petrified Forest National Park, Arizona](#). *Journal of Vertebrate Paleontology* **32**(3):573-586
- **Sues H-D, Fitch AJ, Whatley RL. 2020.** [A new rhynchosaur \(reptilia, Archosauromorpha\) from the Upper Triassic of eastern North America](#). *Journal of Vertebrate Paleontology* **40**(2):e1771568
- **Sues H-D, Olsen PE. 2015.** [Stratigraphic and temporal context and faunal diversity of Permian-Jurassic continental tetrapod assemblages from the Fundy rift basin, eastern Canada](#). *Atlantic Geology* **51**(1):139-205

- Sues H-D, Schoch RR. 2013. [Anatomy and phylogenetic relationships of *Calamops paludosus* \(Temnospondyli, Stereospondyli\) from the Triassic of the Newark Basin, Pennsylvania](#). *Journal of Vertebrate Paleontology* **33**(5):1061-1070
- Sulej T. 2002. [Species discrimination of the Late Triassic temnospondyl amphibian *Metoposaurus diagnosticus*](#). *Acta Palaeontologica Polonica* **47**:535-546
- Sulej T. 2007. [Osteology, variability, and evolution of *Metoposaurus*, a temnospondyl from the Late Triassic of Poland](#). *Palaeontologica Polonica* **64**:29-139
- Sulej T, Majer D. 2005. [The temnospondyl amphibian *Cyclotosaurus* from the Upper Triassic of Poland](#). *Palaeontology* **48**(1):157-170
- Swofford DL. 2002. [PAUP*. Phylogenetic analysis using parsimony* 4.0](#). Sinauer, Sunderland, Massachusetts.
- Szulc J, Racki G, Jewula K, Środoń J. 2015. [How many Upper Triassic bone-bearing levels are there in Upper Silesia \(southern Poland\)? A critical overview of stratigraphy and facies](#). *Annales Societatis Geologorum Poloniae* **85**:587-626
- Teschner EM, Chakravorti S, Sengupta DP, Konietzko-Meier D. 2020. [Climatic influence on the growth pattern of *Panthisaurus maleriensis* from the Late Triassic of India deduced from paleohistology](#). *PeerJ* **8**(1):e9868
- Teschner EM, Sander PM, Konietzko-Meier D. 2017. [Variability of growth pattern observed in *Metoposaurus krasiejowensis* humeri and its biological meaning](#). *Journal of Iberian Geology* **44**(1):99-113
- Tsai CH, Fordyce RE. 2014. [Juvenile morphology in baleen whale phylogeny](#). *Naturwissenschaften* **101**(9):765-769
- Tykoski RS. 2005. [Anatomy, ontogeny, and phylogeny of coelophysoid theropods](#). D. Phil. Thesis, The University of Texas at Austin
- University of Michigan. 1957. [The President's report to the Board of Regents for the academic year 1955-1956](#). Ann Arbor: University of Michigan
- von Meyer E. 1842. [Labyrinthodonten-Genera](#). *Neues Jahrbuch für Mineralogie, Geographie, Geologie, Paläontologie* **1842**:301-304
- von Zittel KA. 1887–1890. [Handbuch der Paläontologie. Abteilung I. Paläozoologie. Band III. Vertebrata \(Pisces, Amphibia, Reptilia, Aves\)](#). München and Leipzig: Oldenbourg.
- Warren AA, Hutchinson MN. 1988. [A new capitosaurid amphibian from the Early Triassic of Queensland, and the ontogeny of the capitosaur skull](#). *Palaeontology* **31**:857-876
- Warren A, Rozefelds AC, Bull S. 2011. [Tupilakosaur-like vertebrae in *Bothriceps australis*, an Australian brachyopid stereospondyl](#). *Journal of Vertebrate Paleontology* **31**(4):738-753
- Warren A, Snell N. 1991. [The postcranial skeleton of Mesozoic temnospondyl amphibians: a review](#). *Alcheringa* **15**(1):43-64
- Watson DMS. 1919. [The structure, evolution, and origin of the Amphibia. The 'orders' Rachtomi and Stereospondyli](#). *Philosophical Transactions of the Royal Society, Series B* **209**(360–371):1-72
- Watson DMS. 1962. [The evolution of the labyrinthodonts](#). *Philosophical Transactions of the Royal Society of London. Series B, Biological Sciences* **245**(723):219-265
- Wiens JJ. 1995. [Polymorphic characters in phylogenetic systematics](#). *Systematic Biology* **44**(4):482-500
- Wiens JJ. 1998. [Testing phylogenetic methods with tree congruence: phylogenetic analysis of polymorphic morphological characters in phrynosomatid lizards](#). *Systematic Biology* **47**(3):427-444

- **Wiens JJ. 1999.** [Polymorphism in systematics and comparative biology](#). *Annual Review of Ecology and Systematics* **30**(1):327-362
- **Wiens JJ. 2001.** [Character analysis in morphological phylogenetics: problems and solutions](#). *Systematic Biology* **50**(5):689-699
- **Wiens JJ, Bonett RM, Chippindale PT. 2005.** [Ontogeny discombobulates phylogeny: paedomorphosis and higher-level salamander relationships](#). *Systematic Biology* **54**(1):91-110
- **Wiens JJ, Servedio MR. 1997.** [Accuracy of phylogenetic analysis including and excluding polymorphic characters](#). *Systematic Biology* **46**(2):332-345
- **Wiley EO, Mayden RL. 2000.** [A defense of the evolutionary species concept](#). In: Wheeler QD, Meier R, eds. *Species Concepts and Phylogenetic Theory. A Debate*. New York: Columbia University Press. 198-208
- **Wilson JA. 1941.** [An interpretation of the skull of *Buettneria*, with special reference to the cartilages and soft parts](#). *Contributions from the Museum of Paleontology, University of Michigan* **6**:71-111
- **Wiman C. 1914.** [Über die Stegocephalen aus der Trias Spitzbergens](#). *Bulletin of the Geological Institutions of the University of Uppsala* **13**:1-34
- **Witzmann F. 2006.** [Developmental patterns and ossification sequence in the Permo-Carboniferous temnospondyl *Archegosaurus decheni* \(Saar-Nahe Basin, Germany\)](#) *Journal of Vertebrate Paleontology* **26**:7-17
- **Witzmann F, Gassner T. 2008.** [Metoposaurid and mastodonsaurid stereospondyls from the Triassic-Jurassic boundary of Portugal](#). *Alcheringa* **32**(1):37-51
- **Witzmann F, Schoch RR, Hilger A, Kardjilov N. 2012.** [Braincase, palatoquadrate and ear region of the plagiosaurid *Gerrothorax pulcherrimus* from the Middle Triassic of Germany](#). *Palaeontology* **55**(1):31-50
- **Woodruff DC, Carr TD, Storrs GW, Waskow K, Scannella JB, Nordén KK, Wilson JP. 2018.** [The smallest diplodocid skull reveals cranial ontogeny and growth-related dietary changes in the largest dinosaurs](#). *Scientific Reports* **8**(1):1-12
- **Yates AM, Warren AA. 2000.** [The phylogeny of the 'higher' temnospondyls \(Vertebrata: Choanata\) and its implications for the monophyly and origins of the Stereospondyli](#). *Zoological Journal of the Linnean Society* **128**:77-121
- **Zeigler KE, Heckert AB, Lucas SG. 2003.** [The vertebrate fauna of the Upper Triassic \(Revueltian\) Snyder quarry](#). *New Mexico Museum of Natural History and Science Bulletin* **24**:71-79
- **Ziet**